# Removal of Cadmium Ions from Aqueous Solutions by Batch Biosorption on Pomelo Peel

Pin Jia Chong[1], Masniroszaime Md. Zain[2*]

[1,2]*School of Chemical Engineering, Taylor's Lakeside University, Malaysia*

**Corresponding email: Masniroszaime.MdZain@taylors.edu.my*

*Abstract*— **Pomelo peel as an agricultural waste is used to test the feasibility of it in removing cadmium ions from aqueous solution. Pomelo peel contains high amount of pectin which consists of functional groups that are able to bind with cadmium ions. The feasibility of pomelo peel as biosorbent to remove cadmium ions from aqueous solution is conducted in batch with pH ranges from 1 to 6, contact time ranges from 0 to 240 minutes and concentration of initial cadmium ions ranges from 25 to 100 mg/L as variables. The efficiency of untreated and pre-treated pomelo peels will also be compared. Biosorption isotherms can be generated using Langmuir and Freundlich models and kinetics of sorption process can be analyzed using pseudo-first order rate equation and pseudo-second order rate equation.No results have been shown as the experiment is still on going. However, it is strongly supported by theories and other researched papers that it is feasible for agricultural waste to be used as biosorbent in treating cadmium from aqueous solution.**

*Keywords*— Adsorption, Agricultural Waste, Biosorption, Cadmium, Pomelo Peel

## 1. Introduction

The natural occurring heavy metals have been a threat to living organism for their high toxicity. Cadmium as a heavy metal can be found in natural activities or man-made activities. Through these activities, many of the water sources are being contaminated with cadmium as it is highly soluble in aquatic environment. The carcinogenic cadmium mainly exposes to human through their diet. Contaminated soil and water causes the uptake of cadmium by crops and animals which are part of human diets and can cause failure of organs by accumulating in the tissues.

Primarily, cadmium accumulates in the liver where low molecular weight protein called Metallothionenins (MT) will form complexes with cadmium[1]. These complexes will release to various organs through blood and accumulates in the kidneys[2]. Since the body is poor in excreting cadmium and cannot actually metabolically degrade it into less toxic substance, even a small amount of cadmium accumulated in the body can cause serious health risk[3].Hence, it is essential to minimize or prevent cadmium from entering our body.

There are several ways of treating cadmium from aqueous environment. Traditional methods such as precipitation, membrane filtration, ion exchange, absorption and co-precipitation are high in cost, difficult to maintain and low in efficiency[4].The most economical and effective method of all the treatments is adsorption using mainly activated carbon as adsorbent. However, activated carbon as adsorbent is not very economical and which is why agricultural waste by products are being researched to explore the feasibility. Agricultural wastes are not only economical and effective but most importantly, they are environmental friendly and can be regenerated easily. They can also be found abundantly in most places and are non-toxic.

In this research, pomelo peel is chosen because the availability is abundant in Southeast Asia and they are rarely being researched. They contain high level of pectin which is a natural occurring polysaccharide in its cell walls and between the cell walls. Pectin consists of functional groups such as carboxyl groups, ether and amide which bind with cadmium ions to form complexes in the solution[5, 6]. The content of pectin of several fruit by products have been studied and compared. Pomelo peel is found to have the highest pectin content among them[7].

Studies have shown that pretreating agricultural wastes with chemicals can be more effective than non-treated ones[8, 9, 10]. Agricultural wastes that are chemically modified can extract soluble organic compounds and improve chelating efficiency[11, 12, 13, 14]. Acidic pretreatment has proved to be effective in eliminating impurities and ions that are dominating the binding sites[10]. Hence pretreated pomelo peels will also be compared to untreated pomelo peels.

### 1.1 Research Objectives

The objectives of this research were to explore the feasibility of removing cadmium ion from aqueous solution using untreated and pretreated pomelo peel by conducting batch experiments. The untreated and pretreated pomelo peels were compared to identify the best pretreatment. Also, the effects of solution pH, initial cadmium ion concentration and contact time were studied to identify the optimum conditions for this biosorption process.

## 2. Methodology

### 2.1 Preparation of Pomelo Peels

Pomelo peels were collected and washed with deionized water to eliminate any foreign particles and water soluble materials. The washed pomelo peels were cut into small pieces of 1 to 2 cm and dried in forced air convection oven (PROTECH, Model FAC-350) at about 60°C or below for approximately 48 hours or until the weight of the pomelo peels is constant to ensure all the moisture in the pomelo peel is being eliminated. The dried pomelo peels were blended in blender (Magic Bullet) and sieved using 500 µm cut size sieve to increase the surface area of biosorption.

Fig.1aImage of Pomelo Peel.

Fig. 2b Pomelo Peel cut into 1-2cm

Fig.2cImage of Blended Dried Pomelo Peel

Fig. 2dImage of Sieved Pomelo Peel

### 2.2Pretreatment of Pomelo Peels [15]

The general procedures for preparing the pomelo peel are the same as section 2.1. Dried and sieved pomelo peel was washed with isopropyl alcohol to form PPI. PPI was washed with sodium hydroxide to form PPIS and citric acid to form PPIC. PPIS was

washed with citric acid to form PPISC. Experiment will be conducted using untreated and pretreated pomelo peels.

### 2.3Determination of Effect of Solution pH

The effect of solution pH was determined by agitating 0.1g of untreated or pretreated pomelo peel and 100ml of 50 mg/L cadmium nitrate solution using shaker for 24 hours with a speed of 150rpm. The solution pH was adjusted by adding droplets of NaOH or $HNO_3$ ranging from pH 1 to pH 6. The experiment was conducted in room temperature. A graph of equilibrium cadmium ion capacity against pH of solution was plotted to see the effect of solution pH.

### 2.4Determination of Effect of Initial Cadmium Ion Concentration (Isotherm Experiment)

The effect of initial cadmium ion concentration was determined by agitating 0.1 g of untreated and pretreated pomelo peel with concentration of cadmium nitrate solution ranging from 25 mg/L to 100 mg/L for 24 hours at room temperature with a speed of 150rpm. The pH of the solution was kept constant at pH 4 by adding droplets of NaOH or $HNO_3$. Equilibrium isotherms were generated using the results. Langmuir model was described by:

$$q_e = q_{max} b C_e/(1+bC_e) \quad (1)$$

andFreundlich model was described by:

$$q_e = K_F C_e^{1/n} \quad (2)$$

where,
$q_e$ = equilibrium cadmium ions capacity (mg/g),
$q_{max}$ = maximum uptake capacity (mg/g biosorbent),
$C_e$ = equilibrium concentration (mg/l solution),
b = Langmuir equilibrium constant.
$K_F$ and n = Freundlich constants charactieristic of the system.

### 2.5Determination of Effect of Contact Time (Kinetic Experiment)

The effect of contact time to biosorption process was determined by agitating 0.1g of untreated and pretreated pomelo peel with 100 ml of 50mg/L of cadmium nitrate solution using shaker with different contact times ranging from 0 to 240 minutes with constant speed of 150 rpm at room temperature. The pH of the solution was kept constant at pH 4 by adding droplets of NaOH or $HNO_3$. Pseudo-first order rate equation and pseudo-second order rate equation were used to analyze the kinetic of biosorption. Pseudo-first order rate equation was described by:

$$\ln(1-q_t/q_e) = -k_1 t \quad (3)$$

and pseudo-second-order equation wasdescribed by:

$$t/q_t = (1/K_2 q_e^2) + (t/q_e) \quad (4)$$

where,
$q_t$ = weight of solute adsorbed per gram of biosorbent (g solute/g biosorbent),
$q_e$ = weight of solute adsorbed per gram of biosorbent at equilibrium (g solute/ g biosorbent)
t = contact time
$k_1$ = rate constant of pseudo-first-order sorption and
$k_2$ = rate constant of pseudo-second-order sorption.

### 2.6Cadmium Analysis

Capacity of cadmium ions per gram of pomelo peel biosorbentwas determined by using mass balance. The equilibrium capacity of cadmium ions was calculated using the equation:

$$q_e = V(C_i-C_e)/m. \quad (7)$$

Where,
$q_e$ = equilibrium cadmium ions capacity (mg/g),
V = the suspension volume (l),
m = the mass of biosorbent (g),
$C_e$ = cadmium ions concentration at equilibrium (mg/l),
$C_i$ = initial cadmium ions concentration (mg/l).

The residual cadmium concentration was analyzed using flame atomic adsorption spectrophotometry (FAAS).

## 3. Conclusions

Since the experiment is still on going, the results of the experiments have yet to be compared. However, with reference and support of many researched papers, using agricultural wastes to remove harmful cadmium are feasible and economical. It is also an environmental friendly substitution to other adsorbents. This is important for wastewater treatment to remove cadmium before releasing the wastewater into the environment as to avoid exposure of this highly toxic heavy metal to living organisms.

## References


[1] S. Angshuman, R. Geethanjali and K. Vishnuvardhan, "A brief review on the effect of cadmium toxicity: From cellular to organ level," *International Journal of Bio-Technolgy and Research,* vol. 3, no. 1, 2013.

[2] H. Gonick, "Nephroxicity of Cadmium & Lead," *Indian J Med Res,* 2008.

[3] M. Waalkes, "Cadmium carcinogenesis," *Mutation Research,* 2003.

[4] E. Lodyga-Chruscinska, "Biosorption of heavy metals - Modern and cheap method of polluted wastewater treatment," *Food Chemistry and Biotechnology,* vol. 74, 2010.

[5] Z. Mukhiddinov, D. Khalikov, F. Abdusamiev and C. Avloev, "Isolation and structural characterization of a pectin homo and ramnogalacturonan," vol. 53, 2000.

[6] F. Pagnanelli, S. Mainelli, F. Veglio and L. Toro, "Heavy metal removal by olive pomace: biosorbent characterization and equilibrium modeling," *Chemistry Engineering of Science,* vol. 58, 2003.

[7] K. Hasnah and O. Normah, "Pectin content of selected local fruit by-products," *J. Trop. Agric. and Fd. Sc.,* vol. 28, no. 2, 2000.

[8] S. Marina, K. Dragana and P. Jelana, "Potential of Agro-Based Waste Materials as Adsorbents of heavy Metal Ions from Water," University of Novi Sad, Faculty of Technology, Noci Sad, Serbia, 2013.

[9] W. Nitin and P. Vidyan, "Cadmium Removal from Aqueous Solution by Modified Low Cost Adsorbent(s): A State of the Art," *International Journal of Civil, Structural, Environmental and Infrastructure Engineering Research and Development,* vol. 3, no. 4, pp. 17-26, 2013.

[10] L. Vijayaraghavan and Y. Yeoung-Sang, *Biotechnol. Advan.,* vol. 26, pp. 266-291, 2008.

[11] P. Badot and G. Crini, "Application of chitosan, a natural amino polysaccharide, for dye removal from aqueous solutions by adsorption processes using batch studies: A review of recent literature," *Prog. Polym. Sci,* vol. 33, pp. 399-447, 2008.

[12] G. Crini, "Recent developtmets in polysaccharide-based materials used as adsorbents in wastewater treatment," *Prog. Polym. Sci.,* vol. 30, pp. 38-70, 2005.

[13] I. Gaballah, D. Goy, E. Allain, G. Kilbertus and J. Thauront, "Recovery of copper through decontamination of synthetic solutions using modified barks," *Met. Metall. Trans. B,* vol. B28, pp. 13-23, 1997.

[14] B. Pejic, M. Vukcevic, I. Pajic-Lijakovic, M. Lausevic and M. Kostic, "Mathematical modeling of heavy metal ions (Cd2+, Zn2+ and Pb2+) biosorption by chemically modified short hemp fibers," *Chem. Eng.,* vol. 172, pp. 354-360, 2011.

[15] S. Wanna and K. Pairat, "Pretreated Pomelo Peel As Biosorbent of Cadmium Ion From Aqueous Solution," 2010.

# Characterisation of By-Products from Torrefaction of Palm MesocarpFibre

Eng Yee Theng, VeenaDoshi*

*Department of Chemical Engineering, Taylor's University, Malaysia*

**Corresponding email: VeenaADoshi.ArunKumarDoshi@taylors.edu.my*

*Abstract*— **Torrefaction is a mild thermal conversion, usually used as a pre-treatment process prior to pyrolysis and gasification process. It is used to increase the energy density and improve the handling, storage, and transport of the biomass. However, torrefaction process produces liquid and gaseous by-products. Characterisations of the by-products are important before commercialising the process. In torrefactionof palm mesocarp fibre, main compounds found in the liquid product are acetic acid and phenol, whereas the main permanent gases produced are carbon dioxides and carbon monoxide.**

*Keywords*— Torrefaction, Mesocarp Fibre, Torrefaction Volatiles

## 1. Introduction

Bioenergy is an alternative energy sources replacing fossil energy that causes less harm to the environment. Biomass residues are abundant, carbon dioxide neutral with minimal amount of sulphur and nitrogen [1]. However, lignocellulosic biomass has high moisture, low bulk energy density and difficult to transport, handle, store and feed into existing combustion system[2]. Palm mesocarpfibre (PMF) is one of the biomass produced through palm oil milling process and it is 12-15% of fresh fruit bunch by weight[3]. The abundance of the biomass may lead to serious environmental issue if it is not treated.

Thermal conversion technologies are commonly used to develop the energy from biomass, such as pyrolysis, direct combustion, gasification and liquefaction [2]. Higher efficiencies of fuel production or consumption can be achieved by undergoing pretreatments. Raw biomass has high moisture content and low energy density compared to fossil fuel. It also difficult to be grinded and have hygroscopic behaviour that causes inability to be stored for a long period of time [2]. These limitation are able to be improved by a thermolysis process namely torrefaction. Torrefaction is a thermal pre-treatment that perform at temperatures of 200°C to 300°C at an inert atmosphere. This process improved energetic value, hydrophobicity and friability of the biomasses. Mass loss of the biomass through the process is mainly caused by dehydration and devolatisation of hemicellulose component [4]. This greatly increases the energy density of the biomass.

Studies on the volatiles have been done for other lignicellulosic biomass torrefaction, for example, Prins[5]has done studies on composition of volatiles produced for torrefaction of willow and larch,and volatiles of reed canary grass, wheat straw and willow torrefaction process were study with the aid of TGA-FTIR by Bridgeman [6]. Less attention has been paid to volatile products produced during torrefaction of oil palm biomass. With the potential of commercialising process and start up oil palm biomass torrefaction plant, the volatiles produced will be of larger amount. Therefore, studies on the characteristic of the gas and liquid by-product are crucial. Thus, in this study, characteristics of gas and liquid by-productfrom torrefaction of PMF are examined. The temperature of torrefaction process are 220°C, 250°C and 280°C, which represent light, moderate and severe torrefaction temperature respectively. Permanent gases produce are typically carbon dioxide and carbon monoxide, with traces of hydrogen and methane[7]. While liquids are expect to contain mainly acetic acid and phenol.

## 2. Material and Methods

### 2.1 Material

Palm MesocarpFiber (PMF) was obtained from local palm oil mill in Seri Ulu Langat Palm Oil Mill in Dengkil. The oil palm wastes were oven-dried at 105°C for 24 hours to eliminate free moisture content in it. Dried oil PMFwasmilled into particle sizes between the ranges of 0.5 mm to 2.00 mm. It is then sieved using Retsch sieve shaker. The samples will be stored in air-tight containers to avoid moisture contact with the samples.

### 2.2Torrefaction Process

PMF undergo torrefaction process in a bench-scale torrefaction reactor. The sample weight is 25g for each run and it is placed in the reactor at room temperature. Nitrogen gas of 150ml/min at STP is used to inert the system for30 minutes before commencing heating. The reactor is heated at 10°C/min. The experimental temperature of 220°C, 250°C and 280°C will be used to representing mild, moderate and severe torrefaction. The retention time of the torrefaction process is at 0.5h and 2h for each temperature. Torrefaction will produce three phases of products. Torrefied solid biomass is the main product which has been studied over the years. Therefore, the focus of this study is on the liquid and gaseous product. After the torrefaction process, samples were cooled and weighed to determine the solid yield. Volatile liquid are collected in a liquid trap at the base of the reactor. The condensed liquid wasweighed and placed in amber glass container and stored in a cold environment for further analysis.

Permanent gaswascollected in gas bags across the wholetorrefaction process. First gas bag was collected after purging the reactor with nitrogen for 30 minutes. Gas bag 2 was taken at 10th minute of ramping. When the temperature of reactor reaches experimental temperature, third gas bag is collected. It is followed by collection of gas bag at 15 minutes interval till the end of residence time and the last gas bag was collected 30 minutes after that.

### 2.3 Gas Analysis

Agilent Technologies 7890A Gas Chromatograph with TCD and FID was used. Oven temperature is 60 °C, hold for 14 min and pressure is maintained at 20 psi.

### 2.4Liquid Analysis

Liquid samples are diluted to 5wt% with Propan-2-ol before introducing to the Gas-Chromatograph-Mass-Spectrometry (GC-MS) unit. Agilent HP-5ms(30 m × 0.25 mm × 0.25 µm) capillary column was installed in an Agilent Technologies 7890A Gas Chromatograph with 5975C Mass Spectrometer. Helium is use as carrier gas at 30 cm/s, constant flow. The initial oven temperature is 40°C, hold for 1 minute, ramp up at 15°C/min to 100°C, thenfurther ramping at 10 °C/min to 210 °C and hold for 1 minute, then ramping at 5 °C/min to 310 °C and hold 8 minutes. The MSD source at 300 °C, quadrupole at 180 °C, transfer line at 290 °C, scan range 45 to 450 amu. The standard to quantify phenol is taken from Phenol-mix 19 by Dr. Ehrenstorfer GmbH.The pH of the liquid produced are analysed by Mettler-ToledoS20-K SevenEasy pH Meter.

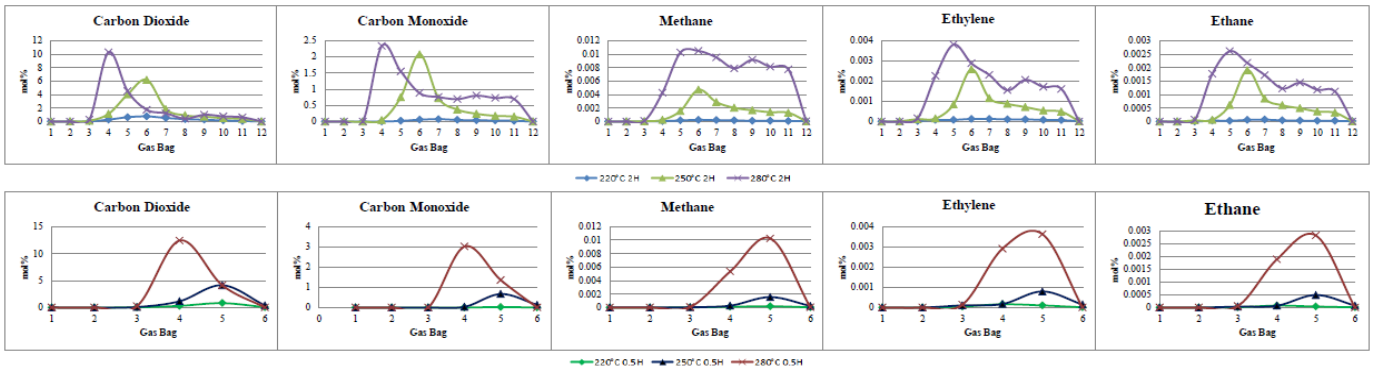


**Figure 1 Concentration of gas produced across torrefaction process of PMF using GC-FID**

## 3. Results and Discussions

### 3.1 Mass Yield and pH Value

The mass yields are in weight percent of the initial raw biomass. Liquid mass yield of torrefaction of PMF shows an increasing trend by increasing of both residence time and temperature. Longer residence timeallows the lignocellulosiccomponents to further breakdown and gives a lower mass yield,thus, higher energy density. Compared the mass yield to review from [4], the mass yield of lower than results from this experiment, but it shows a similar trend. This could be cause by different reactor configuration and sample size with [7]. pH value of the liquid produced are at relatively high acidity except for mild torrefaction at 0.5 hour. This could be compared to GC-MS results in Table 2, at this mild condition, main compound of acetic acid is of relatively lower concentration.

**Table 1 Mass Yields of Torrefaction of PMF**

| Temperature (°C) | Residence Time (Hours) | Solid Yield (wt%) | Liquid Yield (wt%) | Liquid pH Value |
|---|---|---|---|---|
| 220 | 0.5 | 92.95% | 2.54% | 3.29 |
| 220 | 2 | 84.87% | 4.09% | 2.01 |
| 250 | 0.5 | 84.69% | 7.62% | 2.09 |
| 250 | 2 | 72.18% | 12.02% | 2.13 |
| 280 | 0.5 | 68.06% | 20.47% | 2.02 |
| 280 | 2 | 58.60% | 21.00% | 2.05 |

### 3.1Gas Chromatography-Mass Spectrometry

The compounds present in liquid by-product through are mainly acetic acid and phenol; its concentrations are tabulated in Table 2. Higher concentration of these compounds pairs with higher severity condition[5]. However, acetic acid for torrefaction temperature of 2 hours shows decreasing trend across the temperature. This may cause by error in measurement of sample density by syringe with error of ±0.2ml, causes over or under dilution. Other major compounds presents are furfural, 1-Hydroxy-2-butanone, and other phenolic compounds. More phenolic compounds were found in the samples compared to the woody biomass from Prins's study, with only traces of phenol.

**Table 2 Concentrations of Main Compounds in Liquid By-product**

| Temperature (°C) | Residence Time (Hours) | Acetic Acid Concentration (mg/L) | Phenol Concentration (mg/L) |
|---|---|---|---|
| 220 | 0.5 | 9756.8 | 944.2 |
| 220 | 2 | 187870.8 | 11480.0 |
| 250 | 0.5 | 146177.6 | 9728.7 |
| 250 | 2 | 162507.6 | 20073.6 |
| 280 | 0.5 | 188971.4 | 20379.0 |
| 280 | 2 | 109413.7 | 24801.0 |

### 3.1 Gas Chromatography-Flame Ionisation Detector

Gas bags were collected across the duration of experiment to observe the content of the gas produced by torrefaction of PMF with time frame stated in Section 2.2. Figure 1 displays permanent gases produced at each gas bag. Reaction zone starts at Bag 3, where temperature reaches operating temperature and gaseous product starts to produce.At higher temperature, more gases are produced and it is eluted out earlier compared to lower operating temperature with only small amount of permanent gas produced. The main gaseous products are carbon dioxide ($CO_2$) and carbon monoxide (CO), with small amount of methane, ethylene and ethane. Removing high amount of $CO_2$favours the quality of solid fuel produced, as O/C ratio reduced [6]. However, treatments on CO and $CO_2$ before releasing to the environment and recovery of methane gas will be essential for commercialising of the process.

## 4. Conclusion and Recommendation

Yield of torrefaction products is dependent on temperature and residence time. By increasing these parameters, mass yield of solid PMF decrease, while the liquid yield increases. In torrefaction process, solid product qualities are at priority, but considering environmental regulation and issues, optimisation between the product and by-products are required. Increasing the severity of the process increases the acetic acid and phenol concentration in the liquid product. These compounds are required to be treated as high concentrations are detected. Gaseous products are mainly $CO_2$ and CO. High amount of permanent gases produced during the starting of reaction zone. Concentration permanent gases increase with temperature. Further studies on treatments of torrefaction by-product waste are essential.

## References

[1] K. M. Sabil, M. a. Aziz, B. Lal, and Y. Uemura, "Effects of torrefaction on the physiochemical properties of oil palm empty fruit bunches, mesocarp fiber and kernel shell," *Biomass and Bioenergy*, vol. 56, pp. 351–360, Sep. 2013.

[2] W.-H. Chen and P.-C. Kuo, "A study on torrefaction of various biomass materials and its impact on lignocellulosic structure simulated by a thermogravimetry," *Energy*, vol. 35, no. 6, pp. 2580–2586, Jun. 2010.

[3] Y. L. Chiew, T. Iwata, and S. Shimada, "System analysis for effective use of palm oil waste as energy resources," *Biomass and Bioenergy*, vol. 35, no. 7, pp. 2925–2935, Jul. 2011.

[4] J. J. Chew and V. Doshi, "Recent advances in biomass pretreatment – Torrefaction fundamentals and technology," *Renew. Sustain. Energy Rev.*, vol. 15, no. 8, pp. 4212–4222, Oct. 2011.

[5] M. J. Prins, *Thermodynamic analysis of biomass gasification and torrefaction.* .

[6] T. G. Bridgeman, J. M. Jones, I. Shield, and P. T. Williams, "Torrefaction of reed canary grass, wheat straw and willow to enhance solid fuel qualities and combustion properties," *Fuel*, vol. 87, no. 6, pp. 844–856, May 2008.

# Preparation and Stability of Graphene Nanofluids Using Ionic Liquid Analogues

Yan Kai Fang[1], RashmiGangasa Walvekar[1*], Shahbaz Kaveh[1]

[1]*School of Engineering, Department of Chemical Engineering,Taylor's University, Malaysia*

**Corresponding email: RashmiGangasa.Walvekar@taylors.edu.my*

*Abstract*—**In this research, functionalized grapheneoxide nanoparticles are dispersed in ammonium and phosphoniumbased deep eutectic solvents (DESs) to form stable graphenenanofluids (GNFs) without the aid of surfactant. Different molar ratio of salts and hydrogen bond donors (HBDs) are used to synthesize DESs for the preparation of different concentrations of GNFs (0.01 wt%, 0.02 wt% and 0.05 wt%). Homogeneous solutions of nanofluidsare expected to be formed byultrasonic homogenization process. Stability studies are carried out through visual observation and stability validation is made by centrifuging the GNFs samples. This ensures that there is no particle agglomeration and formation of sediments in the nanofluids. From the work, it is found that nine samples of GNFs from phosphonium based DESs are highly stable.**

*Keywords*— deep eutectic solvents, graphenenanofluids, stability

## 1. Introduction

Nanofluids are seen to be a new emerging product that strikes the impetus of researchers in the nanotechnology field. Fluids containing dispersed millimeter or micrometersized solid particles are faced with downsides such as abrasion, increased pressure drop of the flow channel and clogging issues due to the weak suspension stability.These drawbacks can be seen through the work from the researchers at Argonne National Laboratory (ANL) in the United States[1].The behaviour of the minute nanoparticlesare analogous to liquidmolecules[2].These nanofluids, as compared with conventional liquid suspensions,have a larger relative surface area are beneficial in terms of high dispersion stability, reduced pumping power and prevention of clogging issue in flow passages[3].Stabilization of nanofluids can be achieved in numerous ways such as chemical functionalization to favour interactions with host liquid, electrostatic repulsion through formation of electrical double layer solution and finally the use of surfactants. However, the surfactants can deteriorate irreversibly at modest temperature typically above 60°C [4]. Graphene nanoparticles (GNPs), being the first two-dimensional atomic crystal with superior properties has attracted the attention of the research community in the nanofluids advancement. In green chemistry, DESs serve as an alternative to conventional fluids and traditional ionic liquids due to the non-toxicity, biodegradability and non-reactivity with water properties[5]. DESs can be made by the combination of organic halide salts and an organic compound known as hydrogen bond donor (HBD) in which hydrogen bonding can exist between the HBD and the halide ion[6].

In this paper, the work encapsulates the dispersion of GNPs into particular type of DESs to synthesizedifferent concentrations of graphene oxide nanofluids without the aid of surfactant. Stability studies are carried out in order to ensure the GNFs synthesized are stable with no particle agglomeration. This is done through visual observation to determine the presence of suspended particles or sediments in the nanofluids and validated with centrifugal studies.

## 2. Materials and Methods

### 2.1 DESs Synthesis

The chemicals, namely choline chloride ($C_5H_{14}ClNO$)and methyl triphenylphosphonium bromide ($C_{19}H_{18}PBr$) as salts and ethylene glycol ($C_2H_6O_2$) and triethylene glycol ($C_6H_{14}O_4$) as HBDs were purchased from Merck Millipore. The chemicals were used without further purification. Synthesis of DESs was performed by suspending different molar ratios of salt with their corresponding HBD. Table 1 presents the compositions of the different DESs synthesized in this research (abbreviated as DES 1 to DES9).

Table 1.Synthesized DESs compositions and their abbreviations

| Salt | HBD | Molar ratio (Salt:HBD) | | Abbreviation |
|---|---|---|---|---|
| | | Salt | HBD | |
| Choline chloride | Ethylene glycol | 1.00 | 1.75 | DES 1 |
| | Ethylene glycol | 1.00 | 2.00 | DES 2 |
| | Ethylene glycol | 1.00 | 2.50 | DES 3 |
| Choline chloride | Triethylene glycol | 1.00 | 3.00 | DES 4 |
| | Triethylene glycol | 1.00 | 4.00 | DES 5 |
| | Triethylene glycol | 1.00 | 5.00 | DES 6 |
| Methyl triphenylphosphonium bromide | Ethylene glycol | 1.00 | 3.00 | DES 7 |
| | Ethylene glycol | 1.00 | 4.00 | DES 8 |
| | Ethylene glycol | 1.00 | 5.00 | DES 9 |

### 2.2 GrapheneNanofluids Synthesis

Subsequently after the DESs were prepared, 27GNFs were synthesized by the addition of graphene oxide. In this study, graphene was purchased from Graphene Supermarket, United States. The graphene was functionalized through oxidation with hydroxyl group before utilized in the synthesis of GNFs. The functionalized graphene oxide was weighed and added accurately to produce the desired concentrations of GNFs (0.01 wt%, 0.02 wt% and 0.05 wt%). Table 2 presents the different concentrations of the various GNFs synthesized from DESs (abbreviated as GNF 1 to GNF 27).

Table 2. Synthesized GNFs compositions and their abbreviations

| DES | Abbreviation | | |
|---|---|---|---|
| | Concentration (wt%) | | |
| | 0.01 | 0.02 | 0.05 |
| DES 1 | GNF 1 | GNF 2 | GNF 3 |
| DES 2 | GNF 4 | GNF 5 | GNF 6 |
| DES 3 | GNF 7 | GNF 8 | GNF 9 |
| DES 4 | GNF 10 | GNF 11 | GNF 12 |
| DES 5 | GNF 13 | GNF 14 | GNF 15 |
| DES 6 | GNF 16 | GNF 17 | GNF 18 |
| DES 7 | GNF 19 | GNF 20 | GNF 21 |
| DES 8 | GNF 22 | GNF 23 | GNF 24 |
| DES 9 | GNF 25 | GNF 26 | GNF 27 |

### 2.3 Stability Studies

After the GNFs were synthesized, all the samples were undergone ultrasonic homogenization process for approximately 5 minutes. This was done using Bandelin Electronic Sonopuls HD3200 ultrasonic homogenizer with frequency of 20kHz and the pulse setting of 5 seconds with 10 seconds intervals.The samples were cooled with water as the temperature of the samples will increase during the homogenization process. Visual observation was used to monitor the presence of any suspending particles or sediment and select stable GNFs.Nanofluids stability was validated usingScanspeed 1730R bench top microcentrifuge at 1000, 5000, 10000 and 15000 rpm.

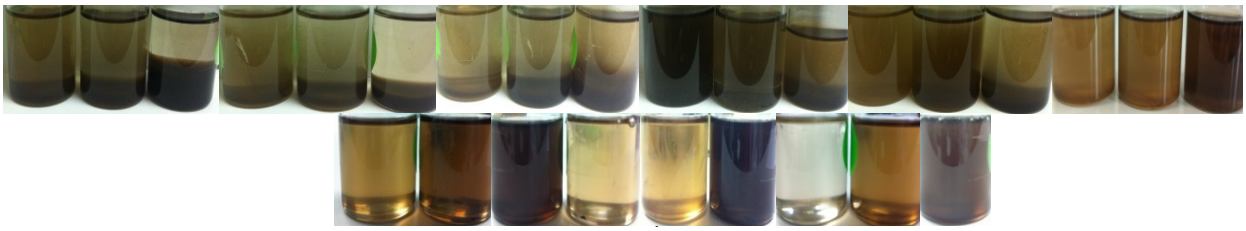

Figure 1.Four weeks after GNFs have undergone ultrasonic homogenization (from left – GNF 1 to GNF 27).

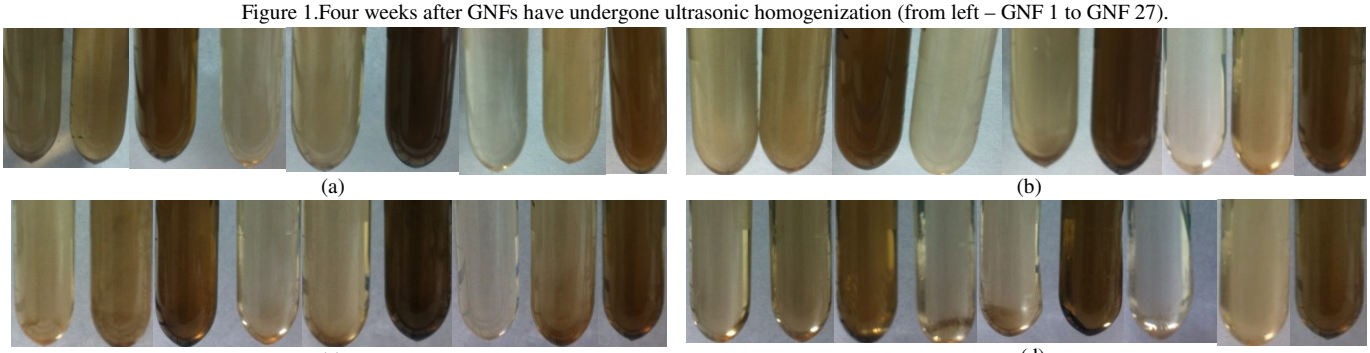

(a) (b) (c) (d)

Figure 2.Stable GNFs (from left: GNF 19 to GNF 27) after centrifugation process at different rpm (a) 1000rpm (b) 5000rpm (c) 10000rpm (d) 15000rpm

## 3. Results and Discussion

Figure 1 depicts27synthesized GNFs after the ultrasonic homogenization and observed for four weeks. Significant sediments were observed from GNF 1 to GNF 18 while GNF 19 to GNF 27have formed stable solutions as there is no visible suspended particles or sediment. This can be explained as nanoparticles in nanofluids have large surface area and the incessant particles collision from Brownian agitation leads to strong van der Waals interactions. However, the collision can cause particle agglomeration and the particles settled out of suspension due to their weight [4]. Figure 2 presents immediate images of stable GNFs after centrifugation process. It is found that all GNFs still possess strong stability.

### 3.1 Effect of GNFs Concentration on Stability

Through visual observation from Figure 1, it can be said that as the GNFs concentration increases, a decrease in stability is observed. This is true as the concentrations of GNFs from the same DES (e.g. GNF 1, GNF 2 and GNF 3)increases,moresediment of GNPs in the GNFs is settled out. The supernatant solutionschange colour from darker brown to lighter brown, indicating that more GNPs have dissolved in the lower concentration of the GNFs from the same DES.

### 3.2Effect of Mole Fraction of SaltandHBDon Stability

For the same GNFs concentration from different DESs (e.g. GNF 1, GNF 4 and GNF 7), themole fraction of salt decreases from DES 1 to DES 3. From Figure 1, the stability increases with decreasing mole fraction of salt. Lower salt content indicates higher hydrogen bond donor content in the DESs. With higher content of hydrogen bond donor, the presence of hydroxyl groups increases which strengthens the hydrogen bonds between the polar DESs and GNPs.

### 3.4Effect of Type of Salt and HBD on Stability

From this research, it has been shown that the stable GNFs (GNF 19 to GNF 27) can be synthesized from the DESs with methyl triphenylphosphonium bromide as salt and ethylene glycol as HBD. Both the HBDs in this experiment are organic solvents and it has been proven that well-dispersion behaviour of GNPs in these organic solvents is achieved [7]. Due to the rich hydrophilic oxygen-containing groups especially the hydroxyl group in polar organic solvents like ethylene glycol and triethylene glycol, the GNPs can be readily dissolved[7].

## 4. Conclusions

In this research work, the preparation of DESs and the synthesis of different concentration of GNFs (0.01 wt%, 0.02 wt% and 0.05 wt%) using functionalized graphene oxide without any surfactant are presented. Ultrasonic homogenization process was performed on the synthesized GNFs to prevent particles agglomeration and sedimentation of GNPs in GNFs. Stability studies using visual observation was also carried out to monitor and determine the stable GNFs which can be formed. The results achieved from the experimental work have shownnine stable GNFs (GNF 19 to GNF 27) being left for four weeks after the ultrasonic homogenization process and stability validation is made using centrifugation process.

For further improvements and recommendations on this work, myriadtypes of salts and HBDs and molar ratio combinations can be explored to synthesize suitable DESs for the preparation of stable GNFs without the addition of surfactant. In addition, the stability studies of GNFs synthesized can be made better by carrying out using zeta potential analysis to study the sedimentation of GNFs.

## Acknowledgment

This work is supported by the Chemical Engineering Department ofthe University of Malaya.

## References

[1] Choi, U.S. and T.N. Tran, *Experimental studies of the effects of non-newtonian surfactant solutions on the performance of a shell-and-tube heat exchanger.* Recent Developments in Non-Newtonian Flows and Industrial Applications, The American Society of Mechanical Engineers, 1991. **124**: p. 47-52.

[2] Choi, S.U.S. and J.A. Eastman, *Enhancing thermal conductivity of fluids with nanoparticles*, in *ASME International Mechanical Engineering Congress & Exposition*. 1995: San Francisco, CA.

[3] Saidur, R., K.Y. Leong, and H.A. Mohammad, *A review on applications and challenges of nanofluids.* Renewable and Sustainable Energy Reviews, 2011. **15**(3): p. 1646-1668.

[4] Taylor, R., P. Phelan, and G. Rosengarten. *Critical review of the novel applications and uses of nanofluids*. in *Proceedings of the ASME 2012 3rd Micro/Nanoscale Heat & Mass Transfer International Conference*. 2012. Atlanta, Georgia, USA.

[5] Abbott, A.P., et al., *Deep eutectic solvents formed between choline chloride and carboxylic acids: Versatile alternatives to ionic liquids.* Journal of the American Chemical Society, 2004. **126**(29): p. 9142-9147.

[6] Shahbaz, K., et al., *Densities of ammonium and phosphonium based deep eutectic solvents: Prediction using artificial intelligence and group contribution techniques.* Thermochimica Acta, 2012. **527**(0): p. 59-66.

[7] Paredes, J.I., et al., *Graphene oxide dispersions in organic solvents.* Langmuir, 2008. **24**(19): p. 10560-10564.

# Mechanical Behaviour of Thermoplastic Starch/Montmorillonite/Alumina Trihydrate Nanocomposites

Firnaaz Ahamed[1], Siew Wei Phang[1,2,*], Tin Sin Lee[2]

[1]*Department of Chemical Engineering, School of Engineering, Taylor's University, Malaysia,*

[2]*Department of Chemical Engineering, Faculty of Engineering and Science, University Tunku Abdul Rahman (UTAR), Malaysia*

**Corresponding email: SiewWei.Phang@taylors.edu.my*

*Abstract*— **Thermoplastic starch (TPS) has exhibited great potential to replace synthetic polymers in commercial applications. However, TPS lacks in some of the crucial mechanical properties. This study proposes the novel combination of *cassava* starch, montmorillonite (MMT) and alumina trihydrate (ATH) to improve the mechanical properties of the nanocomposite. Loadings of MMT and ATH were varied between 1 to 6 wt% and 26 to 37 wt%, respectively, and the mechanical properties were evaluated through tensile testing according to ASTM D882. Presence of both MMT and ATH showed increase in maximum tensile stress and Young's modulus up to 5.08 MPa and 57.56 MPa, respectively, while elongation at break is greatly diminished to 39.2%.**

*Keywords*— Thermoplastic starch; Montmorillonite; Alumina trihydrate; Nanocomposites, Mechanical Properties

## 1. Introduction

Widespread and serious environmental concerns caused by conventional plastics as well as the overdependence on petroleum resources has led to the development in production of bio-based and biodegradable plastics derived from renewable resources. TPS is a biodegradable biopolymer that is manufactured through gelatinization of starch by application of shear and heat in the presence of plasticizers like water and/or glycerol [1]. Starch is an excellent choice to be made into TPS as it is inexpensive and abundantly available [2]. However, TPS exhibits very poor resistance to water and consequently inferior mechanical properties compared to synthetic polymers [2, 3]. Various nanofillers and additives can be incorporated into TPS to improve its properties and nanoclays are one of the most commonly used reinforcement fillers in many different polymer matrices due to its environmentally benign nature, abundant availability and low cost [2, 3]. Similarly, ATH is an inorganic, non-toxic and environmentally friendly flame-retarding compound that also greatly influences the mechanical properties of polymers. However, both MMT and ATH are only effective within a certain loading and excessive amount can lead to adverse effects on mechanical properties of the nanocomposites. MMT is recorded to be effective within 3 to 6 wt% [2-4] while ATH is expressed to be deteriorative to mechanical properties at above 60% [5]. To the best of the authors' knowledge, combination of TPS, MMT and ATH in the form of nanocomposite has never been investigated. The aim of this research is to investigate the influence of varying loadings of MMT and ATH on mechanical properties of TPS/MMT/ATH nanocomposites.

## 2. Experimental

### 2.1 Materials

*Cassava* starch was purchased from SCS Food Manufacturing Sdn. Bhd., Malaysia. Glycerol was obtained from Merck Sdn. Bhd., Malaysia. Untreated MMT (NANOLIN DK® nanoclay) was purchased by FCC®, Inc., China. ATH (Micral® 9400) was supplied by J.M. Huber Corporation, USA, with a purity of 99.5% and laboratory formulated distilled water was used for TPS processing.

### 2.2 Design of Experiments

A full factorial experimental design was employed with two-level factors – loadings of MMT and ATH, generating a total of four formulations labeled F1 to F4. A control sample, F0, with no MMT and ATH was included for clear comparison of properties of pure TPS with that of nanocomposites. The composition of each formulation and corresponding levels of factors are shown in Table 1.

Table 1. Formulations and corresponding levels of factors

| Factors | F0 | F1 | F2 | F3 | F4 |
|---|---|---|---|---|---|
| MMT (wt%) | 0 | 1 | 6 | 1 | 6 |
| ATH (wt%) | 0 | 26 | 26 | 37 | 37 |

The experimental results were carefully interpreted by means of statistical analysis using Minitab® 16.1.1 software. The individual main effects and interaction effects of each factor were cautiously analyzed.

### 2.3 Preparation of TPS/MMT/ATH Nanocomposite Films

100 g of starch was added along with 55 phr of glycerol and 15 phr of distilled water. The mixture was thoroughly stirred. MMT and ATH was subsequently added in appropriate amount according to the experimental design, in that order, and thoroughly mixed. The mixture was melt-extruded in twin-screw extruder (SHJ-20, Nanjing Giant Machinery Co., Ltd., China) with barrel temperatures set in the range of 155 °C to 170 °C from feeding point to the die and screw rotation speed within 300 to 360 rpm. The obtained nanocomposite pellets were molded using 25-ton hydraulic hot press (LS-22009-25, Lotus Scientific Sdn. Bhd., Malaysia) before cut into dumbbell shape for tensile testing.

### 2.4 Methods

Tensile tests were performed on each specimen according to the ASTM D882 on Tensile Tester Machine Series 5582 (Instron®, USA) with elongation rate set at 50 mm/min. The maximum tensile stress, Young's modulus and maximum elongation at break were recorded for each specimen. The fractured surfaces of specimens were examined through scanning electron microscope (SEM), VP-SEM S-3400N (Hitachi, Ltd., Japan) at 1000 times magnification.

## 3. Results and Discussion

Tensile testing on sample F0 yielded Young's modulus, maximum tensile stress and elongation at break with values of 0.046 MPa, 0.34 MPa and 535.7% in average, respectively. The mechanical properties for the rest of the samples are shown in Fig. 1. Mechanical properties of melt-extruded pure TPS with 20 to 25 wt% of glycerol content are reported to be in the range of 5.43 to 6.79 MPa and 37.21 to 74.49% for maximum tensile stress and elongation at break, respectively [6]. As compared to findings by Moscicki et al. [6], the difference is mainly attributed to the high glycerol and water content that is employed for all the formulations in this research. In fact, 32 wt% of glycerol and 9 wt% of water was used in this experimental study. The main reason to employ such high plasticizer content was to improve the processibility of the nanocomposites in extruder in the presence of ATH. Through numerous trial runs prior to this study, it

was discovered that any lower water and glycerol content would render the formulations thick and thus, unable to be extruded out through the die when substantial amount of ATH is present.

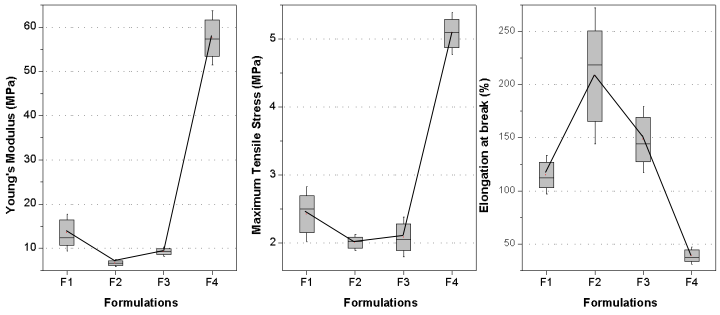


Fig. 1 Mechanical properties of different formulations with boxplots indicating standard deviations of data

It is clearly evident from Fig. 1 that increment of MMT to 6 wt% in F2 results in reduction in maximum stress, Young's modulus and corresponding increase in elongation at break. This observation could be due to agglomeration of MMT due to high content of MMT. This is supported by other researches that reported that maximum threshold of MMT content in TPS is about 5 wt% [2-4]. Sample F3 with increment of ATH to 37 wt% also exhibited poorer mechanical properties than F1 and slightly better than F2. Conversely, sample F4 displayed by far the most superior mechanical strength, with almost four and twofold increase in Young's modulus and maximum stress, respectively, but resulted in great decline in elongation at break, by almost threefold.

The interaction and main effects of MMT and ATH loading is clearly represented in Fig. 2. There are clear interactions between the two factors although the main effects of ATH are far more prominent than main effects of MMT on the responses. Nevertheless, increment in both ATH and MMT content causes increase in Young's modulus and maximum tensile stress while elongation at break diminishes.

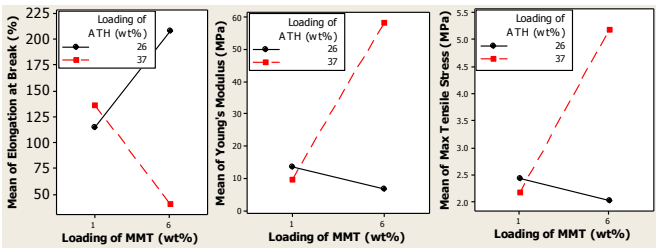


Fig. 2 Interaction plots of MMT and ATH loadings on mechanical properties

Although the effect of ATH is found to be far more prominent in improving mechanical properties of TPS, MMT is often favoured as evident from many previous researches mainly because the effect of MMT is significant even in small amounts [2-4]. In contrast, high loadings of ATH is necessary before the effect on mechanical properties become evident [5]. In fact, increment of MMT from 1 wt% to 6 wt% from F3 to F4 resulted in increase of Young's modulus and maximum tensile stress by about 520% and 143%, respectively.

The mechanical properties obtained through tensile testing are further supported by the SEM micrographs at 1000 times magnification as presented in Fig. 3. In general, all formulations show poor homogeneity, where large grains of unprocessed starch molecules are clearly visible. Native granular starch molecules are not completely destroyed and thus, failed to form a continuous phase. Smaller aggregates seen in the images could be attributed to agglomeration of MMT and/or ATH molecules. In overall, there is poor dispersion of molecules throughout the entire polymer matrices caused by inadequate bonding between the components resulting in poor mechanical properties. Samples F1, F2 and F3 show significant plastic deformation prior to failure where the materials are greatly stretched causing visible cracks to form.

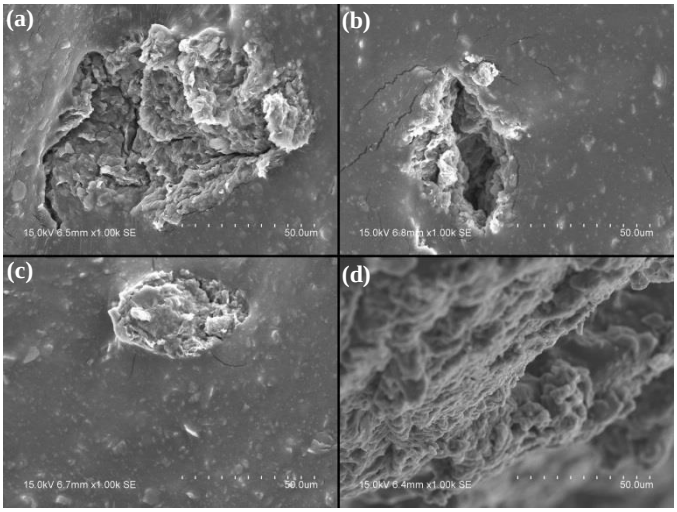


Fig. 3 SEM micrographs of fractured points of (a) F1, (b) F2, (c) F3, (d) F4

Conversely, sample F4 shows very little or almost insignificant deformation before fracture. Significant creases and crazing in samples F1, F2 and F3 could have been the result of progressive recrystallization which is common in glycerol plasticized TPS [7].

## 4. Conclusions

A novel biodegradable TPS/MMT/ATH nanocomposite was prepared through melt-extrusion. Presence of MMT and ATH greatly improved maximum tensile stress and Young's modulus of the nanocomposites but greatly declined elongation at break, making the nanocomposites highly brittle. The results also indicated that nanocomposites with MMT content below 6 wt% shows better mechanical properties and high MMT content results in agglomeration. In general, SEM results revealed very poor dispersion of molecules within the polymer matrices due to inadequate bonding between the components. The bonding between the components could be strengthened through chemical or irradiation cross-linking. SEM images also displayed fine cracks as a result of recrystallization. Proper choice of plasticizer is necessary to reduce the extent of recrystallization in TPS nanocomposite.

## Acknowledgment

The authors' greatly acknowledge the Faculty of Engineering and Science, University Tunku Abdul Rahman (UTAR), Kuala Lumpur Campus for providing testing facilities and instrument support.

## References

[1] R. Shanks and I. Kong, "Thermoplastic Starch," in *Thermoplastic Elastomers*, A. El-Sonbati, Ed., ed: InTech, 2012, pp. 95-116.

[2] V. P. Cyras, L. B. Manfredi, M.-T. Ton-That, and A. Vazquez, "Physical and Mechanical Properties of Thermoplastic Starch/Montmorillonite Nanocomposite Films," *Carbohydrate Polymers*, vol. 73, pp. 55-63, July 2008.

[3] H.-M. Park, X. Li, C.-Z. Jin, C.-Y. Park, W.-J. Cho, and C.-S. Ha, "Preparation and Properties of Biodegradable Thermoplastic Starch/Clay Hybrids," *Macromolecular Materials and Engineering*, vol. 287, pp. 553-558, 2002.

[4] D. Schlemmer, R. S. Angelica, and M. J. A. Sales, "Morphological and Termomechanical Characterization of Thermoplastic Starch/Montmorillonite Nanocomposites," *Composite Structure*, vol. 92, pp. 2066-2070, August 2010.

[5] P. Kiliaris and C. D. Papaspyrides, "Polymer/Layered Silicate (Clay) Nanocomposites: An Overview of Flame Retardancy," *Progress in Polymer Science*, vol. 35, pp. 902-958, July 2010.

[6] L. Mościcki, M. Mitrus, A. Wójtowicz, T. Oniszczuk, A. Rejak, and L. Janssen, "Application of Extrusion-Cooking for Processing of Thermoplastic Starch (TPS)," *Food Research International*, vol. 47, pp. 291-299, July 2012.

[7] B. Chen and J. R. G. Evans, "Thermoplastic Starch–Clay Nanocomposites and their Characteristics," *Carbohydrate Polymers*, vol. 61, pp. 455-463, 9/21/ 2005.

# CFD Simulation for Gas Chlorine Dispersion

Yan Wei Goh, Chien Hwa Chong*, Chin Hong Lim

*School of Engineering, Taylor's University,*
*No 1, Jalan Taylor's,47500Subang Jaya, Selangor, Malaysia*
**Corresponding author : Tel.:+60169320389, E-mail: ChienHwa.Chong@taylors.edu.my*

*Abstract*— **Chlorine gas is one of the toxic and corrosive gases. The chlorine gas colour is yellowish-green, which is difficult to visualise. It is denser than the air and persists to human breath at ground level. This gas could cause major health problem such as chest pain, difficulty breathing, headache, burns, lung damage and more when human exposed to chlorine gas. The objective of this study is to perform a CFD simulation of chlorine gas dispersion in urban area during terrorist's attacks and develop a system to countermeasure chemical attacks. It is hypothesised that analysing the gas flow helps to design a more effective approach in capturing it. To achieve these objectives, CFD simulation of gas dispersion in an urban area by taking account of obstacles. After analysing the gas dispersion, a system is design to mitigate the damage done to the surrounding by reduce the concentration of chlorine gas at different levels. This will provide human with more response time to evacuate in an affected area. In conclusion, this model is useful in improving the security and securing the safety of people.**

*Keywords*— Chemical attacks, CFD simulation, chlorine gas dispersion model

## 1. Introduction

In 1995, many citizens were injured and died when a nerve gas attack on the Tokyo subway by an apocalyptic religious cult [1]. Bombing of World Trade Center and terrorist attack in Sabah, Malaysia were a few cases initiated by terrorists in past decade. These were once unthinkable and we now need to prepare to face it in the future with an anti-terrorism system.

To cope against such terrorism, an elaborate and a sophisticated system is required. To acquire such advanced system involves three main challenges viz. surveillance, consistent research and rapid diagnosis. Surveillance is the first step of the system in monitoring the air, water, soil, and food [2]. Secondly, consistent research and development are to ensure advancement or improvement of technology to use in anti-terrorism [1]. Rapid diagnosis also enables the system to store a large amount of database or reference point on current existing chemical weapon to analyze and identify the hazardous chemical involved [1].

After identify the chemicals, countermeasures can be formulated involving rescue operation, treatment and nullifying the effects of chemical attacks. With the early detection of an attack, nimble operations can be dispatch to evacuate people in the area, help those who are affected. First aid is given to those who are in critical condition until they were stabilized to be sent to hospital for further treatment. Nullifying the effects of chemical attacks would be to keep the effects of an attack as small as possible by containing the gas from spreading.

Having a system readily to response to these incidents could save more lives in shorter amount of time as time is of the essence in saving lives. Little attempts have been carried out by researchers to create and implement the system. This is because researches on countermeasures such as capturing chlorine gas are rather scarce. There are not much of research were conducted on chlorine gas dispersion by experimental field. Thus, less CFD models on chlorine gas were developed and there are no CFD studies done on chlorine gas adsorption by any researchers.

## 2. Literature Review

### 2.1 Chemical Properties

Table 1: List of toxic chemical used in industry and in chemical attack.

| Chemical | Boiling point, °C | Melting point, °C | Vapour density | Odor |
|---|---|---|---|---|
| Chlorine | -34 | -101 | 2.5 | Pungent |
| Phosgene | 8 | -126 | 3.4 | New mown hay |
| Sarin | 147 | -57 | 4.86 | Weak fruity odour |
| Hydrogen cyanide | 26 | -14 | 0.941 | Oil of bitter almond |
| Ammonia | -33 | -78 | 0.6 | Pungent |

Table 1 list of some toxic chemical used in industry and also in chemical attack. Most of the chemical have low boiling point and remain as colourless gas at 25°C. For human to detect these gases would be impossible with sight. However, it is possible for human to detect the gases by the odour briefly at the time of initial exposure. These gas are toxic and it is dangerous to inhale or skin contact with these gases. Table 2 show the exposure limit and health effects if exposed too long.

Table 2: Odor detection threshold, exposure limit and health effect of toxic chemicals.

| Chemical | Odor detection threshold, ppm | Exposure limit, ppm | Health effect |
|---|---|---|---|
| Chlorine | 0.01 | 1 | burns, frostbite |
| Phosgene | 0.125 | 0.1 | irritation, burns, death |
| Sarin | | 0.00002 | irritation, suffocation, death, drooling |
| Hydrogen cyanide | 2-5 | 4.7 | irritation, suffocation, death |
| Ammonia | 1-5 | 35 | burns |

### 2.2Dense Gas Field Experiment

Some large scale experiments related to dense gas dispersion were conducted before 1992. These experiments were conducted in response of public pressure to quantify the potential hazards of some chemicals [3]. Experiment conducted at China Lake, California was sponsored by US Department of Energy to quantify LNG safety issues. At the same time, LNG and LPG were also releases by Shell Company at Maplin Sands (UK) to study atmospheric dispersion and vapour cloud combustion. Freon and nitrogen mixture were used in Thorney Island (UK) test series to collect information about the potential consequences of unconfined vapour cloud explosion on Flixborough disaster. Last three test experiments were carried out at US Department of Energy's Liquefied Gaseous Fuels Spill Test Facility located near Mercury, Nevada[3]. First test, 'The Desert Tortoise' involved ammonia test series were conducted due to public concern over several accidental release of ammonia in rail accident. Secondly, nitrogen tetraoxide of 'The Eagle' was released to resolve public concern about the threats from the shipment of nitrogen tetraoxide collected from the deactivation of the Titan missile system. Lastly, 'The Goldfish' tests were released of hydrogen fluoride to evaluate the potential hazards of hydrogen fluoride accidental releases from petroleum refining operation (Havens 1992).

### 2.3 CFD Simulation of Dense Gas Dispersion

CFD was used to model gas dispersion. Each model has its own configuration (turbulent Schmidt number and k-ε).However, a poor model will lead to wrong prediction and may greatly effect on human and financial resources [2]. Results from CFD predictions are not reliable and required validation by comparing with real experimental results. Therefore, validations of models with experimental results are important to ensure that these models are adequate to use for certain prediction.

## 3. Research Methodology

### 3.1 Case 1: Simulation of the Jack Rabbit chlorine release experiment (Trial 2)

The Jack Rabbit experiment is one of very few field experiments on chlorine gas dispersion. The JR experiment consists of 5 trials (Trial 2-PC, Trial 5-PC, Trial 6-PC, Trial 7-PC, Trial 8-PC). Trial 2 is a 'pilot test' with release of 1 ton pressurized liquefied gas at ambient temperature while Trial 5, 6, 7, and 8 are 'record tests' releasing 2 tons of pressurized chlorine[4]. Chlorine gas is released from 3 inch downward pointing outlet pipe from the tank elevated 2 m above the ground.The JR experiment Trial 2 will be simulated in CFD and the geometry used is a 2D geometry of the size 240 m x 25 m. The source of chlorine gas will be in the middle of the geometry and 2 m above the ground. Trial 2 had limited data as the systems were being set up and being tested that time [4]. An estimated mass flow rate release is 40 kg/s which is calculated from release of 1 ton of chlorine gas in 23 s.

Table 3.The JR experiment data[4].

| Distance from the source, m | Concentration, ppm |
|---|---|
| 50 | 2030 |
| 100 | 2240 |

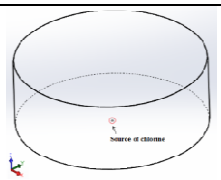

Fig. 1 Geometry for case 1.

### 3.2 Governing Equation

The incompressible gas flow can be described using following equation[5]:

Continuity: $\frac{\partial \rho}{\partial t} + \frac{\partial (\rho u_i)}{\partial x_i} = 0$ (1)

Momentum balance: $\frac{\partial \rho u_i}{\partial t} + \frac{\partial (\rho u_i u_j)}{\partial x_j} = -\frac{\partial p}{\partial x_i} + \frac{\partial}{\partial x_j}\left[u\left(\frac{\partial u_i}{\partial x_j} + \frac{\partial u_j}{\partial x_i}\right) + \lambda \frac{\partial u_k}{\partial x_k}\right] + \rho g_i$ (2)

Dispersion of the chlorine gas in the atmosphere occurs through mean fluid flow and diffusion (effect of turbulent and molecular diffusion) can be represented by the following equation[5]:

Species transport equation : $\frac{\partial}{\partial t}(\rho Y_i) + \nabla.(\rho u Y_i) = -\nabla.J_i + S_{\Phi i}$ (3)

d) Diffusion flux of species $i$: $J_i = -(\rho D_i + \frac{u_t}{Sc_t})\nabla Y_i$ (4)

## 4. Results and Discussion

From Fig. 2, the chlorine gas released from the 2 meter above the ground tends to persists so low to the ground and formation of low level gas cloud. This is caused by gravity slumping (The decrease in cloud height of a flowing dense gas due to the effects of gravity) which is also called negative buoyancy [6]. However, it is expected for gas denser than air to have this behavior.

According to [4], the stored JR chlorine was released two phase due high pressure which will generate small aerosol drops and chemical deposition on the ground will occur.In this case, some important processes such as chemical reaction, influence of complex terrain or obstacles such as vegetation or buildings were ignored [4]. Realizable *k*-ε model is used to create this profile as it can provide more realistic results [6].

Fig. 2 also show that concentration of chlorine is maximum in the center of the flow coming out from the source from time 0 s to 23 s. This is due to the momentum jet release from a high pressurized tank. The concentration of chlorine is reducing as it travels further away from source.

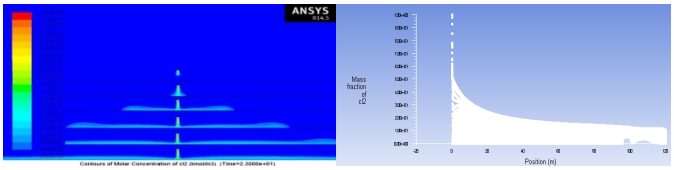


Fig. 2Change of chlorine concentration profile in 23s of release (left).
Fig. 3 Concentration of chlorine vs distance at 20 s after release (right).

Fig. 3 show the concentration of chlorine at any distance away from the source after 20 s the gas is released. Concentration of chlorine (mass fraction) at distance of 50 m and 100 m are 0.02 and 0.015 which is 2000 ppm and 1500 ppm respectively. To validate the results, the JR experiment data is compared. There is a difference of 30 ppm at distance of 50 m while 740 ppm difference at distance of 100 m. The CFD was able to predict the concentration of chlorine at distance of 50 m with a little of difference but a huge gap for distance of 100 m. This is due to some factors (wind speed, 2 m depression, surface roughness) were not taken into account. The downwind concentration of chlorine increases if there is wind blowing more chlorine away from the source.

## 5. Conclusion

The *k*-ε model used in this case provides realistic results as shown in chlorine gas concentration profile. However, there are some factors such as meteorological conditions were not taken into consideration. This could affect much in the result as now it seems to be in steady state. Besides that, there is the possibility that the chlorine properties input were assumed to be ideal case could cause fluctuations in results. CFD simulation is more reliable for gas dispersion prediction provided more factors are taken into account.

## References

[1] F. J. Manning, C. Maczka, C. E. Lawson, J. K. Holliday, and J. Tinker, "Improving Civilian Medical Response to Chemical or Biological Terrorist Incidents: Interim Report on Current Capabilities," *National Academy Press*, 1998. [Online]. Available: http://www.nap.edu/openbook.php?record_id=9519&page=R3. [Accessed: 12-May-2014].

[2] A. S. Khan, A. M. Levitt, and M. J.Sage, "Biological and Chemical Terrorism: Strategic Plan for Preparedness and Response," vol. 49, no. Cdc, 2000.

[3] J. Havens, "Review of dense gas dispersion field experiments," *J. Loss Prev. Process Ind.*, vol. 5, no. 1, pp. 28–41, Jan. 1992.

[4] S. Hanna, R. Britter, E. Argenta, and J. Chang, "The Jack Rabbit chlorine release experiments: implications of dense gas removal from a depression and downwind concentrations.," *J. Hazard. Mater.*, vol. 213–214, pp. 406–12, Apr. 2012.

[5] M. Kiša, Ľ. Jelemenský, O. Mierka, and J. Stopka, "Comparison of CFD Modelling with Small-Scale Field Experiments of Chlorine Dispersion *," vol. 58, no. May, pp. 429–434, 2004.

[6] S. M. Tauseef, D. Rashtchian, and S. a. Abbasi, "CFD-based simulation of dense gas dispersion in presence of obstacles," *J. Loss Prev. Process Ind.*, vol. 24, no. 4, pp. 371–376, Jul. 2011.

# Potential of biosorbent on treatment of industries wastewater

Gui Jit Liang[1], Kaveh Shahbaz [2*]

[1.2], *School of Engineering, Taylor's University, Malaysia*

**Corresponding email: adam_jl@hotmail.com,Kaveh.Shahbaz@taylors.edu.my*

*Abstract*— **Banana peel as biosorbent is one of the biodegradable remover for heavy metal, which safe and cheap source among all the others. The objective of this study was to study the efficiency of zinc to be removed. Besides that, parameter was important for biosorption such as pH 1-5, temperature 25 – 40ºC, biosorbent dosage 1- 5g as well as size of biosorbent 0.6 - 1.6mm. The banana peel was dried in oven with 60ºC for 24 hours under acidified condition for purification. Optimum condition at pH 5 temperature 40ºC, size 1.6 mm and dosage 5g the maximum biosorption was obtained and given 94.24% of removal efficiency**

*Keywords*— Adsorption, Biosorbent, Industries wastewater, Non-linear isotherm,

## 1. Introduction

Present age of rapid grow in industries area that contribute with high concentration of highly toxic heavy metal to the environment such as lead, cadmium, zinc, copper, nickel as well as arsenic compound. There are many methods to remove the heavy metals but these methods tend to cost prohibitive and also non-biodegradable. However, physisorption and chemisorption are involved chemical reaction between the surfaces of the absorbent while biosorption is under physiochemical process that can allow the contaminants attach on the biomass body with naturally. Basically, the benefits of biosorption compare to the other methods include low cost and also minimize the chemical waste to the environment. Therefore, banana peel has been introduced to become a biosorbent for the further research.

The banana peel has been selected as a suitable biosorbent for the removal of SMS (single metal system) from the wastewater and there is a preliminary study for the treatment of SMS by optimizing (pH, Dosage of adsorbent, Temperature and Size of adsorbent). Moreover, Biosorption of maximum uptake will be found from using mathematical modeling as non-linear isotherm model and equilibrium kinetic models [5]. Biosorbent process will get analyzed through using analytical technic.

All in all, the studies show that the banana peel can successfully be used for the adsorption of removing the heavy metal in real industries wastewater. The non-linear isotherm model and equilibrium kinetic models are presented good adjustment and it can conclude that the non-hazardous ago-waste materials can be used to remove industries wastewater to overcome water pollution.

## 2.0 Methodology

### 2.1 Stock solution of metal ions

Stock solution of zinc ion was prepared with distilled water from their salts. The stock solution will be sealed tightly and store in room temperature.

### 2.2 Preparation of biosorbent

Banana peel was cut into piece and wash with HCL in incubator for an hour to remove impurities and then distilled water will be used to remove excess acid on the peel. Process peel will then dried in oven with 60ºC for 24 hours. Sample collected and repeated same washing procedure to ensure impurities was removed completely and dried it again. The final product was sieved into different sizes, which are 0.6, 0.8, 1.0, 1.25 and 1.6mm.

### 2.3 Analytical part

In this section some of the important analytical instrument will be implemented to analyze the result of the before and after to make a comparison on the biosorption process. Inductively coupled plasma optical emission spectroscopy is a highly advance technical to analyze mixture or multiple component and also sensitive to small amount of element in the solution [2]. Inductively coupled plasma optical emission spectroscopy (ICP) is argon plasma and the light measurement that emitted by the element in a sample introduced into an inductively coupled plasma optical emission spectroscopy (ICP) source.

### 2.4 Design of experiment

In this study, Design Expert software, Version 7.1 (Stat-Ease Inc., USA)was being used for experiment design of the removal efficiency of zinc from using banana peel as a biosorbent [8].Actual and coded of parameters are presented. The coded was designed with maximum (+1) and minimum (-1) [8].

Parameter level in actual and coded for removal of zinc using banana peel as a biosorbent

| Parameter | Low level | High level |
|---|---|---|
| pH | 1 (-1) | 5 (+1) |
| Temperature (ºC) | 25 (-1) | 40 (+1) |
| Dosage (g) | 1 (-1) | 5 (+1) |
| Size (mm) | 0.6 (-1) | 1.6 (+1) |

## 3.0 Results and Discussion

### 3.1 Effect of pH on removal of zinc

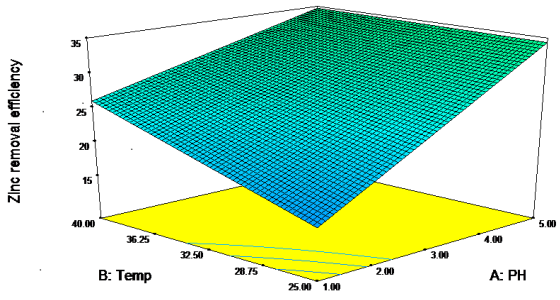


Fig. 1. Respond surface plot of zinc removal using banana peel, zinc removal efficiency against temperature and pH.

In fact, the banana peel is highly affected by the change of pH. When the initial pH value of stock solution changes from 1 to 5 the efficiency of removal was getting higher. Acidic condition was required for banana peel but when it beyond the optimum pH the efficiency will decrease. At lower pH value, hydrogen ions increase while competes with the metal ions for the available active site so when it comes to high pH the adsorption does not active [1]. pH had been studied up to 5.As can be seen from Fig 1 temperature and pH increase, the removal efficiency also increase.

3.2 Effect of temperature on removal of zinc

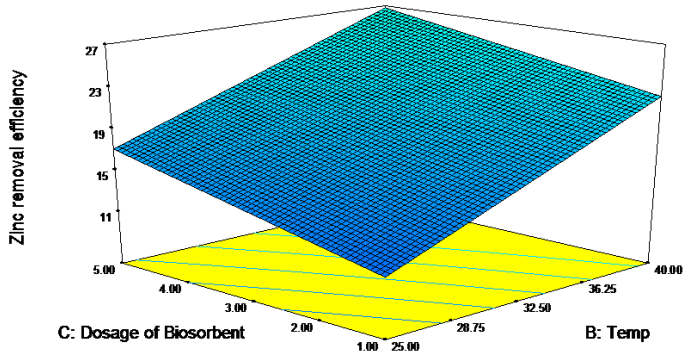


Fig. 2.Respond surface plot of zinc removal using banana peel, zinc removal efficiency against dosage of biosorbent and temperature.

Temperature is another important factor for this biosorption. The plot shown when the temperatures increase, the removal efficiency also increase. This might due to the increase in energy of metal ions and lead to move freely moving ions. Thus, it could increase the opportunities of metal ions with active site. The temperature was studied up to 40ºC.

3.3 Effect of dosage on removal of zinc

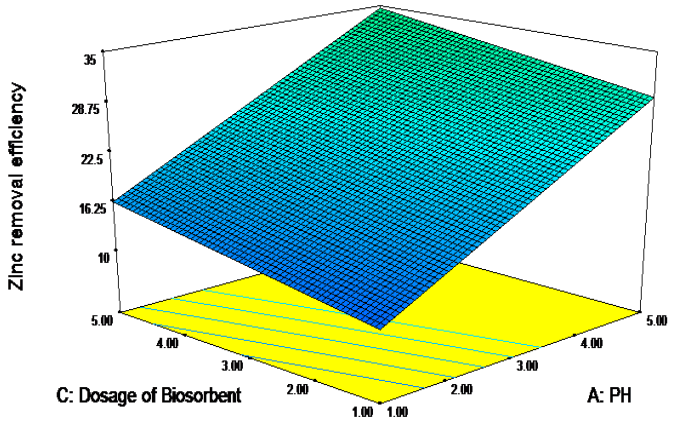


Fig. 3.Respond surface plot of zinc removal using banana peel, zinc removal efficiency against dosage of biosorbent and pH.

Shows that dosage of biosorbent at 5g is the maximum removal of zinc were obtained. Increase the amount of biosorbent also will increase the number of active size and this can make more opportunities for the metal ions bind with the active site, which lead to the high removal of zinc [3].

3.4 Effect of sizes on removal of zinc

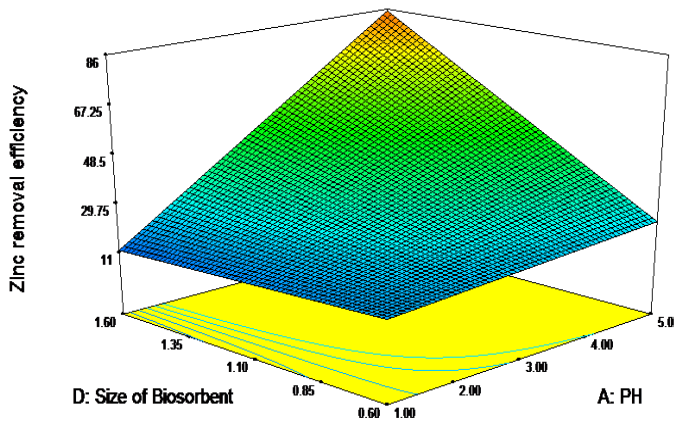


Fig. 4. Respond surface plot of zinc removal using banana peel, zinc removal efficiency against size of biosorbent and pH

Effect of size of biosorbent on adsorption of zinc was observed using different particle size from the range of 0.06 to 1.6mm. Results show that the bigger particle size was having higher adsorption. Although, the smaller particle have bigger surface area to volume ratio but the reaction take place on bigger size of biosorbent when the pH increase simultaneously. The optimum condition gives higher zinc removal efficiency on bigger size of biosorbent. The size of biosobent was done up to 1.6mm.

## Conclusions

The banana peel was selected to be a biodegradable and also a low cost with market available biosorbent for removal zinc in wastewater. This biosorption reaction was highly dependent on basic parameter, which is pH, temperature, and size of biosorbent and dosage of biosorbent used. The biosorption was rapidly increased when the dosage of biosorbent increase. The pH studied showed that biosorbent take place in acidic condition but beyond the optimum parameter and the efficiency will drop eventually. Temperature increase this absorption significantly and also the size, which increase the efficiency proportionally.

## References

[1]. Anwar, Jamil, Umer Shafique, Waheed-uz-Zaman, Muhammad Salman, Amara Dar, and Shafique Anwar. “Removal of Pb(II) and Cd(II) from water by adsorption on peels of banana .” Bioresource Technology 2010, no. 101 (2009): 1752–1755

[2]. Vedat, Yilmaz, Arslan Zikri , Hazer Orhan , and Yilmaz Hayriye . "Selective solid phase extraction of copper using a new Cu(II)-imprinted polymer and determination by inductively coupled plasma optical emission spectroscopy (ICP-OES) ." *Microchemical Journal* , no. 114 (2014): 65-72.

[3]. Suantak , kamsonlian , Balomajumder Chandrajit, and Chand Shri. "A potential of biosorbent derived from banana peel for removal of As(lll) from contaminated water ." *BioIT* 3, no. 2 (2012): 269-275.

**[4].** Muhammad Aqeel Ashraf, Karamat Mahmood, Abdul Wajid, Mohd. Jamil Maah,Ismail Yusoff. “Study of low cost biosorbent for biosorption of heavy metals .” International Conference on Food Engineering and Biotechnology . Singapoore : IACSIT Press , 2011**.**

[5]. Geankoplis, christie John. Transport Processes and Seperation Process Principles. United States of America: Bernard Goodwin, 2003.

[6]. Lawrence K, Wang, Chen Jiaping Paul, Hung Yung-Tse, and Shammas Nazih K. Heavy metals in the environment. United state of America: Taylor & Francis Group, 2009.

[7]. Juliana Q , Albarelli , Rabelo Rodrigo B , Santos Diego T , Beppu Marisa M , and Meireles M. Angela A . “Effects of supercritical carbon dioxide on waste banana peels for heavy metal removal .” The Journal of Supercritical Fluids , no. 58 (2011): 343-351.

[8]. Kaveh, Shahbaz , Mjalli Farouq S, Ali Hashim Mohd , and AlNashef Inas M. "Elimination of All Free Glycerol and Reduction of Total Glycerol from palm Oil-Based Biodiesel Using Non-Glycerol Based Deep Eutectic Solvents ." *Taylor & Francis*, 2013: 1184-1193.

# Removal of Glycerol from Palm Oil-Based Biodiesel Using New Ionic Liquids Analogous

Kah Chun Ho[1], Kaveh Shahbaz[1*], Rashmi Gangasa Walvekar[1]

[1] *Department of Chemical Engineering, Taylor's University, Malaysia,*

**Corresponding email: Kaveh.Shahbaz@taylors.edu.my*

*Abstract*—**At the end of transesterification reaction, produced biodiesel have to be purified from the byproduct glycerol before employed as diesel substitute. The glycerol content must meet the limit set by the EN 14214 and ASTM D6751 international biodiesel standards. In this work, seven new ternary deep eutectic solvents (DESs) were synthesised from choline chloride (ChCl) as salt and two hydrogen bond donors (HBDs), namely glycerol and ethylene glycol. These DESs were employed as extraction solvent to remove total glycerol from palm oil-based biodiesel. The results revealed that synthesised DESs have higher removal efficiency of total glycerol than free glycerol. The maximum removal efficiency of free and total glycerol was attained by DES 3 at molar ratio 0.5:1 (DES3: biodiesel).**

*Keywords*— deep eutectic solvent, biodiesel, glycerol, removal, palm oil, purification

## 1. Introduction

Biodiesel is a clean-burning fuel synthesized from renewable resources. The conventional method for biodiesel synthesis is alkali catalyzed transesterification between triglyceride and alcohol such as methanol to produce fatty acid methyl ester (FAME) and glycerol as shown in Fig 1 [1]. Potassium hydroxide (KOH) is commonly used as alkali homogeneous catalyst [1].

$$\text{Triglyceride} + \text{Methanol} \xleftrightarrow{catalyst} \text{Glycerol} + \text{FAME}$$

Fig. 1 General reaction scheme for triglycerides transesterification [1]

At the end of transesterification, the produced biodiesel still contains trace amount of glycerol that need to be purified to meet the biodiesel international standards. The high glycerol content increases viscosity of biodiesel subsequently leads to choked fuel systems, injector fouling and upsets engine's performance [2].

Several biodiesel glycerol removal processes are wet washing, dry washing and membrane extraction [3]. Water washing produced significant amount of wastewater and product loss. On the other hand, dry washing uses solid adsorbents and contributed to the landfill environmental issues [3]. Membrane extraction can reduce the glycerol content to the requirement but it involves high production cost and lower the product yield [1].

Lately, ionic liquids (ILs) have received great attention for its unique properties [4]. Nevertheless, the costly raw materials and complicated ILs' synthesis had retarded the its widespread application [2]. A new solvent called DES was discovered as ILs analogous because similarity of favorable properties [5, 6]. DES is an eutectic mixture formed by certain ratio of halide salts and HBDs associated by strong hydrogen bonds [7]. In contrast to ILs, high purity of DESs can be synthesised easily at low cost and thus makes them potential extraction solvents for large-scale applications [2, 7-9].

The aim of this work to synthesize new ternary DESs using ChCl as salt and two HBDs, specifically glycerol and ethylene glycol as extraction solvent to eliminate total glycerol from palm oil-based biodiesel in accordance to ASTM D6751 which is 0.24 weight % [2].

## 2. Experimental Section

### 2.1 Materials

Palm oil (Yee Lee Sdn Bhd) was purchased from local mart. D6584 kit contains calibration standard solutions and two internal standard solutions was purchased from Agilent Technologies, Malaysia. The derivation agent was also purchased from Agilent Technologies, Malaysia. Choline chloride ($C_5H_{14}CINO$) as salt, glycerol ($C_3H_8O_3$) and ethylene glycol ($C_2H_6O_2$) as HBDs with high purity (≥ 99%) were obtained from Merck, Malaysia for the synthesis of DESs without further purification. Methanol (99.8%) and KOH pellet were also supplied from Merck, Malaysia. Mass fraction of water in these chemicals is kept below $10^{-4}$.

### 2.2 Transesterification Reaction

500g of palm oil was transferred into a beaker heated by water bath at $60^{O}$C. Excess methanol was prepared in molar ratio of methanol: palm oil at 10:1 for higher yield of biodiesel. KOH as a base catalyst (1wt% of palm oil) was dissolved in methanol to prepare homogenous potassium methoxide. Potassium methoxide was added to the palm oil and stirred at constant speed of 600 rpm for two hours. Then, the mixture was cooled to ambient temperature before transferred to a separation funnel. After all-night settling, the upper layer (biodiesel phase) was then separated from lower layer (rich glycerol phase) [6].

### 2.3 DESs Synthesize

In this work, ChCl as salt and two HBDs, specifically glycerol and ethylene glycol were selected to synthesize seven ternary DESs as extraction solvents. DESs were synthesized in a tight and humidity-safe screw-capped bottle to prevent any contamination with atmospheric moisture [10]. Magnetic stirrer was employed to mix the salt and HBDs in different molar ratios at $80^{O}$C and 300 rpm until a homogeneous colourless liquid appeared [10]. Table 1 presents the composition of different DESs and its abbreviation.

Table 1. Compositions of the synthesized DESs.

| DES Abbreviation | Molar ratio | | |
|---|---|---|---|
| | ChCl | Glycerol | Ethylene Glycol |
| **1** | 1 | 1 | 1 |
| **2** | 1 | 2 | 1 |
| **3** | 1 | 1 | 2 |
| **4** | 1 | 2 | 2 |
| **5** | 2 | 1 | 1 |
| **6** | 2 | 2 | 1 |
| **7** | 2 | 1 | 2 |

### 2.4 Extraction Process

Synthesized DESs were added to the produced biodiesel independently at various DES: biodiesel ratios (0.5:1, 1:1, 2:1 and 2.5:1). The vials were then swirled at 300 rpm using orbital shaker at ambient temperature for two hours. After two hours of settling, the top layer (extracted biodiesel) was separated and analysed by Gas Chromatography (GC) [7]. The total glycerol was determined by Equation 1.

$$Total\ \ glycerol = G + 0.25MG + 0.146DG + 0.103TG \quad (1)$$

where G=glycerol, MG=Monoglyceride, DG=Diglyceride and TG=Triglyceride in weight percentage [6].

### 2.5 Analytical Method

The total glycerol content in biodiesel before and after extraction was conducted in accordance to analytical methods from EN 14105 and ASTM D6584-07. It were analyzed by a HP 6890N GC equipped with cool-on-inlet, capillary flame ionization detector (FID) with electronic pneumatics control (EPC), analytical column DB-5ht (15 m × 0.32 mm × 0.1 µm film) and a 530 µm inner diameter high-temperature retention gap. The analytical procedures were performed similar to research work done by K. Shahbaz, et al. [7].

## 3. Results and Discussion

### 3.1 Synthesize of DESs

After 90 min of mixing and heating, colourless liquid appeared at room temperature except for DES 5. DES 5 exists as semisolid at room temperature. As general, all synthesized DESs (except DES 5) were used as extraction solvents at ambient conditions which reduce the energy consumption.

### 3.2 Removal of Free Glycerol

The free glycerol and total glycerol content of the produced biodiesel are 0.1422 wt% and 0.9279 wt% which are higher than the acceptable values by ASTM D6751.

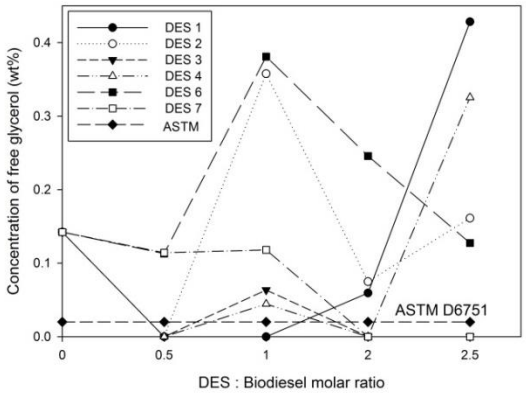


Fig. 2 Free glycerol content after extraction by the synthesized DESs

It is evident from the Figure 2 that the all DESs reduce glycerol content at molar ratio of 0.5:1 (DES: biodiesel) then free glycerol fraction rises with increasing DES: biodiesel ratio (1:1) and decreases at higher DES: biodiesel ratio (2.1) and increases after that. DES 6 was not able to remove free glycerol at all tested molar ratio of DES: biodiesel in accordance to ASTM D6571 specification.

DES 3 was able to reduce the free glycerol content to zero at all tested molar ratios except 1:1 (DES: biodiesel), which implies all free glycerol was eliminated successfully. In addition, the free glycerol removal profiles show that the free glycerol removal efficiency decreased with the increase in the mole fraction of glycerol in DESs. This is in good agreement with the work done by [6]. On the other hand, the free glycerol removal efficiency improved with the increase in the mole fraction of ethylene glycol in DESs. This behavior is substantiated by similar work where ethylene-based DESs have higher free glycerol removal efficiency than glycol-based DESs [11].

### 3.3 Removal of Total Glycerol

Based on the equation 1, the total glycerol was determined by free glycerol and bound glycerol (MG, DG and TG). As shown by Figure 3, the total glycerol profile is similar to the trend exhibited by free glycerol. It should be highlighted that DES 3 has successfully removed the total glycerol content below the ASTM D6571 specification at all tested molar ratios. The removal efficiency of total glycerol using DES 3 ranged from 87.25 to 97.65% when increasing the molar ratio of DES: biodiesel. Besides, DES 3 able eliminated all free glycerol and total glycerol at the minimum DES: biodiesel molar the ratio; 0.5:1.Comparing to former research using ChCl-based DES

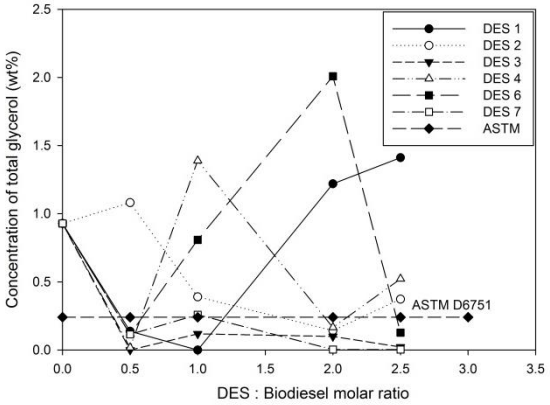


Fig. 3 Total glycerol content after extraction by the synthesized DESs

[7], it justifies the high performance of experimental synthesized ternary DESs in total glycerol removal.

## Conclusion

In this study, seven new ternary DESs had been synthesized from ChCl salt and HBDs, namely glycerol and ethylene glycol. Six synthesized DESs that exist as liquid at room temperature were employed as extraction solvents to remove free and total glycerol from palm oil-based biodiesel. Most of the synthesized DESs were not successful to remove free glycerol in accordance with the ASTM specification except DES 3 at molar ratios DES: biodiesel of 0.5:1, 2:1 and 2.5:1. On the contrary, synthesized DESs showed higher total glycerol removal efficiency except DES 1 and 6. As overall, DES 3 was found to be the best extraction solvent to eliminate all free glycerol and total glycerol at minimum usage of DES.

## References

[1] I. M. Atadashi, M. K. Aroua, A. R. Abdul Aziz, and N. M. N. Sulaiman. (2012). The effects of water on biodiesel production and refining technologies: A review. *Renewable and Sustainable Energy Reviews*, vol. 16, 3456-3470.

[2] M. Hayyan, F. S. Mjalli, M. A. Hashim, and I. M. AlNashef. (2010). A novel technique for separating glycerine from palm oil-based biodiesel using ionic liquids. *Fuel Processing Technology*, vol. 91, 116-120.

[3] M. Berrios and R. L. Skelton. (2008). Comparison of purification methods for biodiesel. *Chemical Engineering Journal*, vol. 144, 459-465.

[4] C. Yue, D. Fang, L. Liu, and T.-F. Yi. (2011). Synthesis and application of task-specific ionic liquids used as catalysts and/or solvents in organic unit reactions. *Journal of Molecular Liquids*, vol. 163, 99-121.

[5] A. P. Abbott, D. Boothby, G. Capper, D. L. Davies, and R. K. Rasheed. (2004). Deep Eutectic Solvents Formed between Choline Chloride and Carboxylic Acids: Versatile Alternatives to Ionic Liquids. *Journal of the American Chemical Society*, vol. 126, 9142-9147.

[6] K. Shahbaz, F. S. Mjalli, M. A. Hashim, and I. M. AlNashef. (2011). Using Deep Eutectic Solvents Based on Methyl Triphenyl Phosphunium Bromide for the Removal of Glycerol from Palm-Oil-Based Biodiesel. *Energy & Fuels*, vol. 25, 2671-2678.

[7] K. Shahbaz, F. S. Mjalli, M. A. Hashim, and I. M. ALNashef. (2010). Using Deep Eutectic Solvents for the Removal of Glycerol from Palm Oil-Based Biodiesel. *Journal of Applied Sciences*, vol. 10, 3349-3354.

[8] K. Huang, Y.-L. Chen, X.-M. Zhang, S. Xia, Y.-T. Wu, and X.-B. Hu. (2014). SO2 absorption in acid salt ionic liquids/sulfolane binary mixtures: Experimental study and thermodynamic analysis. *Chemical Engineering Journal*, vol. 237, 478-486.

[9] R. B. Leron, A. Caparanga, and M.-H. Li. (2013). Carbon dioxide solubility in a deep eutectic solvent based on choline chloride and urea at T = 303.15–343.15 K and moderate pressures. *Journal of the Taiwan Institute of Chemical Engineers*.

[10] F. S. G. Bagh, K. Shahbaz, F. S. Mjalli, I. M. AlNashef, and M. A. Hashim. (2013). Electrical conductivity of ammonium and phosphonium based deep eutectic solvents: Measurements and artificial intelligence-based prediction. *Fluid Phase Equilibria*, vol. 356, 30-37.

[11] K. Shahbaz, F. S. Mjalli, M. A. Hashim, and I. M. AlNashef. (2013). Elimination of All Free Glycerol and Reduction of Total Glycerol from Palm Oil-Based Biodiesel Using Non-Glycerol Based Deep Eutectic Solvents. *Separation Science and Technology*, vol. 48, 1184-1193.

# Uptake of Heavy Metal Ions from Aqueous Solution via Biosorption by the Fungus *Rhizopus Oryzae*

Jayasilan Selvam[1], Masniroszaime[2*], Kaveh Shahbaz[3*]

[1]*School of Engineering ,Taylor's University, Malaysia*

**Corresponding email:silan_jaya@hotmail.com*

*Abstract*—**Biosorption is a process of binding of opposite charges to the surface of a biomass. In this study, *RhizopusOryzae* has been used as a biomass to remove copper ions. The study was carried out in batch and effects of pH (1-5),temperature ($25^0$C-$55^0$C), biomass dosage (0.5g-5g) and initial metal concentration (30mg/l-80mg/l) were investigated. The research showed that copper ions were removed at higher initial metal concentration, low biomass dosage, low temperature and high pH.**

*Keywords*— Biosorption, *Rhizopusoryzae*, Heavy metals

## 1. Introduction

Accumulation of heavy metal ions in aquatic medium is at worrying state in this era of industrialization. Heavy metals are being released to the environment via various activities such electroplating industry, semiconductor industry and mining [1]. Cadmium has huge potential to human and environment. Exposure to cadmium at elevated level can cause kidney damage and bone degeneration [2].Copper on the other hand can cause irritation of the eyes, vomiting and diarrhea.Non- biodegradability and toxicity nature of heavy metals is seen as a main issue and thus treatment of heavy metals wastewater is vital [1]. Conventional treatment includes precipitation, ion exchange, filtration and electrolysis.

Biosorption is a new method being studied to remove heavy metals. The biosorption process involves a solid phase (sorbent) and a liquid phase (solvent) containing a dissolved species to be sorbed (sorbate) [1]. Due to higher affinity of the sorbent for the sorbate species, the latter is attracted and removed. Compared with the conventional treatment method, biosorption process deals potential advantages such low operating cost, non-toxic, minimization of chemical sludge and environmental friendly [3]. Various biomasses like fungi, alga, yeast and bacteria have been used by researchers previously. Biosorption by fungi has showed excellent results since fungal biomass offers advantage of having high percentage cell wall [1]. This subsequently shows tremendous metal binding properties. *Rhizopus oryzae* a strain from the *Rhizopus* family is an example of fungi that grows well in tropical and subtropical region. *Rhizopus oryzae* is non-toxic fungi and is widely used in fermentation of tempeh, a soy bean based food product[4].

## 2. Materials and Method

### *2.1 Preparation of biosorbent*

*Rhizopus Oryzae* was extracted from tempeh. The tempeh was obtained from a local market. A small portion of the tempeh was scrapped and carefully placed onto potato dextrose agar plates. The plates were left to incubate at $35^0$C for 3 days. After 3 days, the plates are removed and the spores are washed with distilled water. The solution is then centrifuged at 200 rpm to obtain the solid portion (spores of *Rhizopus oryzae*). The spores are then oven dried at $80^0$C before it was ground in mortar and sieved with an average size of 1mm.

### *2.2 Preparation of adsorbate*

The reagents used were of analytical grade and was prepared at room temperature. The stock solutions of cadmium and copper were prepared by dissolving a weighed quantity of copper sulphate in deionized distilled water. Further dilution was done for different concentration.

### *2.3Biosorption Studies*

Batch biosorption experiments were carried out in laboratory scale. The experimental design and optimization was carried out as indicated by the Design Expert Software, version 7.1. The experiment was done in 250ml Erlenmeyer flasks. About 50 ml of the metal stock solutions was transferred to the flask and 0.5 g of biomass was contacted with the solution at $50^0$C and pH of 1.00. The flask was then agitated at 200 rpm for 4 hours at shaker incubator. After the separation of biomass from solution via centrifugation, the residual concentration of copper was determined using Inductive Coupled Plasma (ICP). Optimization was then carried out with the aid of Design Expert Software, version 7.1

## 4. Results

### 4.1 Effect of dosage on removal efficiency of copper

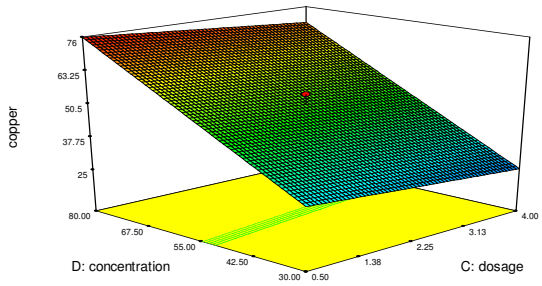


Fig 1: Respond of removal efficiency against initial metal concentration and biomass dosage

Figure 1 above shows the surface respond of removal of copper at different values of initial metal concentration and dosage of biomass. From the chart above, it is seen that the highest removal efficiency was achieved at high concentration and low biomass dosage. The optimum concentration and dosage are 80mg/l and 0.5 grams respectively. Low biomass dosage may attribute to interference between the binding sites [1].

### 4.2 Effect of dosage and temperature on removal efficiency of copper

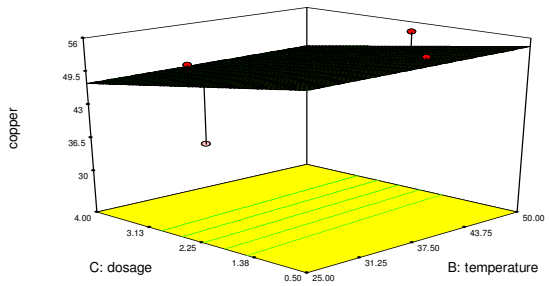

Fig 2: Respond of removal efficiency against temperature and biomass dosage

Figure 2 states the surface respond of removal of copper at different dosage of biomass and temperature. From figure above, it is seen that maximum removal of copper ions were achieved at low temperature and low dosage. The optimum dosage and temperature that gaves highest removal was recorded at 0.5 grams and $25^0$C respectively. Enzymatic systems of the fungi cells are disturbed when temperature changes occurred. However, in this study change in temperature is not significant to the removal of metal ions.

## 4.3 Effect of pH and concentration

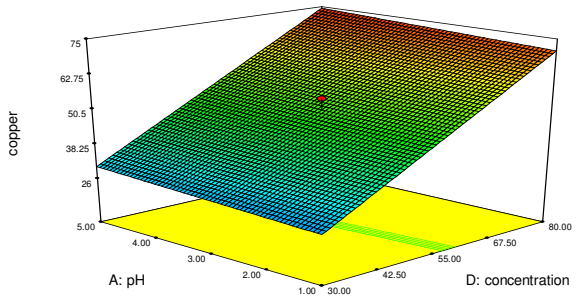


Fig 3: Respond of removal efficiency against pH and initial metal concentration

Figure 3 above shows the surface respond of removal of copper at different values of initial metal concentration and pH of metal solution. From the chart above, it is seen that the highest removal efficiency was achieved at high concentration and high pH. The optimum concentration and pH are 80mg/l and 5.00 respectively. Ph affects the biosorption process in way whereby it disturbs the activity of the functional groups in the biomass. At low pH, rise in positive charge density on the sites of biomass surface creates obstacle for the metal cations to attach onto the surface of biomass [4]. This as a result of repulsive forces. At high pH, the surface of biomass is more negatively charged and thus biosorption of positive copper ions are maximum at pH of 5.

## 4.4 Effect of temperature and pH

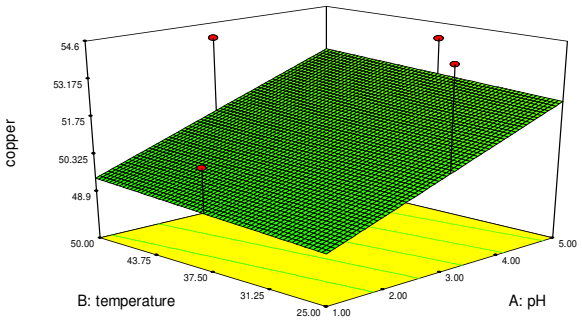


Fig 4: Respond of removal efficiency against pH and temperature

Figure 4 above relates the removal efficiency of copper with respect to temperature and pH. Low temperature and high pH gives the largest removal efficiency. This was achieved at $25^0$C and pH of 5.00.

## 7.Conclusions

In conclusion, it can be said that the fungus *Rhizopus Oryzae* has proved to be a biomass that has ability to remove heavy metals present in water. This was achieved via the process biosorption. By varying different parameters, the optimum conditions for highest removal efficiency are known. Copper ions were removed at higher initial metal concentration, low biomass dosage, low temperature and high pH.

## References

[1] Nilanjana, D. &Vimala, R. (2007). Biosorption of heavy metals – an overview.*Indian Journal of Biotechnology,*7, 159-169.

[2]YihMin,S, ChingYi,H, Fu Lin, C, Li Chun,C. (2010). Biosorption of lead,mercury and cadmium ions by Aspergillusterreus immobilized in a natural matrix. *Polish Journal of Microbiology,*1, 37 - 44.

[3]Nirmal Kumar, J.(2012). Removal of heavy metals by biosorption using freshwater alga Spirogyra hyaline.*Journal of Environmental Biologyy,*33, 27-31.

[4]William Shurtleff.& Akiko Aoyagi. (1979). *The Book of Tempeh.* New York, Harper & Row Publishers.

[5] Hajar, M. (2010). Biosorption of cadmium from aqueous solution using dead biomass of brown alga *Sargassum.African Journal of Environmental Science and Technology.*4(7), 412 – 418.

# Potential of Microalgae on the Production of Biodiesel

Jovian J. Maynardo, Veena Doshi*, Jeevan Raj Rajanren

*School of Engineering, Taylor's University, Subang Jaya, Selangor, Malaysia*

**Corresponding email: veenaadoshi.arunkumardoshi@taylors.edu.my*

*Abstract*— **Microalgae as biomass is one of promising renewable and alternatives energy sources, which is clean and completely biodegradable. The aim of the present work was to study the effect of different light intensities on the growth rate of *Nannochloropsis* oculata. Moreover, the effect of different drying temperatures were studied as well with respect to the lipid yield obtained. The microalgae was cultured in a photobioreactor with light intensities of 3000, 5000, and 7000 lux. The harvested culture were then dried at drying temperatures of 70, 85, and 100°C before undergoing extraction. At 5000 lux, the microalgae culture reached the optimum growth condition and achieved the highest specific growth rate of 0.236 day$^{-1}$ with the shortest generation time of 2.9 days, followed by 7000 and 3000 lux. The optimum drying temperature was determined to be 85°C for the highest lipid yield of 6.80%.**

*Keywords*— biodiesel, microalgae, lipid, *Nannochloropsis oculata*, photobioreactor, growth rate, drying, extraction

## 1. Introduction

The world consumption and needs on energy has been greatly increased, but it is not followed and balanced by the energy sources. Renewable energy has become very promising since it is clean, environmental friendly, and completely biodegradable. Biomass is one potential source of alternative renewable energy to the fossil fuel besides other sources, such as hydro, wind, solar, geothermal, wave, and tidal. One source of biomass is microalgae which contributes on the production of biodiesel from the lipid (oil) content of the algae.

As the fastest growing plant, microalgae or microphyte is relatively easy to be grown and requires little amount of nutrition. Algae as the second generation biofuel is more promising since other first generation crops like palm oil, which are already used as food sources, have depended on market demand [1]. Despite of these advantages, algae technology is relatively new and a lot of research on this field is still on going. The biofuel produced from algae still lacks stability and the cost is very high which is currently in the range of $0.42-0.97/L in 2012 [2]. Moreover, the current biodiesel processing involves expensive cultivation and downstream process with overall efficiency of ten thousand lower than the conventional fossil fuel [3]. Therefore, further research and study should be done to make the algae biofuel more reliable which includes optimisation on the cultivation and the efficient downstreamprocessing method.

Light intensity is one important growth parameter which has not been fully studied yet. The general range of optimum light intensity exists as 2,500-7,000 lux,but it is still considered as a wide range [4]. More precise and accurate value should be obtained since light intensity plays important role of microalgae growth which will affect the photosynthesis process and contribute to the oil content of microalgae.Pre-treatment process like algae drying is usually done before the extraction to increase the extraction efficiency which depends on the drying temperature and period.There were only a few studies on the algae drying. Moreover, only one single drying temperature and period was often used in the previous experiment. Thus,its effect on the extraction efficiency cannot be observed [5].

This project covered the production of biodiesel from microalgae starting from species selection followed by cultivation in photobioreactor, drying, chemical extraction of lipid, transesterification, and ended with the purification of the produced biodiesel. The optimum light intensities as one growth parameter with respect to the growth rate was to be determined. The optimum drying temperature with respect to the lipid yield would be specified as well.

## 2. Methodology

### 2.1 Microalgae

The microalgae used in this experiment was *Nannochloropsis oculata* which was obtained from Algaetech Int. Sdn Bhd (Kuala Lumpur, Malaysia) in liquid form. This microalgae strain has a diameter of 1-2 µm and classified as eukaryotic green marine microalgae [6].

### 2.2Cultivation

The cultivation of the microalgae was carried out in 250 ml photobioreactor. F/2 medium (Algaetech Int. Sdn Bhd, Kuala Lumpur, Malaysia) was used as the nutrient source for the microalgae. The volume ratio of microalgae inoculum to the medium was 1:10.Three different light intensities within the current optimum range were tested in this experiment, which were 3000, 5000, and 7000 lux as the controlled variable. Phototropic period of 24:0 (light : dark hours) was used.The culture temperature was monitored and maintained at 18-25°C, whereas the pH was kept at 7-8.5 with salinity of 20-24 gram/litre. The culture was aerated with the air flow rate of 2-4 litre/min. To study the growth, culture density was measured daily by 2ml sample taking, centrifuging, and measuring the amount of biomass which would be expressed in gram/ml.The growth curve would be plotted and the specific growth rate was calculated by the equation:

$$Growth\ rate, K' = \frac{1}{t_2 - t_1} Ln\left(\frac{N_2}{N_1}\right) \quad (1)$$

Where Nis the biomass at time t during the exponential phase.

### 2.3Harvesting and Drying

The cultures were harvested after two weeks which was at the exponential phase of the microalgae. It was then centrifuged at 4000 rpm for 10 minutes. The algae drying process was carried out in the oven (FAC-350, Protech, Malaysia). Three different drying temperatures would be tested in his experiment, which were 70, 85, and 100°C with the same drying period of 24 hours. The biomass yield was calculated by dividing the weight of obtained dried biomass by the culture volume.

### 2.4Lipid Extraction

Lipid extraction from biomass was performed by using hexane-isopropanol (3:2 v/v) at 25°C for 7 hours. 75 ml of the solvent mixture was added to every gram of dried biomass. Filtration was then done before transferring the mixture into the separating funnel where the top dark green layer containing lipid and the solvent would be taken and heated up to get the pure lipid.Transesterification process was carried out at temperature of 65°C for 4 hours. 10 gram (12.6 ml) of methanol would be added for every gram of lipid. 10 wt% of potassium hydroxide (KOH) as a base (alkali) catalyst was used in the experiment. The top transesterified biodiesel rich phase would be taken and washed with 300 v% of water to get the final biodiesel product [7]. The lipid yield from microalgae would be calculated by the equation:

$$Lipid\ yield, Y\% = \frac{W_L}{W_{DA}} \quad (2)$$

Where $W_L$ and $W_{DA}$ are the weights of the extracted lipids and the dried algae biomass, respectively.

### 2.5Error Analysis

One dimensional ANOVA (Analysis of Variance) with fixed effect was used to analyse the error and variance involved in the experiment.

## 3. Results and Discussion

### 3.1Effect of Light Intensity on the Microalgae Growth Rate

The growth of the microalgae cultures was studied by measuring the culture density for two weeks with respect to different light intensities as shown in Fig. 1. The plotted culture density would then construct the growth curve of the microalgae. It was observed that the culture would undergo the highest and optimum growth at light intensity of 5000 lux, followed by 7000 lux and 3000 lux. At 5000 lux, the culture started to undergo the exponential phase on the fourth day of culture and reached the peak at 1.9 gram/litre culture after three days before experiencing declining and constant growth rate. At 7000 lux, the culture first underwent obvious lag phase that made the growth lower than 3000 lux culture for the first two days, before it could slowly surpass the 3000 lux and have higher growth at the end. The longer lag phase at 7000 lux was due to the culture's difficulty to adapt on the high light intensity at low culture density since very high amount of photons and heat absorbed per cell were experienced. As the culture density increased with constant light intensity, this issue would be tolerated [8].

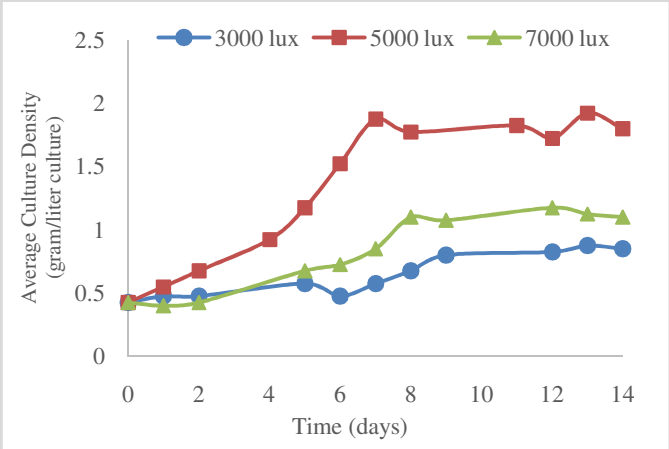


Fig. 1. Different growth of microalgae cultures with respect to the different light intensities.

The growth curves allowed the specific growth rate, divisions per day, and generation (doubling) time to be determined for different light intensities as shown in Table 1.It was determined that the highest specific growth rate of the culture was achieved at light intensity of 5000 lux, which would give specific growth rate of 0.236 $day^{-1}$and 0.340 divisions per day with generation/doubling time of almost 3 days. It means 5000 lux as the optimum light intensity obtained from this experiment was within the current optimum range from previous study which was from 2500 to 7000 lux [8]. At 7000 lux, the specific growth rate was 0.208 $day^{-1}$ which was 12% lower than that at 5000 lux. It also took longer time for the microalgae at 7000 lux to double its amount, which would take 3.3 days. This might occur because the microalgae had reached beyond a certain point at which higher light intensity might damage the cell and would result in declining growth. This is called photo-inhibition which explains too strong lighting may generate excess heat and damage microalgae cell [9]. At 3000 lux, the culture underwent the lowest specific growth rate due to insufficient lighting provided.

Table 1. Growth parameters obtained at different light intensities.

| Light Intensity (lux) | Specific Growth Rate, K' ($day^{-1}$) | Divisions per Day ($div.day^{-1}$) | Generation/Doubling Time (days) |
|---|---|---|---|
| 3000 | 0.174 | 0.251 | 4.0 |
| 5000 | 0.236 | 0.340 | 2.9 |
| 7000 | 0.208 | 0.301 | 3.3 |

### 3.2Effect of Drying Temperature on the Lipid Yield

The percentage of extracted lipid to the biomass with respect to the different drying temperatures is shown in Fig. 2. The highest microalgae lipid yield was obtained at drying temperature of 85°C. At this temperature, the lipid yield reached 6.47% which was slightly lower than the previous reported yield of 6.80% [7]. There was no significant differences on the lipid yields at drying temperature of 70°C and 85°C, but the lipid yield dropped much at 100°C.

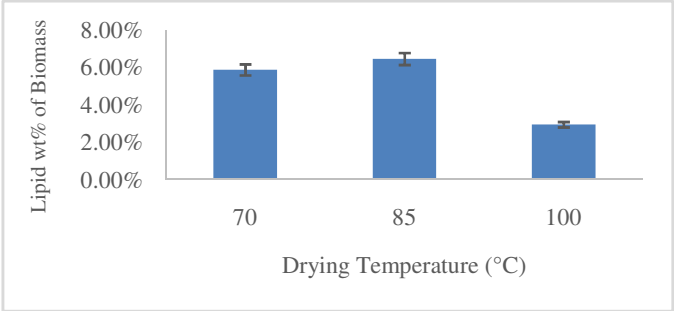


Fig. 2. Lipid yield obtained at different drying temperatures.

## 4. Conclusions and Future Work

From this experiment, the optimum light intensity for the growth of microalgae *Nannochloropsis oculata* was 5000 lux, which would give the highest specific growth rate of 0.236 $day^{-1}$ with the shortest generation time of 2.9 days during the exponential phase. The second highest growth rate was achieved at 7000 lux, whereas 3000 lux gave the lowest growth rate and longest generation time.

The optimum drying temperature was achieved at 85°C which gave highest lipid yield of 6.47%.

There were two specific parameters tested as the limitations of this experiment, which were constant light intensity and drying temperature. Other light intensity and drying related parameters might be taken into account as well to enhance this experiment, such as increasing light intensity, wave length (colour) of lighting, source of light, flashing, phototropic period, drying period, and drying method. Moreover, different algae species might be considered as well since only one algae species is used in this experiment.

## Acknowledgment

The authors are grateful to Taylor's University(Selangor, Malaysia) for the financial support of this work.

## References

[1] A. Demirbas, "Use of Algae as Biosources," Energy Conversion Management, vol. 2010, no. 51, pp. 2738-2749, 2010.
[2] A. Demirbas and M. F. Demirbas, "Importance of Algae Oil as a Source of Biodiesel," Energy Conversion and Management, vol. 2011, no. 52, pp. 163-170, 2010.
[3] B. J. Gallagher, "The Economics of Producing Biodiesel from Algae," Renewable Energy, vol. 2011, no. 36, pp. 158-162, 2010.
[4] D. Simionato, S. Basso, G. M. Giacometti and T. Morosinotto, "Optimization of light use efficiency for biofuel production in algae," Biophysical Chemistry, vol. 2013, no. 182, pp. 71-78, 2013.
[5] B. J. Gallagher, "The Economics of Producing Biodiesel from Algae," Renewable Energy, vol. 2011, no. 36, pp. 158-162, 2010.

[6] D. Hibberd, “Notes on the taxonomy and nomenclature of the algal classes Eustigmatophyceae and Tribophyceae,” Journal of the Linnean Society of London, vol. 1981, no. Botany 82, pp. 93-119, 1981.
[7] R. Halim, B. Gladman, M. K. Danquah and P. A. Webley, “Oil extraction from microalgae for biodiesel production,” Bioresource Technology, vol. 2011, no. 102, p. 178–185, 2010.
[8] D. Simionato, S. Basso, G. M. Giacometti and T. Morosinotto, “Optimization of light use efficiency for biofuel production in algae,” Biophysical Chemistry, vol. 2013, no. 182, pp. 71-78, 2013.
[9] I. S. Suh and C.-G. Lee, “Photobioreactor engineering: Design and performance,” Biotechnology and Bioprocess Engineering, vol. 8, no. 6, pp. 313-321, 2003.

# Drying Kinetics of Medicinal Herbs

Chun Hong Khek[1], ChienHwa Chong[1*]Adam Figiel[2],Antoni Szummy[3], Aneta Wojdyło[4]

[1]*School of Engineering, Taylor's University,*
*No 1, Jalan Taylor's,47500Subang Jaya, Selangor, Malaysia*
**Corresponding author: Tel.:+60169320389, E-mail: ChienHwa.Chong@taylors.edu.my*
[2 3]*Institute of Agricultural Engineering, Wroclaw University of Environmental and Life Sciences, Chelmonskiego 37/41 Street, Wroclaw 51-630, Poland.*
[4]*Department of Fruit and Vegetable Technology, Wroclaw University of Environmental and Life Sciences, Chelmonskiego 37/41 Street, Wroclaw 51-630, Poland.*

***Abstract*—**
**The objective of this study is to investigate the drying kinetics of medicinal herbs using convective drying and hybrid drying techniques. Five herbs with different characteristics were selected viz. Strobilanthuscrispus (SC), cassia alata (CA), andrographispanaculata (HB), phyla nodiflora (PN), and clinacanthusnutans (SG). Samples were subjected to convective drying and vacuum microwave drying, it was found that the drying time reduced from average of 6.5 hr to less than 30 min to reach equilibrium moisture content (EMC). The drying efficiency improved by a factor of 13 for average and up to 20 times depending on the nature of leaves.**

***Keywords*— natural herbs, drying, drying kinetic, hybrid drying, convective drying, advance drying**

## Introduction

Drying is a complex operation involving heat and mass transfer. According to Mujumdar (2011), the transport of moisture during drying process may occur following one or more different mechanisms of mass transfer including

a.) Liquid diffusion/evaporation
b.) Knudsen diffusion (freeze drying)
c.) Vapour diffusion

A typical drying behaviour can be descripted as in Fig. 1. where drying are divided into three phases, first is initial transient period, follow by constant rate period and failing rate period. During initial transient period, drying happened primarily on the surface of herb leaves. In a typical convective air drying characteristics, the transient behavior happened typically at first half an hour of drying for a convective drying process. Next, the constant rate period is happening to mainly middle part of the leaves, where the moisture is slowly diffuse out. Lastly, the failing rate period is happened for internal moisture where it took time for diffusion to happen, and hence, the rate of drying decreases with time.

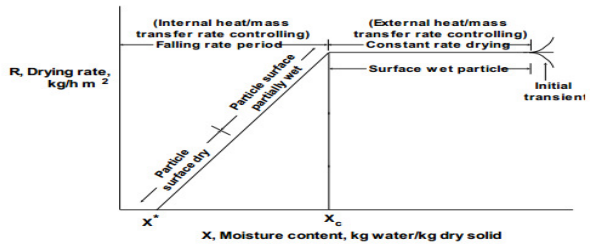


Figure 1: Typical drying behavior

More than century, a conventional convective drying technique has been used to dry biomaterials, the drying time is improved using higher drying temperature. . However, its often decrease the product quality of biomaterial due to biochemical changes. According to Sharma and Prasad (2004), the drying time can be reduced using the microwave technology. Microwave energy able to penetrate through the sample and allow generation of heat at the inner layer of the sample, which gives a much more uniform drying than a convective drying method. The quality of finished product also can be assured because of much shorter drying time that reduced the tendency of oxidation by air (Yoshinori, 2009). However, difficulties in optimising microwave drying technique as microwave power selection varies from one product to another; bad setting often result in lower product quality and high energy consumption.

As an initiative to improve the performance of microwave technique, vacuum is implemented into microwave drying technique, which can reduce the processing time and maximum temperature of samples. The differential in vapor pressure between surrounding the surface of the sample, moisture can diffuse out rapidly due to higher energy state (vacuum lower the boiling point). In addition, Figuel (2009) reported that microwave pulse setting is more effective than continuous microwave energy input.

The objective of this study is to investigate the drying kinetics of medicinal herbs dried using vacuum microwave drying (VM) and combined convective-vacuum microwave drying (CVM).

## Materials and Methods

### Materials

*Strobilanthuscrispus* (SC), *cassia alata* (CA), *andrographispanaculata* (HB), *phyla nodiflora* (PN), and *clinacanthusnutans* (SG) were purchased from TKC herbal nursery Sdn. Bhd. ,Seremban, Negeri Sembilan, Malaysia. Stem of herbs were removed and cleaned before subject to drying.

### Bone drying

The samples will undergo bone drying using forced convective hot air dryer (Model FAC-350, ProTech, Country) following ASTM D1348-94 to get bone dry weight. The operating condition from this ASTM is 105°C for 24 hours.

### Convective drying

Samples of herbs were spread as a single layer on a tray to dehydrate until equilibrium moisture content (EMC) is achieved. Convective drying was carried out at set point temperature of 40, 60 and 80°C. The initial moisture of the leaves is tested with a humidity analyser, and can also be calculated using the equation (1).

$$MC = \frac{Initial\ weight - bone\ dry\ weight}{bone\ dry\ weight} \qquad (1)$$

In this study, moisture ratio is determined from equation (2).

$$\mathrm{MR} = \frac{M_T - M_E}{M_O - M_E} \qquad (2)$$

Where MR is the moisture ratio, $M_T$is the moisture at time T, $M_E$ is the EMC value, and $M_o$ is the initial moisture content

### Vacuum microwave drying (VM)

100g of herbs were subjected to a vacuum microwave dryer (SM-200, Plazmatronika,Poland) that had a revolving vacuum drum with radius of 0.18m and length of 0.27m; two magnetrons of 1200W, the power is adjustable. The drying experiments were performed at 480W with operating conditions of 4.0 to 6.0 kPa. The VM drying was set at 30sec microwave pulses followed by 5sec break. The drum was rotated at 6rpm. Drying is carried out until EMC is achieved.

## Results and Discussion

Fig. 2 shows the drying of medicinal herbs using the convective air drying and VM techniques.Referring to the drying kinetics of herbs dried using convective air drying method, moisture content of 0.6 g $H_2O$/g DM and 0.1g $H_2O$/g DM were identified as critical moisture content. It is indicated using a vertical red color line. Other drying characteristics are initial transient period(right region), first falling rate period (middle region), and 2nd falling rate period(left region) (Chuan Lim,2010).The initial transient period fall in the range of 0.6 to 0.8 g $H_2O$/g DM. No constant rate period could be due to the moisture on the surface of the leaves were removed quickly by the forced convective hot air (Figuel, 2009) As drying proceed and crosses the vertical line, entering the middle zone, which is 1st falling rate periodwith moisture content in the range of 0.2 to 0.8g$H_2O$/g DM, the drying rate started to drop from 0.04 to 0.01 g $H_2O$/g DM m. min. It is due to moisture losses due to diffusion via spaces between cells and pores of leave to the surface. The continuous diffusion of the moisture reduced the efficiency of heat transfer (Chong,2010).Furthermore, it was found that the drying duration was ranged from 6 to 8 hrat temperature and air velocity of 50°C and 0.8m/s, respectively. Around 44 to 60% of total drying time fall under 2nd falling rate period which is ranged from 0 to 0.2g$H_2O$/gDM with decrease of drying rate from 0.02 to 0.01 g $H_2O$/g DM m. min. The diffusivity of the moisture from internal part to the surface is relatively low, which prolonged the drying period (Chuan Lim,2010)

For VM drying, the critical moisture points were indicated by the vertical red color lines which divide the initial transient period, 1st falling rate period and 2nd falling rate period. The drying rate at the transient period is ranged from 0.15 to 0.25g $H_2O$/g DM m. min at moisture content of 0.6 to 0.8 g $H_2O$/g DM. It is extremely fast compared to convective air drying as the moisture content are removed using microwave energy with the aid of vacuum condition. This technique reduces the vapor pressure, giving a bigger drive force for moisture to diffuse into the air and changes its physical states (Figuel, 2009). As drying progress from right to left, 1st falling rate period appear, the drying rate decreased from 0.1 to 0.02g $H_2O$/g DM m. min with moisture content ranged from 0.1 to 0.65 g$H_2O$/g DM.Microwave energy able to generate heat to internal part of the leaves, making the heat transfer and mass transfer happened effectively even the moisture content is low (Chong, 2010).A third critical moisture point was found in Fig 3.Drying rate is still high as microwave energy generated heat by changing the electromagnetic field up to 300M times per second encourages the mass transfer of moisture.

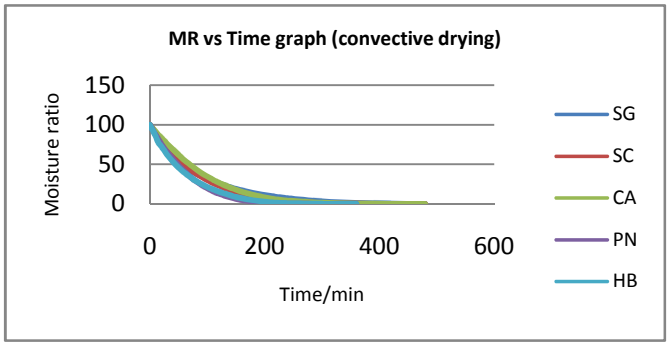


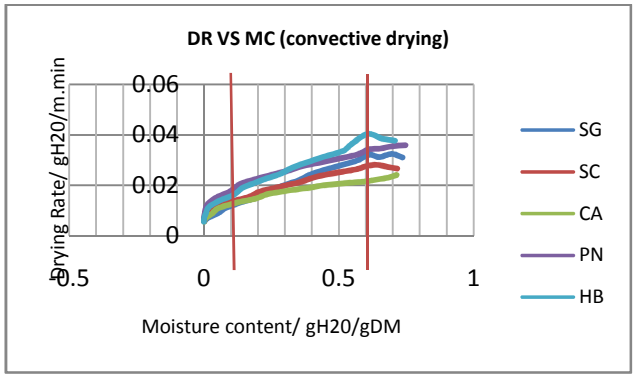


Figure 2: Drying kinetic of herbs for convective drying method

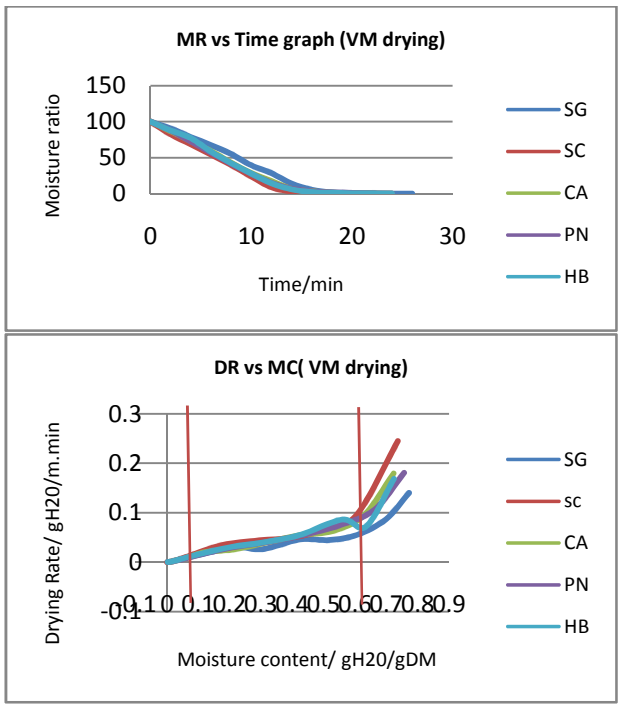


*Figure 3: Drying kinetic of herbs for VM method*

## Conclusion

In conclusion, vacuum microwave drying is a much more efficient drying method that gives significant improvement in drying time for herbs processing which potentially gives much better product quality due to short drying period and higher rehydration properties. VM microwave method often do not give indication of initial transient period in herb drying due to the rapid and more uniform dehydration. The drying efficiency is improved by average of 13 times and up to 20 times depending on nature of leaves.

## References

[1] Nussinovitch, A, Hershko, V., (1996). Gellan and vegetable coatings.Carbhydrate Polymers 30, 185-192

[2] Madamba, P.S., Driscoll, R.H.,Buckle, K.E., (1996). The thin layer drying characteristic of garlic slices. *Journal of Food Engineering* 29, 75-97

[3] Maroulis, Z.B., Kiranoudis, C.T., Marinos-Kouris, D., (1995). Heat and mass transfer modeling in air drying of foods. *Journal of Food Engineering 26, 113-150*

[4]Yoshinori Itaya,Shiegekatsu Mori, (2009). Recent R&D on Drying Techology in Japan. *Drying technology, Taylor and Francis Group, pp1187-1196*

*[*5] Chuang limLaw, ChienHwa Chong, Adam Figuel, (2010), Intermittent Hot Air, Dehumidified Air, Heat Pump and Convective Cum Vacuum Microwave Drying Characteristics and Models*, AJChE2010, vol 10, No.1, 50-55*

[6] Adam Figuel, (2009), Drying kinetics and quality of vacuum-microwave dehydrated garlic cloves and slices. *Journal of Food Engineering 94 (2009) 98-104*

# Degradation of Low Density Polyethylene/Starch Blend in Acid and Base

Meow Shan Khoo[1], Siew Wei Phang[1,2*], Tin Sin Lee[2]

[1] *Department of Chemical Engineering, School of Engineering, Taylor's University, Malaysia,*

[2] *Department of Chemical Engineering, Faculty of Engineering and Science, University Tunku Abdul Rahman(UTAR),Malaysia*

**Corresponding email: SiewWei.Phang@taylors.edu.my*

*Abstract*— **Degradation tests on physical and mechanical properties of LDPE-Tapioca starch blends were studied and characterized by conducting tensile testing and melt flow index(MFI) testing. The chemical degradation using different concentration of sodium hydroxide solution and hydrochloric acid were conducted for duration of 3 and 6 days (the samples to soak into the solutions) are compared with the samples without soaking. Different tapioca loading 0phr, 5phr, 10phr,15 phr and 20phr were used for each study. In overall, tensile tests showed decrease trend as the loading of starch increased. However, increased trend showed from 15phr to 20phr for both solutions due to the xcessive small particles of starch tend to agglomerate.**

*Keywords*— Degradation, starch, low density polyethylene, acid, base.

## 1. Introduction

Critical environmental issue from non-biodegradable plastics is continuously becoming the major concern over years even efforts have been made such as recycle. The durable and indestructibility of non-biodegradable plastic characteristics are the contributing factors as they enter waste stream[1]. Petroleum depleting will adversely affect the production of conventional plastic since petroleum is one of their raw materials[2]. For all these, hence, a viable method to reduce the environment impacts is to change the non-biodegradable plastic into biodegradable plastics by adding or mixing with other biodegradable material. Starch is abundant, low cost and degradable that can be added to the common used plastic-low density polyethylene (LDPE). LDPE is resistive to chemical attack due to its high density packed structure with long hydrophobic chain[3]. However, one of the major challenges in the making of biodegradable plastic is the weakness in physical properties of biodegradable plastic and the capability to withstand aging. Aging is a process where a product gradually loses its original design function and efficiency with time that is intolerable in engineering.

In this study, pure LDPE and LDPE with various tapioca starch compositions were tested for its physical properties and biodegradability to examine the best blend composition of this type of biodegradable plastic.

## 2. Material and Methods

### 2.1 Materials and Equipments

Different formulations of LDPE-starch blend were prepared with LDPE resin grade MFI 2.5 from Petlin (Malaysia) Sdn. Bhd. Tapioca native starch powder was purchased from Thye Huat Chan Sdn.Bhd. The chemicals used were purchased from Chemolab Malaysia with the concentration of 5 molarity was then diluted to 2 molar and 4 molar of solutions.

### 2.2 Design of Experiments

The compositions of starch and low density polyethylene mixtures were tabulated and showed as below.

Table 1. Various Formulations in Preparing Samples for Extrusion

| Formulation | LDPE (phr) | Starch (phr) | Total (phr) |
|---|---|---|---|
| 1 | 100 | 0 | 100 |
| 2 | 100 | 5 | 105 |
| 3 | 100 | 10 | 110 |
| 4 | 100 | 15 | 115 |
| 5 | 100 | 20 | 120 |

**Note: phr indicates parts per hundred.*

### 2.3 Preparation of LDPE/ Tapioca Starch Blend

The mass of LDPE-tapioca starch polymer blends were weighted and blended using twin screw extruder (SHJ-20, Nanjing Giant Machinery Co., Ltd, China) at 7 rpm and 170$^{o}$C. The extruded samples were cooled by water and fed into pelletizer. The pellets samples were dried in the oven to remove moisture at 60$^{o}$C for a day. The pellets samples were moulded using 25-ton hydraulic hot press (LS-22009-25, Lotus Scientific Sdn. Bhd, Malaysia) under 180$^{o}$C. The moulded 150mmx150mmx1mm samples are cut into dumbbell shape.

### 2.4 Methods

The chemical aging of LDPE-starch blends were tested by soaking samples into sodium hydroxide solutions and hydrochloric acid with concentration of 2molarity and 4 molarity for a period of 0,3, and 6 days. Samples were took out and rinsed with distilled water, oven dried at 60°C for a day.

Young's modulus of elasticity, tensile strength and elongation at break were obtained from tensile tests. The dumbbell shape samples were tested using (Model 4302 Series IX) Instron Universal Testing Machine based on ASTM D1882 standard with 2kN load cell and crosshead speed of 50mm/min. For each formulation, chemical solution, concentration and day to degrade, three samples were tested and the average values are obtained.

Melt Flow Index of the samples were carried out based on ASTM D1238-01. Sufficient amount of samples are pushed inside MFI machine and a load is put to allow the flow of samples. The cut samples were weighed and the time is recorded. The values were converted to mass per 10 minutes.

## 3. Results and Discussion

### 3.1 Mechanical Testing

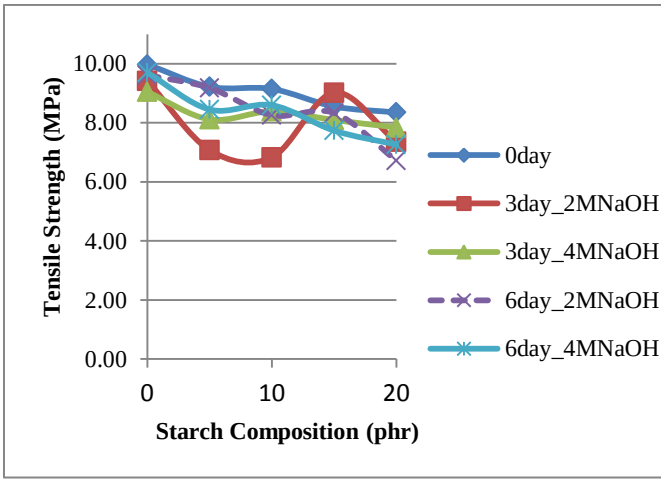


*Note: phr indicates parts per hundred.*

Figure 1. Tensile Strength against Starch Composition with different Molarity of Sodium Hydroxide solutions in Three Different Degradation Days.

. Fig. 1 shows, in overall, the decrease in tensile strength as starch composition increased. This shows good trend which supported by R.R. Ali, et al.[4]. The LDPE and LDPE blend were submerge into sodium hydroxide solution, gelatinization happened and the starch inside the blend started to differentiate and reduced the intermolecular interaction between matrix, causing the tensile strength to decrease significantly[5]. As the composition raise up to 15phr, the well-blended sample will be having sufficient free radical that established interaction between the cross linking[5]. Further increment in the composition will result in decrease of tensile strength because the excessive small particles of starch tend to agglomerate rather than forming interaction with the cross linking, which result in weakening of mechanical strength.

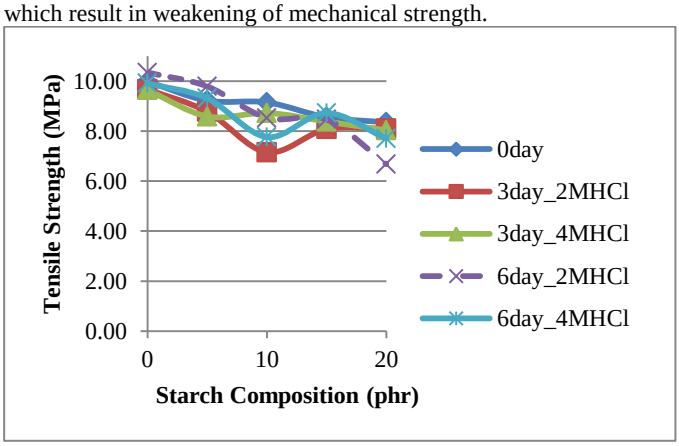


*Note: phr indicates parts per hundred.*

Figure 2. Tensile Strength against Starch Composition with different concentration of Hydrochloric acid in Three Different Degradation Days

Fig. 2 shows, the graph of tensile strength versus starch composition with and without day(s) to degrade in different concentration of hydrochloric acid solutions. The slightly increased of tensile strength from 15phr of starch to 20phr of starch can be compared again using Roshafima R.A, et al tensile strength versus starch loading result. The same explanations of Fig.1 are applied for this case also.

Table 2.Melt Flow Index of LDPE-Starch blend using different Concentration of Sodium Hydroxide solutions and Different Day(s) for Degradation.

| **Solution** | **NaOH** | | | | |
|---|---|---|---|---|---|
| **Molarity(M)** | | **2** | **4** | **2** | **4** |
| **Day(s) for soaking** | **0** | **3** | | **6** | |
| **Composition (LDPE/TS)** | **MFI value (g/10 min)** | | | | |
| **100phr/0phr** | 3.0 | 2.7 | 2.7 | 2.8 | 2.7 |
| **100phr/5phr** | 2.2 | 2.7 | 2.6 | 2.5 | 2.5 |
| **100phr/10phr** | 2.5 | 2.7 | 2.6 | 2.7 | 2.8 |
| **100phr/15phr** | 2.6 | 2.7 | 2.5 | 2.7 | 2.5 |
| **100phr/20phr** | 2.8 | 2.2 | 2.5 | 2.4 | 2.2 |

*Note: phr indicates parts per hundred.*

Table 3. Melt Flow Index of LDPE-Starch blend using different Concentration of Hydrochloric acid in Three Different Degradation Days

| **Solution** | **HCl** | | | | |
|---|---|---|---|---|---|
| **Molarity (M)** | | **2** | **4** | **2** | **4** |
| **Day(s) for soaking** | **0** | **3** | | **6** | |
| **Composition (LDPE/TS)** | **MFI value (g/10 min)** | | | | |
| **100phr/0phr** | 3.0 | 2.7 | 2.8 | 2.8 | 2.7 |
| **100phr/5phr** | 2.2 | 2.8 | 2.7 | 2.9 | 2.7 |
| **100phr/10phr** | 2.5 | 2.8 | 2.7 | 2.9 | 3.0 |
| **100phr/15phr** | 2.6 | 2.6 | 3.0 | 2.4 | 3.2 |
| **100phr/20phr** | 2.8 | 2.4 | 2.5 | 2.2 | 3.5 |

*Note: phr indicates parts per hundred.*

From Table 2 and Table 3, MFI showed fluctuated results. The result for 0phr, 5phr and 10phr mix did not present any significant changes in MFI value because the starch mix composition is relatively low, in comparing with overall structure. The raised in the MFI value indicates that the viscosity of the blend is lower than the pure LDPE mix[4]. This is because the homogeneous mix of the irregular shape's tapioca starch, which incurred an increment of spacing between molecules, lead to a drop in intermolecular forces between polymer coils[4]. There is also a possibility that the blending process enhanced the formation of particle-matric interaction, causing the blend to become smoother and hence increase in the mobility[4].

## 4. Conclusions

In conclusion, NaOH solutions showed significant degradation from the 0 day samples through MFI test and tensile strength especially for day 3 samples. HCl solutions samples showed fluctuated results in MFI. The observation will still be carried out until day 30 to determine the degradation conditions of the samples.

## References

[1]R. Narayan, *"Biodegradable Plastics"*1993.
[2]M.P. Journal and A. Chauhan, "*Environment-friendly Biodegradable Polymers and Their Applications*"vol.7, no.2, pp.62-67,2012.
[3] R. Chandra and R. Rustgi,*"Biodegradable Polymers*", vol. 23, no.97, 1998, pp. 1273-1335
[4] R.R. Ali, W.A.W.A.Rahman, R.M.Kasmani, H.Hasbullah, N. Ibrahim, A.N.Sadikin,and U.A. Asli,"*Characterization and Degradation Analysis of Tapioca Starch Based Biofilms*"no.12,pp.591-594,2013.
[5] R.R. Ali, W.A.W.A.Rahman, R.M.Kasmani, H.Hasbullah,"*Tapioca Starch for Disposable Packaging Ware*", vol. 32, pp. 1711-1716, 2013.

# Sintering Behavior of Forsterite with Manganese Oxide ($MnO_2$) as Doping Agent

Kumanan Angumuthu[1], Jeffrey Chin Kong Leong[1*]

[1]*School of Engineering, Taylor's University, Malaysia,*

**Corresponding email: JeffreyKongLeong.Chin@taylors.edu.my*

*Abstract*—**Forsterite ($Mg_2SiO_4$) powder was synthesized by using magnesium and talc with assistance of ball milling and subsequent heat treatment. Manganese doped forsterite was prepared at weight percentage of 0.05%,0.1%,0.2%,0.5% and 1.0wt% by adding manganese oxide before ball milling. The undoped and manganese doped forsterite was sintered at temperature ranging from 1200 C to 1600 C. Relative density, fracture toughness and microhardness was tested for biomedical application of forsterite.**

*Keywords*— Sintering, Forsterite, Bioceramic, Mechanical Properties, Manganese Oxide

## 1. Introduction

Forsterite is excellent in biomedical application especially in bone implant due to its composition which consists of magnesium and silicon, important elements in bone calcification process.Forsterite fracture toughness ( $K_{IC} = 2.4$ MPa $m^{\frac{1}{2}}$ ) are superior to hydroxyapatite and lower limit reported for corticol bone [1], and study on bioactivity of nanostructured forsterite, with grain size of 31nm has shown bioactivity and bioresorbability are on par with hydroxyapatite[2]. Forsterite also possesses melting point of 1890 $^oC$ with excellent electrical insulation, thermal expansion, and chemical stability[3].

Sintering is the traditional method of ceramic manufacturing which is used to transform fine ceramic powder into solid body using high temperature treatment. The basic tenet of sintering is to join particles without melting it, so the sintering temperature usually set below the melting point of the material.[4]The most commonly used sintering technique for forsterite production are based on the conventional pressureless sintering in air atmosphere. This method of consolidation requires high temperature, slow heating rate and long holding time to produce above 99% dense body, characterized by having large-grained microstructure and low mechanical properties [5].

Thus, this research aimed at synthesizing pure nanocrystalline forsterite powder and develops a process that would ultimately lead to the densification of the ceramic body at low temperature without compromising on the forsterite phase stability and inducing grain coarsening. Besides, the research will also explore the use of sintering additive such as $MnO_2$ which will be incorporated into forsterite to see the potential method in improving the sintering of forsterite.

## 2. Methodology

### 2.1 Preparation of Forsterite Powder

Talc ($Mg_3Si_4O_{10}(OH)_2$, Sigma-Aldrich, 99% purity) and magnesium oxide (MgO,Merck, 97% purity) was individually added to 500ml beaker using 100ml ethanol ($C_2H_5OH$,Merck) as solvent. Manganese Oxide were measured using Electronic Balance and added to the beaker containing the talc. The weight of talc, magnesium oxide and manganese oxide used for each sample is shown in Table 1. Both beaker was put in Ultrasonic Mixer for 2min to ensure homogeneity. After 2min, contents of both beaker was mixed and undergoes ultrasonic mixing for 30min.

Table 1: Ratio of Talc, MgO and MnO2 used for each sample

| Weight Percentage (wt% $MnO_2$) | Talc (g) | MgO (g) | $MnO_2$ (g) |
|---|---|---|---|
| 0 | 16.32 | 8.680 | 0 |
| 0.05 | 16.31 | 8.676 | 0.0125 |
| 0.1 | 16.30 | 8.672 | 0.025 |
| 0.2 | 16.29 | 8.663 | 0.05 |
| 0.5 | 16.24 | 8.641 | 0.125 |
| 1.0 | 16.16 | 8.593 | 0.25 |

The mixture was ball milled at 350 rpm using 5mm zirconia ball for 3 hours followed by heat treatment in oven for 24 hours at 60 $^oC$. The powder from oven is sieved using 212$\mu m$ metal sieve. The sieved powder was pressed in uniaxial pressing machine at 30MPa to compact the powder into disc (20mm dia. x 5mm thickness) and bar (32 x 13 x 6) mm using hardened steel mould. The sample were labeled. The pressed sample was sintered at different temperature (1200 $^oC$, 1300 $^oC$, 1400 $^oC$, 1500 $^oC$ and 1600 $^oC$) at the rate of 10$^oC$ /min for 2 hours.

### 2.2 Bulk Density Measurement

The bulk density of the forsterite will be determined by using Archimedes method by using water as medium. The bulk density was determined by precisely calculating the dry weight, suspended weight and saturated weight of forsterite.

The dry weight was calculated through measurement of geometric dimension (cylindrical for disc and cube for bar) and sample mass. The suspended weight was measured in a dish submerged in water after the electronic balance (Mettler-Toledo, Switzerland) are set to zero. The saturated weight are measured immediatelyafterwards to get weight of water-saturated forsterite. Equation 1 will be used to calculate the bulk density after the measurements are taken.

$$\rho_{bulk} = \frac{W_{dry}}{W_{sat} - W_{susp}} \rho_{water} \quad (1)$$

Where $\rho_{bulk}$ is the bulk density of the sample, $W_{dry}$ is the dry weight, $W_{sat}$is the saturated weight, $W_{susp}$ is the suspended weight, and $\rho_{water}$ is the density of water.

### 2.3 Young's Modulus

The Young moduli of forsterite ceramic was measured by using sonic resonance method (GrindoSonic: MK5 "Industrial", Belgium). ASTM E1876-97 (1998) is the standard used in this test. First, dimensions (width, length, and thickness) of ceramic sample was measured. The sample was put into the instrument which will determine the resonance frequency of the sample. Equation 2 will be used to calculate the Young's modulus:

$$E = 0.9465\left(\frac{mF_f^2}{b}\right)\left(\frac{L}{t}\right)^3 T_c \quad (2)$$

Where m is the mass of bar in gram, b is the width of the bar in mm, L is the length of the bar in mm, t is the thickness of the bar in

mmand Tc is the correction factor, and Ff is the fundamental resonance frequency of the bar in flexure in Hz

### 2.4 Vickers Hardness Test

Vickersindentation test will be used to determine the hardness of forsterite ceramic by using standard microindentation device (Matsuzawa, Japan). ASTM E384-99 (1999) and ISO 14705 (2000) are the standards used as quality control in this test. The indentation was made using pyramidal diamond indenter with a load of 50g. The indentation was applied slowly and held for 10 seconds. The pyramidal impression left by the indenter are measured with microscope to nearest $0.1\mu m$, thus the value of average diagonal (2a) are obtained. Equation 3 is used to determine the hardness.

$$H_v = \frac{1.854P}{(2a)^2} \quad (3)$$

Where Hv is the hardness (GPa) , P is the applied load (kgf) and 2a is the average diagonal ($\mu m$).

### 2.5 Fracture Toughness Determination

Fracture toughness test will be evaluated by using crack measurement method and using Niihara's formula shown in Equation 4. [6] The principle are same as Vickers indentation test, however measurement of radial cracks from the pyramidal impression was measured by microscope to determine the fracture toughness.

$$K_{IC} = 0.203\left(\frac{c}{a}\right)^{-\frac{3}{2}} H_v . a^{\frac{1}{2}} \quad (4)$$

Where $K_{IC}$ is the fracture toughness in MPa $m^{1/2}$, c is the length of measured crack from the center of indentation at half of the average length of two indent diagonals ($\mu m$)and $H_v$ is the hardness(GPa).

### 2.6 Microstructural Evaluation

X-Ray diffraction (XRD) (RigakuGeiger-Flex, Japan) was used to characterize the phase stability and crystal lattice present. The results from XRD was compared with standard reference JCPDS-ICCD (Joint Committee for Powder Diffraction Standard – International Center for Diffraction Data) file.

Field emission scanning electron microscope (FESEM) (Zeiss AURIGA, Germany) will be used to evaluate the grain size and microstructure. The grain size was measured from FESEM micrograph using standard line intercept method as outlined in ASTM E112-96 (2004). Average grain size was calculated by using Equation 5 proposed by Mendelson (1969).

$$D = 1.56\left(\frac{C}{MN}\right) \quad (5)$$

Where C is the total length of test line, M is the magnification of FESEM micrograph and N is the number of intercepts.

## 3. Expected Results & Discussion

### 3.1 Densification and Grain Size

Sara et.al [7] has studied the sintering behavior of pure forsterite. The highest relative density of 90.7% is achieved at temperature of 1500 C, while highest fracture toughness and Vickers microhardness are achieved at temperature of 1400 C. In ceramics, dopants are shown to increase densification with controlled grain size.[8] Thus, doping forsterite with manganese oxide are expected to increase the relative density of forsterite beyond 90.7%.

Formation of enstatite (MgSiO3) during sintering also present as challenge in obtaining pure forsterite. Grain size determines the physical property of ceramic. Experiment has shown that grain boundary diffusion of Si is the rate-controlling step for grain growth in forsterite.[9] Doping will induce segregation along the grain boundary by altering the surface and interfacial composition. Segregation plays a major role in grain boundary migration; a key element in controlling grain size.[8] Currently, the lowest grain size reported in the literature is 25 -45 nm. [1]

### 3.2 Fracture Toughness and Hardness

The highest fracture toughness for pure forsterite was achieved by Fathiet. al. [10] of 3.61 MPa $m^{1/2}$ and toughness of 940 Hv. The author achieved this in temperature of 750 $^{o}$Cand dwell time of 15 hours, however when temperature increased to 850$^{o}$C, the hardness and fracture toughness started to decline. These phenomena are attributed to grain coarsening that happen when sintered at elevated temperature for long time.

## 4. Conclusions

In this study, manganese oxide doped forsterite powder was successfully synthesized by using ball milling.Experimental data to develop sintering profile and determination of mechanical integrity of sintered forsterite are not yet developed.

**Acknowledgment**

The author is grateful for the support provided by University Malaya.

**References**

[1] M. Kharaziha and M. H. Fathi, "Synthesis and characterization of bioactive forsterite nanopowder," *Ceram. Int.*, vol. 35, no. 6, pp. 2449–2454, Aug. 2009.

[2] F. Tavangarian and R. Emadi, "Nanostructure effects on the bioactivity of forsterite bioceramic," *Mater. Lett.*, vol. 65, no. 4, pp. 740–743, Feb. 2011.

[3] F. Tavangarian and R. Emadi, "Effects of fluorine ion and mechanical activation on nanostructure forsterite formation mechanism," *Powder Technol.*, vol. 203, no. 2, pp. 180–186, Nov. 2010.

[4] D. Kolar, "Chemical research needed to improve high-temperature processing of advanced ceramic materials (Technical report)," *Pure Appl. Chem.*, vol. 72, no. 8, pp. 1425–1448, 2000.

[5] Z. Huang, M. Gotoh, and Y. Hirose, "Improving sinterability of ceramics using hybrid microwave heating," *J. Mater. Process. Technol.*, vol. 209, no. 5, pp. 2446–2452, Mar. 2009.

[6] K. Niihara, R. Morena, and D. Hasselman, "Evaluation of K Ic of brittle solids by the indentation method with low crack-to-indent ratios," *J. Mater. Sci. …*, vol. 1, pp. 13–16, 1982.

[7] S. K. Y. Lee, C. Y. Tan, S. K. L. Lai, R. Tolouei, M. Amiriyan, B. K. Yap, and S. Ramesh, "Sintering behaviour of forsterite bioceramics," *2011 Natl. Postgrad. Conf.*, pp. 1–3, Sep. 2011.

[8] M. N. Rahaman, *Ceramics Processing and Sintering*, Second Edi. New York: CRC Press, 2003.

[9] T. Hiraga, C. Tachibana, N. Ohashi, and S. Sano, "Grain growth systematics for forsterite ± enstatite aggregates: Effect of lithology on grain size in the upper mantle," *Earth Planet. Sci. Lett.*, vol. 291, no. 1–4, pp. 10–20, Mar. 2010.

[10] M. H. Fathi and M. Kharaziha, "Two-step sintering of dense, nanostructural forsterite," *Mater. Lett.*, vol. 63, no. 17, pp. 1455–1458, Jul. 2009.

# Production of Activated Carbon from Sugarcane and Coconut Shell

Joan Na Lee, Xiao Yien Lim*

*Energy Research Group, School of Engineering, Taylor's University, Malaysia*
**Corresponding email: XiaoYien.Lim@sd.taylors.edu.my*

*Abstract*— **Activated carbon (AC) produced from the biomass that are widely available in Malaysia is opted as an efficient and low cost technique to capture gaseous pollutants, which are sulphur dioxide ($SO_2$) and carbon monoxide (CO). The biomass are first prepared by carbonizing them at different temperatures to study the effect of temperatures on the char produced. Successful chars are then subjected to impregnation with KOH solution for activation. Once AC is obtained, it will be placed in an adsorption column and its efficiency at adsorbing $SO_2$ and CO gases will be studied.**

*Keywords*— Activated carbon, biomasses, impregnation, adsorption

## 1. INTRODUCTION

As of today, the amount of greenhouse gases (GHGs) in the atmosphere is increasing rapidly due to the emissions of exhaust gases from the industrial factories that mainly use fossil fuels such as coal and petroleum as their energy source. Besides that, the number of vehicles on the road is increasing significantly over the years which contributes more exhaust gases that further worsen the environment.Accumulation of the concentration of gases such as CO and $SO_2$ would impact the environment adversely if there are no actions taken to control them. Air pollution resulted from the combustion of fossil fuels and coal which emit $SO_2$can cause acid rain as well as many types of respiratory diseases due to the formation of ground level ozone[1]. On the other hand, the concentration of CO in the Northern Hemisphere is increasing at rate of 1% per year[2]. This would eventually lead to an increase in the concentration of $CH_4$ due to reaction with hydroxyl radicals to form hydroperoxy radicals ($HO_2$), which destroy the ozone layer.

The process of adsorption using activated carbon using waste biomass is opted as the most efficient way used to adsorb the pollutant gases as the starting material is cheap and the operating cost is low as compared to other alternatives such as wet scrubbing system [1].Therefore, in this study, a novel adsorbent derived from the combination of sugarcane and coconut shell. The adsorbent will be developed using different ratios of compositions (1:1, 1:3, 3:1 of sugarcane and coconut shell respectively). Particle size of 2 – 5 mm of the samples are prepared and subjected to the process of carbonization prior to chemical activation using potassium hydroxide (KOH) which increases the total surface area of the adsorption sites. Different flow rates of the exhaust gas from petrol engine are studied to investigate which conditions will yield an adsorbent with the highest efficiency of capturing CO and $SO_2$ gases.

## 2. RESEARCH METHODOLOGY

### 2.1 Materials

Sugarcane is collected from a vendor in Port Dickson, Malaysia whereas the coconut shells were provided by supplier from DST Technology, Malaysia.

### 2.2. Preparation of Activated Carbon

Sugarcane is washed with tap water to remove impurities. The dried sugarcane is then sundried for storage purpose. Washed sugar cane is then grind using blender and sieved to particle size of range between 2 to 5 mm. Once obtained the sieved sugar cane, it is washed with distilled water and dried in oven for 24 hours at 110 °C. 40g of dried sugarcane is placed in ceramic trays and into the furnace (KSL-1100X) for the carbonization process to take place at 500 °C for 2 hours under constant flow of pure $N_2$ gas. The resulting char obtained from the carbonization process will be chemically activated by soaking with 0.1M of KOH solution with an impregnation ratio of 1:50. The resulting mixture will then be dried in the oven at temperature of 110 °C for 24 hours. Once dried, the impregnated char produced will be subjected to carbonization at 500 °C for 2 hours under constant flow of pure $N_2$ gasto produce sugarcane activated carbon (SAC). Similar procedure will be conducted for coconut shell to produce coconut shell activated carbon (CAC) but with impregnation ratio of and 1:1.

### 2.3. Experimental Set-up

Adsorption column with 1:10 diameter to height ratiowill be filled with activated carbon with bed height of 30mm. At room conditions (temperature of 25 °C and pressure 1 atm), the experiment is first started by starting on the petrol engine that has been filled with engine oil. The tube that connects the exhaust is then connected to the inlet probe of the adsorption column and the gas flow rate can be adjusted by adjusting the valve and using a flow meter. The initial gas flow rate value used is 20 mL/min and the gas is allowed into the adsorption column for about 3 minutes to allow the concentration of the gas treated to reach steady state. Next, gas analysis meter (BTU 4400 Gas Analyser) is inserted into the probe to measure both the initial and final concentration of $SO_2$ and CO gases at time interval of 10 minutes. The procedure is then repeated with different gas flow rates of 5, 10 and 15 mL/min, with different composition of biomass (sugarcane and coconut shell powder with ratio of 1:1, 1:3 and 3:1) as well as to conduct replication for each set of sample. Once the experiment is over, the engine is switched off and the tube is disconnected from the adsorption column probe.

## 3. RESULTS AND DISCUSSION

Table 1: Carbonization of Sugarcane at Different Temperatures

| Temperature Used (°C) | Observation | Comment |
|---|---|---|
| 500 |  | Char is produced |

| Temperature Used (°C) | Observation | Comment |
|---|---|---|
| 600 |  | Half of the sugarcane turned into ashes |
| 700 |  | Completely turned into ashes |
| 800 |  | Completely turned into ashes |

Table 2: Carbonization of Coconut Shell at Different Temperatures

| Temperature Used (°C) | Observation | Comment |
|---|---|---|
| 500 |  | Char is produced |
| 600 |  | Slight ashes are produced |
| 700 |  | Completely turned into ashes |

Carbonization is a process that involves thermal decomposition of carbonaceous material in which to eliminate non-carbon species [3].Thus, after the process of carbonization, the char will contain more than 90% of carbon content and remaining content consists of ashes which enables the char to be a functional AC [4]. Based on Table 1 and 2, it is shown that at temperature of 500 °C produced perfect chars for both sugarcane and coconut shell as compared to other higher temperatures. It is also noticed that the yield of the char produced reduced with increasing temperature of the carbonization. This is due to the reason that more volatile matters were being released, which therefore, gives rise to an increase in fixed carbon content [5]. The suitable range to carbonize sugarcane is between the range of 500 – 550 °C [6], whereas for coconut shell, it is shown that at lower temperature (250 – 500 °C) of carbonization is able to produce activated carbon with larger surface area and pore volume [5]. Hence, in this study, the process of carbonization of sugarcane and coconut shell will be conducted at 500 °C.

Table 3: Before and After Carbonization of SAC Impregnated with KOH solution

| Before | After | Comment |
|---|---|---|
|  |  | Ashes are produced |

The resulting char is then subjected to process of chemical activation using KOH solution.The benefits of activating char via chemical activation are that it requires lower temperature for the carbonization process as well as shorter time is required for activation. Moreover, chemical activation helps to increase the surface area of AC[7]. Besides that, surface basicity of the AC will increase as well [8]. Activation of char also helps to enlarge the diameters of the pores created during the process of carbonization. This evidently helps prepare the AC to have higher capability of $CO_2$ capture [9]. However, referring to Table 3, it showsthatashes were produced when impregnatedsugarcane charwascarbonizedat 500 °C for 2 hours. Ashes do not chemically combined with the carbon surface of AC as they are non-carbon or mineral additive [8]. Impurities present in ashes become saturated as well when the char is subjected to activation process via carbonization [8,9]. Therefore, high ash content is considered undesirable for AC as it will reduce the efficiency of its adsorption capacity as well as its mechanical strength [8]. Since ashes are produced instead of char during activation, hence, it is decided that the activation process of the impregnated char is omitted.

## 4. Conclusions and Future Work

Based on the results obtained, SAC and CACwill be produced by carbonizing at 500 °C, impregnate with 0.1M KOH solution and dried in oven at 110 °C for 24 hours. The efficiency of different composition of SAC and CAC will then be studied in an adsorption column to determine its capacity at adsorbing $SO_2$ and CO gases.

## References


[1] A. C. Lua and J. Guo, "ADSORPTION OF SULFUR DIOXIDE ON ACTIVATED CARBON FROM OIL-PALM WASTE," *Journal of Environmental Engineering,* 2001.

[2] M. A. K. Khalil and R. A. Rasmussen, "The global cycle of carbon monoxide: Trends and mass balance," vol. 20, no. (1–2), 1990.

[3] F. a. Derbyshier, "Porosity in carbons: Characterization and applications," *Porosity in carbons,* p. 277, 1995.

[4] M. Plaza, C. Pevida, B. Arias, J. Fermoso, M. Casal, C. Martín, F. Rubiera and J. Pis, "Development of low-cost biomass-based adsorbents for postcombustion," *Fuel,* pp. 2442-2447, 2009.

[5] J. Katesa, S. Junpiromand and C. Tangsathitkulchai, "EFFECT OF CARBONIZATION TEMPERATURE ON PROPERTIES OF CHAR AND ACTIVATED CARBON FROM COCONUT SHELL," vol. 20(4), no. 269-278, 2013.

[6] M. Ruiz and C. Rolz, "Activated Carbons from Sugar Cane Bagasse," vol. 10 (4), no. 429–432, 1971.

[7] J. Sahira, A. Mandira, P. B. Prasad and P. R. Ram, "Effects of Activating Agents on the Activated Carbons Prepared from Lapsi Seed Stone," vol. 3(5), 2013.

[8] A. H. Abdullah, A. Kassim, Z. Zainal, M. Z. Hussien, D. Kuang, F. Ahmad and O. S. Wooi, "Preparation and Characterization of Activated Carbon from Gelam Wood Bark (Melaleuca cajuputi)," Vols. 7, No. 1, no. 65-68, 2001.

[9] S. M. Manocha, "Porous Carbon," *Sadhana Vol. 28, Parts 1 & 2,* p. 335–348, 2003.

# Removal of Antibiotics from Synthetic Wastewater by Advanced Oxidation Processes (AOPs)

Mohamad Farid bin Che Wil[1*], Rajesh Nithyanandam[1]

[1]*School of Engineering, Taylor's University, Malaysia*

**Corresponding email: faridchewil@gmail.com*

*Abstract*—**In this study, Fenton's Reagents process was used for the treatment of water containing Amoxicillin antibiotics of 100 mg/L concentration. The molar concentration (0.1M, 0.2M, 0.3M, 0.35M, and 0.4M) of Fenton's reagents was varied with different ratio of ferrous sulphate to hydrogen peroxide. COD and BOD reduction after treatment were calculated and optimum ratio was determined. Total Suspended Solid (TSS) formed after treatment was also measured.**

*Keywords*— Amoxicillin antibiotics, Fenton's reagent, Advanced Oxidation Processes (AOPs)

## 1. Introduction

One of pharmaceutical compound namely antibiotics have been detected in worldwide in environmental matrices (e.g. water and wastewater) and their presence on ecosystem has been known for 30 years[1]. The presence of the antibiotics in environment is at low level, but with continuous input of this compound may lead potential risk to the aquatic and terrestrial organism[2]. Hence, antibiotics have emerged as one of pollutant to the environment. Common antibiotics (with their concentration) found in wastewater are Sulfonamides: sulfamethoxazole (0.02–0.58 (μg/L), fluoroquinolones: ofloxacin (6–52 ng/L), ciprofloxacin (6–60 ng/L) bacteriostatic: trimethoprim (0.11–0.37 μg/L) Penicillin group: penicillin G (0.025 μg/L)[2].

The using of antibiotics is to sustain health condition of living organism such as human, animal and plant. The consumed antibiotics by organisms are excreted through urine or feces and sent to the sewage or manure[3]. This is one of route how antibiotics can emerge on the environment. Besides that, antibiotics are also can be found in different environmental compartment such as hospital effluent resulted from heavy used from human and veterinary medicine[4]. The emerging antibiotics in environment cause the formation of resistant microorganisms that causing problem to public health and also result to imbalance microbial ecosystem. Antibiotics could produce toxic effect that affects microbial community and other living organism in environment.

The objective of this study is to investigate removal of the antibiotics from synthetic wastewater by degrade it using Fenton's reagent process. The degradation is measured in term of COD and BOD reduction after the treatment at different molar concentration of Fenton's reagent.

## 2. Methodology

### 2.1 Preparation of Synthetic Wastewater

This synthetic wastewater contains amoxicillin antibiotics at 100 mg/L concentration. Amoxicillin antibiotics was obtained from Poliklinik Cahaya, Selangor is dissolved in distilled water and stored at 4℃.

### 2.2 Fenton's Reagent Experiment

500 mL of synthetic wastewater was poured into 4 500mL beaker. The pH of this synthetic wastewater was adjusted to pH between 2 -3 by adding several drops of 30% of sulfuric acid for optimum Fenton's reaction[5]. Fenton's reagent molar concentration of 0.1M with different ratio (1:2, 1:4, 1:8, and 1:10) of ferrous sulphate to hydrogen peroxide was added for each beaker and stir with stirrer for 30 minutes. After 30 minutes sample was taken for COD, BOD, and TSS test. Similar procedure was repeated for 0.2M, 0.3M, 0.35M, and 0.4M of molar concentration of Fenton's reagent.

### 2.3 Chemical Oxygen Demand (COD) Test

COD reagent such as sulfuric acid reagent, standard ferrous ammonium sulfate titrant (FAS) (0.10M), potassium dichromate digestion solution (0.01667M), and ferroin indicator solution was prepared. The 1.5ml sample mixed with 3.5ml sulfuric acid reagent and 1.5ml potassium dichromate was heated for 2 hours at 150℃. The heated mixture then was cooled at room temperature and mixed with 2 drops ferroin indicator and titrate with 0.10M until color change from blue-green to reddish brown. Blank sample also was prepared in same manner as sample. Below is the equation to calculate the COD value:

$$FAS\ Molarity\ (M) = \frac{volume\ 0.0167\ K_2Cr_2O_7\ titrated\ (mL}{Volume\ FAS\ used\ in\ titration\ (mL)} \times 0.10 \quad (1)$$

$$COD\ \left(\frac{mg}{L}\right) = \frac{(A-B)\times M\times 8000}{mL\ sample} \quad (2)$$

Where A = FAS for blank
B = FAS for sample
M = FAS molarity
8000 = miliequivalent weight of oxygen x 1000 mL/L

### 2.4 Biochemical Oxygen Demand (BOD)

BOD reagent (iodine azide solution, starch indicator, standard sodium thiosulfate titrant, manganous sulfate solution and dilution water) was prepared. 2 BOD 300 ml bottle was prepared. 1.5ml sample is diluted with dilution water inside each BOD bottles. One bottle is labelled with day-0 and another bottle with day-5. The day-0 bottle was mixed with 1ml of manganous sulfate, 1ml iodine azide and 1ml concentrated sulfuric acid. 200 mL was taken from day-0 bottle for titration with sodium thiosulfates solution till colourless. The day-5 bottle was wrapped with aluminum foil and incubates at 20℃ for 5 days. After 5 days titration was done as day-0 bottle. Below is the equation to calculate BOD value.

$$BOD\ \left(\frac{mg}{L}\right) = \frac{D_1 - D_2}{P} \quad (3)$$

Where $D_1$ = DO diluted sample for day-0 bottle (mg/L)
$D_2$ = DO diluted sample for day-5 bottle (mg/L)
P = decimal volumetric fraction of sample used

Note: 1 ml sodium thiosulfates = 1 mg DO/L

### 2.5 Total Suspended Solid (TSS)

Weight of a filter paper was measured. By using the filter paper, sample was filtered to obtain the suspended solid. The filtrate was dried together with the filter paper in oven at 103 to 105℃ for 1 hour. After 1 hour the weight dried filter paper was measured again. The increased value of the weight corresponding to value of total suspended solid. Below is the equation used to measure the TSS value.

$$TSS\ \left(\frac{mg}{L}\right) = \frac{(A-B)\times 1000}{V} \quad (4)$$

Where A = weight of filter + dried residue, mg
B = weight of filter, mg
V = volume of sample, mL

## 3. Result and Discussion

### 3.1 COD Reduction at Different Ratio of $Fe^{2+}/H_2O_2$.

Value of COD of the synthetic wastewater before the treatment was 125.33 mg/L. After treatment with 0.1M and 0.2M of Fenton's reagent COD value of the synthetic wastewater was reduced to certain value. Treatment was done for 30 minutes and foam was produced during the reaction and the color of water also was changed to reddish color. Figure 1 below shows reduction of COD after treated with 0.1M and 0.2M of Fenton's reagent.

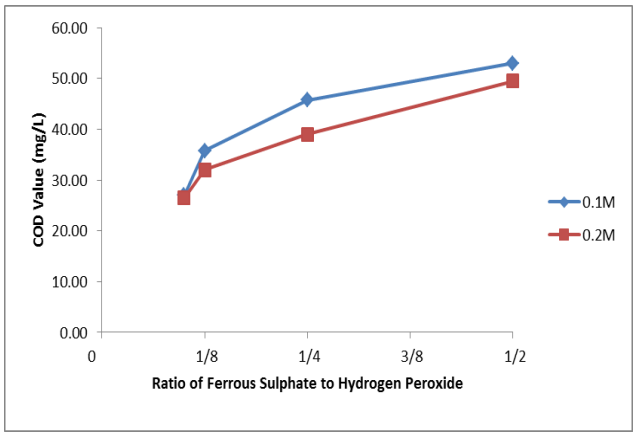


Figure 1 COD Reduction at Different Ratio of Ferrous Sulphate to Hydrogen Peroxide of Different Concentration of Fenton's Reagent

For 0.1M of Fenton's reagent, the COD reduction is increased as the ratio of $Fe^{2+}/H_2O_2$ decreases. However, further decreasing of $Fe^{2+}/H_2O_2$ will not increase the reduction of COD due to higher concentration of $Fe^{2+}$ that will directly react with hydroxyl radical[6]. The maximum COD reduction at 0.1M is occurred at 1/10 ratio of $Fe^{2+}/H_2O_2$. The value of COD at this ratio is 27.00 mg/L and the reduction was 78%.

At 0.2M of Fenton's reagent, the COD reduction is showed similar behavior as at 0.1M where, the COD reduction is increased as the ratio of $Fe^{2+}/H_2O_2$ decreases. However, the COD reduction at 0.2M is higher than COD reduction at 0.1M. Other study also shows that, the COD reduction is increased as the concentration of Fenton's reagent increase[7]. The maximum COD reduction was occurred at 1/10 where the COD value is 26.50 mg/L and percentage of reduction is 79%. From literature review the COD reduction will be increased as the Fenton's reagent concentration increased[7].

## 4. Conclusion

From this study, the COD reduction is increase as the ratio of $Fe^{2+}/H_2O_2$ decreases. However as reported in other study, further decreasing of $Fe^{2+}/H_2O_2$ will not increase the COD reduction due to higher concentration of $Fe^{2+}$.

This study also shows that, as the concentration of Fenton's reagent increase, the COD reduction also increases. This behavior also was reported in other study. Maximum of COD reduction for 0.1M occurred at 1/10 at the percentage of 78%. At 0.2M the maximum COD reduction also occurred at 1/10 at the percentage of 79%. This study result only up to 0.2M. However, result for 0.3M, 0.35M, 0.4M will be done.

## References

[1] V. Homem and L. Santos, "Degradation and removal methods of antibiotics from aqueous matrices--a review.," *J. Environ. Manage.*, vol. 92, no. 10, pp. 2304–47, Oct. 2011.

[2] M. Klavarioti, D. Mantzavinos, and D. Kassinos, "Removal of residual pharmaceuticals from aqueous systems by advanced oxidation processes.," *Environ. Int.*, vol. 35, no. 2, pp. 402–17, Mar. 2009.

[3] M. O. Uslu and I. A. Balcioğlu, "Comparison of the ozonation and Fenton process performances for the treatment of antibiotic containing manure.," *Sci. Total Environ.*, vol. 407, no. 11, pp. 3450–8, May 2009.

[4] B. Huerta, E. Marti, M. Gros, P. López, M. Pompêo, J. Armengol, D. Barceló, J. L. Balcázar, S. Rodríguez-Mozaz, and R. Marcé, "Exploring the links between antibiotic occurrence, antibiotic resistance, and bacterial communities in water supply reservoirs.," *Sci. Total Environ.*, vol. 456–457, pp. 161–70, Jul. 2013.

[5] E. S. Elmolla and M. Chaudhuri, "Degradation of the antibiotics amoxicillin, ampicillin and cloxacillin in aqueous solution by the photo-Fenton process.," *J. Hazard. Mater.*, vol. 172, no. 2–3, pp. 1476–81, Dec. 2009.

[6] E. Elmolla and M. Chaudhuri, "Optimization of Fenton process for treatment of amoxicillin, ampicillin and cloxacillin antibiotics in aqueous solution.," *J. Hazard. Mater.*, vol. 170, no. 2–3, pp. 666–72, Oct. 2009.

[7] R. Nithyanandam and R. Saravanane, "Treatment of Pharmaceutical Sludge by Fenton Oxidation Process," *Int. J. Chem. Eng. Appl.*, vol. 4, no. 6, pp. 359–364, 2013.

# Comparison of Different Methods for Extraction of Herbs

Mu'ammar Rusydi Shapheri[1*], Rajesh Nithyanandam[2]

[1,2]*Chemical Engineering Department, School of Engineering, Taylor's University, Malaysia*

*muammarrusydishapheri@sd.taylors.edu.my

*Abstract*—**Pegaga is used as prevention and treatment against cellular injury diseases as they contain antioxidant. Therefore, study on the best method of extraction to maximize the yield recovery of antioxidant components is vital. There are four extraction methods to be studied. Ultrasonic Assisted Extraction is the best method by showing values of 1350 mg GAE/100 g DW, 599 mg CE/100 g DW and 79 % scavenging activity on TPC, TFC and DPPH respectively. In a nutshell, this project has a possibility to create an important impact to society due to the fact that human always relies on remedies for diseases prevention and treatment.**

*Keywords*— *Centella Asiatica* (Pegaga), Extraction, Antioxidant

## 1. Introduction

Human civilization has used herbal medicines for millions of years as prevention and treatment of diseases. This is due to the fact that these herbal medicines contain beneficial biologically active components to improve health and well beings. One of the most important active component that exists in these herbs is antioxidant compounds. Antioxidant has the ability to counteract harmful cell damaging free radicals which is known to cause cellular injury such as cancer [1]. Therefore, studies on the best method of extraction to maximize the yield recovery of antioxidant compounds should be the main focus in performing this research.

In this study, *Centella Asiatica* or known as Pegaga by local Malaysian is chosen as a focused herb of interest due to its significant properties of antioxidant activity. Antioxidant properties of Pegaga will be used as a criterion to determine the best method of extraction. Pegaga is subjected to four extraction methods which are Conventional Solid-Liquid Extraction, Conventional Soxhlet Extraction, Hot Water Extraction / Infusion and Ultrasonic Assisted Extraction. After extractions, the extract crudes/samples from the methods will be subjected to antioxidant compound assay (Total Phenolic Content (TPC) assay and Total Flavonoid Content (TFC) assay) and antioxidant activity assay (DPPH free radical scavenging activity). These assays will evaluate the performance of each methods. The method which shows the highest recovery of phenolic and flavonoid compounds (antioxidant compounds) and together with highest antioxidant activity is selected as the best method of extraction.

### 1.1 Objective

The objective is to choose the best method of extraction of Pegaga herb among four extraction methods based on evaluation of highest antioxidant compounds recovery and highest antioxidant activity of the extract crude.

### 1.2 Theoretical Framework on Extraction Mechanism

Extraction is a process of separation to obtain desired bioactive components from a plant [2]. It occurs based on two physical phenomenon which are diffusion process through cell wall and washing out of the bioactive components once the cell wall is broken. Each extraction procedures must consist of two stages. First stage is steeping of Pegaga vegetal material in solvent to facilitate swelling of cell. Second stage is mass transfer of active components from material to solvent by osmotic process and diffusion [3].

## 2. Methodology

### 2.1 Material and Chemicals

Powdered form Pegaga (Ethno Resources Sdn. Bhd., Malaysia), ethanol (Astral Lab, Malaysia ), Folin Ciocalteus phenol reagent, gallic acid and sodium hydroxide (Merck, Germany), sodium carbonate and (+)-catechin (Labchem, Malaysia), sodium nitrite and aluminium chloride (Systerm, Malaysia), 2,2-diphenyl-1-picrylhydrazyl (DPPH) (Sigma Aldrich, USA). All chemicals used in the experiments were standard analytical grade.

### 2.2 Extraction Methods

#### *2.2.1 Conventional Solid-Liquid Extraction*

2 gram of powdered form Pegaga was extracted with 30 ml of extraction solvent (40% ethanol+60% water) in a 100 ml glass conical flask at 65°C for 60 minutes. The mixture was shaken in a Digital Orbital shaker (Yih Der, Model LM-400D, China) at a constant speed under controlled temperature. The extraction was carried out in triplicate [2].

#### *2.2.2 Conventional Soxhlet Extraction*

2 gram of powdered form Pegaga was placed in extraction thimble. The thimble is then transferred into the Soxhlet apparatus (Favorit, Model HS-1678, Malaysia). Pegaga was then extracted with 30 ml of extraction solvent (40% ethanol+60% water) for 8 hours. The equipment was operated by continuously bring the sample into contact with recycled solvent. The extraction was carried out in triplicate [3].

#### *2.2.3 Hot Water Extraction / Infusion*

2 gram of powdered form Pegaga was infused with 30 ml of distilled water at 80°C for 10 minutes. The mixture was stirred with a glass rod while maintaining constant temperature. The extraction was carried out in triplicate [1].

#### *2.2.4 Ultrasonic Assisted Extraction*

2 gram of powdered form Pegaga was mixed with 30 ml of extraction solvent (40% ethanol+60% water) in a conical flask and placed in the Ultrasonic equipment. The mixture was subjected to a sonication period of 40 minutes and at a temperature of 55°C. The extraction was performed by Ultrasonic assisted equipment (Soluzioni Technologiche Inc., Model Sonica 5300EP S3, Italy). The extraction was carried out in triplicate [3].

### 2.3 Antioxidant Compound Assay

#### *2.3.1 Determination of Total Phenolic Content (TPC)*

Pegaga crude extract was diluted 50 times. 1 ml of diluted extract was added to 1 ml of 10 fold dilution Folin-calcalteu Reagent. 0.8 ml of sodium carbonate (75%, w/v) was added after 4 minutes followed by 2 hours incubation at room temperature. The absorbance was measured adjacent to a blank at 765 nm by using UV light spectrophotometer (Dynamica, Model RB-10 spectrophotometer, Malaysia). 1 ml of sample was replaced with 1 ml of deionized water to prepare the blank. Gallic acid was used for standard curve calibration and the calibrated equation was $y = 0.9726x + 0.0234$ ($R^2$=0.9746). Milligrams of gallic acid equivalent per 100 g dried weight (mg GAE / 100 g DW) was used to express the results. Each extract sample was analyzed in triplicate [2].

*2.3.2 Determination of Total Flavonoid Content (TFC)*

0.25 ml of Pegaga extract was firstly mixed with 1.25 ml deionized water. 0.075 ml of 5% (w/v) sodium nitrite solution was added then followed by 0.15 ml of 10% (w/v) aluminium chloride. After 5 minutes, 0.5 ml of 1M sodium hydroxide was added and followed by addition of 0.275 ml of deionized water. Its absorbance was measured at 510 nm by using UV light spectrophotometer (Dynamica, Model RB-10 spectrophotometer, Malaysia). 0.25 ml of Pegaga extract was replaced with 0.25 ml of deionized water to prepare the blank. (+)-catechin was used for standard curve calibration and the calibrated equation was y = 3.3216x ($R^2$=0.9821). Milligrams of (+)-catechin equivalent per 100 g dried weight (mg CE / 100 g DW) was used to express the results. Each extract sample was analyzed in triplicate [2].

## 2.4 Antioxidant Activity Assay

*2.4.1 DPPH free radical scavenging activity assay*

0.1 ml of Pegaga extract was mixed with 3.9 ml of ethanolic DPPH (60µM). The mixture was allowed to settle for 30 minutes at ambient temperature. The absorbance was measured against blank at 517 nm by using UV light spectrophotometer (Dynamica, Model RB-10 spectrophotometer, Malaysia). Blank used was ethanol. Simultaneously, negative control (0.1 ml ethanol + 3.9 ml ethanolic DPPH) absorbance was also measured three times. Average was taken used as a constant for calculation in Equation 1. The results were expressed as scavenging (%).Each extract sample was analyzed in triplicate [2].

$$Scavenging\ (\%) = \frac{A_o - A_1}{A_o} \times 100\% \quad (1)$$

$A_o$ = Absorbance of sample, $A_1$ = Absorbance of negative control

## 3. Research Outcomes and Discussion

The effects of different method of extractions on the recovery of antioxidant compounds and antioxidant activity is shown in Fig 1. Ultrasonic assisted extraction shows domination on TPC, TFC and DPPH with values of 1350 mg GAE/100 g DW, 599 mg CE/100 g DW and 79 % scavenging activity thus selected as the best method.

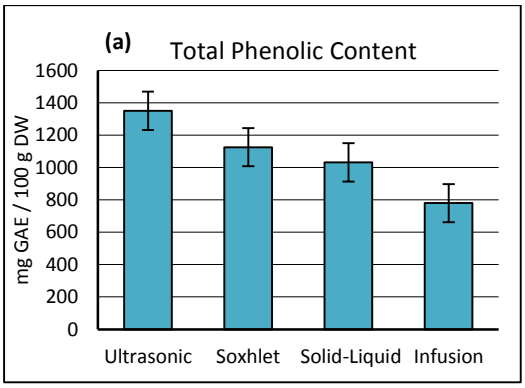


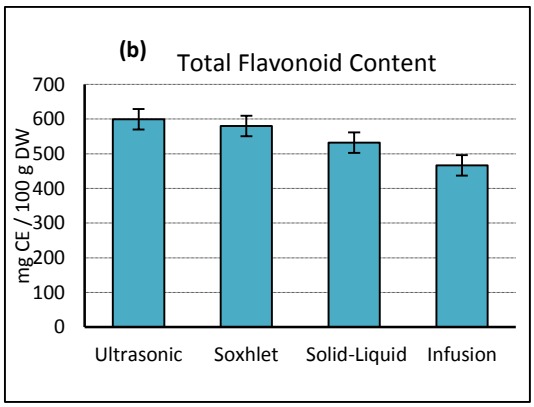


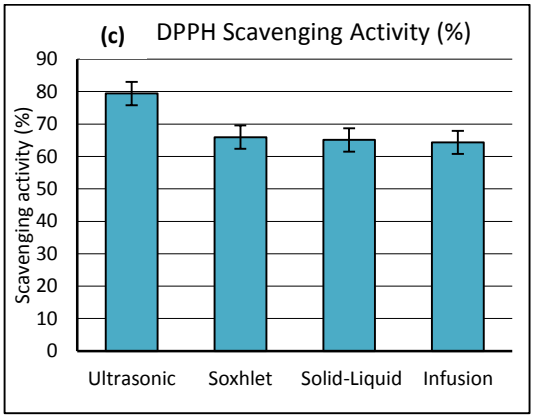


Fig. 1 Effect of methods of extraction on (a) TPC, (b) TFC, (c) DPPH assays. **Note: Standard deviations are represented by error bars.

Ultrasonic dominations can be explained by its application of high-frequency sound waves to enhance interaction between solvent and vegetal material. High speed ultrasonic vibration results in enormous quantity of bubbles in the liquid. These bubbles will collapse progressively thus producing mechanical, physical and chemical effects that will rupture the vegetal material cell membranes. This will promote the release of extractable compounds and improve mass transfers by intensifying solvent penetrations into cellular materials [3, 4]. High recovery amount of phenolic and flavonoid compounds in Fig. 1 (a) and (b) can be used as a reasonable justification on high DPPH % of ultrasonic method shown in Fig.1(c). High antioxidant activity is related to phenolic and flavonoid compounds availability as they act as hydrogen donating free radical scavengers [2]. The author's results can be benchmarked to the findings by [4], which state that ultrasonic extraction is a simpler and effective method to recover bioactive compounds in herbs.

Each method was carried out based on the best parameters settings (e.g. solvent concentration, temperature, etc.) found from literature review. This was done to ensure the extraction processes behave in the best manner. This will also ensure that the best yields of antioxidant compounds and activity from each extraction methods will be obtained. This explains the rationale behind the methodology selections.

## 4. Conclusion

Ultrasonic assisted extraction is the best method as it shows significance recovery of antioxidant compounds and show the highest antioxidant activity for Pegaga herb with values of 1350 mg GAE/100 g DW, 599 mg CE/100 g DW and 79 % scavenging activity on TPC, TFC and DPPH. In a nutshell, this project has a possibility to create an important impact to society due to the fact that human relies on antioxidant remedy for cancer prevention and treatment. Knowledge on the best method of extraction is important in order to maximize bioactive component yields extracted from Pegaga. This is to ensure world's blooming demand on antioxidant remedies is satisfied. This will also help Malaysian herbal marketing industry growth globally.

## References

[1] F. Pittela, "Antioxidant and cytotoxic activities of Centella Asiatica (L) Urb.," *International Journal of Molecular Science*, no. 10, pp. 3713-3721, 2009.

[2] K. Chew, "Effect of ethanol concentration, extraction time and extraction temperature on the recovery of phenolic compounds and antioxidant capacity," *Internation Food Research Journal*, no. 18, pp. 571-578, 2011.

[3] M. Bimakr, "Ultrasound-assisted extraction of valuable compounds from winter melon (Benincasa hispida) seeds," *International Food Research Journal*, vol. I, no. 20, pp. 331-338, 2013.

[4] A. Gupta , "Modern extraction methods for preparation of bioactive plant extracts," *International Journal of Applied and Natural Sciences*, vol. 1, no.1, pp. 8-26, 2012.

# Stability Studies of Graphene Nanolubricants Using Ionic Liquid Analogues

Noor Arliya Shaharuddin[1], Rashmi G. Walvekar[1*], Kaveh Shahbaz[1]

[1]*Chemical Engineering, Taylor's University, Malaysia,* [1]*Chemical Engineering, Taylor's University, Malaysia*

**Corresponding email: RashmiGangasa.Walvekar@taylors.edu.my*

***Abstract*— One of the ways to enhance lubricant's thermophysical properties is to add nanoparticles (Graphene oxide nanoparticles (NPs)) as an additive that becomes a nanolubricant. Previous studies of nanolubricants using palm oil have been known to improve the wear and friction of a lubricant, but it is not stable. This is because nanoparticles are not soluble in oils. An alternative solution would be to add solvents, namely ionic liquids (ILs). ILs are organic salts with low melting points that reduce wear and friction. They have a huge range of liquid temperature, high thermal stability and low vapour pressure. However, they are expensive as they require complicated preparation procedure. Recently, Deep Eutectic Solvents (DESs) have been recognized as an alternative of ILs. Since they are environmentally-benign solvents and represent common properties as that of ILs but are cheaper. DESs are said to be able to stabilize nanolubricants through strong hydrogen bond interactions. Multiple tests are done on different DES/nanoparticle concentrations to deduce their stability and thermophysical properties. To synthesize DES, various organic salts and Hydrogen Bond Donors (HBDs) are mixed with different molar ratios. Nanolubricants are synthesized with different concentrations of Graphene oxide NPs and the stability tests were made for all samples. This research is able to determine stable DES-based nanolubricants.**

*Keywords*— Deep eutectic solvent, nanographene oxide, ionic liquid, nanolubricant.

## 1. Introduction

The objectives of this study are to synthesize different DESs and to prepare stable nanolubricants without surfactants at various graphene oxide NP concentrations.

Lubricants play a major role in many fields of technology-related processes to lessen frictional resistance, save the surfaces of contact from wear, lower heat and provide cooling, decrease emissions and boost fuel economy [1]. The stability of nanolubricants is an important character in which many studies have found to be a challenge [7]. Most nanolubricants use surfactants to enhance the stability as the surface tension is lowered. However, surfactants are not able to withstand high temperatures as the bonding between the surfactants and nanoparticle can be destructed [6].

Previous studies have shown that adding nanoparticles into biolubricant base fluid improves the thermophysical properties, thus the efficiency. Nanoparticles like graphene NPs, for instance, can be used as an additive to lubricants, thus producing nanolubricants, as they are safe, environmentally-benign and can be found all over [5]. It has gained high attention because of its enhanced thermophysical properties and heat transfer performance, as well as their potential applications in numerous fields that include thermal power generation, refrigeration, cooling and many more [2]. However, graphene NPs reacts negatively towards the lubricating properties of biolubricants when the temperature increases. Nano-based biolubricants are not stable because nanoparticles are not able to disperse into the lubricants [4].

Over the recent years, ILs have been discovered for their unusual properties as the replacement of biolubricants. ILs are organic salts that have low melting points and the characteristics of a huge range of liquid temperature, high thermal stability and low vapour pressure, non-flammable with insignificant volatility, able to be miscible with water and organic solvents and unique electrochemical properties. They have a considerable potential for use as "green" solvents for industrial processes [3].

However, synthesis of ionic liquids involves many high-priced chemicals and long preparation and purification procedure which increase their costs. Due to expensive ILs, DESs can be utilized as cheaper alternatives. Currently, DESs are being the subject of research as well as industry because of their potential as environmentally-benign solvents and their benefits such as non-toxicity, non-reactivity with water, and being biodegradable. In fact, DESs represent common solvation properties with ILs. They are formed by mixing two or more components and have low melting points compared to their compounds. In other words, DESs are created from mixtures of organic halide salts with an organic compound which is an HBD that is able to form a hydrogen bond with the halide ion [3].

## 2. Methodology

### 2.1 Chemicals and materials

Methyltriphenylphosphonium bromide (MTPB) and glycerol were purchased from Merck Chemicals (Malaysia) with high purity (>99%), and graphene oxide NPs from Graphene Supermarket US (USA) with diameter of 60 nm and centrifugal device (Scan Speed 1730R).

### 2.2 Synthesis of DESs

This study involves four DES samples. To synthesize DES, a salt (MTPB) and a Hydrogen Bond Donor HBD particle (glycerol) were selected and mixed at four different molar ratios, as shown in Table 2.1. The mixed chemicals were stirred using a magnetic hot plate stirrer (WiseStir SMHS-3 by Daihan Scientific Co., Ltd.) for approximately 2 to 3 hours until a colourless liquid can be observed with temperature of 90˚C. Table 2.1 shows the compositions of glycerol and MTPB and the abbreviations.

Table 2.1. Compositions of synthesized DESs and their abbreviations

| Salt | HBD | Molar ratio (salt:HBD) | DES |
|---|---|---|---|
| MTPB | Glycerol | 1:2.5 | 1 |
| | | 1:3 | 2 |
| | | 1:4 | 3 |
| | | 1:5 | 4 |

### 2.3 Synthesis of Nanolubricants

Graphene oxide NPs with different concentrations (0.01, 0.015 and 0.02 wt%) and all the DESs were weighed using a weighing balance (BEL Engineering) were added to each of the sample to produce nanolubricants [4]. Then, each sample was sonicated using a probe sonicator (Bandelin Electronic UW 3200), for two times for about 4 minutes each. This method which is called two-step method is the most economic method for the production of nanolubricants, hence the most popular method among many others [7]. Table 2.2 shows the compositions of the lubricants.

Table 2.2: Compositions of nanolubricants and their abbreviations

| DES | Molar ratio, MTPB : Glycerol | Concentration (%wt) | Abbreviation |
|---|---|---|---|
| 1 | 1 : 2.5 | 0.01 | NL 1 |
| | | 0.015 | NL 2 |
| | | 0.02 | NL 3 |
| 2 | 1 : 3 | 0.01 | NL 4 |
| | | 0.015 | NL 5 |
| | | 0.02 | NL 6 |
| 3 | 1 : 4 | 0.01 | NL 7 |
| | | 0.015 | NL 8 |
| | | 0.02 | NL 9 |
| 4 | 1 : 5 | 0.01 | NL 10 |
| | | 0.015 | NL 11 |
| | | 0.02 | NL 12 |

## 2.4 Stability Analysis

There are two methods used- sedimentation and centrifugal methods.

a) Sedimentation method

The stability of each sample was observed visually from the amount of sediments at the bottom through a direct light. The sample that had the least sediment would be the most stabilised compound [2]. Observations with photographs were made every two weeks for about six weeks until present time to determine the highest stability samples [7].

b) Centrifugal method

This method is to confirm the stability test at a short amount of time [6]. The centrifugal device (Scan Speed 1730R) was used and all the samples of a total of 12 were put into the device for 10 minutes. Four sets of nanolubricants were made to be set to four different rotational speeds- they are 1000 rpm, 5000 rpm, 10000 rpm and 15000 rpm. The before and after photographs were taken to compare [6].

## 3. Results and discussion

The following photographs in Figure 3.1, Figure 3.2 and Figure 3.3, were taken every two weeks for six weeks to observe the progress of the stability test.

Figure 3-1: From left, NL 1, 2, 3, 4, 5, 6, 7, 8, 9, 10, 11 and 12 on the second week.

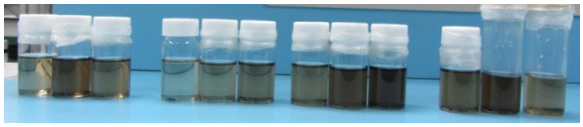

Figure 3-2: From left, NL 1, 2, 3, 4, 5, 6, 7, 8, 9, 10, 11 and 12 on the fourth week.

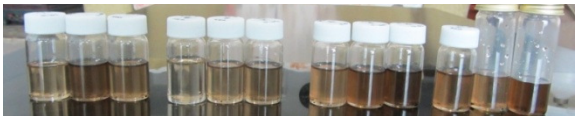

Figure 3-3: From left, NL 1, 2, 3, 4, 5, 6, 7, 8, 9, 10, 11 and 12 on the sixth week.

It can clearly be observed that all the nanolubricants are stable through the colours and very few graphene oxide NPs can be seen at the bottom of the vial bottle. The nanolubricants on the second, fourth and sixth week did not have any differences physically, as seen from the photographs above. However, to confirm the stability of all the nanolubricants, a centrifugal method was used, as explained in the previous section of methodology. A before and after photographs for four sets of nanolubricants for four different rotational speeds- 1000 rpm, 5000 rpm, 10000 rpm and 15000 rpm are shown below.

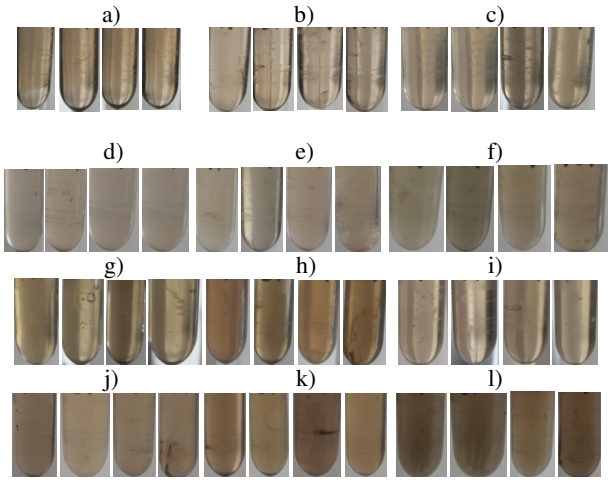


Figure 3-4: Centrifugal method samples after centrifugal method of 1000 rpm, 5000 rpm, 10000 rpm and 15000 rpm for a) NL 1, b) NL 2, c) NL 3, d) NL 4, e) NL 5, f) NL 6, g) NL 7, h) NL 8, i) NL 9, j) NL 10, k) NL 11 and l) NL 12

Referring to Figure 3.4, no sediments can be seen after going through the centrifugal test. This confirms that all the nanolubricants synthesized are stable [7]. In this study, the main emphasis is that no surfactant was used as a stabiliser. According to Derjaguin, Verway, Landau and Overbeek (DVLO), the nanolubricants are stable because they have an adequate high repulsion as compared to the attractive force. Thus, the nanolubricants are considered to be stable [7]. This is also due to the hydrogen bond interactions between the DESs and graphene oxide NPs, owing to the presence of hydroxyl groups in glycerol and the unique structure of graphene oxide NPs. It is known that graphene oxide NPs have many functionalized groups such as carbonate, hydrogen, carboxyl, phenol, carbonyl and ether that contribute to the susceptibility of the strong hydrogen bonds [4].

## 4. Conclusions

Graphene oxide NPs can be easily dispersed in glycerol-based DESs even without a surfactant for six weeks until present time. This is mainly because of the presence of strong hydrogen bonds between the DESs and graphene oxide NPs. The further experimental research on thermophysical and tribological properties of nanolubricants containing graphene oxide NPs at various temperatures will be conducted in the future work.

## References

[1] Castillo Marcano, S. J., et al. (2012). "Nanolubricants for diesel engines: Related emissions and compatibility with the after-treatment catalysts." Tribology International(0)..

[2] Fuxian Wang, L. H., Zhengguo Zhang, Xiaoming Fang, Jinjing Shi and Wenshi Ma (2012). "Surfactant-free Ionic Liquid-Based Nanofluids with Remarkable Thermal Conductivity Enhancement at Very Low Loading of Graphene." Nanoscale Research Letters **1**: 7.

[3] Kaveh Shahbaz, S. B., Farouq Sabri Mjalli, Mohd Ali Hashim and Inas Muen AlNashef (2012). "Prediction of glycerol removal from biodiesel using ammonium and phosphunium based deep eutectic solvents using artificial intelligence techniques." Elsevier **118**: 8.

[4] Rashmi, W. and A. G. Zen. (2013). Tribological Evaluation of Nano Graphene Platelets as an Additive to Biolubricant Base Fluid. EURECA 2013. T. Padmesh**:** 3.

[5] Rensselar, J. V. (2010). Unleashing the Potential of Ionic Liquids. Tribology and Lubrication Technology, STLE**:** 8.

[6] Sayantan Mukherjee, S. P. (2013). "Preparation and Stability of Nanofluids-A Review." IOSR Journal of Mechanical and Civil Engineering (IOSR-JMCE) **9**(2): 63-69.

[7] Wei, X. and L. Wang (2010). "Synthesis and thermal conductivity of microfluidic copper nanofluids." Particuology **8**(3): 262-271.

# Optimization of Plastic Bag for Algae Growth

C.K. Thein[1], N.M. Razali[2], M. M. Shamel[3], S. W. Phang[4]

[1]*Mechanical Engineering Department, Taylor's University Lakeside Campus, Malaysia,* [2,3,4]*Chemical Engineering Department, Taylor's University Lakeside Campus, Malaysia.*

**ChungKet.Thein@taylors.edu.my*

*Abstract*—**Rising interest to find an alternative source for fossil fuels as the energy is the main reason to grow algae in large amount which algae is recognizes as one of the biodiesel is made from. Algae is primitive organism with a simple cellular structure and have a large surface to volume body ratio, and it grows rapidly fast, usually double their biomass within 24 hours while during exponential growth, the biomass doubling time can be as short as 3.5 hours [1]. This aim of this paper is to design a plastic bag for algae growth so that the cost of the algae production will be reduced. The plastic bag was designed by considering the amount of light intensity uptake by the algae at the middle of the plastic bag is enough for its growth. The design also based on the maximum load that the plastic can take in order to sustain the weight of the water and algae inside of it. The designated plastic bag was simulated by using finite element analysis (FEA) to test its toughness.**

*Keywords*—Algae, Biodiesel, Finite Element Analysis

## 1.0 Introduction

Fossil fuels such as petroleum, natural gas, coal are non-renewable, which being consumed over 80% are the main sources of energy and been consumed for so many years. The depletion of the sources urge the needs to find a new resources [2]. Biodiesel and bioethanol are among the possibilities renewable fuel that gained great interest. However, the cost of growing the algae might be expensive and there is also cheaper techniques which risk in contamination problem.

Among the techniques that are available, algae cultivation in the plastic bag is the most economical and reliable method to grow algae. A high density polyethylene is considered to manufacture the plastic bag because of its toughness and durability. The plastic bag needs to exposed to sunlight and able to withstand the weight of water and algae.

This research will be focused on the design of the plastic bag. Before growing the algae inside the plastic bag, the shape of the plastic bag is a critical challenge for the algae to grow. Algae needs sunlight and nutrients to grow. It is stated that, to design effective plastic products to meet with the profitability and quality requirements, the understanding and applying the characteristics of plastics such as load, operating temperature and pressure are required before the design procedure [3]. A safety of factors of 1.5 to 2 is needed in order to get a plastic product with suitable strength and deformation under a fixed load that must not exceed the constraints require.

Moreover, after the designing phase, to get the plastic tested, FEA is very useful in order to analyse the product before the real plastic bagbeing produced. Besides the real test on the prototypes and final products, this FEA helps to improve the design, reduce time consuming with the model design and identify the problems of the designed product quickly and efficiently [3]. FEA is the cost effective way to reduce time and course needed to build numerous real life

The most important is, computer modelling and simulation by the software reduce a large amount of cost need to build numerous real life model to test the various conjunctures.

## 2.0 Methodology

### 2.1 Selection of Material

The type of materials for plastic were compared based on its durability, toughness and price. From the comparison, polyethylene were chosen as the most suitable material for the algae cultivation plastic bag. There are three classes of polyethylene: low density polyethylene (LDPE), linear low density polyethylene (LLDE) and high density polyethylene (HDPE). Since this plastic bag need to be left under the sunlight for a period of time and need to withstand the specific weight and pressure acting on the plastic bag wall, HDPE fitted the criteria.

### 2.2. Plastic Bag Design

Algae need sunlight and nutrient to grow, Gestel stated that amount of light intensity will affect the maximum rate of photosynthesis for the algae to grow. The maximum photosynthesis occurs when the light intensity is 38% [4]. In this paper, a cylindrical shape plastic bag is considered. The maximum distance or the radius of the plastic bag so that the algae will get enough light intensity at the centre of the bag was calculated using the equation (1):

:

$$ln\left(\frac{I_0}{I}\right) = 0.014\ (d) \qquad (1)$$

Where:

$I_o = light\ intensity\ in\ the\ surrounding, \frac{W}{m^2}$

$I = light\ intensity\ at\ the\ middle\ of\ plastic\ bag, \frac{W}{m^2}$

$d = maximum\ distance\ of\ half\ of\ the\ plastic\ bag, cm$

Using equation (1), intensity of the sunlight and the maximum photosynthesis rate related to light intensity, the radius of the cylinder was calculated as 600 mm. The length of the plastic bag was calculated based on the yield strength of the HDPE is 14.5 MPa with the safety of factors of 2. The thickness of the plastic is 0.5 mm and the plastic characteristic is transparent. The thickness will not have a major effect to the light intensity that penetrated the plastic bag. The simplified formula to find the length of the plastic bag which was originally from Hooke's Law is shown in equation (2):

$$l = \frac{\sigma \times 2t}{\rho \times r \times g} \qquad (2)$$

Where,

$l = length\ of\ the\ plastic\ bag, mm$

$\sigma = Yield\ strength, \frac{N}{mm^2}$

$t = thickness\ of\ the\ plastic\ bag, mm$

$r = radius\ of\ the\ plastic\ bag, mm$

$g = gravity, \frac{N}{kg}$

Using equation (2), equation (1) and information of plastic bag, the length of the plastic bag is calculated as 2270 mm. there is several unpredictable in the plastic bag, an uncertainty of 10% is applied to this model which is estimated as 2000 mm.

### 2.3 Model Generation

In order to simplify the model generation, the length of the plastic bag was divided into 10 equally section. Each section, different pressures were acting on the wall by referring to the reference point.

The reference point was the point where the plastic bag was being hanged. Besides that, with the known radius and length of the plastic bag, the force can be calculated applied on the plastic bag based on the mass of algae and water inside was 22 189.7 N.
The plastic bag was simulated using SolidWorks FEA. The curvature based mesh with minimum size of 18.811 mm was used in the simulation. The mesh quality was set to be high so that error will be reduced and the simulation result will yield more accurate.

## 3. Results and Discussion

### 3.1 Simulation Results

Refer to Figure 1, the maximum stress of the plastic bag does not exceed the yield strength. The minimum and maximum stresses from the simulation ware $1.10902 \times 10^{-5}$ Pa and 5.71MPa, respectively. Therefore, the plastic bag will not be break once it's been filled with the load, i.e., water and algae to be grow inside.

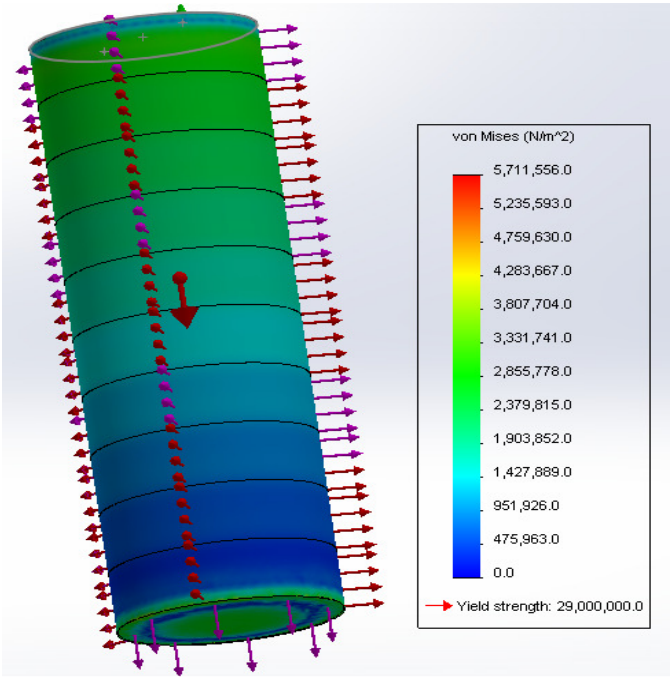


**Figure 1.** Simulation result for stress

The minimum andmaximum displacement of the plastic bag were 0 mm and17.5708mm, respectively. The maximum displacement occurred at the bottom of the plastic where the force from the weight of the water and algae inside was applied.

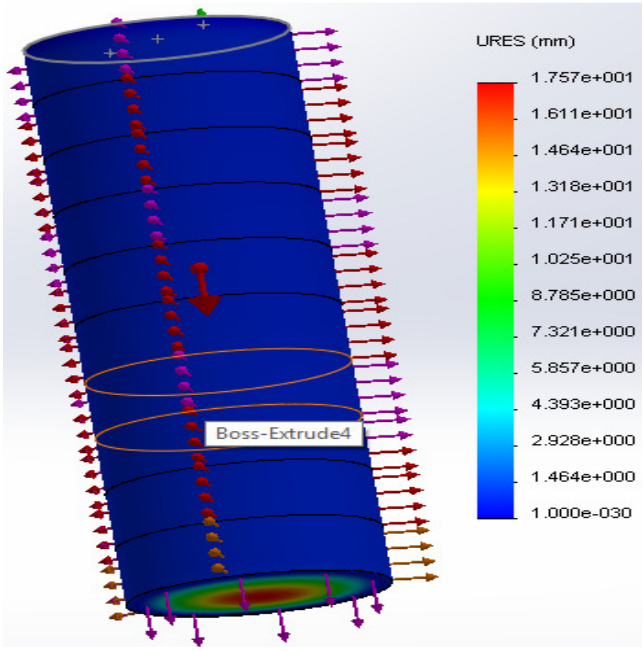


**Figure 2.** Simulation result for displacement of the plastic bag

## 4. Conclusion

Light intensity is the most important thing in making sure that the algae inside the plastic bag especially in the middle will get enough energy source to carry out photosynthesis process. Therefore, it is important to get the maximum percentage of light that will penetrate plastic bag which is enough to supply energy to the algae.
On the other hand, force and pressure that acting on the wall also are very element because higher force and pressure that acting on the wall of the plastic bag will result in higher stress. When this happen, the plastic will not be able to sustain the weight of the water and algae and therefore will definitely break.
Further study of algae growth plastic bag should be carried out with the material that is even better than high density polyethylene, especially the material that is biodegradable. Non-biodegradable plastic is one of the sources that cause pollution in the worldwide since the characteristics of it are indestructibility and durable. So, a biodegradable plastic bag is really important not only for algae growth industry, but in fact for all the applications that use plastic bags in daily live.

## Acknowledgment

Special thanks to School of Engineering Taylor's University, DrThein Chung Ket as main supervisor, not to forget Ms Eunice PhangSiew Wei and Dr Marwan as co-supervisors, for the help throughout completing this project.

## References

[1] Chisti, Y., 2006. *Miocroalgae as Sustainabe Cell Factories.* s.l.:Environ Engineering Management.
[2]Demirbas, A. &Demirbas, M. F., 2010. Energy Conversion and Management. *Importance of Algae Oil as a Source of Biodiesel,* pp. 164-170.
[3] Rosato, D. V. &Rosato, R. V., 2003. *Plastic Engineered Product Design.* 1st ed. Oxford, UK: Elsevier Advanced Technology.
[4] Geste, N. C, Nesbit, A. D, Gordon E. P & Green, C, 2005. *Continuous Ligh May Induce Photosynthetic Downregulation in Onion- Consequene for Groing Biomass Partitioning, Texas, USA*
[5] Brydson, J. A., 1995. *Plastic Materials.* 6th ed. s.l.:Butterworthh-Heinnemann Ltd.
[6] Demirbas, A. H., 2009. Enery Education Science Technology. *Inexpensive Oil and Fats Feedstock for Production of Biodiesel,* pp. 163-168.
[7] Chisti, Y., 2007. Trends in Biotechnology. *Biodiesel from Microalgae Beats Bioethanol,* pp. 126-131.

# Wastewater Treatment by using Natural Coagulant

Nur Fathinatul Akmal binti Saharudin[1*], Rajesh Nithyanandam[2*]

[1,2]*Chemical Engineering Department, School of Engineering, Taylor's University, Malaysia*

**nurfathinatul.akmal@sd.taylors.edu.my*

*Abstract*— **Natural coagulant is a natural based coagulant that can be used in coagulation process of wastewater treatment for reducing turbidity. The objectives of this study were to assess the possibility of using natural coagulants as an alternative to the current commercial synthetic coagulant such as aluminium sulphate and to optimize the parameters related in the working condition of coagulation process. Based on the experimental results, it was concluded that this natural coagulant efficiency which can removed up to 99.1% of turbidity in synthetic wastewater is comparable to the synthetic coagulant.**

*Keywords*— natural coagulant, coagulation, wastewater treatment

## 1. Introduction

In wastewater treatment, coagulation has been practiced since earliest times and the main objective is to remove colloidal impurities hence also removing turbidity from the water. Coagulant is a chemical used that is added to the water to withdraw the forces that stabilizes the colloidal particles and causing the particles to suspend in the water. Once the coagulant is introduced in the water, the individual colloids must aggregate and grow bigger so that the impurities can be settled down at the bottom of the beaker and separated from the water suspension. Aluminium and iron coagulants are commonly used in most industries. However, when aluminium is used as a coagulant in waste water treatment, it can caused several bad effect on human health such as intestinal constipation, loss of memory, convulsions, abdominal colic's, loss of energy and learning difficulties.

Hence nowadays, there has been great attention in the improvement and implementation of natural coagulants in wastewater treatment. These natural coagulants can be formed or extracted from animal, microorganisms and also plant. Natural coagulant chosen for this project is Hibiscus Sabdariffa or also known as Roselle. Roselle seeds were found to be rich in proteins (27.745%) which are soluble in water and carry an overall positive charge when in solution [1]. These positive charge proteins would bind to the negatively charged particles in the solution that cause turbidity. This project was carried out to investigate the efficiency of this natural coagulant to be used in the coagulation process of wastewater treatment.

## 2. Methodology

### 2.1 Materials and Chemicals

Good quality dry seeds of Roselle were carefully selected and collected from Port Dickson, Negeri Sembilan, Malaysia. Industrial wastewater sample is collected from a glove manufacturing company in Selangor, Malaysia. Kaolin with particle size of 0.1-4 μm from Sigma-Aldrich is used to simulate the wastewater turbidity. Chemical used are hydrochloric acid from Astral Lab, sodium hydroxide from Merck and aluminium sulphate also from Merck.

### 2.2 Preparation of Synthetic Wastewater Samples

Synthetic industrial wastewater was prepared by adding chemical to simulate industrial wastewater properties and to be treated in this project. The synthetic water turbidity value was adjusted to be at the same level with the turbidity value of the collected industrial wastewater which is 80 NTU. 10g of dry kaolin was dispersed into 1 litre of distilled water and mixed for 1 hour at 200 rpm. Prepared synthetic wastewater suspensions were allowed to settle for 24 hours before the experiment.

### 2.3 Preparation of Roselle Seed

The seedpods were allowed to dry naturally on the tree to make sure there were fully matured before harvesting the seeds for coagulant production. The seeds were then shelled, crushed, ground and sieved to a fine powder with size of < 250μm. The powder is mixed with water to yield a net positive charge from the water soluble proteins of the seeds. The water coagulant suspension was vigorously shaken for at least 5 min after adding water to fully expand the molecules and then filtered by using 2.5μm filter papers before it can be used. The suspension was stored in a refrigerator to avoid deterioration, hence if the suspension is refrigerated; it can be kept up to one week without deterioration [2].

### 2.4 Experimental Run

There are a few variables that can be affected by temperature such as pH, viscosity, density and floc volume concentration, hence it is very important to maintain and control the temperature for an accurate result. The temperature of the wastewater is remained constant at room temperature throughout the experiment. Sample solution of the coagulants, synthetic wastewater, sodium hydroxide and hydrochloric acid were prepared at suitable concentration to ensure that the experiment would run smoothly and the results can be measured conveniently. In this jar testing experiment, 0.1 M of NaOH and 0.1 M of HCl were used to adjust the pH level to desired pH value of the wastewater.

### 2.5 Coagulation Activity

The optimum condition of coagulation process is where the least dosage of coagulant is needed and the pH value of the condition that can yield the wanted flocs and contributing to clean water. The pH range tested in this experiment is from 2 to 11 and the concentration of coagulant added is between 20mg/l to 200 mg/l. In this jar test experiment, natural coagulant with a concentration of 200mg/l was first added into 200ml of wastewater. The mixtures were rapidly stirred at 120 rpm after the addition of the dose for about 3 minute. The mixtures were then stirred slowly at a speed of 50 rpm to allow it to flocculate for a period of 20 minutes. After sedimentation process for 1 hour, 100 ml of the supernatant liquid was carefully collected without disturbing settled flocs to measure residual turbidity (RT) value. The same coagulation test without the addition of natural coagulant was carried out as a control and the residual turbidity ($RT_C$) value was determined. The coagulant activity and total suspended solid values after coagulation process were calculated.

Coagulation activity was measured as:

$$\text{Coagulation activity} = \frac{(RT_C - RT)}{RT_C} \times 100\ (\%)$$

### 2.6 Analytical method

The turbidity values of the wastewater sample were measured by using a turbidity meter (CyberScan TN 100 IR) from Eutech Instrument in Nephelometric Turbidity Units (±0.01 NTU). The pH values of the wastewater samples were measured by using Professional Benchtop pH meter BP3001 from Trans Instrument with an accuracy of ±0.02. The overhead stirrer used in jar test experiment is R50D Precision Overhead Stirrer from CAT Scientific with an adjustable speed from 50 to 1600 rpm.

## 3. Research Outcomes and Discussion

### 3.1 Effect of pH on coagulation activity of Roselle seed

The study of influence of pH on coagulation activity is important as the solubility of matters and particles are depends on the pH level of the wastewater. Wastewater is mainly consists of negative charge particles and the pH value of where these particles are stable is known as isoelectric point. The optimum pH value for coagulation process of both synthetic and industrial wastewater with initial turbidity of 80 NTU were determined. The initial pH was varied from pH 2 to pH 11with a maximum dosage of 200 mg/l of natural coagulant. Fig. 1 shows the results obtained from jar test experiment for both synthetic and industrial wastewater.

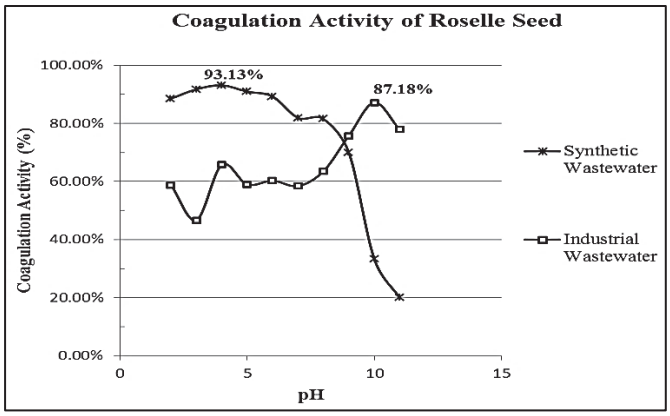


Fig. 1 Effect of pH on coagulation activity of Roselle seeds extract.

As can be seen from Fig. 1, the highest coagulation activity of Roselle seed for synthetic wastewater is at pH 4 with 93.13% turbidity removal. On the other hand, the highest coagulation activity for industrial wastewater is at pH 10 with 87.18% turbidity removal. Coagulation activity of Roselle seed in synthetic wastewater is high at pH range of 6 and below which is in acidic range while coagulation activity in industrial wastewater is high at pH range of 9 and above. The percentage of turbidity removal decreased in the synthetic wastewater for pH 9 and above. This may be caused by excessive addition of sodium hydroxide used as a pH modifier. The reducing in coagulation activity at pH 8 and above suggested that some protein may be denatured at high concentration of sodium hydroxide hence reduced efficiency of coagulation process [3].

### 3.2 Effect of natural coagulant dosage on coagulation activity

Based on Fig. 1, the optimum pH for coagulation process of synthetic and industrial wastewater are 4 and 10 respectively. In this project, optimum dosage of roselle seeds extract for both synthetic and industrial wastewater was determined in their respective optimum pH level and these results are presented in Fig. 2.

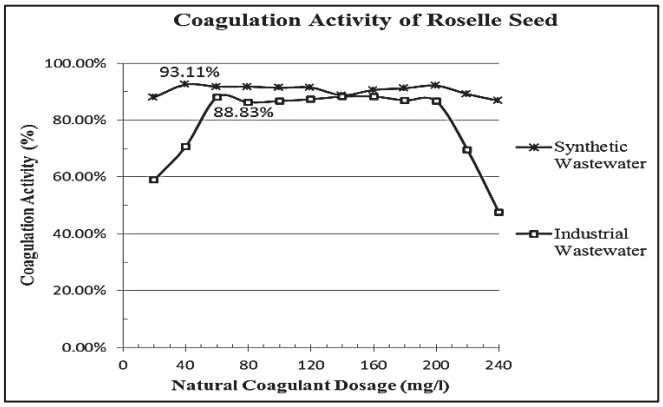


Fig. 2 Effect of coagulant dosage on coagulation activity of Roselle seeds extract.

According to Fig. 2, the optimum dosage of roselle seed extract in the removal turbidity of 80 NTU is 40 mg/l for synthetic wastewater and 60 mg/l for industrial wastewater. The turbidity value was reduced from 80 NTU to 5.5 NTU for synthetic and to 10.3 NTU for industrial wastewater. Coagulation activity of roselle seeds was decreased by increasing dosage of its extract. This declination may be caused by charge reversal and destabilization of colloidal particles due to overdosing of protein.

### 3.3 Coagulation activity of Roselle seed extract

Based on this result, industrial wastewater required higher amount of roselle extract in order to achieve high turbidity removal. This showed that the coagulant activity of roselle seed was reduced when there are unwanted particles existed in the wastewater. This may be caused by the various contaminants existed in the wastewater that inhibit the natural coagulants to perform at their best. Basically the coagulant dosage required to reduce the turbidity level is depend on the characteristic of the wastewater and the aim of the treatment process. Wastewater consists of high amount of negative charge particles required high amount of natural coagulant for complete stabilization.

The highest turbidity removal efficiency for aluminium sulphate was within 82.9-99.0% over wide range of turbidity. The best performance of alum was observed at pH 7 over the selected range of turbidity but its performance decreased to some extent at pH values of 4, 5 and 8. [4]. The highest removal efficiency of roselle seeds was within 81.2 to 93.13% for synthetic wastewater at pH 4 and within 76.8 to 87.18% at pH 10. This showed that the natural coagulant extracted from roselle seeds gave comparable performance with existing synthetic coagulant in coagulation water treatment process.

## 4. Conclusions

The quality of the wastewater treated by using natural coagulant is comparable to the quality of the wastewater treated by commercial coagulant and hence can be used to replace aluminium sulphate as commercial coagulant. The highest removal efficiency of roselle seeds was within 81.2 to 93.13% for synthetic wastewater at pH 4. However, the highest removal efficiency for industrial wastewater was within 76.8 to 87.18% at pH 10. For future work, the optimum method of extraction of each of the natural coagulants can be found. There are various types of protein extraction such as solvent extraction which are using water, oil, sodium hydroxide and alcohol like ethanol to extract the protein out of the seed. The best extraction method would be the one that can extract the most coagulant chemicals out of the kernel. Hence, the best method for extraction of this coagulant can be determined together with the optimum condition such as coagulant dosage, temperature, pH and turbidity of the water.

## References

[1] A. I. Cissouma, F. Tounkara, M. Nikoo, N. Yang, and X. Xu, “Physico Chemical Properties and Antioxidant Activity of Roselle Seed Extracts,” vol. 5, no. 11, pp. 1483–1489, 2013.

[2] E. N. Ali, S. A. Muyibi, H. M. Salleh, M. R. M. Salleh, J. Gombak, I. Islamic, J. Gombak, and C. Author, “Moringa oleifera seeds as natural coagulant” pp. 163–168, 2009.

[3] G. Muthuraman, S. Sasikala, and N. Prakash, “Proteins from Natural Coagulant for Potential Application of Turbidity Removal in Water,” vol. 3, no. 1, pp. 278–283, 2013.

[4] A. Baghvand, A. D. Zand, N. Mehrdadi, and A. Karbassi, “Optimizing Coagulation Process for Low to High Turbidity Waters Using Aluminum and Iron Salts,” vol. 6, no. 5, pp. 442–448, 2010.

# Design an Adsorption Unit for Lake Water Treatment from Taylor's University

Nur Fatinah Abd Aziz[1], Rajesh Nithyanandam[2]

[1, 2]*Chemial Engineering Department, School of Engineering, Taylor's University Lakeside Campus, Malaysia*

**Corresponding email: Rajesh.Rajasekaran@taylors.edu.my*

*Abstract*— **Adsorption process is commonly known to treat water at low cost especially when the adsorbent used are biomass such as agricultural waste. In this study, rice husk was selected as the adsorbent due to the abundant availability in Malaysia and previous study shown the successful removal of different types of heavy metal and dye by adsorption process. Rice husk was prepared at different conditions to select the best for heavy metal removal in lake water in preliminary study. The study continued at column and result obtained was used to identify isotherm and kinetic model that fits the adsorption data.**

*Keywords*— Adsorption; Rice Husk; Natural Adsorbent; Copper

## 1. Introduction

Wastewater treatment is one of the essential processes in industrial area especially when the waste produced from the process is toxic or containing heavy metal that will harm the surrounding if overexposed. Since the clean water source for human is obtained mostly from river, the proper wastewater treatment is needed before being released to the nearby river. However different processes need different kind of water treatment. Therefore a few water treatment processes are developed depending on the type of waste to be treated. The most common process that has been widely used recently is adsorption process. Adsorption method is preferable when compared to other separation such as membrane separation and coagulation/flocculation processes due to the recently use of biomass product as the natural adsorbent to replace the conventional adsorbent such as commercial activated carbon and silica gel [1]. This low cost and unconventional adsorbent can be made from agricultural wastes such as fruit peel [2], sugarcane and peanut shell [3]. Most of the natural adsorbent has been researched to successfully remove the heavy metal and dye from wastewater.

One of the attractions in Taylor's University Lakeside Campus, Malaysia is the lake itself which located at the centre of the campus. The lake is a stagnant body where the main source of the water comes from rain water and the surface runoff from surrounding discharged the pollutants into the lake. The lake water is not polluted with large amount of heavy metal yet but the water still need to be treated to meet the clean water quality standard.

Thus a project is proposed to design an adsorption unit to be used in treating Taylor's University lake water. The main objective of this study is to design an adsorption unit to treat contaminants in lake water by using natural based type adsorbent. A natural adsorbent is chosen based on literature review and the abundant availability in Malaysia in which rice husk is selected to be used in this study. Since adsorption is the main process in this study, a concentration to be study is needed to conduct the research. Based on previous Taylor's University Lake Water 2010 Full Report, amount of copper content in lake water was higher than the Standard A and B for water quality in Malaysia. Thus copper is the heavy metal that will be treating in this study. A series of batch experiment is conducted to test different parameters such as contact time, adsorbent dosage and pH. The selected adsorbent and parameter are further tested in adsorption column and the equilibrium data is prepared to evaluate the adsorbent performance.

## 2. Methodology

### 2.1 Adsorbent Preparation

Rice husk (Type: Short Malinja Paddy R-16) was obtained from local rice mill located in Muar, Johor. The rice husk was sun-dried for 3 days to remove any water content. Preliminary experiment was conducted for water parameters with three different condition of rice husk were used. Rice husk (Type I) was crushed first with blender and sieved at 500 $\mu m$ sieve (Model: RX-812-1) which is equivalent to 35 mesh size. The sample was stored in airtight container for future experimentation. (Type II) The crushed sample was pretreated with analytical grade $H_3PO_4$ for 24 hours to remove any impurities and colour pigments. Sample was filtered with Whatman No.1 Filter Paper oven dried at 110℃ for 24 hours to remove remaining acid. (Type III) The raw rice husk was washed with distilled water several times to remove impurities and colour pigments. Oven dried at 110℃ for 24 hours before being stored in dessicator for future use.

### 2.2 Batch Adsorption Experiment

#### *2.2.1 Preparation of Copper Stock Solution*

10 mg of analytical grade copper sulphate pentahydrate ($CuSO_4.5H_2O$) was dissolved in 500 ml of distilled water. Distilled water was added until the solution reached to 1 litre.

#### *2.2.2 Effect of Contact Time, Adsorbent Dose and pH*

pH of stock solution was adjusted with BP pH meter (Model: 3001 Trans Instrument) to 6.5 using either NaOH or HCl similar to the pH of lake water. 1 g of prepared adsorbent was added to six conical flasks. 200 ml of copper stock solution was transferred to the flasks and agitated at 150 rpm speed with WiseStir Magnetic Stirrer (Model: SMHS-3, DAIHAN Scientific Co., Ltd, Korea) at room temperature 25℃ for different periods. The contact time was set to 10, 20, 30, 40, 60 and 90 minutes. The solution was immediately filtered with Whatmann No. 1 Filter Paper to determine the final copper concentration with PinAAcle 900 AAS Spectrometer (Model: 900F, PerkinElmer Inc., USA). The impurity removed was calculated based on (1) and a graph was plotted for amount of impurities removed against contact time. Optimum contact time was obtained from the graph.

$$q_e = \frac{(C_i - C_e)V}{W} \quad (1)$$

Different dose of adsorbent were added to six conical flasks (0.5 g, 0.7 g, 1.0 g, 1.5 g, 2.0 g and 2.5 g) contained 200 ml of stock solution. pH of stock solution was fixed at 6.5 and stirred at optimum contact time obtained from previous experiment.

pH of copper stock solution was adjusted to five different pH (pH 3, 5, 7, 8, 9) by calibrated with BP pH meter (Model: 3001 Trans Instrument) and 200 ml of stock solution was added to five conical flasks. All solution were stirred with WiseStir Magnetic Stirrer (Model: SMHS-3, DAIHAN Scientific Co., Ltd, Korea) at optimum contact time and adsorbent dosage obtained from previous study.

### 2.3 Column Experiments

Adsorption column was designed using acrylic column with internal diameter of 46 mm and height 460 mm (Height to Diameter Ratio = 10). The column was in down flow mode and peristaltic pump was used for pumping in the lake water. Three different flow rate and bed height were used (3, 5 and 7 ml/min) and (50, 100 and 150 mm) respectively. The effluent sample was collected at time interval of 10 minutes and breakthrough curve was plotted for each of the variables.

#### *2.3.1 Adsorption Studies*

The equilibrium data obtained from column experiment were used to determine the loading behavior of copper removal using rice husk by testing with Freundlich and Langmuir isotherm equations based on (2) and (3) respectively. Linear equations for both models were correlated and the adsorption capacity was obtained.

$$q_e = K_F C_e^{1/n} \quad (2)$$

$$q_e = \frac{q_m K_L C_e}{1 + K_L C_e} \quad (3)$$

#### *2.3.2 Kinetic Studies*

In this work, Thomas model were used and the expression for the model in adsorption column are as (4)**;**

$$\frac{C_t}{C_o} = \frac{1}{1 + exp(k_{Th} q_o \, m/v - k_{Th} C_o t)} \quad (4)$$

Where $k_{Th}$ and $q_o$ were obtained from linear graph plotted to determine the breakthrough curve of $\frac{C_t}{C_o}$ against $t$ . $q_o$ is the equilibrium Cu(II) uptake per g of rice husk adsorbent (mg/g) [4].

## 3. Result and Discussion

### 3.1 Rice Husk Preparation


Fig.1 Different Condition of Rice Husk Used for Preliminary Experiment

### 3.2 Preliminary Experiment using Rice Husk Type I

Table 1. Amount of Turbidity Removed at Different Contact Time using Rice Husk (Type I)

| Initial Turbidity (NTU) | Adsorbent Dosage (g) | Amount of Lake Water (ml) | Contact Time (minute) | Average Final Turbidity (NTU) |
|---|---|---|---|---|
| 3.46 | 1 | 200 | 10 | 3.40 |
| | | | 20 | 3.25 |
| | | | 30 | 2.68 |
| | | | 40 | 2.58 |
| | | | 60 | 3.04 |
| | | | 90 | 3.12 |

Table 2. Amount of Turbidity Removed at Optimum Contact Time and Different Adsorbent Dosage

| Initial Turbidity (NTU) | Contact Time (minute) | Amount of Lake Water (ml) | Adsorbent Dosage (g) | Average Final Turbidity (NTU) |
|---|---|---|---|---|
| 3.46 | 40 | 200 | 0.5 | 5.01 |
| | | | 0.7 | 4.88 |
| | | | 1.0 | 2.54 |
| | | | 1.5 | 2.76 |
| | | | 2.0 | 3.05 |
| | | | 2.5 | 6.34 |

Type 1 rice husk had shown that the optimum contact time where the least value turbidity can be obtained at 40 minutes. However when the experiment continued for different adsorbent dosage, the average final turbidity showed inconsistent value and more turbid after the treatment. This caused by untreated rice husk as the sieved rice husk contained lots of colour pigments and impurities that needed to be removed before being used. Type I rice husk was not used for further column experiment.

For the column study, previous study had shown that removal of Cu(II) equilibrium sorption data using Rice Husk based Activated Carbon fitted Freundlich isotherm and Thomas model [4].

## 4. Conclusion

This study is still ongoing and based on the result obtained in the preliminary study, the sieved rice husk must be treated first before being used as rice husk contained a lot of impurities and release colour pigment once being crushed to smaller forms. However untreated rice husk gave better result for different contact time which showed the high possibility to be used in adsorption process by modifying the rice husk to obtain optimum efficiency. Application of rice husk gives beneficial in economy area by reducing cost in adsorption process and also in the biomass waste treatment.

## References

[1] O. S. Amuda and A. O. Ibrahim, "Industrial wastewater treatment using natural material as adsorbent," *African J. Biotechnol.*, vol. 5, no. August, pp. 1483–1487, 2006.

[2] G. C. Ribeiro, L. M. Coelho, and E. Oliveira, "Removal of Cu(II) from Ethanol Fuel Using Mandarin Peel as Biosorbent," *Bioresources*, vol. 8, no. 3, pp. 3309–3321, 2013.

[3] H. Nadi, M. Alizadeh, and M. Ahmadabadi, "Removal of Reactive Dyes ( Green , Orange , and Yellow ) from Aqueous Solutions by Peanut Shell Powder as a Natural Adsorbent," *Arch Hyg Sci*, vol. 1, no. 2, pp. 41–47, 2012.

[4] N. K. E. M. Yahaya, I. Abustan, M. Faizal, P. Mohamed, O. S. Bello, M. A. Ahmad, E. Campus, and E. Campus, "Fixed-bed Column Study for Cu ( II ) Removal from Aqueous Solutions using Rice Husk based Activated Carbon," *Int. J. Eng. Technol.*, vol. 11, no. 1, pp. 186–190, 2011.

# Personalized Learning in Chemical Engineering Process Control

Po Wei Yoong[1], Douglas Tong Kum Tien[2*]

[1]*Chemical Engineering, Taylor's University, Malaysia* [2]*Mechanical Engineering, Taylor's University, Malaysia*

**Corresponding email: DouglasKumTien.Tong@taylors.edu.my*

*Abstract*—**This study aims to evaluate the effectiveness of student learning experience by introducing a personalized learning approach. Multiple Intelligence Theory (MIT) is used as the basic of this approach. A total of 35 Chemical Engineering students were surveyed to identify their learning preferences. The relationship between the survey result and teaching technique was analysed before a method was proposed to personalize the learning of a specific topic of this subject to the students as an initial experiment.**

*Keywords*— Personalized Learning, Multiple Intelligence, Process Control

## 1. Introduction

Process Control is important in the industry to ensure the product quality, safety and process efficiency and consumption. Every process requires specific design to accommodate its parameters[1][2][3][4]. It is important to have the ability to identify the nature of the process in order to design the control system.

Every individual was brought up in a different environment, teaching methods and thus having a wide diversity of learning profiles[5]. By acknowledging the diversity of learning styles, approaches in learning and intellectual development, we can conclude that no two minds are alike[6]. Thus, a wide range of innovative teaching methods was introduced over the years in order to improve the quality of education and one of them is Personalized Learning.

In a nutshell, the science of human brain is one of the important key areas of study. In the context of education, individual cognitive development is often associated with teaching methods. In one of the findings by [6], they identified the categories of diversity which are Learning Styles, Approaches to Learning and Orientation to Studying and Intellectual Development. These categories explain the effect of personal growth and unique needs in the process of learning.

### 1.1 Objective

The main objective of this research is to study the effectiveness of Personalized Learning in Chemical Engineering module. By introducing Personalized Learning in Engineering Curriculum will not only allow the students to trigger their cognitive skills in learning, at the same time this will act as a self-discovery of their own ability and inner talent that can be utilized in many ways.

## 2. Theoretical Framework

### *2.1. Multiple Intelligence*

From the founding of neuroscience[7], there are substantial relationship of that with learning process. The ability of understanding a theory or fact is closely related to the type of perception and analyzing skills that present naturally within oneself. One could have more than one type of approach in solving problem and it is known as multiple intelligence [1]. During the 1980s a range of intelligence that was proposed and it was then regarded as a base for research. Musical Intelligence, Bodily-Kinestetic Intelligence, Logical Mathematical Intelligence, Linguistic Intelligence, Spatial Intelligence, Interpersonal Intelligence, and Intrapersonal Intelligence are the basic intelligence proposed during the early years and across the centuries, more new intelligence was discovered uniquely in their own way. These intelligence describes how one person interprets and deliver their own view through their individualize approach[8][9]. In a conclusion of this founding is that no two individual would have the same intelligence profile.

### *2.2. Learning Styles*

Understanding personal psychology type is important as the first step in order to make improvement in the effectiveness of their work. The Myers-Briggs Type Indicator described 4 facets of type which are personal integration with the surrounding, "perceiving processes", "judgment processes" and "preferences among the mental processes"[10]. Identification of student's learning patterns would help the educators to enhance their unique dominant by designing effective teaching instrument. For an example, two individual can be an Extrovert but they are different in Judging and Perceiving. At some point, they might show a mixture of two distinguished pattern of a facet, but there will dominance on of the pattern. Research [6] finds that engineering modules are biased towards introverts, intuitors, thinkers and judgers. Through Personalized Learning it is aimed to bring this gap between the current teacher-centered teaching methods close to the unique learning styles of the students.

## 3.0 Research Methodology

The experiment for this study is to be conducted in "Process Control System Design" topic. It is a form of assignment and this topic requires students to relate process integration and equipment specification in the design.

Based on the learning preference of the students, an instrument was proposed to assist in the student's learning process. This instrument is a 3D Rapid Prototype Model, resembled the main equipment of the process in a given case study. It allows the students to relate technical knowledge to the problem statement before generating the solution.

### 3.2. Participants

This study group consists of a total of 35 Year 3 Chemical Engineering students who enrolled in the Process Control module. They are then divided into two groups- Controlled Group (CG) and Uncontrolled Group (UG).

### 2.4 Data Inputs

#### *2.4.1 Pre-test Survey*

This pre-test survey involves students and also the industry. It aims to collect the feedbacks of the students' past experience towards the teaching method of the subject, learning styles, intelligence profile, and also determine the expectation between the industry and the learning institution. Students were given survey forms while interview session was carried out with industrial personnel.

*2.4.2 Post-test Survey*

It is important to run a survey on the Controlled Group in allowing them to comment on their experience with the model they have been using as a tool in their learning process. The areas will be covered in the survey includes the effectiveness of the tool in generating clearer definition of their challenge given, area of improvement of the tool, the importance of the hardware in every module and also the individual motivation to learn.

2.5 Data Analysis

Results from the survey are analyzed to see the population of the learning profiles in the class. This result has to be further validated through student informal interview and also the lecturers because the questionnaire given out to the students are from the source of different culture and background.

Results from the post-test survey are very useful in improving the design of instrument to further enhance the effectiveness in student's learning in class.

## 3. Result

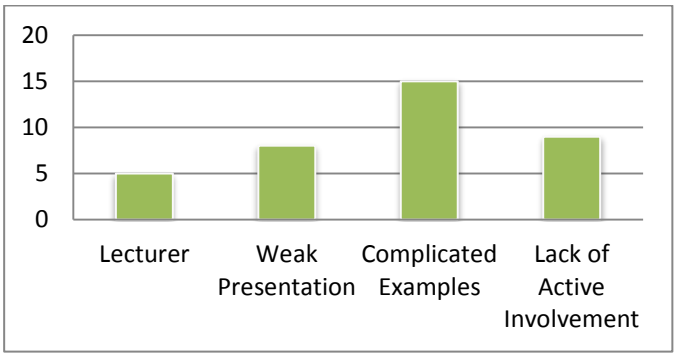


Fig. 1 Student's response towards the module

Engineering subjects requires understanding theoretically and also imaginative applications of the knowledge into real life operations. From Figure 1, about 15 student facing difficulty in relating complicated examples. According to the students, they need additional material in order to visualize the challenge and by saying so, students' need the class to be conducted in an interactive environment too. Out of the 24 students responded to the other 3 reasons of why the module is difficult to understand, 10 of them confessed that they lose interest and motivation in attending classes because they couldn't get the gist of every lecture they attended due to weak presentation by lecturer and also minimum involvement of the students in the class. Thus, for technical topics which need visual and concrete material for understanding, a downsized model would be an effective tool to be used.

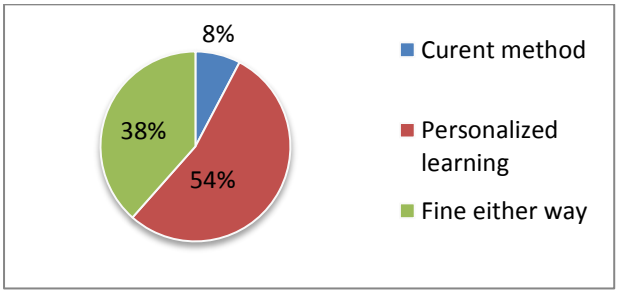


Fig. 2 Student's response towards different teaching methods

The response of students towards different learning methods is illustrated in Figure 2. 54% of them realized the benefits of Personalized Learning after being briefed about what exactly it is all about, while 8% prefers the current method and some of them thought that neither of them will affect their current learning method. The survey extended to discover learning preference of the students in the group. Students who choose to stay with the current method found to be Linguistic dominant as the class material are of more words, while the others are having different Intelligence dominant and learning styles. These responses seem to that personalized learning aimed at each individual's learning style is effective for learning technical subjects in engineering.

## 4. Conclusion

From the study, the results show that personalized learning is suitable for engineering students who are learning technical subjects. They are seen to be more motivated and benefitted form this experiment to personalize their learning. However, this initial experiment model needs to improved and as for the future work, personalized learning are to be designed for other engineering modules.

## 5. References

[1] E. Hosgor, T. Kucuk, I. N. Oksal, and D. B. Kaymak, "Design and control of distillation processes for methanol–chloroform separation," *Comput. Chem. Eng.*, vol. 67, pp. 166–177, Aug. 2014.

[2] J. J. Downs and S. Skogestad, "An industrial and academic perspective on plantwide control," *Annu. Rev. Control*, vol. 35, no. 1, pp. 99–110, Apr. 2011.

[3] T. Chai, S. J. Qin, and H. Wang, "Optimal operational control for complex industrial processes," *Annu. Rev. Control*, vol. 38, no. 1, pp. 81–92, 2014.

[4] M. Kano and M. Ogawa, "The state of the art in chemical process control in Japan: Good practice and questionnaire survey," *J. Process Control*, vol. 20, no. 9, pp. 969–982, Oct. 2010.

[5] M. Liu and P. Yu, "Aberrant Learning Achievement Detection Based on Person-fit Statistics in Personalized e-Learning Systems.," *J. Educ. Technol. Soc.*, vol. 14, pp. 107–120, 2011.

[6] R. Felder and R. Brent, "Understanding student differences," *J. Eng. Educ.*, vol. 94, no. 1, pp. 57–72, 2005.

[7] H. Lalancette and S. R. Campbell, "Educational neuroscience : Neuroethical considerations," vol. 7, no. 1, pp. 37–52, 2012.

[8] Z. Özdilek, "To what extent do different multiple intelligences affect sixth grade students' achievement level on the particle model of matter?," *Procedia - Soc. Behav. Sci.*, vol. 2, no. 2, pp. 4858–4862, Jan. 2010.

[9] H. Sözen, M. Sözen, and A. Tekat, "Comparison of the profiles of the potential teachers in different disciplines based on multiple intelligences theory (Samsun City Sample)," *Procedia - Soc. Behav. Sci.*, vol. 1, no. 1, pp. 943–948, Jan. 2009.

[10] D. Gordon, *People Types & Tiger Stripes*, Third., no. 7. Gainesville, Florida: Centre for Applications of Pshychological Type, 1993.

# Palm Oil Waste as Fuel Source in a DCFC

Sean, M[1], Doshi, V[2]

[1]School of Engineering,Taylor's University,Malaysia, [2]School of Engineering, Taylor's University, Malaysia

*Corresponding email: VeenaADoshi.ArunKumarDoshi@taylors.edu.my

***Abstract*— Biomass is an important renewable source contributing to the world's economy, sustainability and energy security. Direct carbon fuel cells with solid oxide electrolyte (DC-SOFC) has attracted growing attention recently as an efficient generator of electricity. In this research,Palm oil Mesocarp Fiber is used as the raw material to produce biochar. Pyrolysis condition of heating rate and residence time is held constant at 10°C/min and 2 hours respectively. Three set of temperature is used which are 400, 600 and 800 °C. The biochar's is fed into a Solid Oxide Fuel Cell to generate electricity. Biochar produce at 400, 600 and 800 C have surface area of 353.0, 548.6 and 706.0 respectively. Biochar produce from Mesocarp fiber have high surface area and porosity which would make it a suitable fuel source in a DCFC.**

*Keywords*— Direct carbon fuel cells, Biomass, Biochar, Pyrolysis

## 1. Introduction

Global energy demand throughout the world is increasing at a very rapid rate. Much of the energy consumption comes from non-renewable source that contribute heavily to air pollutions and global warming. At least 168 million tons of biomass such as timber, palm oil waste, rice husks, coconut trunk fiberand sugar cane waste is produced annually[1]. This research aim to test lignocellulose biomass as a suitable fuel source in a direct carbon fuel cell (DCFC's). DCFC are a relatively new technology that opens new opportunities to convert carbonaceous fuels to electricity.The biggest attraction in DCFC is that it can run oncarbon products produced from biomass waste called biochar. Biochar are intermediate solid residue of thermal conversion of organic substance formed through the process of pyrolysis of Lignocellulos biomass.

### 1.1Objective

The objective of this research is to:

- Optimize the production of biochar from palm oil Mesocarp Fibre using slow pyrolysis process;
- Characterize the biochar for its carbon properties such as surface area, porosity, structure, carbon content and impurities;
- Measure the performance of the biochar in DCFC;
- Access and optimize biochar carbon properties in generating electricity in a DCFC

A wide variety of biomass material have been used to produce biochar however no work have been done on producing biochar from Mesocarp Fibre. Significant majority of research on biochar are in the areas of soil amendments for fertilization of crops and as an activated carbon for $CO_2$ capture. They have been no work done on using biochar from palm oil waste as a fuel source in a DCFC system.

### 1.1 Scope

Mesocarp Fibre is used as the raw material to produce biochar. Pyrolysis condition of heating rate and residence time is held constant at 10°C/min and 2 hours respectively. Three set of temperature is used which are 400, 600 and 800 °C. The biochar's is fed into a Solid Oxide Fuel Cellto generate electricity.

## 2. Theoretical Framework

### 2.1Direct Carbon Fuel Cells (DCFC)

Direct carbon fuel cells (DCFC) convert carbonaceous fuels directly into electricity. Fine carbon particles are directly oxidized in an electrochemical cells at high temperature ranging from 600°C to 900°C. This process is a half-cell notation where the overall reaction is [2];

Cathode: $O_2\ (air) + 4e \rightarrow 2O^{2-}$ (1)

Anode: $C + 2O^{2-} \rightarrow CO_2 + 4e$ (2)

In this research, Solid Oxide fuel cell is choses as it is the most developed fuel cell with benefits of fuel flexibility and simplicity to operate [2]. Figure 1 depicts the mechanism of a solid oxide fuel cell using carbon as a fuel source.

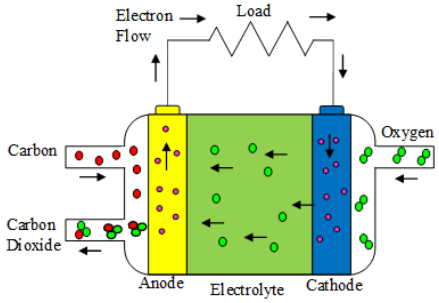


Figure 1: Mechanism of Solid Oxide Fuel Cells [2]

#### *2.1.1 DCFC Fuel Source*

A large number of carbon rich fuels such as coal and activated carbon can be fed into a DCFC.A study on the interaction between carbon and anode in a SOFC using four grades of coal found that the higher the pore size and surface area of the coal the higher the power output of the fuel cell [3].The carbon fuel must be of highly porous material with high surface area to be able to adsorb oxygen which acts as an electrolyte in a SOFC system [3].

### 2.2 Lignocellulose Biomass

Biomass composition can vary depending on biomass type and origin. The term "lignocellulose biomass" is used when referring to woody biomass. The main components of the lignocellulose materials are cellulose, hemicellulose and lignin [4]. Lignin is reported to be the most thermally resistance component in biomass and start to decompose at temperatures above 400 °C [4]. This decomposition of lignin produces some bio-oil but the majority of the lignin remains as a solid and contributes heavily to the mass of the biochar product.

### 2.3Biochar Preparation

Pyrolysis is the thermal decomposition process of biomass which takes place in the absent of oxygen at atmospheric pressure. Biochar are black solid. The biochar is intermediate solid residue, which is formed in the pyrolysis of most biomass. At low temperature and low heating rate process, high bio-char production can be gained from the process [5].A study on the characterization of biochar products from pyrolysis of Miscanthus at a constant temperature of 600°C and varying residencetime of 10, 30 and 60 minutes found that the longer the residence time the more developed the surface area of biochar

[6].A recent studied on the influence of pyrolysis conditions on pore development of oil-palm-shell activated carbons found that as heating rate increase, the initial BET surface, micro and macro pores area also increased [7].However progressive increase in heating rates above 10°C/min gradually reduce the surface areas and pores volume [7].

## 3. Research Methodology

### 3.1Sample Preparation

Palm Oil Mesocarp Fibre was dried at 103°C. The dried palm oil waste is then milled using a cutting mill with a 1 mm blade and then sieve with a Retch sieve shakerranging between 1.00 to 2.00 mm.

### 3.2Pyrolysis Experiment

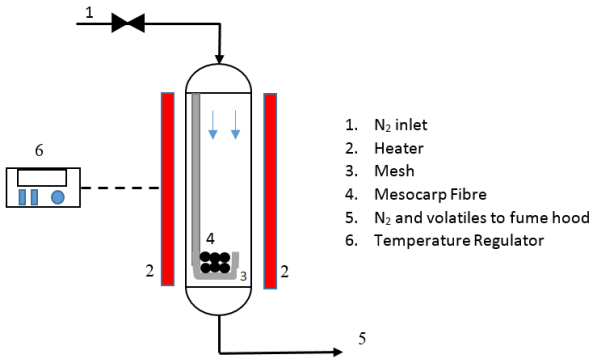


Figure 3: Schematic diagram of the pyrolysis system

The pyrolysis of Mesocarp Fiber samples is carried out using a reactor equipped with an electric furnace heater as shown in Figure 2. 1 g of each sample is placed into the reactor tube on a wire mesh sample holder.Three set of temperatures would be perform at 400, 600 and 800°C. The heating rate of 10°C $min^{-1}$ is chosen as it coincide with slow pyrolysis method in producing high yield of biochar. Pyrolysis residence time is measured from the time when samples in the reactor reached the desired temperature and isothermal heating is held. The experiment will be conducted for residence time of 2 hours. The reactor is purge with nitrogen gas at a rate of 100 l/min to ensure no oxygen is present in the reactor tube.

### 3.3 Mesocarp and Biochar Analysis

Table 1 shows the types of analysis that would be performed on the Mesocarp fibre and biochar.

Table 1: Table of Analysis on biochar and Mesocarp Fiber

| Analysis | Description |
|---|---|
| Proximate | Determine properties of moisture content, volatile matter, fixed carbon and ash content. |
| Ultimate | Determine the carbon, hydrogen, nitrogen, sulphur and oxygen content by weight |
| BET | Brunauer-Emmet-Teller (BET) analyser is used to determine the physical properties of biochar relating to specific surface area and porosity. |
| XRD | X-Ray Diffraction (XRD) analysis is used to determine the atom and molecular crystalline structure of the biochar |

### 3.4Solid Oxide Fuel Cell Test

The biochar is fed into a furnace and heated to a desired temperaute of 550 °C. The heated biochar is then fed into a SOFC device under a variable resistance load, which adjusts the outputs of cell voltage and power. This power output is then measured and the power density (ΔE-I) and current density (ΔP-I) is then calculated and plotted to obtain the ΔE-I and ΔP-I curve.

## 4. Results

### 4.1Thermogravimetric Analysis (TGA) on Mesocarp Fiber

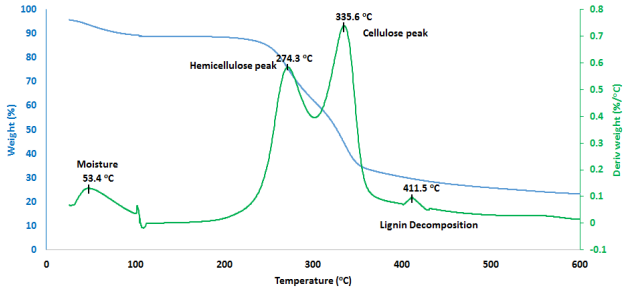


Figure 1: TGA analysis on dry Mesocarp Fiber

The TGA analysis shows the thermal behavior of biomass samples by recording peaks of volatile matter release at different temperature. Four peaks around 53.4, 274.3 and 334.6°C is due to volatiles release from decomposition of moisture, hemicellulose and cellulose while the lignin decomposes at a much higher temperature around 411.5 °C.

### 4.2Surface Area and Pore Size

Table 2 shows the results of $CO_2$ analysis perform for biochar samples at 400, 600 and 800 °C.

Table 2: Results of surface area and pore size at 400, 600 and 800 °C

| Temp (°C) | Surface Area (m2/g) | Total pore area (cm2/g) |
|---|---|---|
| 400 | 353 | 219.38 |
| 600 | 548.6 | 379.4 |
| 800 | 706 | 482.126 |

From table 2, it is clear that the higher the temperature the higher the surface area and total pore area of the biochar. At 400 C, the total surface are is 353 m2/g while at 800 C the surface are is double at 706 m2/g. This indicates a linear relationship between temperature and surface area.

## 5.0 Conclusion

From the research, it was found that the lignin in Mesocarp fiber starts decomposing at 411 °C. Biochar produce from Mesocarp fiber have high surface area and porosity which would make it a suitable fuel source in a DCFC. The carbonization step at high temperature is detrimental to the development of a porous structure in the biochar.

## REFERENCE

[1] Ali, H.I., Irvan, D., M,Nordin.,Azeroo, F.D. (2012). Comparative Study on Characterization of Malaysia Palm Oil Mill Effluent.*Research Journal Chemical Science* 2(12), 1-5

[2] Xavier F.A., Bin Z., Rizwan R. (2010).Innovative biomass fuelled SOFC's for polygeneration. Master's Thesis, Sweden

[3] Desclaux, H.C.,Schirmer, M.,Woiton, E. (2013). Influence of the Carbon/Anode Interaction on Direct Carbon Conversion in a SOFC. *Journal of Electrochemical Science8*, 9125-9132

[4] Yang, H.,Yan, R., Chen, H., Lee, D.H. (2007) Characteristics of hemicellulose, cellulose and lignin pyrolysis. *Fuel 8*, 1781-8.

[5] M. Azri, S., Loh, S.K., Nasrin, A.B., &Choo, Y.M. (2011). Production and Characterization of Bio-Char from the Pyrolysis of Empty Fruit Bunches. *American Journal of Applied Sciences 8* (10), 984-988

[6] Magdalena, D., Piotr, T., Robert, S., Marek, S., Janusz, J. (2013).Biomass Fuels for Direct Carbon Fuel Cell with Solid Oxide Electrolyte.*Journal of Electrochemical Science 8*, 30-239

[7] Aik, C.L., Fong, Y.L., Jia, G. (2005). Influence of pyrolysis conditions on pore development of oil palm shell activated carbon. *Journal of Analytical and Applied Pyrolysis 76*, 96-102

# Removal of Cadmium Ions from Aqueous Solution by Biosorption on Immobilized Microalgae

Siti Azzura Binti Md Lasa[1], Masniroszaime Binti Md. Zain[2]

[1,2]*Chemical Engineering Department, Taylor's University, Malaysia,*

**Corresponding email: Masniroszaime.MdZain@taylors.edu.my*

***Abstract*— Concern on environment is increasing when wastewater contains heavy metals because it can affect health of human and needs to be treated well. In this study, *Nannochloropsis Oculata* was used to remove cadmium ions from aqueous solution. The parameters that affect the biosorption process such initial concentration of metal ions, pH of solution and solid/liquid ratio was studied in batch experiment. The equilibrium data for the biosorption of cadmium ions onto *Nannochloropsis Oculata* was fitted to the Langmuir and Freundlich isotherm. From experimental results, *Nannochloropsis Oculata* could be chosen as one of an alternative biosorbent to remove cadmium ions from aqueous solution due to its high efficiency of biosorption and availability in Malaysia.**

*Keywords*— *Nannochloropsis Oculata*, cadmium, biosorption,

## 1. Introduction

The existence of heavy metals in wastewater has become major environmental concern as they are poisonous to all living organism including human beings. The most hazardous metals ions contaminated in effluent discharge may include cadmium, chromium, copper, zinc, lead, arsenic, and nickel from variety sources such as electroplating, metalliferous mining and electronic industries [1]. Heavy metals are non-biodegradable substances and may accumulate in living organism once they consume the polluted water. Amongst the harmful heavy metals, cadmium is considered as priority pollutant because its toxicity in relatively low dosages. Based on Malaysia Environmental Law, ENVIRONMENTAL QUALITY ACTS 1974, the Malaysia Environmental Quality (Sewage and Industrial Effluent) Regulations, the permissible limit for cadmium ions relesase to environment is 0.01mg/l for Standard A while for Standard B is 0.02 mg/l.

There are many methods used to remove metal ions from wastewater include adsorption, coagulation, flocculation, ion exchange, precipitation, electrodialysis, and ultrafiltration. These methods are reported to be high cost and have several disadvantage aspects such as incomplete metal removal, high cost of reagent, expensive equipment and high energy requirement [1]. Biosorption has become one of alternative method which use biological materials such as agricultural wastes as biosorbents. It is a biological process which uses cell wall of biological materials which segregate the metal ions from aqueous solution [1]. The microalgae cell have high binding capacity due to the cell wall has several functional groups such as amino ($NH_2$), hydroxyl (OH) and carboxyl (COOH) which give negative charge to the cell surface. Since cadmium ions are in cationic form ($Cd^{2+}$), they are adsorbed onto the cell surface because of the different charge ions [2]. This technique claims some advantages such as the reusability of biometerials, low operating cost, no production of other pollutants, and improved selectivity of specific metal ions.

The main objective of this study is to remove cadmium ions from aqueous solution using immobilized microalgae, *Nannochloropsis Oculata* by biosorption process. The effects of initial concentration of cadmium, pH of solution and solid/liquid ratio on the adsorption on cadmium ions are studied. The result obtained is evaluated to investigate the potential of *Nannochloropsis Oculata* as a best biosorbent in removal of cadmium ions.

## 2. Methodology

### 2.1 Material and Chemicals

The *Nannochloropsis Oculata* strain and F/2 medium was purchased from Algaetech International Sdn. Bhd. (Kuala Lumpur, Malaysia) in liquid form. The chemicals used in this study which are cadmium nitrate tetrahydrate Cd $(NO_3)_2.4H_2O$, calcium chloride $CaCl_2$, sodium alginate $C_6H_7O_6Na$ and sodium chloride NaCl were of analytical grade and purchased from R&M Marketing, Essex UK.

### 2.2 Cultivation of microalgae, *Nannochloropsis Oculata*

The medium and conical flasks were sterilized in autoclave machine (Model: SL PMD 2827, Daehan Scientific Co. Ltd.) for 20 minutes at 121°C. 20% of microalgae were used in 100 ml of F/2 medium. The microalgae were placed under light with light intensity of 1800 lux using lux meter (Model: LX-101 Guangzaou Landtek Instrument Co. Ltd) at 25°C. After 14 weeks, the microalgae were harvested by centrifugation at 4000 rpm for 15 minutes to separate from the medium by centrifuge (Model: Universal-32R, Hettich, Germany).

### 2.3 Immobilization of microalgae in alginate beads

The harvested microalgae were suspended with 2% of sodium alginate solution in 1:1 volume ratio in order to get a mixture of algae-alginate suspension. The mixture is then poured into a 50 ml of burette and titrated into a 2% calcium chloride solution. The drops of Na-alginate solution formed into beads around 2 to 3 mm in diameter upon contact with the calcium chloride solution. The beads were left in the calcium chloride solution for 30 minutes at 25 ± 2°C to keep hardening. They were well rinsed with sterile saline solution (0.85%) and stored in refrigerator at 4°C (Model No. SMI 2247802, CKE Holding Sdn. Bhd. Malaysia).

### 2.4 Preparation of synthetic wastewater

The synthetic waste water was prepared using 125 mg/L standard stock solution of Cd (II). This stock solution is prepared from 125 mg of cadmium nitrate tetrahydrate (Cd $(NO_3)_2.4H_2O$) and dissolved in 1L of distilled water

### 2.5 Determination of cadmium uptake by microalgae with different parameters

*2.5.1 Effect of initial concentration*

100 ml of cadmium ions stock solution in four different concentrations, 75mg/L, 125 mg/L, 175 mg/L and 225 mg/L respectively, were prepared and placed in different conical flasks. 1g of alginate beads was weighed using weighing balance (Model: TX 423L, Shimadzu, Japan) and placed in each conical flask. The experiment was carried out triplicate.

*2.5.2 Effect of pH*

The prepared stock solution of cadmium ions were brought to five different pH which are pH 3, pH 5, pH 7, pH 9 and pH 11 respectively by adding hydrochloric acid (HCl) and sodium hydroxide solution (NaOH). The initial pH of each metal solution were adjusted to the required pH by using 0.1M of NaOH and 0.1M of HCl solutions. The pH value was measured using pH meter (Model: BP 3001, Trans Instrument, Singapore). 1 g of alginate

beads were poured into each conical flask. The experiment was carried out triplicate.

*2.5.3 Effect of solid/liquid ratio*

1g of alginate beads was weighed and placed in five conical flasks in different volume of stock solution. The experiment was started by using 50 ml of prepared synthetic wastewater solution followed by 70 ml, 100ml, 150 ml and 200 ml of stock solution. The solution was measured using measuring cylinder. The experiment was carried out triplicate.

### 2.6 Data Analysis

The beakers were then shaken at a constant speed of 100 rpm using Digital Orbital Shaker (LM 400D Yihder Technology, Taiwan) in 45 minutes. After shaken, all samples from each varying variables were separated by filtration through a filter paper (Whatman 125 mm) and were analyzed to find the concentration of cadmium ions by Atomic Absorption Spectrophotometer (Model:900F PerkinElmer, US). All the samples were read three times and the average values were obtained. The amount of heavy metals removed per unit mass of biosorbent was calculated by using the following equation;

$$q_e = \frac{(C_i - C_e)V}{W} \quad (1)$$

While the percentage of biosorption of metal ion can be calculated as equation below,

$$Biosorption\ (\%) = \frac{(C_i - C_e)}{C_i} \times 100 \quad (2)$$

where $C_i$ is the initial metal concentration (mg/L), $C_e$ is the equilibrium concentration of metal solution (mg/L), V is the volume of solution (L), and W is the mass of biosorbent (g).

## 3. Research Outcomes and Discussion

The effect of initial concentration of cadmium solution was studied within the range of 75mg/L to 225 mg/L. From Figure 1, cadmium ions uptake increased with increasing concentration which has been reported by G. Edris which studied of removal of cadmium and lead by *Chlorella Vulgaris* [3]. This is due to the theory that when initial metal ions concentration increase, there is bigger driving force to overcome mass transfer between solid and aqueous phase which lead to increase metal ions adsorption [3].

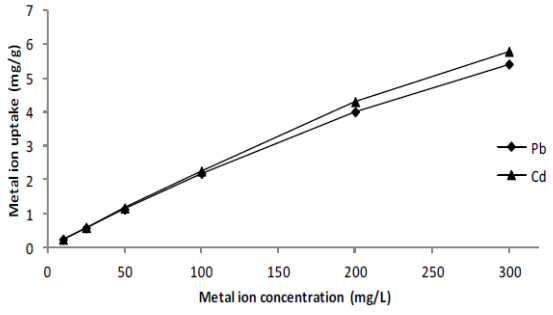


**Figure 1Effect of initial concentration on biosorption of cadmium ions**

The effect of pH on biosorption of cadmium ions onto immobilized microalgae was determined at the pH range of 3-11. From previous study, heavy metals biosorption depends on pH value [4]. Figure 2 showed biosorption capacity increase with pH value but there is no no significant increase above pH 5. This is because pH values affect the active sites of biosorbent and properties of heavy metals in water. At lower pH values the charge on the surface of microalgae is positive and cation adsorption is not desired and hydrogen ions fight with metals ions for their active site. Conversely, at high pH value which is in alkaline phase, there is high repulsion of electrostatic between cations and surface sites which result in high metal uptake. The effect of solid/liquid ratio was investigated by varying the microalgae dosage from 0.5 g to 2.5g with 100ml cadmium stock solution of 125mg/L. The biosorption efficiency increases as the microalgae dosage increases because the amount of sites available for biosorption increases. At optimum biosorbent dosage, further increase of microalgae does not bring to any significant changes because of the saturation of active sites [5].

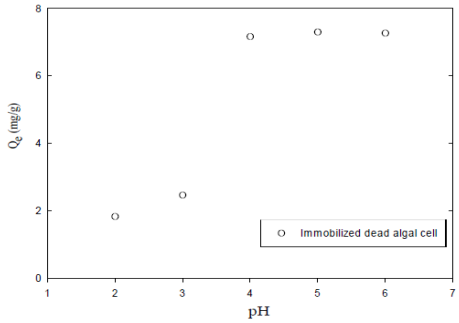


**Figure 2 Effect of pH value on metal ions uptake**

In this study, two isotherm models which are Langmuir and Freundlich were applied to describe surface properties and affinity of the biosorbent used. The Langmuir and Freundlich model can be expressed as follow:

$$q_e = \frac{q_{max} b C_f}{1 + bC_f} \quad (3)$$

$$log\left(\frac{x}{m}\right) = logK_f + \frac{1}{n}\, C_e \quad (4)$$

From Langmuir equation (3), $q_{max}$ refers the maximum amount of cadmium ion adsorbed by the biosorbent and b is the affinity between the adsorbate and adsorbent which indicate the initial slope of the isotherm and $C_f$ refers to concentration of fluid. Higher values of b indicate higher affinity and thus higher sorption efficiency. For Freundlich equation (4), $\frac{x}{m}$ is mass of adsorbate per mass of adsorbent, $K_f$ and $\frac{1}{n}$ are Freundlich capacity factor and intensity parameter respectively.

## 4. Conclusion

The removal of cadmium ions from aqueous solution were carried out in batch experiment with different parameters such as initial concentration of cadmium, pH of solution and solid/liquid ratio. All these parameters which affect the biosorption process were optimized. From the results obtained, *Nannochloropsis Oculata* can be concluded to be a potential biosorbent for removal of cadmium ions. Thus, *Nannochloropsis Oculata* can be used for the development of useful biosorbent materials for heavy metal removal.

## References

[1] M. A. Barakat, "New trends in removing heavy metals from industrial wastewater," *Arab. J. Chem.*, vol. 4, no. 4, pp. 361–377, Oct. 2011.

[2] S. K. Mehta and J. P. Gaur, "Use of algae for removing heavy metal ions from wastewater: progress and prospects.," *Crit. Rev. Biotechnol.*, vol. 25, no. 3, pp. 113–52, 2005.

[3] G. Edris, Y. Alhamed, and A. Alzahrani, "Cadmium and lead biosorption by Chlorella Vulgaris," in *Sixteenth International Water Technology Conference*, 2012, no. Ii, pp. 1–12.

[4] D. Sheikha, I. Ashour, F. A. A. Al-rub, C. Engineering, P. O. Box, G. Gõj, G. Sgqo, Y. Ué, Q. Téy, and T. O, "Biosorption of zinc on immobilized green algae : Equilibrium and Dynamics Studies," *J. Eng. Res.*, vol. 5, no. 1, pp. 20–29, 2008.

[5] G. Değirmen, M. Kılıç, O. Cepelioğullar, and A. E. Pütün, "Removal of copper(II) and cadmium(II) ions from aqueous solutions by biosorption onto pine cone.," *Water Sci. Technol.*, vol. 66, no. 3, pp. 564–72, Jan. 2012.

# Antioxidant Potential of Edible Oils in Malaysia

Xiang Yi Tan[1], Rajesh Nithyanandam[2*]

[1]*Department of Chemical Engineering, Taylor's University, Malaysia,*

[2]*Department of Chemical Engineering, Taylor's University, Malaysia*

**Corresponding email: Rajesh.Rajasekaran@taylors.edu.my*

***Abstract*—DPPH assay was used to determine the antioxidant activity in edible oils. When maintained at room temperature, the order of the effectiveness of free radical scavenging are found to be extra virgin olive oil > rice bran oil > corn oil > palm oil > sunflower oil > groundnut oil > virgin olive oil. Extra virgin olive oil especially has a very high free radical scavenging activity of 27%. The antioxidant activity in edible oils decreased when the temperature were increased to cooking temperature at 80 °C. Quantification of α-tocopherol was performed using a reversed-phase high performance liquid chromatography (RP-HPLC) equipped with photodiode array detector (DAD) at 292 nm. The result shows that rice bran oil has the highest amount of α-tocopherol, which is 17.25 mg per 100g of oil.**

*Keywords*— Antioxidant, α-tocopherol, edible oils, DPPH, HPLC

## 1. Introduction

Edible oils, mainly vegetable oils are rich sources of natural antioxidants. Natural antioxidant is a significant active component in reducing fat oxidation as it removes the free radicals in lipids. Synthetic antioxidants such as butylatedhydroxytoluene (BHT) and butylatedhydroxyanisole (BHA) are reported to have negative effects to human health which lead to liver damage, lung damage and carcinogenesis.This increased the interest towards the study of natural antioxidant potential in edible oils due to their safety to human health.

Free radicals are reactive forms of oxygen which take part in the initiation and propagation of chain reaction in human body.They are highly reactive and harmful to human body as they tend to damage all biological macromolecules including protein, carbohydrates, lipids and DNA within human body.The most common natural antioxidant which can be found in vegetable oils is tocopherol where they react actively with free radicals to form stable compounds in human body. Studies also reveal that antioxidants, especially vitamins E have high free-radical scavenging activity, which help in reducing the risk of diseases such as cancer, neutrological diseases and cardiovascular disease.

The objective of this project is to determine and analyse antioxidant activity in different types of edible oils using DPPH assay. Besides, the effect of heating to antioxidant activity in edible oils is evaluated. High performance liquid chromatography (HPLC) with reverse phase basis was conducted to determine the α-tocopherol content in edible oils.

## 2. Methodology

### 2.1 Materials

Edible palm, sunflower, corn, olive, extra virgin, rice bran and groundnut oils were purchased from local supermarket in Malaysia.

### *2.2 Reagents and Standards*

Methanol, 1,1– Diphenyl -2-picryl-hydrazy (DPPH*), hexane, tetrahydrofuran and α-tocopherol standards of HPLC grade were purchased from Sigma-Aldrich (Malaysia). Ultrapure water was generated by Arium 611UF system (Sartorius Stedim Biotech GmbH, Goettingen, Germany). Standard stock solution of α- tocopherols were prepared in methanol on the day of the experiment.

### 2.3 DPPH Radical Scavenging Method

#### *2.3.1Experiment*

75 µM stock solution of 1,1– Diphenyl -2-picryl-hydrazy (DPPH*) in methanol was prepared. 4 ml of blank solution (contains only DPPH in methanol) was prepared and used as control. The absorbance of the control at 515 nm was measured using a UV-spectrophotometer. 50 µL of oil sample was added to 4 ml of DPPH methanolic solution in a test tube and being wrapped with aluminium foil. All experiments were performed in triplicate. The tubes, in triplicates, were incubated in dark at 25 ° C for 30 minutes. The final absorbance measurements were carried out at 515 nm using a UV – Spectrophotometer. The experiment was repeated with different types of edible oils.

To test for the heating parameter, edible oils, in triplicate were heated to 30 ℃, 40 ℃, 50 ℃, 60 ℃, 70℃ and 80 ℃ respectively and allowed to cool down. Similar steps were carried out to conduct the DPPH experiment. The experiment was then repeated for each type of edible oils. DPPH radical scavenging activity is calculated for each type of oil.

### 2.4High Performance Liquid Chromatography (HPLC) Analysis

Quantification of α-tocopherol content in edible oils using reversed-phase high performance liquid chromatography (RP-HPLC) was performed as described by Gimeno. E (2000) with slight modification.[1]

#### *2.4.1 Equipment*

Separation by HPLC was carried out using a Shimadzu liquid chromatography system (Kyoto, Japan) equipped with a degasser (DGU-20$A_5$), a delivery pump (LC-20AT), an auto sampler (SIL-20A HT) and a column oven (CTO-10AS VP) with a 50 µL sample loop. The detector was a SPD-M20A photodiode-array detector (DAD). The data were stored and processed by LCsolution software (Shimadzu, Kyoto, Japan). The column was a Brownlee C-18 analytical column (150 x 4.4 mm I.D., 5 µm particle size) (Pelkin Elmer, USA).

#### *2.4.2 Samples Preparation*

Oil samples were stored in dark at room temperature (23 – 25 ℃) before the HPLC analysis. Oil sample (about 1 g) was diluted in hexane (1:10). 50 µL of the solution was transferred to a screw-capped tube and diluted with 1 ml of the methanol:hexane:tetrahydrofuran mixture (80:10:10,v/v/v). After being vortexed-mixed and centrifuged (5000 rpm) at 5 min and 10 min respectively, the sample was filtered with a 0.45 µm pore filter and an aliquot of the solution was transferred to an amber-coloured vial. Amber coloured material was used to prevent the loss of α-tocopherol. All the samples are prepared in triplicate. Samples were prepared the day before experiment and were kept in dark at -20 ℃.

#### *2.4.3 Standard Stock Solutions Preparation*

α- tocopherol standard solution of different concentration (0.2, 0.3, 0.5, 1, 3 and 5 mg $L^{-1}$) were prepared for external calibration. The standard curve (concentration against peak area) was calculated by linear regression analysis.The calibration curve constructed was used for quantification of α-tocopherols. α-tocopherol content was expressed in terms of milligrams per 100 g of oil.

*2.4.4 Chromatographic Analysis and Quantification*

The mobile phase was a mixture of methanol-water (96:4, v/v) and eluted at a flowrate of 1 ml/min. The mobile phase was filtered and sonicated before the experiment. The analytical column was kept at 25 ºC. DAD detector was set at 292 nm and total separation time was 15 minutes. The injection volume was 50 µL. Standard solutions were injected into the HPLC before the oil samples to determine the retention time of α - tocopherol. After that, samples of different types of edible oils were analysed. α – tocopherols were identified by comparison of the retention times with the standard α – tocopherol curves. Amount of α - tocopherol can be determined by comparing the peak areas of the samples with the standards.

## 3. Results and Discussion

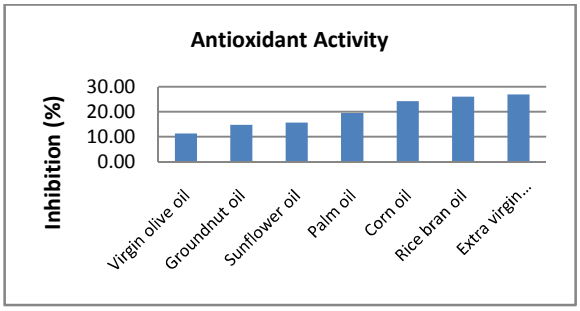


**Figure 3.1 DPPH Scavenging Effect of Edible Oils at room temperature**

As seen from **Figure 3.1**, extra virgin olive oil has the highest DPPH free radical scavenging activity of 27% among all the edible oils tested at room temperature. The result shows that extra virgin olive oil has the most antioxidant content.

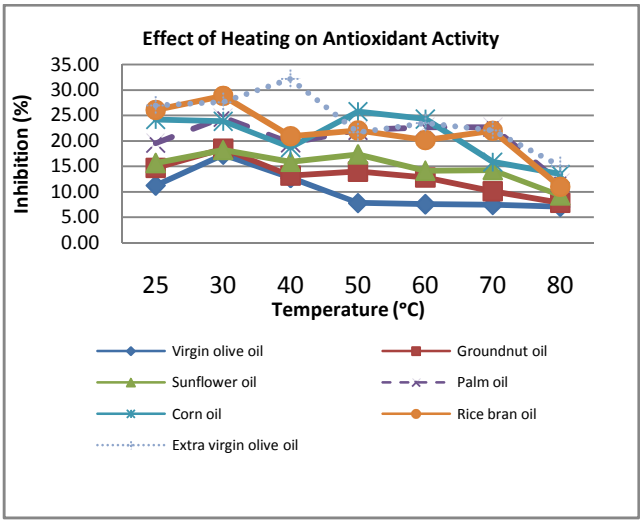


**Figure 3.2 Effect of Heating to Antioxidant Activity in Edible Oils**

It was observed that the antioxidant activity decreased gradually with temperature in **Figure 3.2**. When edible oils were heated to 30 ºC, surprisinglythe DPPH radical scavenging activity for each type of oil increased. According to Tomaino in his studies, heating process might improve the properties of the natural antioxidants in the oils or induces the formation of new compounds which have the same antioxidant properties. This caused the antioxidant activity remained unchanged or even increased even though there were losses of active ingredients.[2]

However when edible oils were heated to 80 ºC, the antioxidant activity of edible oil decreased gradually. Among all the edible oils, virgin olive oil especially showed drastic decrease of its antioxidant activity until it reaches a low inhibition value of 7.08% at 80 ºC. Decrease in antioxidant activity shows that there might be loss of antioxidants when the edible oils were heated to a higher temperature. Another possibility is that the antioxidant properties in the oils might have decreased or disappeared during the heating process, which results in low DPPH radical scavenging ability.

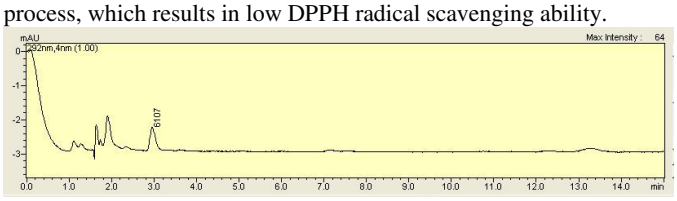


**Figure 3.3 Peak Area for Standard Solution at 1 mg/L**

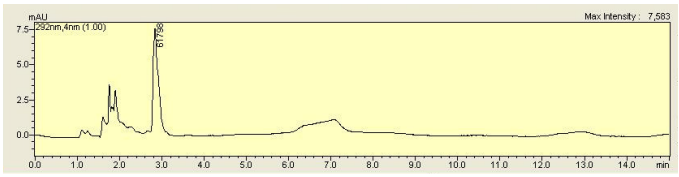


**Figure 3.4 HPLC Chromatogram of Rice Bran Oil**

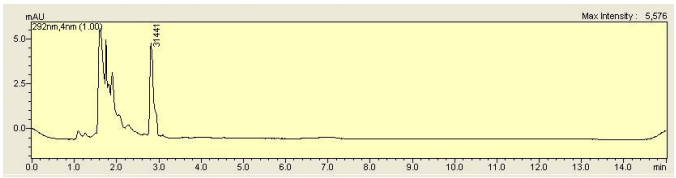


**Figure 3.5 HPLC Chromatogram of Extra Virgin Olive Oil**

**Figure 3.3** shows the chromatogram of the standard solution at 1 mg/L. It was observed that the peak area appeared at around t = 2.9 min. Integration was performed from t = 2.7 min to t = 3.3 min for each concentration to obtained the peak area for α–tocopherol at the particular concentration. The standard curves (concentration against peak area) were calculated by linear regression analysis. The chromatogram for rice bran oil and extra virgin olive oil are shown in **Figure 3.4** and **3.5** respectively. Data of peak areas were collected to calculate the concentration of α–tocopherol in edible oils.

**Figure 3.6 α–tocopherol Content in Edible Oils**

| *Oil Sample* | *α - tocopherol Content (mg per 100 g)* |
|---|---|
| Peanut Oil | 9.34 |
| Extra virgin olive oil | 8.06 |
| Olive Oil | 11.15 |
| Sunflower Oil | 15.32 |
| Palm Oil | 11.54 |
| Corn Oil | 15.73 |
| Rice Bran Oil | 17.25 |

## 4. Conclusion

When maintained at room temperature, extra virgin olive oil has the highest tendency to scavenge free radicals, which shows that it has the largest amount of antioxidants. The loss of antioxidants or the antioxidant properties in edible oils happened when heated to a high temperature of 80ºC. RP-HPLC result shows that rice bran oil has the highest α-tocopherol content.

## References

[1] E. Gimeno, a I. Castellote, R. M. Lamuela-Raventós, M. C. de la Torre, and M. C. López-Sabater, "Rapid determination of vitamin E in vegetable oils by reversed-phase high-performance liquid chromatography.," *J. Chromatogr. A*, vol. 881, no. 1–2, pp. 251–4, 2000.

[2] A. Tomaino, F. Cimino, V. Zimbalatti, V. Venutti, V. Sulfaro, and A. De Pasquale, "Influence of heating on antioxidant activity and the chemical composition of some spice essential oils," *Food Chem.*, vol. 89, pp. 549–554, 2005.

# Modelling of Pyrolysis in Fluidized Bed Reactor – Eulerian Model

Y.C Yan[1], X.Y Lim[1*], W Rashmi[1], C.H Lim[2]

[1]*Energy Research Group, School of Engineering, Taylor's University, Malaysia*

[2]*Environmental Research Group, School of Engineering, Taylor's University, Malaysia*

**Corresponding email: xiaoyien.lim@taylors.edu.my*

*Abstract* – **In this study, an Eulerian model from the Euler approach is implemented to model the fast pyrolysis in a lab-scale fluidized bed reactor. In this 2-D model, laminar viscous model and multi-stage kinetic scheme are used to predict the products' yield from pyrolysis of pure cellulose and red oak at 773K. The simulation results were validated with experimental result obtained by Xue et al (2012) and were discussed.**

*Keywords* – CFD, Pyrolysis, Fluidized Bed

## 1. Introduction

For the past few decades, pyrolysis has been intensively studied as an alternative thermochemical technique to gasification in order to convert biomass to bio-oil [1]. Fast pyrolysis is a process in which the organic materials undergo thermal degradation in the absence of oxygen and the products resides in the reactor for a few milliseconds. The desirable product in the fast pyrolysis of biomass particles is condensable material, tars that form the main product – bio-oil [2]. Despite the advancement made in the pyrolysis for bio-oil production, there are still some technical challenges in pilot scale studies due to cost [3]. In addition, measuring the flow of reacting dense gas-solid is both challenging and limited to latest measuring technique [4]. However, with Computational Fluid Dynamics (CFD) modelling, pyrolysis study can be carried out in a simulated model and this indirectly minimizes the need to conduct expensive and time-consuming experimental testing.

## 2. Research Methodology

### 2.1 Multiphase Model

In this study, the multi-fluid fluidized bed reactor is modelled using the Eulerian model – an Euler-Euler approach. It utilizes the conservation of each phase that relates by the application of kinetic theory in the case of granular flow in fluidized bed reactor [5]. The implementation of Eulerian model permits the modelling of multiple separated interacting phases in lower computational time [6]. Additionally, Eulerian model takes into account the inconsistent density of the biomass due to the chemical reaction in the fluidized bed reactor [4]. This model also allows heterogeneous reaction between phases.

### 2.2 Viscous Model

A study conducted by past researcher on fluidized bed shows that there is no obvious difference in flow prediction with or without turbulence model [7]. In fact, the laminar model shows better performance in predicting the flow in fluidized bed compared to turbulence model [8]. Hence, in this present study, laminar model is selected as the viscous model to simulate the flow inside the fluidized bed reactor.

### 2.3 Chemical Kinetics Model

Fundamentally, the kinetic model of the decomposition of biomass obeys the Arrhenius rate expression [9]. The kinetic mechanism used in this study to model the biomass decomposition is the multi-stage semiglobal kinetic scheme as illustrated in Fig 1 [10, 11, 12]. The decomposition rate of a biomass is the sum of the decomposition of cellulose, hemicellulose and lignin. All the decomposition rates are in first-order. In this study, two different feedstock is used; the pure cellulose and red oak. The red oak consists of 41wt% cellulose, 32wt% hemicellulose and 27wt% lignin. The kinetic parameters of each biomass component are based on the experimental values from literature [10, 13, 14].

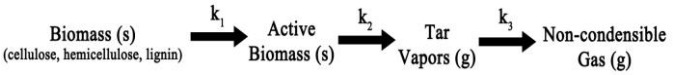


Fig 1 Kinetic scheme for the reactive biomass particles. The biomass are activated and is converted into tar vapors. The tar vapors will undergo cracking which produces non-condensible gas.

### 2.4 Computational Domain and Boundary Conditions

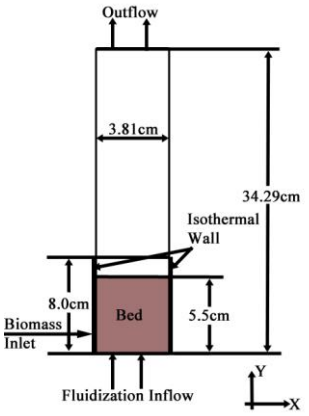


Fig 2 The computational domain of the fluidized bed in this study.

The 2-D model is solved using pressure-based ANSYS Fluent 14.0 as shown in Fig 2. The isothermal wall is defined with a constant temperature of 800K whereas the remaining reactor's wall is defined as adiabatic wall. The inlet for the biomass is located on the left wall with a height of 0.73cm and the bottom of the inlet is 1.335cm above the bottom of the reactor. The biomass is fed into the reactor at $2.67\times10^{-5}$ kg/s with an initial temperature of 300K. The reactor operates at atmospheric pressure. Pure nitrogen gas with an initial temperature of 773K is flowed into the reactor with a superficial velocity of 0.36 m/s. The sand bed is defined with an initial temperature of 773K and a volume fraction of 0.59 with a particle diameter of 0.052cm. The computational domain and boundary conditions stated above are consistent with the benchmark paper by Xue et al. (2012) [4].

The model consists of three phases; the first phase comprises of the nitrogen, tar vapour and non-condensible gas, the second phase is the inert sand bed, and the third phase consists of the biomass components. All simulation is run up to 100s of physical time using parallel runs on Dell Precision T7600. The simulation takes

approximate one week (for pure cellulose) and 4 days (for red oak) to complete.

### 2.5 Mesh Dependency

In order to determine the mesh dependency of the model, three different mesh sizes were compared. The number of elements that were compared was 750, 1700 and 2600. Statistical analysis was conducted on the key parameters of the different mesh sizes to ensure no large deviation. From this study, the deviation from 1700 to 2600 is less than $10^{-3}$. Since, the simulation model in the benchmark paper used 1800 number of elements; hence, in order to give a great deal of confidence on the accuracy of the model, the number of elements selected for this study is 2600.

## 3. Results

The simulation key results are compared and validated with the experimental result conducted by Xue et al. (2012) [4] and are shown in Table 1. The yields of the products are obtained through the surface integral report across the reactor's outlet.

Table 1 Comparison between the product yields (wt%) of pure cellulose and red oak in simulation and experiment [4].

| Approach | Tar | Non-condensible Gas | Outlet Temperature (K) |
|---|---|---|---|
| **Pure Cellulose** | | | |
| **Simulation** | 78.87 | 25.09 | 791.03 |
| **Experimental** | 82.1 | 12.4 | 773.15 |
| **Red Oak** | | | |
| **Simulation** | 79.38 | 24.76 | 789.61 |
| **Experimental** | 71.7±1.4 | 20.5±1.3 | 773.15 |

It is important to first validate the simulation model using pure cellulose as the kinetic scheme described in Fig 1 is based on cellulose and are superimposed on the remaining biomass components. The predicted results for pure cellulose are in a good agreement with the experimental results quantitatively. The yield of tar (78.87%) is under-predicted, whereas the yield of the non-condensible gas (25.09%) is over-predicted. This is understandable due to the fact that this model does not include the creation of char as one of the pyrolysis products, although the yield of char is low (2.2wt %) in the experiment. As the formation of char is an exothermic reaction which gives out 25kJ of energy per kg [15]; hence, the absence of char formation results in lower energy supply for the pyrolysis process in the reactor and eventually causes less bio-oil to be produced. In this model, the biomass components are assumed to be spherical and experience no volume shrinkage during the pyrolysis [5]. This would affect the density change of the biomass during the reaction and over-estimated the biomass loss. The over-estimation of biomass loss would lead to high residual in the simulation, causing formation of tar to decrease.

The red oak simulation on the other hand, shows a higher prediction on the tar yield (79.38%) than the experimental result. This is supported by the fact that the pyrolysis of lignin and hemicellulose is exothermic; hence, supplying more energy for the conversion of biomass to tar [16]. However, the absence of char formation greatly affected the trend of the tar yield, in which the red oak has a lower tar yield (24.76%) compared to the pure cellulose as shown in the experimental result in Table 1. Theoretically, lignin produces more char than tar and the absence of char formation leads to over-estimation of tar yield by the lignin in the simulated model [16].

As for the outlet temperature, the simulation result has the tendency to over-predict. This is due to the assumption made in the simulated model that no energy is loss from the reactor's adiabatic wall. Nevertheless, the deviation of the outlet temperature from the simulated model and the experimental results are less than 2.3%, which is within acceptable range for a simulated model.

## 4. Conclusion

In conclusion, a 2-D CFD model is implemented on the fast pyrolysis process in fluidized bed reactor using the Eulerian model and multi-stage semi global kinetic scheme. The model is validated with experimental results to some extent. Taking account into the absence of char formation, the model shows good agreement with experimental results in tar and gas yield, and reactor outlet temperature.

The CFD model has a good prediction of the biomass pyrolysis in fluidized bed reactor and can be used for different type of biomass in which the composition of cellulose, hemicellulose, and lignin is known. As a future work, the char formation could be included in the biomass decomposition to ensure the whole model can be implemented. Additionally, a 3-D model would be conducted to validate the 2-D model and provide clearer information about the fast pyrolysis behavior in a fluidized bed reactor.

## References


[1] M. Wright and R. Brown, "Comparative economics of biorefineries based on the biochemical and thermochemical platforms," *Biofuel Bioprod Biorefin 1*, pp. 49-56, 2007.

[2] C. Blasi, "Modeling chemical and physical processes of wood and biomass pyrolysis," *Progress in Energy and Combustion Science 34*, pp. 47-90, 2008.

[3] C. Hamelinck and A. Faaij, "Outlook for advanced biofuels," *Energy Policy 34*, pp. 3268-3283, 2006.

[4] Q. Xue, D. Dalluge, T. Heindel, R. Fox and R. Brown, "Experimental validation and CFD modeling study of biomass fas pyrolysis in fludized-bed reactors," *Fuel 97*, pp. 757-769, 2012.

[5] K. Papadikis, A. Bridgwater and S. Gu, "CFD modelling of the fast pyrolysis of biomass in fluidised bed reactors, PartA: Eulerian," *Chemical Engineering Science 63*, pp. 4218-4227, 2008.

[6] P. Mellin, Q. Zhang, E. Kantarelis and W. Yang, "An Euler-Euler approache to modeling biomass fast pyrolysis in fluidized-bed reactors - Focusing on the gas phase," *Applied Thermal Engineering 58*, pp. 344-353, 2013.

[7] C. Loha, H. Chattopadhyay and P. Chatterjee, "Assessment of drag models in simulating bubbling fluidized bed hydrodynamics," *Chemical Engineering Science 75*, pp. 400-407, 2012.

[8] M. Hamidipour, J. Chen and F. Larachi, "CFD study on hydrodynamics in three-phase fluidized beds - Application of turbulence models and experimental validation," *Chemical Engineering Science 78*, pp. 167-180, 2012.

[9] J. White, W. Catallo and B. Legendre, "Biomass pyrolysis kinetics: A comparative critical review with relevant agricultural residue case studies," *Journal of Analytical and Applied Pyrolysis 91*, pp. 1-33, 2011.

[10] A. Bradbury, Y. Sakai and F. Shafizadeh, "A kinetic model for pyrolysis of cellulose," *Journal of Applied Polymer Science 23*, pp. 3271-3280, 1979.

[11] F. Shafizadeh, "Introduction to pyrolysis of biomass," *Journal of Analytical and Applied Pyrolysis 3*, pp. 283-305, 1982.

[12] F. Shafizadeh and A. Bradbury, "Thermal degradation of cellulose in air and nitrogen at low temperature," *Journal of Applied Polymer Science 23*, pp. 1432-1442, 1979.

[13] R. Miller and J. Bellan, "A generalized biomass pyrolysis model based on superimposed cellulose, hemicellulose, and lignin kinetics," *Combustion Science and Technology 126*, pp. 97-138, 1997.

[14] A. Liden, F. Berruti and D. Scott, "A kinetic model for the production of liquids from the flash pyrolysis of biomass," *Chemical Engineering Community 65*, pp. 207-221, 1988.

[15] C. Koufopanosi, G. Maschio and A. Lucchesit, "Kinetic modelling of the pyrolysis of biomass and biomass components," *Canadian Journal of Chemical Engineering 67*, pp. 75-84, 1989.

[16] P. Basu, Biomass Gasification and Pyrolysis: Practical Design and Theory, UK: Academic Press, 2010.

# Preliminary Test of Phytoremediation of Hydrocarbon Contaminated Soil using Plant Species around Taylor's University

Yehga Nikkil Gogulanathan[1], Veena Arun Doshi[2], Salmi Nur Ain Sanusi[3]

[1]*Department of Chemical Engineering, Taylor's University, Malaysia,* [2]*Department of Chemical Engineering, Taylor's University, Malaysia*

**Corresponding email: VeenaADoshi.ArunKumarDoshi@taylors.edu.my*

*Abstract*— **The aim of this paper is to determine the most suitable species of plant found based on 3 species within Taylor's University for phytoremediation of PAH in soil while also determining the range of concentration of diesel the plant species is able to survive. The experiment was conducted within the lab premises of Taylor's University in a controlled environment for 14 days. 3 different species of plants found within Taylor's University was exposed to 5, 10, and 15 g diesel/kg soil in soil while the presence of withering and biomass of the plants was recorded. By the end of the experiment, Species 1 was found the most suited species for phytoremediation as it had no presence of withering, the highest biomass of plants of 49.82g , 5.92g, 60.07g, 48.53g for Fresh Shoot, Dry Shoot, Fresh Root and Dry Root Respectively while Species 2 had withered completely with biomass of 2.03g, 2.30g, and 0.81g and 0.70g for Fresh Shoot, Fresh Root, and Dry Root and Dry Shoot respectively, and Species 3 had partially withered with 31.0g, 3.85g, and 54.86g and 15.58g for Fresh Shoot, Dry Shoot, Fresh Root, and Dry Root respectively. The concentration range of diesel that Species 1 is able to survive is 5g diesel/kg soil and 10g diesel/kg soil.**

*Keywords*— phytoremediation, polycyclic aromatic hydrocarbon, diesel.

## 1. Introduction

Soil pollution is the detrimental alterations of soil based upon anthropogenic activities such as usage of pesticides and herbicides, improper disposal of biological solid, liquid remains, and chemicals wastes from industries and oil spillages which are ever present in industrialized regions. One of the most common of these soil pollutants are the polycyclic aromatic hydrocarbons (PAH) according to the work of Shahsavari et al. [1], which states petro genic hydrocarbons are the most found contaminants which have been known to cause devastating harm within these ecosystems in terms of health and environmental aspects as extensively documented by several recent studies [2] such as the destruction of animal and plant habitats while also having a tendency to develop carcinogens and mutagens as classified by the US Environmental Protection Agency (EPA) [3].

Phytoremediation is a non-damaging biological in-situ soil remediation technique whereby plants are used to treat the soil and sediments that have been polluted by toxic metals, organics, and radionuclides [3]. Based on Cunningham et al. [4], the mechanism by which phytoremediation operates is through either eliminating, isolating or degrading the pollutants contained in the soil via uptake of the roots. This innovative technology is considered to be a viable alternative to remediate the land that have been polluted due to the anthropogenic activities as it is inexpensive compared to orthodox remediation treatments, while also being able to cause a positive effect towards the environment due to the reconstruction of plant cover in the contaminated sites.

Various plant species have found to be grown within the premises of Taylor's University within its natural vegetation. Three species of plants that are found within Taylor's University are chosen for this phytoremediation study of PAH using diesel as a source of soil contaminant. The present study of the preliminary phytoremediation test aims to determine the maximum concentration of diesel which the plants will be able to survive in. This study also aims to determine the most suitable out of the three selected plant species found in Taylor's University that is suitable for phytoremediation of PAH in diesel oil of contaminated soil.

## 2. Method

### 2.1 Preparation of Contaminated Soil

Based on the procedure used by Sanusi [5], the black soil is sieved with a 4mm-sieve to ensure homogeneity of soil components for all portions of the soil used for the plants besides removing abrasive fragments from the soil. 3kg of the sieved black soil is then placed into round pots of dimensions of 30 cm (D) x 20 cm (H) for 3 sets of plants of each of the 3 sets for the 3 different species of plant used.

The diesel fuel used for the experiment was obtained from the nearest petrol station. Different diesel concentrations of 5, 10, and 15 diesel/kg soil for each 3 sets of plant species were prepared. The diesel was mixed with acetone on a 1:1 basis in accordance to methods shown by Xu et al. [6].to evenly distribute the composition of diesel in the soil. The diesel-acetone mixture was then poured into the pots of soil. To further facilitate the mixing process, the diesel: acetone mixture was stirred and mixed rigorously 3 times for 1 week.

After 1 week, the each 6 plants each of the 3 species is then planted into the pots of the differing concentrations and will be left for observation for 14 days.

The plants was watered 3 times per week and the presence of withering was observed weekly for the 2 weeks beginning with the first day of the experiment and the presence of withering was observed.

### 2.2 Measurement of Biomass of Plants

The plants were removed once a week using a spade and the plants were divided into two sections to measure the fresh and dry weight of the shoots and roots in an electronic weighing balance. Then, the shoots and roots are dried in an air convective oven for 24 hours at a temperature of 200$^{o}$C before the shoots and roots are weighed in an electronic weighing balance.

## 3. Results & Discussion

During the 14 day period, it was noted that Species 1 had only slight form of leaf discolouration, and no withered leafs for the pot with 15g/kg diesel while the other 2 pots had no form of discolouration or withering. On the other hand, Species 2 of the plants had completely withered in all pots on the third day. Finally, Species 3, the plants in all 3 pots had shown the presence of withering on day 9 with a steady increase of withering during 14 day period.

### 3.1 Biomass of Plants

Based on the Figure 1, at the end of the 14 day study it is noted that for the highest fresh weight and dry weight of the roots and shoots recorded is the highest at 10 g diesel/kg soil which are 49.82g for Fresh Shoot, 5.92g for Dry Shoot, 60.07g for Fresh Root and 48.53g for Dry Root. Hence it can be said that Species 1 is most suited to survive

within 10g diesel/kg soil of contaminated soil. It is also noted that the biomass of shoot and roots of Species 1 had increased on the final day of the study indicating that the plants of Species 1 are able to grow in a diesel contaminated environment the longest period of time out of the other 2 species of plant that had shown a lower trend in biomass data. This can be attributed due to the fact that Species 1 has a large and extensive root system, having the highest sets of data for biomass of Fresh Root and Dry Root out of the 3 plant species. This results is supported by a study conducted by Muratova et al. which shows that plant species with an extensive rhizosphere region is the region that encourages successful phytoremediation to occur, as with extensive rhizospheres, the plants are unable to tap in resources from beneath the contaminated soil, as deep as 3m [58].

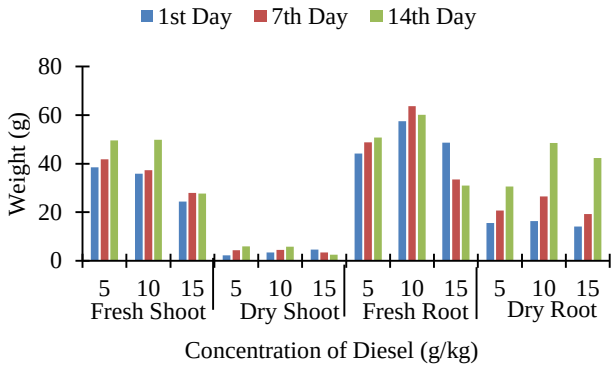


Fig. 1 Fresh and Dry Weight. Of Shoots and Roots of Species 1 in different Diesel Concentrations.

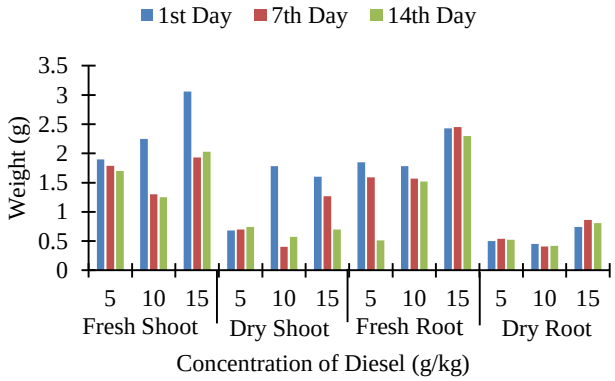


Fig. 2 Fresh and Dry Weight. Of Shoots and Roots of Species 2 in different Diesel Concentrations.

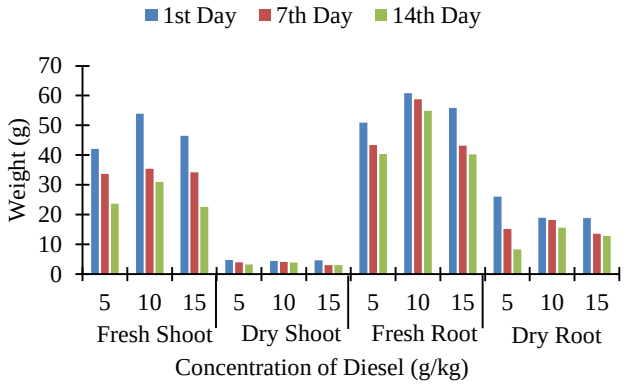


Fig. 3 Fresh and Dry Weight. Of Shoots and Roots of Species 3 in different Diesel Concentrations.

While for Species 2, based on Figure 2, it is noted that the weight is generally the highest for the soil with 15g diesel/kg soil for the Fresh Shoot, Fresh Root, and Dry Root with 2.03g, 2.30g, and 0.81g respectively while, the highest weight for Dry Shoot is of concentration 5g diesel/kg soil with 0.7g. However, it is noted that as time of study passes by, the weight of trend of the fresh and dry weights of roots and shoots for Species 2 reduces. This is consistent with the observation that Species 2 had started to experience withering by day 3, and by the 14th day of the experiment, all plants of all concentrations of species 2 had withered. This can be attributed to the fact that Species 2, has the smallest form of roots as studies and as such, Species 2 has the least extensive root system.

Finally Species 3, based on Figure 3, the general trend shows that the weight of the shoots and roots decrease as the study goes on. This is consistent with the observation that the plants had begun the process of withering during the study. However unlike Species 2, the plants have not completely withered during the period of the study. It is also noted that, the highest dry and wet weights for the root and shoots of Species 3 at the end of the study is recorded for 10g diesel/kg soil which are 31.0g, 3.85g, and 54.86g and 15.58g for Fresh Shoot, Dry Shoot, Fresh Root, and Dry Root respectively. This set of results is in accordance to a study conducted by Adam & Duncan whereby the PAH content of diesel oil that was spilled will remain in the ground for a long time, and alter the characteristics of the soil besides deterring growth and development of the plants around it causing low germination percentage and hindered seed development as the diesel in the soil would prevent oxygen and water uptake between the soil and plants [25].

## 4. Conclusion

After 14 days of experimental observation, it was noted that Species 1 is the most suited to undergo further phytoremediation tests as it is able is able to survive in and grow with minimal leaf discolouration in concentration ranges of 5 and 10g diesel/kg soil. It also shows the highest biomass readings of 49.82g for Fresh Shoot, 5.92g for Dry Shoot, 60.07g for Fresh Root and 48.53g for Dry Root among the 3 plant species on the last day of the study.

Species 2 and 3 is not considered suitable for phytoremediation tests as the plants of Species 2 had completely withered by the end of the experiment while showing a decreasing trend in biomass value with the lowest recorded biomass for 2.03g, 2.30g, and 0.81g and 0.70g for Fresh Shoot, Fresh Root, and Dry Root and Dry Shoot respectively while Species 3 had partially withered with the biomass recordings 31.0g, 3.85g, and 54.86g and 15.58g for Fresh Shoot, Dry Shoot, Fresh Root, and Dry Root respectively for the 14th day of the study.

## References

[1] Shahsavari, E., Adetutu, E.M, Anderson, P.A., & Ball, A.S. (2013). Plant Residues – A Low Cost Effective Bioremediation, Treatment for Petrogenic Hydrocarbon-Contaminated Soil. *Journal of The Science of Total Environment*, vol.443, 766-774.
[2] Meagher, R.B. (2000). Phytoremediation of toxic elemental and organic pollutants." Journal of Current Opinion in Plant Biology, vol.3, 153-162.
[3] Enell, A., Fuhrman, F., Lundin, L., Warfvinge, L. & Thelin, G. (2008). Polycyclic Aromatic Hydrocarbons in Ash: Determination of Total and Leachable Concentrations. *Journal of Environmental Pollution*, vol.152, 285-292.
[4] Cunningham, S.D., & Ow, D.W. (1996). Promises and Prospects of Phytoremediation. *Journal of Plant Physiology*, vol.110, 715-719.
[5] Sanusi, S.N.A. (2013). *Fitoremediasi Hidrokarbon Menggunakan Tumbuhan Paspalum scrobiculatum L. Hack dan Paspalum vaginatum Sw.* M.S. thesis,Universiti Kebangsaaan Malaysia, Bangi, Malaysia.
[6] Xu, S.Y., Chen, X.Y, Wu, W.X, Wang, K.X, Lin, Q. & Liang, X.Q. (2006). Enhanced Dissipation Of Phenanthrene And Pyrene In Spiked Soils By Combined Plants Cultivation. *Journal of Science of the Total Environment*, vol.363, 206-215.
[7] Muratova, A.Y., Dmitrieva, T.V., Panchenko, L.V. & Turkovskaya, O.V. (2008). Phytoremediation of Oil-Sludge–Contaminated Soil. *Journal of International Journal of Phytoremediation*, vol.10, 486.
[8] Adam, G. & Duncan, H. (2002). Influence of Diesel Fuel on Seed Germination. *Journal of Environmental Pollution*, 122(2). 363-370.

# Computer-Aided Training Module for Power System Analysis and Design

Ahmad Ashraf bin Ahmad[1], Reynato Andal Gamboa[2*]

[12]*School of Engineering, Taylor's University, Malaysia*

**Corresponding email: reynatoandal.gamboa@taylors.edu.my*

*Abstract*— **Electrical Transient Analyzer Program (ETAP) is an enterprise solution software widely used for the simulation, design, and analysis of power system networks. ETAP is the power engineers' tool in designing and evaluating power system performance under normal and abnormal condition. The engineer had to be equipped with a good understanding of how the software can be used. Available training on the use of ETAP is quite expensive such that a typical student or an electrical engineer cannot normally afford to pay. This paper presents the details of tutorial workbook intended to help students and power engineers learn ETAP in an easiest possible way. A tutorial workbook on network building, power flow analysis, and fault analysis was developed and tested among a select number of electrical engineering students. On average, 90% of the students find it easier using ETAP with the aid of the tutorial workbook.**

*Keywords*— tutorial workbook, ETAP, power system analysis

## 1. Introduction

Power System Analysis and Design is one of the most important modules taken by a student who want to pursue degree in electrical engineering. Computer software's are developed to aid users to perform complex calculation and task accurately and efficiently. Perform complex calculation manually can be time consuming and inaccurate due to human error. Network modeling tool is computer software developed to aid users of power system to simulate their design prior to implementation. This can be also used to aid student in learning power system [1].

Electrical Transient Analyzer Program (ETAP) is network modeling tool where users can model, simulate and run various analyses on power system. ETAP is a well-known tool widely used in industries and educational institutes around the world. Whereby, top 10 electrical design companies in the world use ETAP. In Malaysia, utility grid owner Tenaga Nasional Berhad (TNB) uses ETAP to design and simulate their electrical power system prior implementation [2]. Hence, this shows the importance for an Electrical Engineer who plans to explore the power system field to learn ETAP. Besides that, students can use the aid of ETAP to learn power systems efficiently applying their theoretical knowledge to work.

Currently there are is two form of learning material available in the market for self-learning basis. One of the materials available is a demo guide book which is a manual [3] presented with the software on some key features on the software. Whereas the other option is, a limited number of video tutorial [4] on key analysis and setup which is a media guide for user to use the software.

In the case on more guidance required, proper training and workshop can be arranged with consultancy firms of the software and the ETAP organization itself. This type of guidance requires cost in exchange of service. Thus, this is a very expensive option usually approached by industries and not individual as many could not afford. Thus, the objective of this research is to develop Computer-Aided Training Module for Power System Analysis and Design. Whereby, a tutorial workbook was developed to aid users in conducting power system analysis and design using network modeling software ETAP. The tutorial workbook produced encompasses network construction fault analysis and load flow analysis. The impact of the tutorial workbook was evaluated in the form of survey conducted on a group of individuals who are learning power systems. Their evaluation on the tutorial workbook are important are used for future development of the workbook.

## 2. Methodology

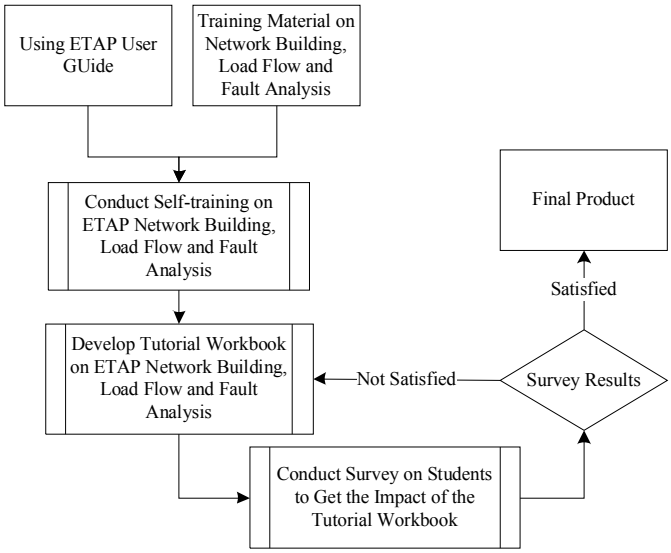


Figure 1: Block diagram of the research methodology

The research methodology approached in this research is shown in Figure 1. The ETAP demo guide book [3] was reviewed and critically analyzed in terms of features and translation of procedures to actions. It can be said that the present guide book are well presented in terms of coloring and proper diagrams are provided for guidance. Some draw backs are found whereby, proper examples on conducting various analyses and constructing networks are not provided. .

Based on the result of analyses performed on the guide book, training materials on network building, load flow and fault analysis was obtained from power system lecturer lab sheets to be used as example in the tutorial workbook. Simultaneously, training material on network building load flow and fault analysis is analyzed and picked to be used in the tutorial workbook as a worked example.

Based on the guide book as reference, the training material obtained was simulated on ETAP as self-training. Whereby, the procedure performed in conducting the simulation will be presented in the tutorial work book in terms of diagrams and explanations. These procedure involved and interpreted was the input for the tutorial work book.

The tutorial workbook made was checked and ensured it encompasses all the fore mentioned features such as network construction, load flow and fault analysis prior to completion.

The tutorial workbook developed was tested on a group ten Electrical and Electronic Engineering students who are currently taking studying the power system module. The students are tested with different tutorial question from the sample practices provided in the tutorial workbook. Upon, completions of the test students are provided with a survey form to retrieve their opinion on the impact of the tutorial workbook.

The survey result was analyzed in terms of bar charts in order to know the impact of the tutorial workbook on network building, load flow and fault analysis prior to using the tutorial workbook and after using the tutorial workbook. Comments and recommendations from students are taken for future improvisation of the tutorial workbook.

Figure 2: Survey results before students using the tutorial workbook

With reference to Figure 2, it can be seen that mostly students have difficulties on using ETAP for the first time because they have no proper training or guidance on using the software. Thus, this proves that the guide book provided by ETAP insufficient and unproductive as many student faced difficulties in performing the highlighted tasks. It can be said that 80% of the students faced problems on building a network on ETAP because they have issues in setting the specifications which was provided.

## 3. Results

Figure 3: Survey results for network building with help of tutorial workbook

Based on Figure 3, it is shown that students find it easier to build their network on ETAP with the aid of the tutorial workbook. This is because the tutorial workbook shows step by step procedure on how to set specifications, where to input the specified values and where the equipment's icons are located. On average, 90% of the students improve their skills on network building on ETAP.

Figure 4 shows 90% of the students are capable to perform load flow analysis on ETAP with the help of the tutorial workbook. The balance 10% of the students gave negative feedback on the tutorial workbook. This may be due to lack of basic understanding of the student on load flow.

Figure 4: Survey results for load flow with help of tutorial workbook

Figure 5: Survey results for fault analysis with help of the tutorial workbook

Based on Figure 5, it can be noted that 90% of the students can perform fault analysis with the help of the tutorial workbook. Aside the help of the tutorial workbook, it is important for students to learn the topic prior simulating their learning on software's.

## 4. Conclusion

Based on the results obtained, the tutorial workbook developed is capable in assisting the students or users to use ETAP. On average, 90% of the students find the tutorial workbook productive and beneficial in assisting them to use ETAP. The remaining 10% of students find that there are rooms for improvement for the tutorial workbook. In conclusion, the tutorial workbook meets it purpose which is to help students to build networks, run load flow and fault analysis on ETAP.

## References

[1] Cobus Strauss Jan de Kock, Practical Power Distribution for Industry, 1st ed. Burlington: IDC Technologies, 2004.

[2] "ETAP Users | Global ETAP Clients for Electrical Power System Solutions." [Online]. Available: http://etap.com/industries/etap-user-list.htm. [Accessed: 4-May-2014].

[3] Operation Technology, Inc., ETAP 7.0.0 Demo Getting Started.: Operation Technology, Inc., 2009

[4] "ETAP Tutorials | Arc Flash Analysis | Load Flow Analysis | Motor Acceleration Analysis | ETAP." [Online]. Available: http://etap.com/training/tutorials-training-videos.htm. [Accessed: 4--May-2014].

# Characterisation and Separation of Brain Wave Signals

Aminath Saadha[1], K. Suresh Manic[1,*], K. Pirapaharan[2], Aravind C.V[1]

[1]*CIARG School of Engineering, Taylor's University, Malaysia* [2]*Department of Engineering, University of Papua New Guinea, Papua New Guinea*

**Corresponding email: SureshManic.Kesavan@taylors.edu.my*

*Abstract*—**Neurons in the brain communicate through electrical impulses that give rise to both electrical and magnetic fields which are categorized into five different band limits. These waves can be measured outside the skull through an Electroencephalogram. The utilisation of brainwave detection in other areas such as biomedical engineering and gaming industry is yet to be explored. Categorisation of different rhythms of brainwaves and brainwave pattern analysis make it easier to identify the mental status of a person. This research aims to develop a hardware and software that is tested using function generators to simulate the EEG signal from the brain. It is observed that the initial results based on the above that the device performs as expected and hence can be used as brain wave signal measuring device.**

*Keywords*— Brain wave, EEG, Signal processing

## 1. Introduction

The human brain can be sub divided into four structures each with a different set of functions [1]. Each movement, perception and thought that we execute has a distinct neural activation pattern. An Electroencephalography (EEG) is a record of this brain activity and characterizes the field potentials ensuing from the combined activity of many neuron impulses. It is measured through surface electrodes placed on the skin of the scalp. There are five different band limits for the brain wave, namely delta, theta, alpha, beta and gamma. These identifiers are characterized based on the frequency range which is normally from 1Hz to 60Hz, with amplitudes of 10 to 100 microvolts [2].

Although EEG has been in use for a relatively long time, little research has been made into the recognition of brainwave patterns and the separation of brainwaves and categorizing them [3]. Moreover the current apparatus available for measuring EEG waves are bulky thus restricting the flexibility of operating conditions and the movement of the user.

This research is aimed to create a device that can acquire brainwaves, identify and differentiate between the different frequencies consisted in the signal with the help of a signal processing software and is also portable thus giving a wider range of operation. The study aspires to provide a better understanding of a person's mental and physical action through the development of a real time brainwave scope. Such a device enable discerning various human afflictions such as a person's mental health by measuring the stress levels and hence provide proper counseling. Real time gaming is another advent that this technology enable by providing the method of creating mind control games.

## 2. Research Methodology

Figure 1 above shows the graphical user interface developed through LABVIEW that displays the real time brainwave signal and the separate components.

The block diagram in Figure 2 indicates the different stages of obtaining the signal and analyzing it to component categories based on its characteristics. The signal is obtained from five different signal generators each of which represent a band of the brainwave signal. It is then passed through a signal conditioning circuit consisting of a 60Hz notch filter, used for eliminating the noise accumulation from the 60 Hz power supply. Since brainwaves are between the frequencies of 3Hz-60Hz the signal passes through a 60Hz low pass filter and a 3Hz high pass filter.

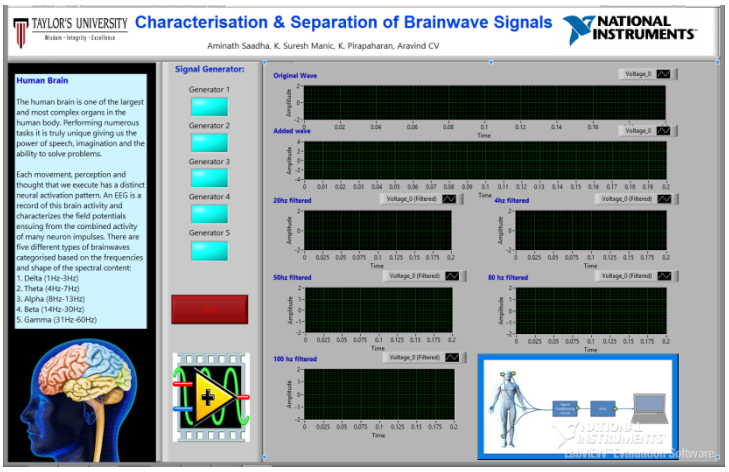


Fig. 1 Graphical user interface developed for the system.

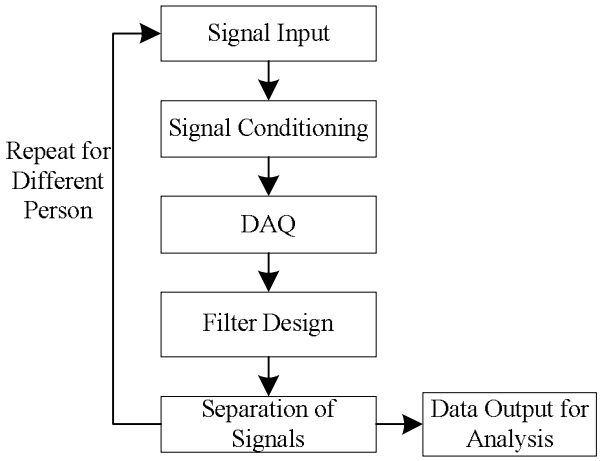


Fig. 2 Methodology used in this brainwave separation analysis.

This removes other frequency bands that are acquired through the sensor. Butterworth filters constructed using LM741 amplifier is used for a smoother response and unity gain in order to eliminate any noise amplification.

The conditioned signal then passes through DAQ 6009, a data acquisition device used for simple data logging and portable measurement. The Nyquist Shannon sampling theory states that the sampling frequency must be twice that of the highest frequency of the signal hence for brainwaves giving a sampling rate of 120 Hz [5]. However for a better reconstruction of the signal since it is of very small amplitude, 15mV a much higher sampling rate of 5 kilo-samples per second is used. Signals that are sampled from the Data Acquisition (DAQ) are sent to a signal processing software, LABVIEW [3]. Within this platform the signals are then added up which represents the actual EEG signal from the brain. Band pass filters are then implemented through the software to analyze the signal and separate it into the components frequencies. Tests are conducted to evaluate the software and assess whether the five different filters in the setup perform correctly.

In test 1, two case studies are conducted since the device is intended to be used for people with different personality, meaning

that the brainwaves vary from person to person. In the first case signals are all within the frequency band of the band pass filter. This test assumes that all the frequencies of brain waves are present in this signal and tests the detection of all the frequencies. In case 2 the signal from a signal generator is changed so that it does not fall in any filter category. This signal assumes that the subject does not produce one frequency of brain wave at that moment and all other frequencies are being detected. Table 1 shows the frequency of signal from each signal generator for the two cases. A second test is designed to check whether the intensity of the brain wave is detected by the software. For this study the amplitude of the 4Hz signal generator is increased from the input while the amplitude of other frequencies is maintained constant.

TABLE 1. Case studies conducted to test the design.

| Case | Signal Generator frequency (Hz) | | | | |
|---|---|---|---|---|---|
| | 1 | 2 | 3 | 4 | 5 |
| 1 | 4 | 20 | 50 | 80 | 100 |
| 2 | 4 | 20 | 50 | 120 | 100 |

## 3. Results Analysis

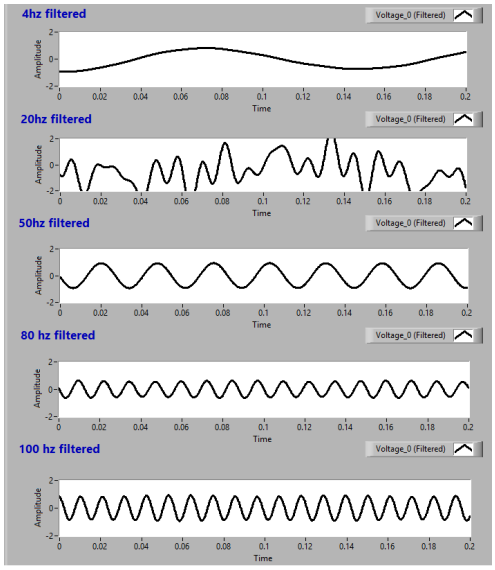


Fig. 3 Results for test 1 case 1

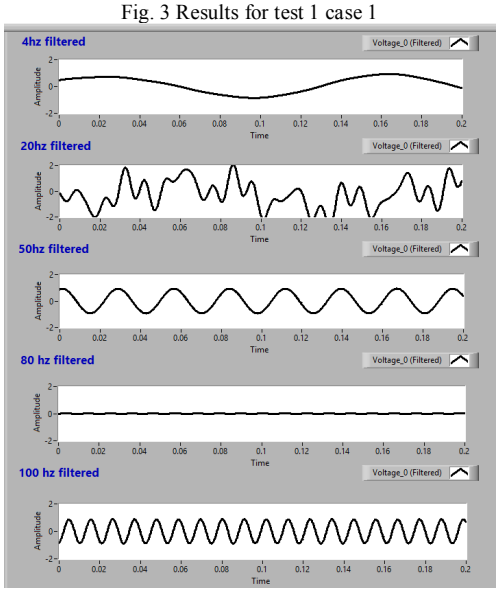


Fig. 4 Results for test 1 case 2

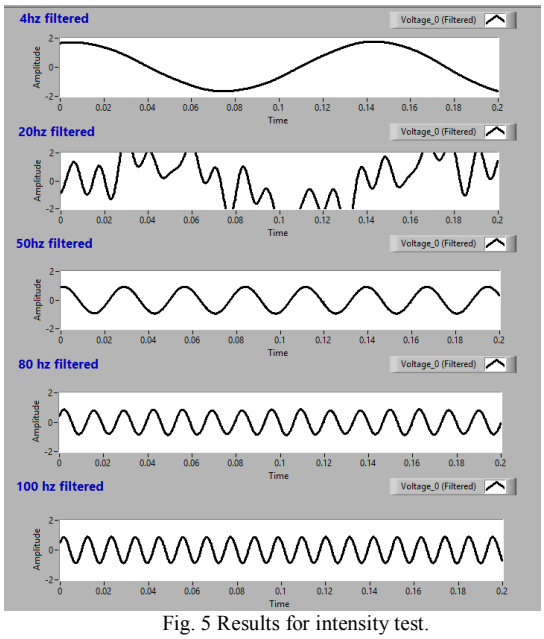


Fig. 5 Results for intensity test.

Figure 3 shows the results from test 1-case 1, where all the signals are detected as shown by their representative amplitudes. However in figure 4 which displays the results for case 2 the amplitude for the 80Hz signal is almost null indicating that there is no signal and that the filters function as expected.

Figure 5 displays the results for test 2 where the detection of intensity of a signal is detected. As expected the amplitude which corresponds to the intensity of the wave is increased which is shown in the greater amplitude of the signal.

## 7. Conclusions

The results from the initial test with signal generators indicate that the software and hardware built for the experiment are performing as expected. The filters that are implemented in the LABVIEW software filters out each band of the signal from the mixed signal which comprises the original input signal. For further studies the signal generators are to be replaced with the electrode and tested to visualize the actual brain waves in real time.

## References

[1] Alan Longstaff, *Neuroscience*, Fifth Edition ed., Elizabeth Owen, Ed. New York, US: Taylor & Francis Group, 2005.

[2] Hoole P.R.P, K. Pirapaharan, SA. Basar, and DLDA Liyanage, SSHMU Senanayake, SRH Hoole R.Ismail, "Autism, EEG and brain electromagentics research," in *Biomedical Engineering and Sciences (IECBES), 2012 IEEE EMBS*, 2012, pp. 5-6.

[3] Ramesh GP, Aravind CV, Rajparthiban R, and N.Soysa, "Body Area Network through Wireless Technology," *International Journal of Computer Science and Engineering Communications*, vol. 2, no. 1, pp. 129-134, January 2014.

[4] Giancarlo Strata, Renato Galli, Sara Gori, Carlo Gneri, Ugo Limbruno, Domenica Di Santo, Mario Mariani, Luigi Murri Roberto Massetani, "Alteration of Cardiac Function in Patients with Temporal Lobe Epilepsy: Different ROles of EEG-ECG Monitoring and Spectral Analysis of RR Variability," *Epilepsia*, vol. 3, no. 38, pp. 363-369, 1997.

[5] Fabio Freschi, "Localization of Sources of Brain Activity: A MILP Approach," *IEE Transaction on Magnetics*, vol. 46, no. 8, pp. 3429 - 3431, August 2010.

[6] Bob W. Van Dijk, Henk Spekreijse Jan C. De Munck, "Mathematical Dipoles are Adequate to Desicribe Realistic Generators of Human Brain Activity," *IEE Transactions on Biomedical Engineering*, vol. 35, no. 11, pp. 960-966, November 1988.

# On-Grid Photovoltaic System for Maximum Demand Reduction at Taylor's University Lakeside Campus

Arasan Bidamally[1], Reynato Andal Gamboa[1*], Aravind CV[2]

*School of Engineering, Taylor's University Lakeside Campus, Malaysia*

**Corresponding email: reynatoandal.gamboa@taylors.edu.my*

*Abstract*— **Demand charge of Taylor's University Lakeside Campus (TULC) electricity usage constitutes 30% of its electricity billing. This means TULC'S maximum demand coincides with the system demand of its power supply provider which charge customer at higher rate under this condition. To reduce the, demand a grid-connected photovoltaic (Grid-PV) module was introduced as a secondary source. The application of this secondary source to reduce maximum demand is yet to be explored and thus hereby presented. The selection of critical load adopted by this Grid-PV system was done through power flow analysis using ETAP® network modeling software. PV sizing was done for the load selected and power flow analysis was conducted to analyze the impact of on-grid PV. It is reported in this work that, an average reduction of 11% on maximum demand can be obtained through the implementation of Grid-PV.**

*Keywords*— Maximum Demand, Photovoltaic, Power Flow Analysis

## 1. Introduction

Taylor's University Lakeside Campus (TULC) is a modern campus that comprises educational and commercial facility [1]. The campus has an average monthly electricity usage of 980MWh and average maximum demand (MD) of 3000kW. The average monthly bill is RM 304,208.76 whereby 30% of the total monthly bill was from demand charges [2]. At TULC the tariff C1 which is used for medium voltage general commercial customer is applied. The standard maximum demand charge imposed is RM25.90 per kW which is can also be considered as peak period rate [3].

Malaysia is a hot and humid country which has an average of 12 hours of daily sunlight and average irradiance per year of 1643 kWh/m$^2$, making it viable for solar energy implementation[4], [5]. Solar energy is regarded as the cleanest technology for electricity production. Typically there are two types of solar PV system which for on-grid and off-grid application. On-grid systems are PV system which is implemented with grid connection. Whereby, off-grid systems stand-alone system used for small scale application[6].

The objective of this research is to reduce the costs spend on demand charges with the introduction of solar energy to act as a secondary source for the TULC campus which reduces the daily energy consumption during the time of peak period. Taylor's University Power Flow Model (TUPFM) developed using network modeling tool and an on-grid PV system which is tapped to critical load selected with respect to size of area available for implementation is designed and tested.

## 2. Research Methodology

Fig.1 shows the block diagram methodology applied for this research. Analysis on maximum demand curve for TULC was conducted to determine the average maximum demand of the system. The electrical network diagram for the campus is modeled using ETAP® as shown in Fig. 4 and load analysis was done to determine the highest power demand of the system. Fig.2 shows that main switch board (MSB) 3 and MSB 4 as the highest contributor for the maximum demand due to high power consumption. MSB 3 is connected to critical sub-loads that have high calculated maximum demand size that will not be viable to size PV with the area available at the campus. Therefore, MSB 4 is opted whereby; it is a mixture of lighting load and critical load. The load selected to be tapped with PV is shown in Fig.3 that is expected to operate consistently compared to other sub-loads that used to power lighting loads which are inconsistent.

The size of PV was based on assumption to power the load for working hours from 9a.m to 5p.m. PV selected is polycrystalline that is suitable for hot and humid condition of Malaysia. The inverter opted is grid tied since it is an on-grid PV system. Load and fault analysis was conducted on TUPFM that was modeled in ETAP®. This is done to analyze the system response to On-Grid and Off-Grid. The results obtained was analyzed on demand reduction and cost savings.

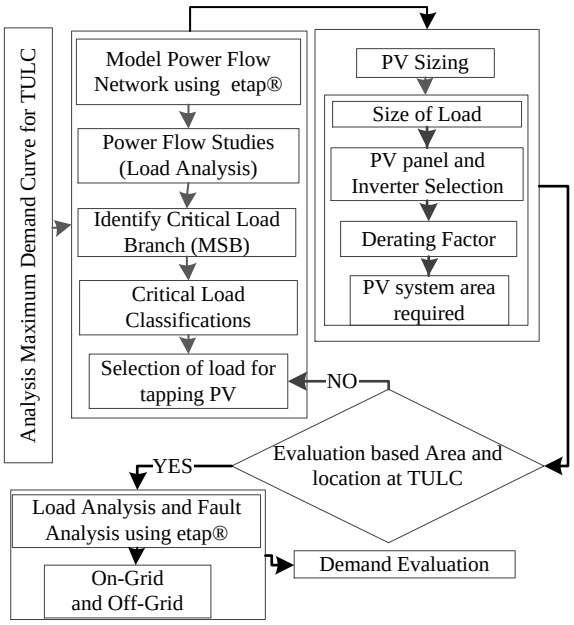


Fig.1 MSB Load of the TUPFM

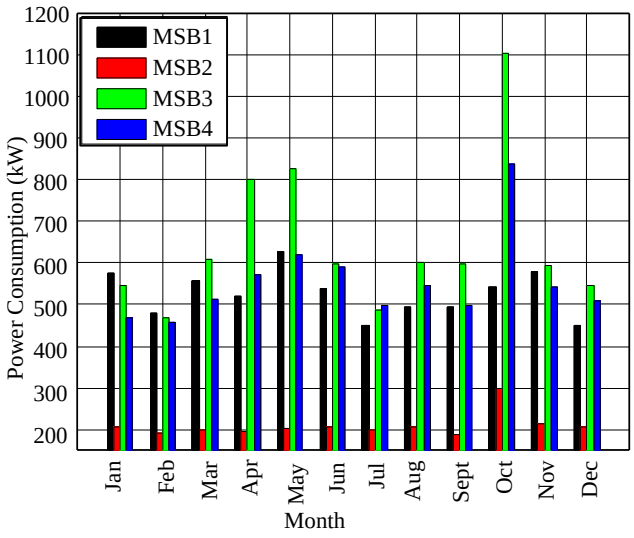


Fig.2 MSB Load of the TUPFM.

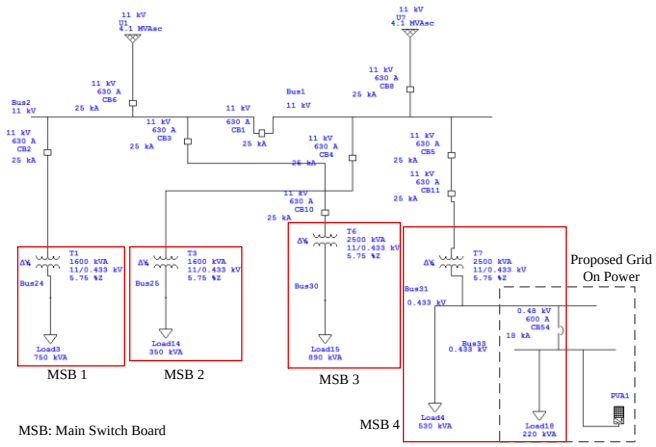


Fig.3 TUPFM Design using Network Modeling Tool.

## 3. Calculations

The ratio ($Ar_{MSB4}$) of selected critical load ($CL_R$) to average load of MSB 4 ($AP_{MSB4}$) was computed as follows

$$Ar_{MSB4} = \frac{CL_R}{AP_{MSB\,4}} \quad (1)$$

Assuming the selected critical load is tapped to PV; new average load of MSB 4 ($NP_{MSB4}$) can be computed by using power consumed by MSB 4 ($P_{MSB4}$)

$$NP_{MSB4} = P_{MSB4} - (Ar_{MSB4} \times P_{MSB4}) \quad (2)$$

Based on the new loading of MSB4, percentage difference ($\%Diff_{MD}$) between existing maximum demand ($P_{MD}$) and new maximum demand ($P_{MD\,(new)}$) was computed

$$\%Diff_{MD} = \frac{P_{MD} - P_{MD(new)}}{P_{MD}} \times 100\% \quad (3)$$

Percentage saving (%Savings) was computed using new maximum demand cost ($NMD_{RM}$) and existing maximum demand cost ($EMD_{RM}$) as follows

$$\%Savings = \frac{EMD_{RM} - NMD_{RM}}{EMD_{RM}} \times 100\% \quad (4)$$

## 4. Results and Discussion

Based on Fig.4 it is noted, that there is a decrement in the power demand as the new maximum demand is lower compared to the existing maximum demand. Thus, this proves that the implementation of on-grid PV to power the critical load reduces the maximum demand. This reduction was taken on the basis that the PV is capable of supplying the demand of the critical load at maximum demand period. Based on Fig.5 it is shown that savings can be made through the implementation of grid-PV on the critical load of MSB 4. Whereby, the PV does not brings return of income but it provides saving through reducing maximum demand charges.

## 5. Conclusions

There is significant impact on the maximum demand with the installation of PV, an average reduction of 11% between new maximum demand and existing maximum demand obtained. Based on the reduction in maximum demand, an average of 9% savings can also be obtained in maximum demand charges. Thus, it can be concluded that implementation of grid-PV can reduce the maximum demand during peak period.

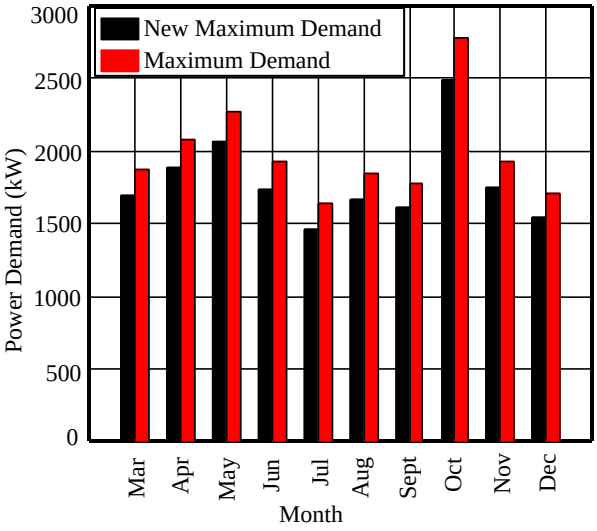


Fig.4 Difference in Maximum Demand based on 2013.

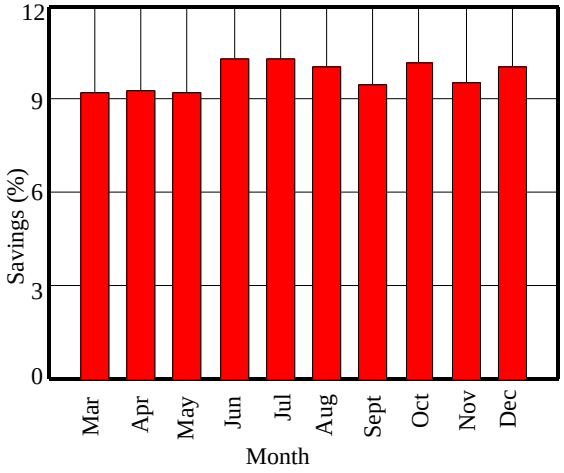


Fig.5 Percentage Saving made based on Maximum Demand 2013.

## References

[1] "ISSUU - Malaysia Landscape Architecture Yearbook 2011 by Charles Teo," *Institute of Landscape Architects Malaysia (ILAM)*, 2011. [Online]. Available: http://issuu.com/carltks/docs/malaysia_landscape_architecture_awards_year_book_2. [Accessed: 11-May-2014].

[2]Aravind CV, Mushtak Al-Atabi, Arasan, and Ramesh GP, "The Case of the Energy Solution to the Eco tourism Model for Sustainable Development using PV/T Technology- IJSER Journal Publication," *Int. J. Sci. Eng. Res.*, vol. 5, no. 4, pp. 174–177, 2014.

[3]T. N. Berhad, "Pricing & Tariff | Tenaga Nasional Berhad," 2014. [Online]. Available: http://www.tnb.com.my/business/for-commercial/pricing-tariff.html. [Accessed: 11-May-2014].

[4]S. C. Chua and T. H. Oh, "Solar energy outlook in Malaysia," *Renew. Sustain. Energy Rev.*, vol. 16, no. 1, pp. 564–574, Jan. 2012.

[5]F. Muhammad-Sukki, A. B. Munir, R. Ramirez-Iniguez, S. H. Abu-Bakar, S. H. Mohd Yasin, S. G. McMeekin, and B. G. Stewart, "Solar photovoltaic in Malaysia: The way forward," *Renew. Sustain. Energy Rev.*, vol. 16, no. 7, pp. 5232–5244, Sep. 2012.

[6]R. Dufo-López, G. Zubi, and G. V. Fracastoro, "Tecno-economic assessment of an off-grid PV-powered community kitchen for developing regions," *Appl. Energy*, vol. 91, no. 1, pp. 255–262, Mar. 2012.

# Estimation of Global Solar Radiation from Meteorological Parameter in Peninsular Malaysia

Chia Wai Kit Louis[1], Reynato Andal Gambol[2*]

[1]*Electrical and Electronic Engineering, Taylors' University, Malaysia,* [2]*Electrical Engineering, Taylors' University, Malaysia*

**waikitlouis.chia@sd.taylors.edu.my;ReynatoAndal.Gamboa@taylors.edu.my*

*Abstract*— **Solar radiation data is vital for designing high precision solar conversion tool. Therefore, temperature-based model is being calibrated according to the weather of Malaysia to calculate the daily solar radiation with high accuracy at any site in Peninsular Malaysia. Statistical performance indicators are used to ensure the accuracy and reliability of the mathematical model.**

*Keywords*— Global Solar Radiation, Temperature, Peninsular Malaysia.

## 1. Introduction

An estimation of 56% increase in the global energy consumption by the end of year 2040 with the fossil fuel to be responsible as the major energy supply is likely to be true as the energy demand for global need has been increasing significantly [1]. It is to be noted that the reliance on the fossil fuel as the main energy supply is not sustainable as the fossil fuel resources will be depleted one day, thus there is a need to look into alternative energy supply and solar energy is one of the most influential energy supply among the renewable energy resources, largely being that there is still a lot of untapped potential in harvesting solar energy.

When it comes to harvesting solar energy, designing high precision solar energy conversion tool requires accurate inputs of solar radiation data [2]. However, solar radiation data measured by high precision measuring tools is very limited in Peninsular Malaysia and are only available at some specific sites across the country due to the high cost of installing them such as pyranometer and pyrheliometer to determine the solar radiation level [3]. Therefore, it is suggested to estimate the global solar radiation using climatological parameters such as sunshine duration, temperature, precipitation data, relative humidity etc. which are relatively easier to get from the local meteorological stations in Peninsular Malaysia.

Although there are a lot of research done in developing empirical models to determine the global solar radiation across the whole world, only a few empirical models are catered for Malaysia's climate. Most of the empirical models are only focusing in location like Perlis, Kelantan and Terengganu [4-6], while others are just journals reviewing the potential of harvesting solar energy in Malaysia [7]. Thus, the mission of this research is to find a mathematical model to calculate estimated solar radiation with practical accuracy using temperature and geological parameters so that it can be used at sites throughout the whole Peninsular Malaysia where solar radiation measurement is absent.

## 2. Objective

The objectives of this research are illustrated as followed:

(i) To develop a mathematical model for estimating daily global solar radiation from extraterrestrial radiation, meteorological data and geographical parameters.

(ii) To test the reliability of the empirical models by comparing the measured value and the calculated value in Peninsular Malaysia.

## 3. Methodology and Data

The temperature model has been selected to be the category of solar radiation model to start with because it is widely available from local meteorological station. Although sunshine duration hour is equally easier to get from the meteorological station, it is found that all the local meteorological stations have stop measuring sunshine duration since 1999. Therefore, it is not viable to come out with a sunshine duration model without any current measurement data to validate the model.

Daily meteorological parameters data are then collected exclusively from 5 selected stations throughout Peninsular Malaysia, namely Alor Setar, Ipoh, Kluang, Kuala Terengganu and Termerloh as shown in Fig 1. The data is divided into two parts to be used for two purpose, installation and validation. For the installation part, the data from 2001 to 2005 is computed into the selected models to derive the empirical coefficient. After then, the derived empirical coefficient is used to calculate the solar radiation data.

As for the validation part, the measured solar radiation data from the meteorological stations in 2013 will be used to compare with the calculated solar radiation data by using a set of statistical performance indicator.

### 3.1 Solar Radiation Model

In this research, two solar radiation models will be chosen to be modified, namely Hargreaves model and Bristow and Campbell model in which the parameter inputs are daily maximum temperature and minimum temperature.

#### *3.1.1 Hargreaves Model*

An empirical model is proposed by Hargreaves and Samani to calculate the solar radiation with maximum and minimum temperature as inputs [8].

$$\frac{H}{H_0} = a(T_{max} - T_{min})^{0.5} \quad (1)$$

$H$ is the daily total solar radiation incidental on horizontal surface and $H_o$ is the daily total solar radiation incidental on extraterrestrial horizontal surface. The unit for both $H$ and $H_o$ is MJ/m$^2$ day. It is proposed that coefficient, $a=0.16$ for interior regions and $a=0.19$ for coastal region [9].

#### *3.1.2 Bristow and Campbell Model*

An empirical model is later proposed by Bristow and Campbell in which the daily global solar radiation, $H$ is an exponential function of temperature difference, $\Delta T$ [10].

$$\frac{H}{H_0} = a[1 - \exp(-b\Delta T^c)] \quad (2)$$

Empirical coefficient, a, b and c can be derived by using regression analysis on the measured meteorological data from year 2001 to year 2005.

The value of the total solar radiation on extraterrestrial horizontal surface can be calculated using the equation (3) [11].

$$H_0 = \frac{24}{\pi} G_{sc} A \left[1 + 0.033 \cos\left(\frac{360N}{365}\right)\right] \quad (3)$$

$$A = \left(cos\varphi\, cos\delta\, sin\omega + \frac{\pi}{180}\omega\, sin\varphi\, sin\delta\right) \quad (4)$$

The solar constant value, $G_{sc}$ is 1367 W/m$^2$. N is the day number in which 1 January to be 1 and 31 December to be 365. $\varphi$ is the latitude of the site. Solar declination, $\delta$ and sunset hour angle, $\omega$ can be calculated from the equation (5) and (6).

$$\delta = 23.45 \sin\left[\frac{360}{365}(284 + N)\right] \quad (5)$$

$$\omega = \cos^{-1}(-tan\varphi\, tan\delta) \quad (6)$$

### 3.3 Statistical Method

Table 1 show the detail of the performance indicators which are going to be used to evaluate the calculated solar radiation data from the calibrated models against the measured solar radiation data from meteorological station.

Table 1: Statistical performance indicators

| Performance Indicator | Equation |
|---|---|
| Coefficient of determination ($R^2$) | $R^2 = 1 - \frac{\sum_{i=1}^{n}(H_{i,m} - H_{i,c})^2}{\sum_{i=1}^{n}(H_{i,m} - \overline{H_m})^2}$ |
| Root mean square error (*RMSE*) | $RMSE = \left[\frac{1}{n}\sum_{i=1}^{n}(H_{i,c} - H_{i,m})^2\right]^{1/2}$ |
| Mean percentage error (MPE) | $MPE(\%) = \frac{1}{n}\sum_{i=1}^{n}\left(\frac{H_{i,c} - H_{i,m}}{H_{i,m}}\right) \times 100$ |
| Mean absolute percentage error (MAPE) | $MPE(\%) = \frac{1}{n}\sum_{i=1}^{n}\left\|\left(\frac{H_{i,c} - H_{i,m}}{H_{i,m}}\right)\right\| \times 100$ |

The symbol *i* denotes the *ith* value of the solar radiation value and *N* is the size of the solar radiation data. As for the symbol *c* and *m*, they denote as the calculated and measure solar radiation values respectively. $\overline{H_m}$ is the average measured solar radiation value.

It is suggested that value for *RMSE*, *MPE* and *MAPE* to be close to zero to indicate the accuracy of the calibrated model. As for $R^2$, value close to 1 is desired indicating a strong match between the measured and calculated solar irradiance data.

## 7. Conclusions

In conclusion, the parameters for the solar radiation model is the temperature-based model. The reason for choosing this parameter is that the air temperature data is easy to be obtained from the local meteorological station. Aside from this, it is to be noted that the sunshine duration data is only available up till 1999, thus it is not practical to come out sunshine duration based model as there is no data to validate this specific parameter model.

5 years data is collected from 5 stations throughout Peninsular Malaysia to gauge the accuracy and feasibility of the calibrated models for calculating the daily irradiation incident on horizontal surface. The empirical coefficient is calculated using the data from 2001 to 2005 and the developed empirical model is validated using 2013 data through the use of statistical performance indicator.

## References


[1] US Energy Information Administration (2013). *International Energy Outlook 2013.*

[2] I. Korachagaon, V. Bapat (2012). General formula for the estimation of global solar radiation on earth's surface. *Renewable Energy,* 41, 394-400.

[3] F. Besharat, A. A. Dehghan and A. R. Faghih (2013). Empirical models for estimating global solar radiation: a review. *Renewable and Sustainable Energy Review,* 21, 798-821.

[4] I. Daut, M. Irwanto, Y. Irwan, N. Gomesh and N. Ahmad (2011). Combination of Hargreaves method and linear regression as a new method to estimate solar radiation in Perlis, Northen Malaysia. *Solar Energy,* 81, 2871-2880.

[5] W. W. Nik, M. Ibrahim, K. Samo and A. Muzathik, "Monthly mean hourly global solar radiation estimation. *Solar Energy,* vol. 86, pp. 379-387, 2012.

[6] S. Ibrahim, I. Daut, Y. M. Irwan, M. Irwantoa, N. Gomesh and A. Razliana. (2012). An Estimation of Solar Radiation using Robust Linear Regression Method. *Energy Procedia,* 18, 1413-1420.

[7] S. A.N., I. Daut, M. Irwanto, Z. Farhana, N. Razliana and A. Z. (2012) Potential of Solar Energy Harvesting in Ulu Pauh, Perlis, Malaysia using Solar Radiation," *Energy Procedia,* 14, 1503-1508.

[8] Hargreaves GH, Samani ZA. (1982). Estimating potential evapotranspiration. *Journal of Irrigation and Drainage Engineering,* 108(IR3), 223-30.

[9] Hargreaves GH. (1994). *Simplified coefficients for estimating monthly solar radiation in North America and Europe.* Department of Biological and Irrigation Engineering, Utah State University, Logan.

[10] Bristow KL, Campbell GS (1984). On the relationship between incoming solar radiation and daily maximum and minimum temperature. *Agriculture and Forest Meteorology,* 31, 59-166.

[11] Soteris A. Kalogirou (2009). *Solar Energy Engineering: Processes and Systems. Oxford, UK: Elsevier.*

# Automated Attendance Capture System

Jonathan Chin Eu Tsun*, Chew Wei Jen, Florence Choong Chiao Mei

*School of Engineering, Taylor's University Lakeside Campus, Malaysia,*

**Corresponding email: Jonathan.EuTsun@gmail.com*

*Abstract*—**Current attendance system that uses face recognition do not track the presence of the students in class before determining if the students should be marked present. This results to an unreliable system as once it has marked the attendance of the students, they are able to skip the rest of the lecture. In this paper, an automatic attendance capturing system that is able to track the presence of students provided that they are present for a set duration of time is proposed. This system tracks the students based on the number of times they are recognized in a frame obtained from the video of the class. From the number of times they are recognized against the total frames of the video, the system can compute whether the students are present or not. From the results, it is found that the system is able to track and ensures that the students are present for a set duration of time before marking their attendance which improved the reliability of face recognition for attendance capturing system.**

*Keywords*— Attendance System, Image Processing, Face Detection and Recognition, Tracking

## 1. Introduction

Capturing the attendance of people is a task commonly performed every day. For example, in the workplace, bosses need to be able to know whether the staff have reported to work while in academia such as schools and universities, the attendance of students are also needed to be taken to track their status. Therefore, it is important that the attendances taken are accurate and fast so that it does not consume too much time. Traditionally, universities have often used the conventional method of calling names and signing of attendance sheet to record the attendance of the students. This old method has proven to be very tedious especially for big classes and can easily be compromised through the help of fellow students signing on behalf of their friends. With that, automatic attendance systems which use face recognition have been proposed as a solution to the problems faced by traditional methods.

By applying image processing for attendance capturing, precious time can be saved as the system will take the attendance of the students automatically without the need of human operation. Furthermore, it is impossible for another person to fake his attendance as his face is required in order for him to be recognized and marked present. There are many attendance capturing systems out there that uses face recognition. The one proposed by Balcoh et al [1] suggested the implementation of image enhancement before performing the face detection and recognition, whereas Kawaguchi et al [2] proposed the usage of two camera where one will detect the position of the student and the other is used to capture the image of the student for detection and recognition. Shehu et al [3] proposed an autonomous system which stores successfully recognized images so that the system can identify the students in the future even when the student's facial features may have changed.

All these systems have their advantages but it is found that they share a common flaw which is that the systems proposed repeatedly captures the picture of the students to ensure that they do not miss out a student. Hence, once a student has been successfully recognized, his attendance is taken and he is able to skip the rest of the lecture without worrying about his attendance being mark absent. This shows that current systems proposed are not that reliable as once the attendance of that student is taken by the system, he is able to skip the rest of the class and still be marked present.

Therefore, an automatic attendance capturing system that is able to track the students is proposed in this paper. This system uses existing face detection and face recognition system to accurately detect and recognize the students. Then, it will track each student to ensure that they remain in the class for a certain period of time before taking their attendance. Therefore, the major contribution of this project is the improvement of the reliability of the systems proposed previously by introducing an algorithm that tracks the students to ensure that they are present for a set duration of time before taking their attendance.

## 2. Methodology

### 2.1 Experimental Procedures

Figure 1 illustrates the proposed method. During a lecture, a webcam attached to a laptop will continuously capture a video of the class. At fixed time intervals during the lecture, a frame of the video of the class is obtained and passed to the laptop which will perform histogram equalization as what was proposed by Balcoh et al [1] before being sent for face detection. Detected faces are then passed through a filter which isolates false detection. Faces detected are then cropped and passed to the face recognition system. Before the experiment is carried out, a database of faces for students in the lecture are collected for the face recognition system. The face detection method used was proposed by Viola-Jones et al [4] due to its high accuracy and low false detection whereas the face recognition method used is Eigenfaces [5] as it is able to recognize slightly tilted face which is very important as students will be moving their heads from time to time during the lecture and may not maintain the same angle at all times.

When a student is recognized, he is awarded a point. If the lecture has not ended then the results will be stored and the steps are repeated from the start until the lecture has ended. The attendance of that student is then determined based on the number of points collected which is the number of times that student is recognized against the system's counter that adds continuously if there are faces detected in a frame. For example, if the system captures 50 frames from start to the end of a lecture and faces are detected in those 50 frames, the system's counter will be 50 and if student X is recognized 40 times out of those 50 frames, student X will have a total point of 40. By taking the points accumulated against the system's counter, the calculation of the percentage of which of the student is in the class which in this case is 40 divided by 50 which means that student X is present for 80% throughout the class will be calculated. Based on the threshold defined, the system will then determine if the student is present or absent. After computing the attendance of the student, the attendance is saved into an Excel spreadsheet.

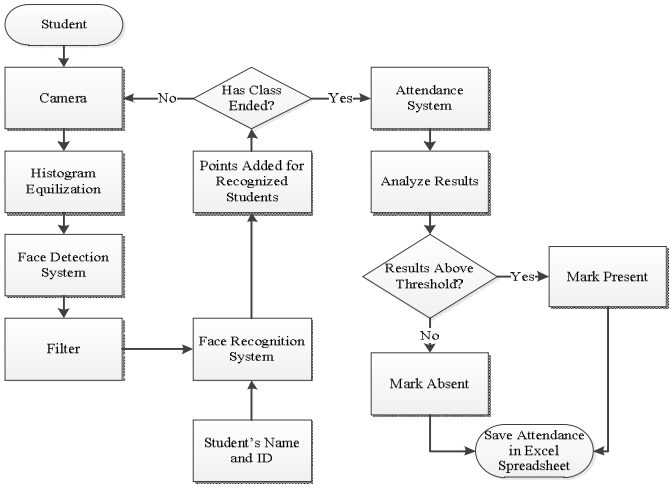


Figure 1: Project Flowchart

## 4. Results and Discussion

For a class test of three students who have their faces in the database, 32 frames were taken from the video of the class. The external webcam captures the frame of the video for the class and sends it to the laptop where the face detection and face recognition is done. A small class was used due to the limitation of the webcam used that causes the resolution of faces from the third row onwards to become too low for recognition purposes. The results are split into face detection, face recognition and attendance.

### 4.1 Face Detection

Figure 2 and 3 demonstrates the detection rate of the system. As seen in both figure 2 and figure 3, boundary boxes were placed around the detected faces. Table 1 shows the results obtained from the face detection system. As 32 frames were taken, student A and student B were actually present throughout the video whereas student C was not present during the start of the video, resulting to him actually being present in the remaining 26 frames. Number of times detected shows the success rate of the face for student A, B and C being detected by the system. By taking the number of times detected over the number of times present in the frame, the face detection rate of the system in this case is 100%. This shows that the face detection method proposed by Viola-Jones et al [4] is very efficient.

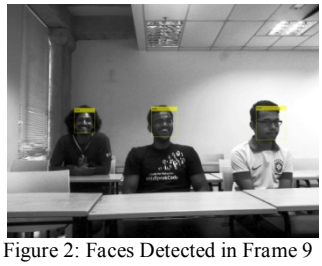

Figure 2: Faces Detected in Frame 9

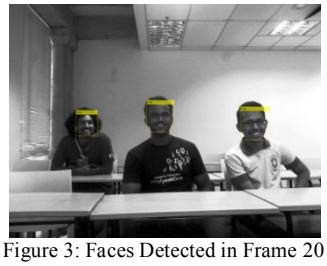

Figure 3: Faces Detected in Frame 20

Table 1 Results of Face Detection System

| Student | A | B | C |
|---|---|---|---|
| Number of times actually present in the frames | 32 | 32 | 26 |
| Number of times detected | 32 | 32 | 26 |
| Face detection rate (%) | 100 | 100 | 100 |

### 4.2 Face Recognition

Table 2 shows the results obtained from the recognition system. Based on the recognition rate obtained, it can be said that the system is quite accurate as the lowest recognition rate is 88%. Student A was able to be recognized in all the 32 frames whereas student C is only able to be recognized 23 times out of the 26 frames the student was actually in. This could be due to the threshold set in the recognition system to filter out students who are not registered into the database, which is also the same reason why student B could not be recognized a 100%. Another reason could be due to the angle at which the face was detected. This could be resolved by ensuring that the training database for the Eigenface recognition system [6] consists of images of that student's face tilted at certain angle.

Table 2 Results of Face Recognition System

| Student | A | B | C |
|---|---|---|---|
| Number of times detected | 32 | 32 | 26 |
| Number of times recognized/tracked | 32 | 29 | 23 |
| Face recognition rate (%) | 100 | 90 | 88 |

### 4.3 Attendance

Table 3 gives the results obtained from the attendance system. The total time in class (%) refers to the percentage in which each student's are present throughout the 32 frames and is computed by taking number of times recognized/tracked divided by the system's counter. As there are faces detected in all 32 frames, the system's counter is 32. Student A has a total time in class percentage of 100% which means that he was present throughout the 32 frames. As student C was not present for the first few frames, his total time in class percentage is definitely lower. Based on the results obtained, it can be seen that the attendance system is dependent on the face detection and face recognition system. From the results obtained for student B, even though he was present throughout the entire 32 frames, the system was only able to recognized him 29 times therefore his total time in class percentage is 90% when it should be actually 100%. This can be rectified by improving the face recognition system. As the threshold of the system was set to 70%, which means if the students have a total time in class percentage of 70 and more, their attendance will be marked present. Since all the students have met the requirement, they are all marked present.

Table 3 Results of Attendance System

| Student | A | B | C |
|---|---|---|---|
| Number of times recognized/tracked | 32 | 29 | 23 |
| Total time in class (%) | 100 | 90 | 71 |
| Attendace | 1 | 1 | 1 |

## 5. Conclusions

The proposed system is able to track the students to ensure that they are present for a set duration of time before taking their attendance as seen from the results shown in the results and discussion section. The attendance system relies on the face detection and recognition system in order to track the students present in the class. Therefore it is important that both the face detection and face recognition have a high success rate. For future works, the face recognition system is required to be improved as it may sometimes fail to recognize the students as shown in the results obtained for student B. In addition, by using a better camera, the size of the classroom and number of rows can be increased.

## References

[1] Naveed Khan Balcoh, M. HaroonYousaf, Waqar Ahmad and M. IramBaig . "Algorithm for Efficient Attendance Management: Face Recognition based approach." IJCSI International Journal of Computer Science Issues, Vol. 9, Issue 4, No 1, July 2012

[2] Y. Kawaguchi, T. Shoji, W. Lin, K. Kakusho, and M. Minoh, "Face Recognition-based Lecture Attendance System." The 3rd AEARU Workshop on Network Education, pp. 65-69, 2005

[3] Shehu V and Dika, A., "Using real time computer vision algorithms in automatic attendance management systems." Information Technology Interfaces (ITI), 32nd International Conference, pp.397-402, 21-24 June 2010

[4] Paul Viola and Michael J. Jones, "Robust Real-Time Face Detection."International Journal of Computer Vision 57(2), 137–154, 2004

[5] M.A. Turk, A.P. Pentland, "Face Recognition Using Eigenfaces." Proceedings of the IEEE Conference on Computer Vision and Pattern Recognition, Maui, Hawaii, USA, pp. 586-591, 3-6 June 1991

# Electromagnetic Analysis of a Novel Outer Rotor Permanent Magnet Generator

Kamalinni Mohan Raj[1], Aravind CV[2*], R.N.Firdaus[2]

[1]*CIARG, Taylor's University, Malaysia,* [2]*Universiti Tecknical Malaysia, Melaka*

**Corresponding email: aravindcv@ieee.org*

*Abstract*— **Newer types of synchronous generators were being developed for typical applications in the past decade due to the advancements in high power density permanent magnets. An outer rotor generator which can typically be applied for wind power and electric vehicle applications are proposed in this paper. The design of the structure is done through analytical calculations and the analysis to optimize the machine parameters are done through numerical analysis. This paper proposes the electromagnetic analysis of a novel outer rotor permanent magnet generator. The designed machine which has 18 slots and 20 poles generates a voltage of 150V when running at 1200 rpm.**

*Keywords*— permanent magnet synchronous generator, torque density, cogging torque

## Introduction

In the Permanent Magnet Synchronous Machine (PMSM), the rotor can be positioned in two ways which is in the inside (inner rotor type) and on the outside (outer rotor type). The key factor in designing a better machine lies in maximizing the power density of the machines. This is usually done through the optimization of parameters like the position and shape of the magnet with respect to the static electromagnetic field [1]. Placing the rotor on the outer surface yields a better torque compared to that of the inner rotor [2]. A fractional horse power outer rotor permanent magnet generator is designed and its electromagnetic design analysis is presented. Attempts by researchers on the study of placing the rotor in inner and outer surface is documented in the literature [3].The outer rotor PMSM derives significant improvement due to the longer radius compared to the inner rotor design. They are found in significant applications such in mechanical cutters [4] and wind turbines [5-6]. The purpose of this research is to design an outer rotor structure generator that can be coupled with a wind turbine generator. The machine is designed with 18 slot and 20 poles catering to the three blade structure of the wind turbine in place. A detailed analysis of the electromagnetic analysis is presented in this paper.

## Methodology

Fig.1 shows the flowchart of the methodology employed in the machine. The ratings of the generated voltage based on the sizing are computed using the Equation (1) to Equation (3). The generated voltage (Q) of the machine is derived as

$$Q = Magnetic\ laoding\ (B_{avg}) XElectrical\ Loding\ (ac) \quad (1)$$

$$Q = 1.11\ \pi^2 K_c K_d (B_{avg}\ DL)(ac\ D)\ n_s\ 10^{-3} \quad (2)$$

$$Q = 1.11\ K_c K_d\ (B_{avg}\ L)(ac)\frac{{v_a}^2}{n_s}\ 10^{-3} \quad (3)$$

where

$K_c$: *Pitch factor* $K_d$: *Distribution factor*

$D$: *Outer diameter of the machine* $L$: *Stack length*

$v_a$: *Rotational speed* $(= \pi D n_s)$

$n_s$: *Synchronous speed*

Fig.2 shows the cross section view of the designed machine and Fig.3 shows the exploded view of the design. Table 1 shows the corresponding values of the designed machine.

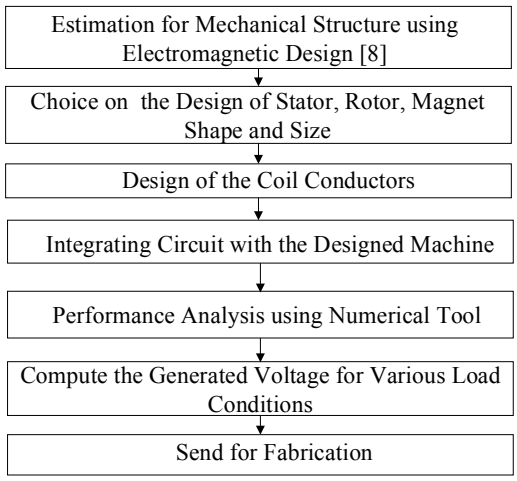


Fig.1 Methodology used for the design of the machine

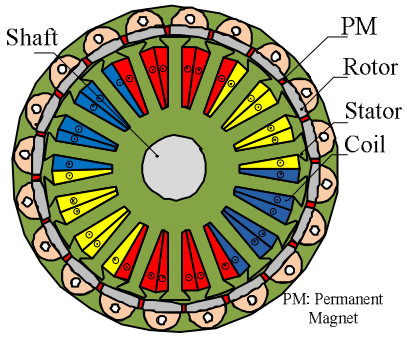


**Fig.2** Cross Section Area of Design

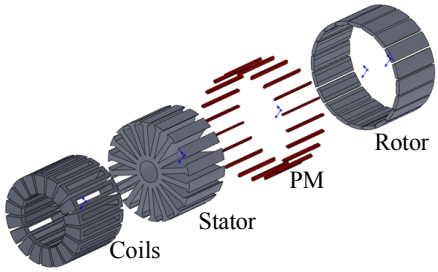


**Fig.3** Exploded View of Design

**TABLE 1. Designed Machine Parameter**

| Parameter | Units |
|---|---|
| Outer diameter | 100 mm |
| Outer rotor inner diameter | 93mm |
| Air gap length | 0.5mm |
| Shaft diameter | 10 mm |
| Stack length | 50 mm |
| Turns per phase | 158 |
| Rated current | 10 A |

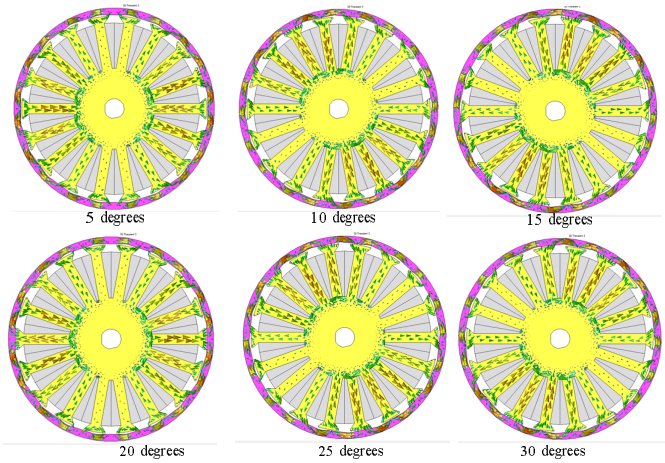


**Fig.5** Magnetic flux density at various rotor positions

The magnetic flux density for one pole pitch value is shown in Figure 5. This magnetic flux density computed through simulation confirms with the designed value earlier for proper excitation and operations of the proposed machine. The electrical parameters of the voltage, current and power are computed in order to conduct an analysis on the performance of the machine. The voltage and the power generated are calculated using a dummy resistive load and the rotor is rotated. The computation is done for both static and dynamic conditions. The voltage and power generated is then computed for various positions of the rotor when a constant current is applied. The same procedure is done with constant frequency applications and the rotor is rotated for various speeds.

## Results and Discussion

Figure 6, shows that as the rotational degree value increases, the magnetic flux decreases slightly during the static condition. Figure 7 shows that as the voltage generated increases from 0 V to 25 V, there is a drastic increase in the magnetic flux. However, as the voltage increases further, there is only a slight increase in the magnetic flux. In a machine, when the voltage increases, this results in an increase in the magnetic flux as the voltage is proportional to the flux when the speed of rotation in a machine is fixed. Figure 8 shows that as the speed of rotation increases, there is a gradual linear increase in the voltage generated by the design because in DC machines, the speed of rotation is directly proportional to the voltage of the machine. Based on the graphs, it can be concluded that the voltage of the machine produced is 150V. The maximum power produced is 250W at 1200 rpm.

## Conclusions

Through mechanical variations on the design, a better torque is produced when the diameter of the rotor is increased. By optimising the pole design a novel structure is proposed in this research. The electromagnetic design analysis of such a machine presents encouraging power density improvements. Initial investigations reveal a generated voltage of 150V when the design runs at 1200 rpm. This machine is ready for fabrication and is to be integrated with an application (in this case a small size laboratory wind turbine).

## References

[1] E. Muljadi and J. Green, "Cogging Torque Reduction in a Permanent Magnet Wind Turbine Generator," in *21st American Society of Mechanical Engineers Wind Energy Symposium Reno, Nevada,* pp. 1-5, Jan. 14-17, 2002.

[2] CV Aravind, M Norhisam, I Aris, D Ahmad and M Nirei, "Double Rotor Switched Reluctance Motors: Fundamentals and Magnetic Circuit Analysis," in *IEEE Student Conference on Research and Development (SCORED2011) Kualalumpur,* pp. 294-299, Jan. 2011.

[3] I. Tarimer and C. Ocak, "Performance Comparison of Internal and External Rotor Structured Wind Generators Mounted from Same Permanent Magnets on Same Geometry," *Electronics and Electrical Engineering*., vol. 92, no. 4, pp. 65-70, July. 2009.

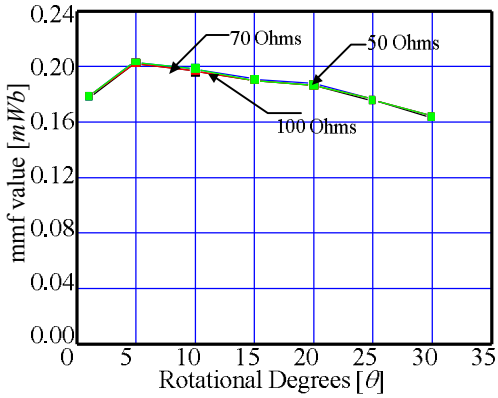


**Fig.6** Static Characteristics of MMF in Coil

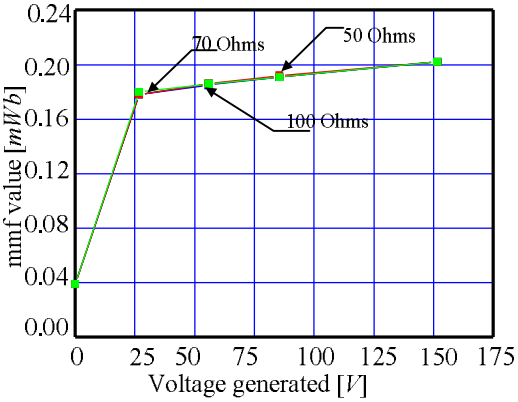


**Fig.7** Transient Characteristics of MMF in Coil

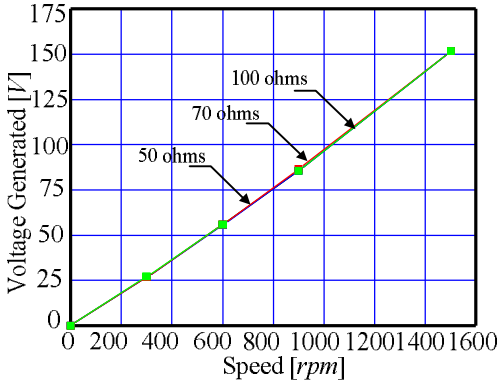


**Fig.8** Generated Voltage

[4] M Norisam, S Ridzuan, RN Firdaus, CV Aravind, H Wakiwaka, and M Nirei, "Comparative Evaluation on Power Spped Density of Portable Permanent Magnet Generators for Agricultural Application," *Progress In Electromagnetics Research,* Vol.129, 345-363, May. 1,2012.

[5] Mayouf. Messaoud and Rachid. Abdessamed, "Modeling and Optimization of Wind Turbine Driving Permanent Magnet Synchronous Generator," *Jordan Journal of Mechanical and Industrial Engineering,* pp.489-494, 2001.

[6] Aravind CV, SC Tay, A Jagadeeswaran and RN Firdaus, "Design of MAGLEV-VAWT with modified Magnetic Circuit Generator," in *Second International Conference on Electrical Energy Systems, Chennai India,* Jan. 7-8, 2014.

[7] Aravind CV, Rajparthiban, Rajprasad, Wong YV, Grace and I Stanley, "A Novel Magnetic Levitation Assisted Vertical Axis Wind Turbine Design Procedure and Analysis," in *8th International Colloquium on Signal Processing and applications, Kualalumpur,* pp. 93-98, Mar. 22-23, 2012.

[8] C Aravind Vaithilingam and C Kamalakannan, *Design of Electrical Apparatus*. Chennai India: Charulatha Publications Chennai India, 2003.

# Design and Development of Signage Displays

Kai Meng, Liaw[1], Irda Hassan[2]

*School of Engineering, Taylor's University Lakeside Campus, Malaysia.*

**Corresponding email: liaw.kaimeng@gmail.com , NurmalaIrdawaty.Hassan@taylors.edu.my*

*Abstract*— **Previously, operating the signage displays using microcontroller already existed. Displays were wired to the microcontroller and updated through software programme. There is limitation with this method due to wired connections to use software to update the displays. In this paper, another further approach will be carried on by only using mobile phone to update the displays through GSM module. Solar energy will be the source of energy for this project.**

*Keywords*— GSM, Microcontroller, Signage

## 1. Introduction

Signage has been used to convey messages and information to the people. It has evolved from conventional to the digital signage. During the old days, conventional signage has been utilized using printed papers or handwritten. Digital signage normally used in industries such as food and beverage industries, shopping malls, universities and also highways to show information and messages. Normally, all the displays are linked to a control system whereby update process can be done. In other words, displays update can only be done in one place only. Therefore, to ease the job for people, updates should be able to carry out anywhere not necessary at one place. This paper shows how GSM module can be used as interaction with the microcontroller to improve the signage displays update.

## 2. Objectives and Scopes

### 2.1 Objectives

I. To write and upload the source code for the microcontroller chips

II. To build a MCU circuit board to interface with the GSM modem and 8 x 8 dots matrix displays

III. To build the multiple 8 x 8 dots matrix displays.

*IV.* To power up the signage displays using solar energy.

### 2.1 Scopes

I. Using mobile phone to update the information displays instead of using software.

II. Avoid unnecessary travelling to update the displays for the digital signage.

III. Using solar panels to power up the project.

## 3. Literature Reviews

Lim Sheng has done a project on Multi-level dots matrix display. The overall design of his project is to display the information on the matrix display by using Visual Basic software through PIC microcontroller [1]. In his paper, he describes that changing of content can be done by reprogramming the codes in the microcontroller. In other words, is to refresh the memory and download a new source code into it. The main components in his project are a LED matrix display and microcontroller. Information is programmed into the PIC 18F877A microcontroller and decoded it to enable all the port from Port A to give bits to 48 LED in the dot matrix column. Proteus VSM Source Code Editor is used to programme the code.

Huang Wei described on how to use web-based remote control as user interface to change the contents in the LED Dot Matrix Display [2]. User can send data and control this LED panel using web browser. Web controller will generate a web page after connection is established from the computer. Instructions will appear in the web page on how to enter messages. These data will transfer to the web controller via internet protocol. These data will be transmitted using IR transmitter to the LED matrix display. The whole process is a one way signal transmission.

Siti, Isolehah had used mobile phone with GSM modem to send text message to user in her project, Smart Security Atert System via SMS [3]. AT89S52 chip interfaced with sensor ,GSM module and the alarm circuit. Whenever there is sign of break in, programmed AT89S52 chip will send signal to the relay driver circuit. This driver will operate the GSM modem in the mobile phone to send alert SMS to the user and switch on the alarm.

According to the previous studies shown, different methods of interfaces has been use for updating their displays contents. Lim Sheng has used PIC microcontroller to display the informations on dot matrix display. Through computer, visual basic programe is used to change the information on the dot matrix displays. Range of microcontrollers are wide. For instants, PIC and Atmel microcontroller. Any microcontroller can be used as interface as long as appropriate assemble languages are used for programming. As for Huang Wei ,the signage display is configured using websites whereby web controller is applied in his project.

As for this project, method proposed is sending messages using mobile phone, received by GSM and transmit the information from GSM to the microcontroller. Lastly, information stored in the microcontroller will be display in the dots matrix display. The microcontroller chip that will be used is Atmega328P chips from ATMEL company. Compared to PIC microcontroller, Atmel chip is relatively bigger in size compared to PIC chip. Atmel chip has serial capability whereby PIC do not have this feature [4]. Serial Capability allows coding to be programmed into the Atmel chip using Serial to USB converter connect to the Arduino Software where sketch uploads can be done. PIC chip uses pipelining which the Atmel did not. Pipelining means every instruction in memory has to be fetched only can be executed.

## 4. Methodology

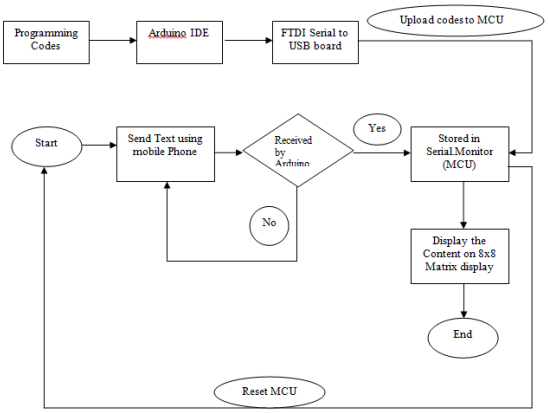


Fig. 1 A flow chart for full project design.

The hardware in this project will be the ATmega328P chips, GSM modules, LED dot matrix display and solar panels. Software parts will be the programming codes which will be uploaded into the microcontroller chip using FTDI serial to USB converter through Arduino IDE program.

### 4.1 Setting up Atmega328P microcontroller board, LED dot matrix displays and GSM module.

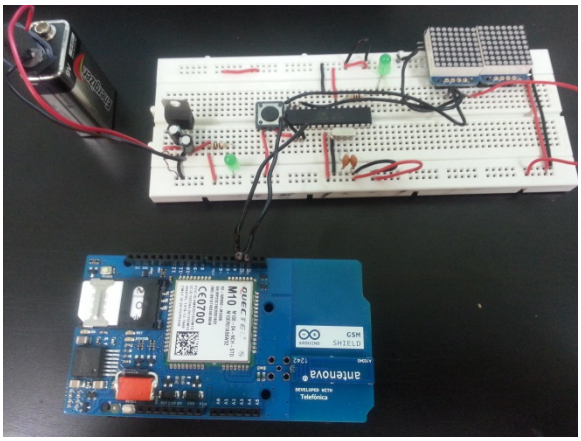

Fig. 2 Prototype inclusive of Atmega328P MCU board,LED matrix display amd GSM module

### 4.2 Programming Code Sketching.

Programming code will be written and compile in Arduino IDE software.

### 4.3 Code uploading into Atmega328P chip.

FTDI serial to USB converter will be used for serial communication purposes. Once the software and the Atmega328P successfully recognized, coding can be upload into the microcontroller chip.

### 4.4 PCB Board for Atmega328P.

The Atmega328P will be using PCB board for the final end product.

### 4.5 Solar panels to power up the entire modules and enclosure to protect the microcontroller circuits.

Suitable solar panels will be used and place outside on the enclosure to generate power for the project and charge the battery. The whole project will be place into the enclosure for protection purpose.

## 5. Expected Results

Table 1. LED dot matrix display output.

| Input (SMS) | Expected Output on displays |
|---|---|
| Text message will be sent from mobile phone. | Dot matrix will show the content on the LED display. |

## 6. Conclusions

In conclusion, Atmega328P set up has to be extra careful as the chip is very sensitive especially the operating voltage. Crystal and capacitors are important to have in the connection of ATmega328P for programming purposes. Microcontroller plays the important role in this project. It is used as the interfacing circuits between the LED dot matrix display and GSM module. Serial programming is the major work in this project to programme the ATmega328P.

## References

[1Lim Sheng, K (2007 ). *Multi-Level LED Dot Matrix Display Panel*. Melaka, Malaysia: Universiti Teknikal Malaysia Melaka, Faculty of Electronic and Computer Engineering.

[2]Huang Wei,C(2009). Implementing Web-Based Remote Control System For LED Dot Matrix Display.Taiwan: Southern Taiwan University,Department of Electrical Engineering.

[3]Siti, Isolehah (2011 ). *Smart Security Aleert System via SMS*. Melaka, Malaysia: Universiti Teknikal Malaysia Melaka, Faculty of Electronic and Computer Engineering.

[4] Lucio Di Jasio, Tim Wilmshurst, Dogan Ibrahim, John Morton, Martin P. Bates, Jack Smith, David W Smith, Chuck Hellebuyck (2007). *PIC Microcontrollers: Know It All: Know It All.* Newne

# Design and Development of Colour Sorting Robot

Lim Jie Shen[1*], Irda Hassan[2**]

[1.2]*School of Engineering, Taylor's University, Malaysia*

** jefflim88@gmail.com ** nurmalairdawaty.hassan@taylors.edu.my*

*Abstract*— **This paper shows a new approach for continuous recognition and sorting of objects into desired location. Image or colours processing nowadays attract massive attention as it leads to possibility of widening scope of application in different field with the help of modern technology. A colour sorting robot is researched, designed and created with Arduino UNO microcontroller, TCS3200D colour sensor, servo motor and other electronic components. The system has the ability to sort the object according to their colours into respective colour station in minimum time. Specific programming code for this system is written.**

*Keywords*— Colour recognition, colour sorting, programming, robot, microcontroller.

## 1. Introduction

The ability to differentiate colours is essential for human's life as it gives us the awareness about the changes in surrounding through our vision [1]. Moreover, by exploiting the ability of colour capture, intelligent machine gains the function to differentiate, sort and organise. The project includes sensors that detect colour of the object then sends info to Arduino Uno which in turn adjust the servo motor which located just below the ball slider to move it up and down [2]. Based upon the colour detected, the slider will move down with the angle of 30º, 50º and 70º depends on the object colour. The stations are in red, green and blue respectively. After every ball placement, the slide will go back to its default angle position, awaiting the next colour ball.

Throughout the years, many people has tried to use various ways to programme and create intelligence robot in various ways to have respective function or achieving goals. Some of the claims made have contributed directly or indirectly to the researched done in this paper. Ying-Hao Yu, et al. 2011, found that a new way in construction turned out to be the upcoming technologies that can be used to accommodate private indoor robots that move with owners and lend them a helping hand when needed [3]. In many cases, the interactions of a few robots are needed to carry out certain task, whereby it is crucial to fully control robots to operate at level which is desired [4]. This Colour Sorting Robot is developed with the purpose of minimising the cost, optimising the productivity and reducing human mistakes.

The objectives of this project are summarised as below:

i. To sort the object according to their respective colours.
ii. To write colour recognising code and sorting programming code.
iii. To research best way to slide down the ball to station
iv. To sort the object to the desired station accordingly.
v. To integrate colour recognising, sorting and motor with Arduino.
vi. To test and troubleshooting on the efficiency of the system.

## 2. Approach and Methodology

### 2.1 The Significant of the Project

The challenge often occurred in industry that involves colour sorting system such as diamonds industry or food industry such as separation of rice, coffee, other cereals that can be solved via this project are:

i. The speed of colour sorting process by an operator is very slow. This is due to the limitation of response time for a human eye. The eyes will always take some time to see an image and project this to the brain to initiate visual sensation. After the brain has received the image, it will take some time for the brain to determine the colour of the object too. However, this limitation can be covered by using a computer. In this project, Arduino Uno, the microcontroller is used to increase the speed of colour sorting.

ii. The accuracy of colour sorting process by an operator is very low. This is because an operator will need to handle hundreds or thousands of objects each day, tiredness will usually cause some fault when colour is being divided or sorted. It is very common for an operator to make this error. However, a machine will not have this problem. A machine will give accurate result even after it has repeated a process for billions of times unless fault to the system occurs. In this project, servo motor is used to substitute the operator and thus increase the accuracy of colour sorting.

iii. The implementation cost for a colour sorting process using the operator is very high. If an industry needs to sort a bulk quantity of product, many workers are needed and with the implement shift and overtime system, the total sum of cost will be relatively high. This will definitely cause the company more then what they actually needed to pay. With the implication of this system, basically large sum of salary can be saved for better used.

The project is important as it can helps in colour sorting-related industry as the system will basically improve overall performance of sorting system.

i. This system will increase the speed and accuracy of colour sorting process.
ii. This system will cut-down the cost of colour sorting process.
iii. This system will overall optimize the productivity of an industrial

### 2.2 Approach

Colours are light waves that are no different than the electromagnetic waves emitted by cell phones. It is our brain cells that interpret them as real colours. For robot, the simplest way they can use to detect colours is by uses the filters of three main colours, which is red, green and blue and compared the value on the light reflected on it. The value taken will then send signal to Arduino which analyse which colour is the object. For this to work, a programme is written so the microcontroller will carry out the colour sensing and recognising task correctly.

### 2.3 Tools

The colour sorting robot code was program using Arduino software. Programming code is researched and written in order for the colour sorting robot to carry out recognition and sorting mechanisms. The connection is done by connecting wires to connect up Arduino UNO which act as microcontroller, servo as well as colour sensor.

### 2.4 Methods

The method used in this project is to use the Arduino Uno act as the brain that is used to receive signal from TCS3200D which is the colour sensor, and at the same time, send a signal to the servo which function to move the ball slider up and down at different angle. It starts from research of previous journals, identification of parts and components, to project testing and troubleshooting. Light intensity test and colour selection test are carried out as shown in Fig.1

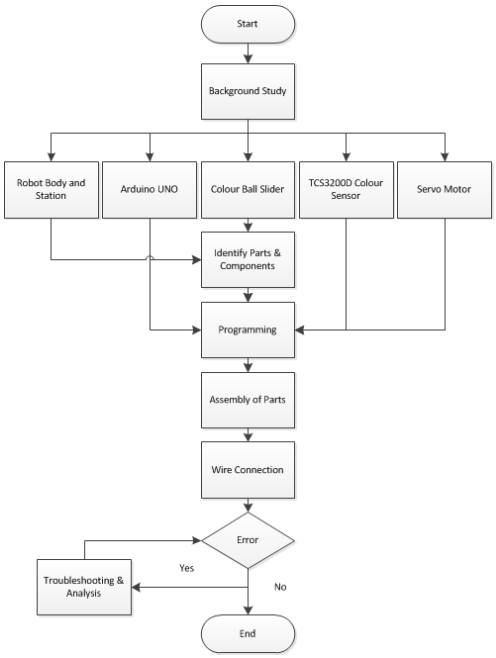


Fig. 1 The flowchart of method used during project.

## 3. Results and Discussion

### 3.1 Data Collection

The method for a colour sensor to recognise it is by using the green, blue and red filter to detect a common colour and see which colour filter has the highest value recorded. If the ball is blue in colour, the blue (B) filter has the highest value compared to other red and green filter as shown in the first 4 lines of the monitoring lines in the Fig. 2 below. The last 4 lines showing that, the colour of next ball, which is red, has the highest red (R) filter value. The RGB value can be checked using many design or paining software such as Adobe Photoshop.

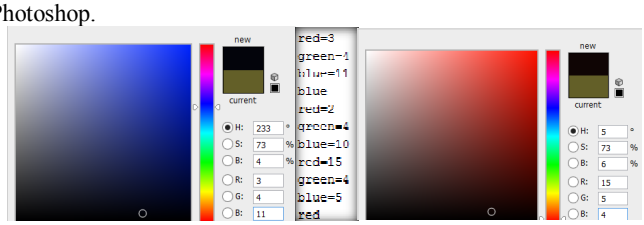


Fig. 2 Colour monitoring in Arduino Programme and Adobe Photoshop that showing blue colour on the left and red colour on the right respectively.

### 3.2 Light Intensity Test

The test is carried out indoor and outdoor to recorded the result and the value shows that the RGB value taken indoor is more or less higher than the one taken outdoor. This is due to the present of more than single light out door which affected the results. Tests taken indoor and outdoor are shown in Table 1 and Table 2 respectively.

Table 1. Table showing the value of RGB filter during indoor test.

| Ball Colour | Average Filter Value | | |
|---|---|---|---|
| | Red filter (R) | Blue filter (B) | Green Filter (G) |
| Red | 17 | 6 | 5 |
| Blue | 3 | 11 | 6 |
| Green | 3 | 3 | 6 |

Table 2. Table showing value of RGB filter during outdoor test

| Ball Colour | Average Filter Value | | |
|---|---|---|---|
| | Red filter (R) | Blue filter (B) | Green Filter (G) |
| Red | 18 | 13 | 9 |
| Blue | 7 | 12 | 8 |
| Green | 2 | 5 | 7 |

It can be seen in the table 1 and 2 that value of the filter is different when tested outdoor and indoor. The presence of other light had causing the TCS3200 D colour sensor filters to have RGB value that are closer to each other. For example, the most obvious results is when tested with green ball outdoor, the green filter and blue filter showed very close result. This might cause the system to detect it as a flaw and not carried out as planned when the two filter share the same reading. This cause the system fails to detect if it is blue ball or green ball.

In order to get optimum result, there are few steps needed to be considered throughout the experiment which is listed below.

i. In the situation where more than one light is present, it is advisable to just focus on a single light surface.
ii. Outside light should be avoided to prevent the presence of too many unwanted light.
iii. Testing result will be more reliable indoor or in a confined space.
iv. Test must be carried out for few times to obtain average results.

### 3.3 Colour Selection Test

The test is carried out to determine what colour of the ball can be best detect by colour sensor TCS3200D. The variety colours of the balls used are blue, red, green, yellow, purple as well as orange.

Table 3. Table showing RGB value of filters with different colour balls.

| Ball Colour | Average Filter Value | | |
|---|---|---|---|
| | Red Filter(R) | Blue Filter (B) | Green Filter (G) |
| Red | 17 | 6 | 4 |
| Blue | 3 | 12 | 7 |
| Green | 3 | 4 | 7 |
| Yellow | 15 | 6 | 14 |
| Purple | 13 | 6 | 15 |
| Orange | 14 | 6 | 12 |

It can be seen in the Table 3 that either two or all three of red, green and blue filter show result that is not too much differ from one another when the colours tested is not the primary colours. The secondary colours such as yellow, purple and orange cannot be detected as easily as colours such as red, green and blue. For example, the orange colour ball is not suitable to be chosen as a tested object as it has R filter and G filter values that are too close to each other.

## 4. Conclusions

In order to create a smart robot that can recognised colour ball and placed them at the correct location using robotic arm, research in length is needed. There are existing robot using PIC microcontroller but there are not many created using Arduino Programme. The real contribution of this system is that it is able to shorten the time needed to sort the colour hence making this system more efficient than the existing one. This robot works by integrating of colour sorting and sorter movement mechanisms and was designed with the purpose of large amount of materials and objects can be sort out in a shorter time with minimum mistake, and to cut-down the cost of whole process.

## References

[1] Khojastehnazhand, M., Omid, M., and Tabatabaeefar, A., "Development of a lemon sorting system based on colour and size" Journal of Plant Science, Vol. 4, No. 4, pp. 122-127, 2010.
[2] David Avishay, Veselin Pavlov and Ivan Avramov "Designing and testing a calibrating procedure for combining the coordination systems of a handling robot and a stationed video camera", Robotics and Computer-Integrated Manufacturing, Vol. 27, pp. 514-520, 2011.
[3] Ying-Hao Yu, N.M. Kwok, Q.P. Ha "Color tracking for multiple robot control using a system-on-programmable-chip", Automation in Construction,Vol. 20, pp.669-676, 2011.
[4] Yongtae Do, "Intelligent worm sorting using robot vision", Procedia Engineering, Vol 41. 41, pp. 917-922, 2012.

# Blade Shape Design and Analysis on the Optimal Direction of Impact for Vertical Axis Wind Turbine

Wei Jie Lou[1], Aravind CV[1*]

[1]*Computer Intelligence Applied Group, Taylor's University, Malaysia,*

**Corresponding email: aravindcv@ieee.org*

*Abstract*— **Wind energy as a viable renewable is reliable and economical for stand-alone systems. Vertical Axis Wind Turbine is getting popular due to the fact Malaysia is lacking of cut-in speed, is viable methods used to harvest wind energy for a low power generation. The power production is highly dependent on the blade shape with respect to the wind flow. In order to increase its output power, the design and optimize the blade design using Computational Fluid Dynamic modelling through different standard blade shapes. Based on the analysis the blade with the highest lift coefficient is chosen. It is observed that NACA4518 have a higher lift coefficient compared to others at an angle of attack at 15°.**

*Keywords*— CFD, NACA, VAWT

## 1. Introduction

The advantage of implementing Vertical Axis Wind Turbine (VAWT) is the ability to generate electricity at low wind speed. However, the design and the position can be highly influential on the output of VAWT. Therefore, the objective of this research is to design and optimize the blade for a VAWT model based on five different NACA profile. These profiles are chosen based on past research done [1-4]. The background of this work is due to the limitations on the choice of the NACA profile [1-3]. Therefore, addition of different NACA profiles into this research to determine the suitable NACA profile to be implemented into the VAWT design. The simulations of these NACA profiles are tested with a numerical tool to determine the drag and lift coefficient which will be discussed in Methodology part. Besides that, the computer aided tool is the used to design the prototype integrated with the NACA profile chosen based on the results from the CFD simulation. This paper would report the simulation results at the Results session.

## 2. Design Methodology

Based on the lift force equation given as in Equation (1)

$$L = \frac{1}{2}\rho u^3 A C_L \quad (1)$$

where L is the lift force, $C_L$ is the lift coefficient, ρ is the air density in kg/m$^3$, u is the wind speed in m/s and A is the area of blade in m$^2$. From the equation, it can be observed that the air densities, wind speed, the size of the blade and lift coefficient are the factors affecting the lift force of the wind turbine. Therefore, CFD tool is used to obtain the lift coefficient of the NACA profiles selected and modelling tool is used to design the blade. Project flowchart is shown in Figure 1. The NACA profiles are simulated under CFD 2-D model and it is solved using pressure-based ANSYS Fluent 14.0 using the setting as shown in Figure 2. The NACA profile coordinate is imported into geometry and a basic airfoil shape is constructed. Then, a mesh surface is created around the airfoil to simulate the surrounding of the airfoil as shown in Figure 3. The accuracy of the results is depending on the mesh size. The more define the meshing, the more accurate the result is. The solver is launched to define the boundary condition for the simulation. Spalart-Allmaras model is used as the setting of boundary condition to give accurate results as this model is normally used to analyze the airflow. After the boundary condition is set, the solution is needed to be initialized to ensure the value is as inputted.

After the confirmation, it is ready to run the calculations after the number of iterations is changed to 3000. The higher number of iterations can provide high accuracy results. Once the setting is done, the calculation is then started until the results are converged. The results of five NACA profiles at angle of attack 15° are shown in Figure 4.

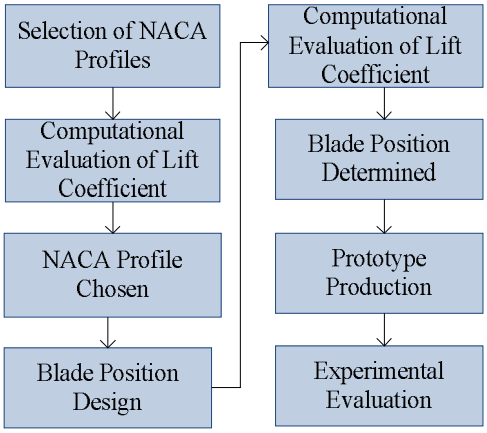


Figure 1 shows the project flowchart.

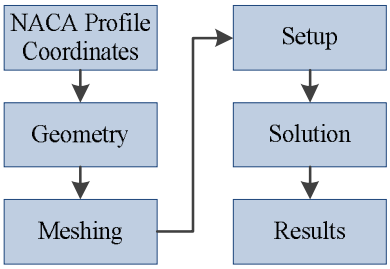


Figure 2 shows the CFD simulation flowchart

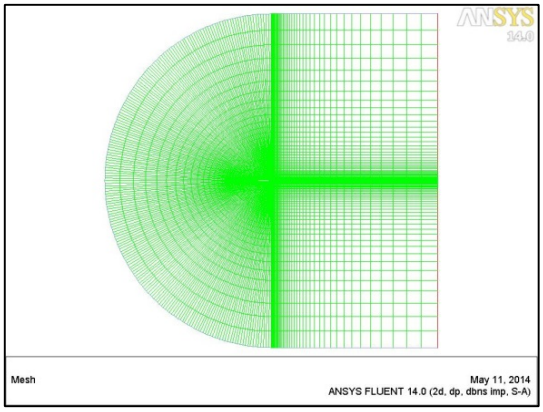


Figure 3 Airfoil meshing

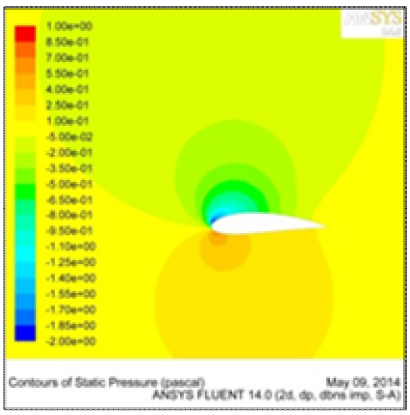


NACA 4518

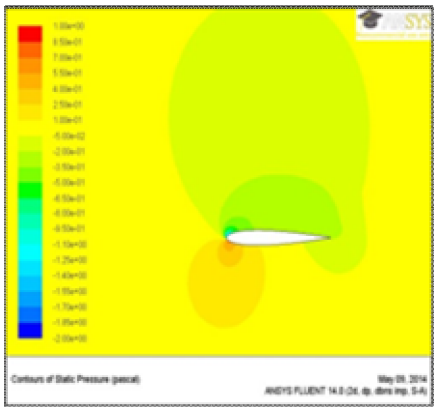

NACA 0012

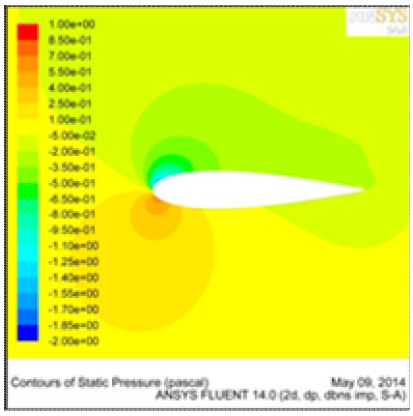


NACA 0018

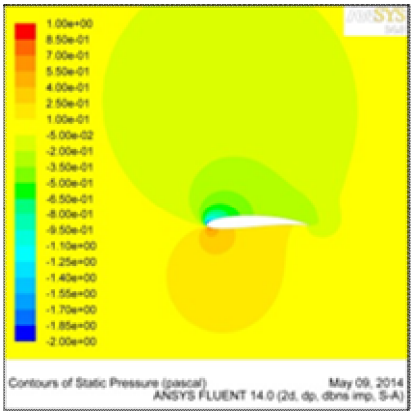


NACA 4612

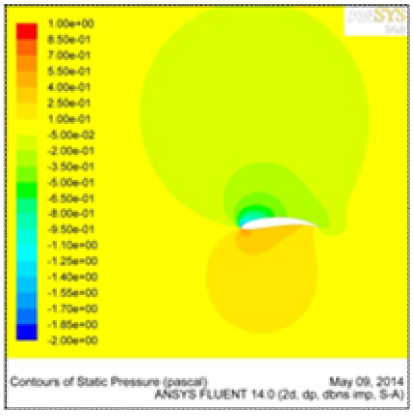


NACA 8612

Figure 2 shows the graph of Lift Coefficient versus Angle of Attack.

## 3. Results

Five different NACA profiles are simulated using numerical tool and are compared for lift coefficient. The NACA profiles are namely NACA0012, NACA0018, NACA4612, NACA8612 and NACA4518. The blade lift force and lift coefficient can be obtained by simulating the NACA profiles. Figure 5 shows the graph of angle of attack versus the lift coefficient. Based on the simulation, it is noticed that profile NACA4518 produces highest lift coefficient at attack of angle of 15° compared with the other four NACA profiles. Table 1 shows the lift coefficient of the NACA profiles selected.

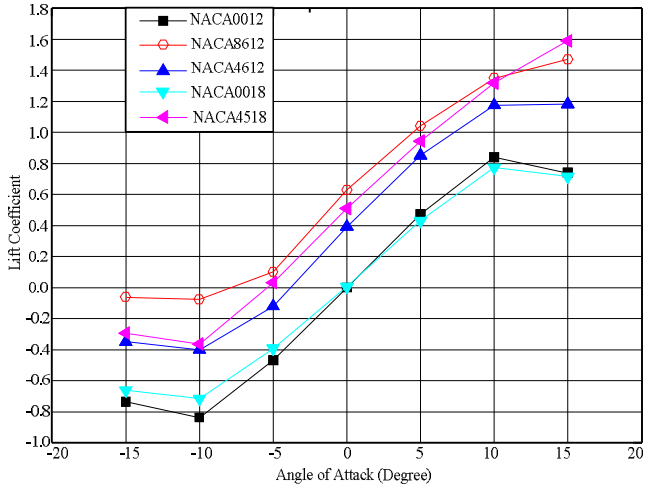


Figure 2 shows the graph of Lift Coefficient versus Angle of Attack.

Table 1 Lift Coefficient of NACA profiles at angle 15°

| NACA Profile | Lift Coefficient |
|---|---|
| NACA0012 | 0.7383058 |
| NACA8612 | 1.4679458 |
| NACA4612 | 1.1804521 |
| NACA0018 | 0.7147175 |
| NACA4518 | 1.587083 |

## 4. Conclusions

It can be observed that NACA4518 have higher lift coefficient compared to others at an angle of attack at 15°. Therefore, it is chosen as the blade profile for the VAWT prototype. Experimental data would be able to collect once the VAWT prototype is developed.

## References

[1] SC Tay, Aravind CV, Rajparthiban "Analysis and Positioning of Blade Structure for the Maglev Assisted Vertical Axis Wind Turbine" Engineering Undergraduate Research Catalyst Conference (EURECA13), Kualalumpur,1-2 July.2013.

[2] CV Aravind, R Rajparthiban, R Rajprasad, YV Wong " A novel magnetic levitation assisted vertical axis wind turbine- Design procedure and anlaysis" Proceedings of the 8th IEEE signal processing and its applications, 93-98, 2012.

[3] M Khan, Rajprasad, Rajparthiban, CV Aravind "Optimization of PMSG based 8 blade magnetically levitated variable pitch low speed VAWT" Applied Mechanics and Materials, Vol.492, 113-117, 2014.

[4] Md Nahid Pervez and Wael Mokhtar, "CFD study of Darreous Vertical Axis Wind Turbine" in 2012 ASEE North Central Section Conference. Grand Valley State Univeristy, Grand Rapids. 2012.

[5] M.C. Claessens, "The Design and Testing of Airfoils for Application in Small Vertical Axis Wind Turbines". Faculty of Aerospace Engineering, Delft University of Technology. 2006.

# Design a Suitable Soft Computing Tool for Hopper Type Process

Sarath Ananthasivam[1], Suresh Manic Kesavan[2]

[1,2] *School of Engineering, Taylor's University Lakeside Campus, Malaysia,*

**Corresponding Author: SureshManic.Kesavan@taylors.edu.my*

*Abstract* – **In this paper, a method is proposed to design an optimal PID controller a nonlinear hopper type tank system. Because of its nonlinearity, it is very difficult to develop a single transfer function for the entire systems. Hence, in this work, the entire tank system is modeled in four different operating regions such as 40%, 60%, 80% and 100%. The developed model is then considered to design the appropriate controller using the Firefly Algorithm (FA). The performance of the controller is assessed using the error parameters such as ISE, IAE, ITSE and ITAE. The firefly based controller offered better result compared to the existing conventional controller design methods and the soft computing algorithms such as Particle Swarm Optimization (PSO) and Bacterial Foraging Optimization (BFO). The controller for this project is designed using a soft computing tool and then it will be implemented into the system.**

*Keywords* - Hopper process, Soft computing tool, BFO Algorithm, Hybrid Algorithm

## 1. Introduction

In recent years, soft computing tools are widely used in the engineering industries for modeling, monitoring and controlling the processes. In the literature, a number of soft computing tools are developed and implemented by most of the researchers. Soft computing tools are the user defined software, which can do an assigned work based on operator's choice. In this, in order to successfully produce a specific function, a particular program will have to be written. The proposed research is on developing a soft computing based PID controller for hopper type process which is a class of non-linear system. Hence, it is necessary to choose a best algorithm to choose and to design the controller for the hopper tank process.

There is a class of soft computing tools that could be used for this application. Some of them are Proportional Integral Derivative controller (PID) and Fuzzy Logic Controller (FLC). Proportional Integral Derivative Controller is the more popular controller and is widely used in control systems because of its multivariable process and it provides better controlled responses. On the other hand, Fuzzy Logic Controller will simply provide the best solution for missing information by a control system through hardware or software [4].

There are many different algorithms that could be used for a non-linear tank. BFO algorithm is one of the algorithms that could be used. Based on a study done on the behavior of the bacteria, it is encouraged to use this algorithm for computational purposes [5].

The algorithm used in this research is the Firefly Algorithm (FA). This algorithm is a metaheuristic inspired algorithm. It was developed from the fireflies flashing patterns. This flashing light is produced chemically from their lower abdomen [6]. In order to optimize it, the flashing light is formulated and an optimized algorithm is formed [7].

This paper's aim is to compare two (2) or more algorithms and come up with an optimized algorithm. The new algorithm will be implemented by running simulation using MATLAB/Simulink.

## 2. Objectives

There are a few objectives identified in this research. The first objective is in order to find the transfer function; a mathematical modeling will need to be performed. The second objective would be, selecting the most appropriate design and algorithm using the generated transfer function and process. The third objective would be designing the most appropriate controller that will be used for the process. The last objective would be to obtain the best result by performing a simulation using the soft computing tool for the process.

## 3. Theoretical Framework

Figure 1 below represents a mathematical model of a conical tank. The general equation can be written as follows:

$$\tan\theta = \frac{R}{H} = \frac{r}{h} \quad (1)$$

It also can be written as,

$$F_{out} = b\sqrt{h} \quad (2)$$

Where, b is a constant value which is equal to 4.3.

Hence,

$$\frac{dV}{dt} = F_{in} - F_{out} \quad (3)$$

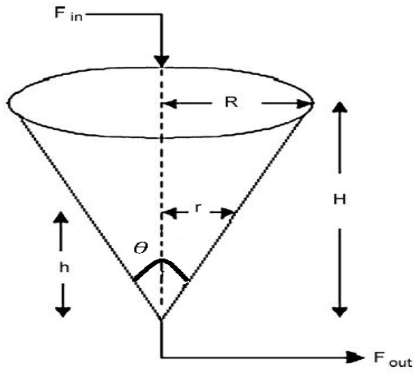


Figure 1: Mathematical model of a conical tank

## 4. Methodology and Data

Figure 2 below is the flowchart that shows the project development flow. Information was gathered at the initial stage for further understanding the process for running the simulation. Simultaneously, journals and case studies on other researchers are reviewed and compared with to identify an appropriate controller. Secondly, an experimental setup is completed to get the required results for the simulation. The transfer function is then calculated based on the results gained from the experimental setup. Using the transfer functions, an algorithm is developed. The PID controller is tuned based using the algorithm that was developed.

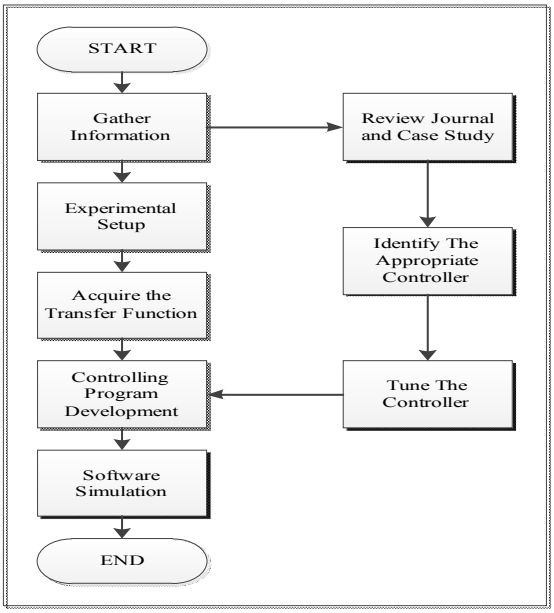


Figure 2: Flow Chart for the overall process for the project

## 5. Results and Discussion

Figure 3 below shows the Firefly Algorithm (FA) developed using the MATLAB/Simulink for the non-linear tank. The algorithm above was developed based on the results of real-time experimental setup for the hopper tank that was tested on. The algorithm was developed for a PID controller only.

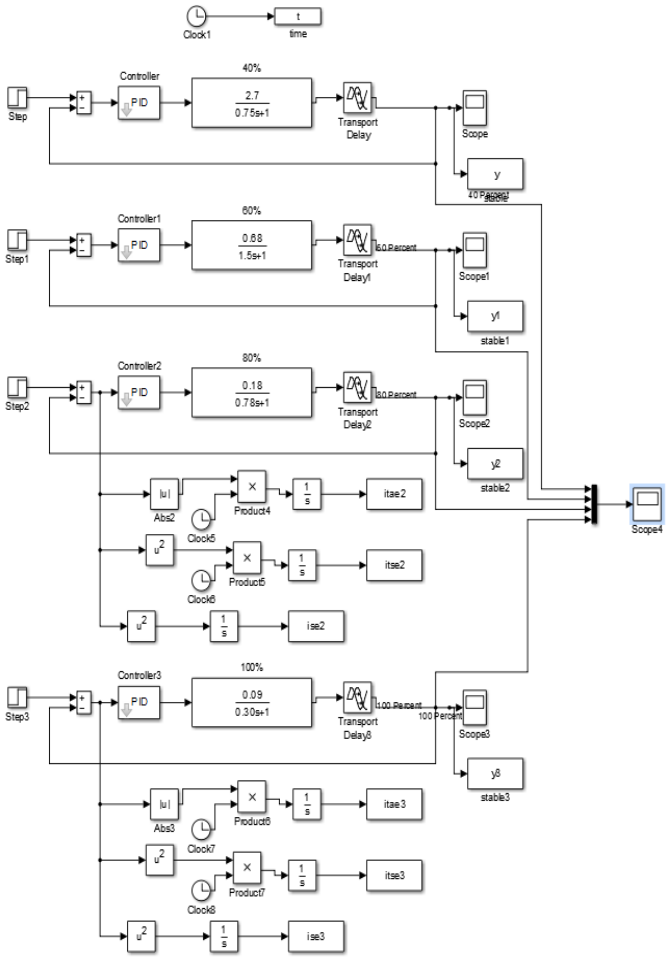


Figure 3: MATLAB/Simulink Design for Firefly Algorithm (FA)

Table 1: PID Tuning Parameters

| Step input | Kp | Ki | Kd |
|---|---|---|---|
| 40% | *0.3187* | *0.4471* | *0.0093* |
| 60% | *0.9702* | *0.8075* | *0.1381* |
| 80% | *2.1062* | *1.8021* | *0.0010* |
| 100% | *1.1821* | *2.9135* | *0.0237* |

Table 1 above shows the PID tuning parameters generated by the Firefly Algorithm (FA). The PID tuning was done for the step input of 40%, 60%, 80% and 100% of the valve opening.

Figure 4: MATLAB/Simulink Generated Result for Firefly Algorithm (FA)

Figure 4 above shows the generated results from the Firefly Algorithm (FA) in MATLAB/Simulink. The results are generated for four (4) different transfer functions. Based on the generated results above, when valve is opened at 40%, the rise-time is lower, hence producing the most optimum results.

## 6. Conclusions

After comparing the various methods used, Firefly Algorithm (FA) seems to produced and optimized result with a low rise time and a low overshoot. As far as the process can withstand an overshoot of 5% and below, it is within an acceptable range.

## References

[1] V. Rajinikanth, K. Latha, 2012. "Setpoint weighted PID controller tuning for unstable system using heuristic algorithm", *Archives of Control Science*, Vol.22 No.4, p.481-505.

[2] V. Rajinikanth, K. Latha, 2012. "Internal model control-proportional integral derivative controller tuning for first order plus time delayed unstable systems using bacterial foraging algorithm", *Sci. Res. Essays*, Vol.7 No.40. p.3406-3420.

[3] K. Latha, V. Rajinikanth, P. M. Surekha, 2013 "PSO-Based PID Controller Design for a Class of Stable and Unstable Systems". *ISRN Artificial Intelligence*. Vol.2013, p.11.

[4] R.Sivakumar, K.Suresh Manic,V.Nerthiga, R.Akila, K.Balu, 2010. "Application of Fuzzy Model Predictive Control in Multivariable Control of Distillation Column". *International Journal of Chemical Engineering and Appplicaion,* Vol.1 No.1, p.38-42.

[5] Riya Mary Thomas, 2013. "Survey of Bacterial Foraging Optimization Algorithm".*International Journal of Science and Modern Engineering (IJISME),* Vol.1 No.4, p.11.[5] Zadeh, Lotfi A., 1994 "Fuzzy Logic, Neural Networks, and Soft Computing". *Communication of the ACM*, Vol37 No. 3, p.77-84.

[6] N.Sri Madhava Raja, K.Suresh Manic and V.Rajinikanth, 2013. "Firefly algorithm with various randomization parameters: An analysis". *Swarm Evolutionary and Memetic Computing*. SEMCCO 2013, LNCS8297, pp.110-121.

[7] X.S.Yang, 2009. "Firefly Algorithm (FA) for Multimodal Optimization". *Lecture notes in computer sciences,* Vol.5792, p.169-178.

# Design and Implementation of a Hybrid Controller Performance on a Hybrid Photovoltaic

Muhammad Abdullah Rosdi[1], Mohammad Taghi Hajibeigy[2*]

[1]*School of Engineering, Taylor's University, Malaysia,* [2]*School of Engineering, Taylor's University, Malaysia*

**Corresponding email: mohammadtaghi.hajibeigy@taylors.edu.my*

*Abstract*— **This paper explains the design of a temperature controller for a photovoltaic thermal (PVT) panel. The controller reads and compare the temperature on the solar panel and on the water tank and drives a water pump based on the difference of the temperature. An algorithm is develop and simulated on PROTEUS 8. The experimental testing is yet to be done at this stage.**

*Keywords*— Photovoltaic (PV), Photovoltaic Thermal (PVT), hybrid photovoltaic, temperature controller, hybrid device controller, heat collector

## 1. Introduction

Continuous efforts to effectively utilizing solar energy has been made for years by using solar photovoltaic (PV) cells – a semiconductor device consists of n-p layer divided by a boundary layer. PV cells absorbs solar radiation by allowing photons to pass through its outer layer. These photons energize the free electrons in the n-silicon layer. With a load connected to the PV cell, the energized electron would travelled in the circuit and back to the cell. This phenomenon is what known electricity generation through a PV cell. Such behavior generate heat on the PV cell. At certain temperature, the electrical efficiency of a solar cell will drop, hence a solar panel system won't be able to fully utilize the energy coming to it [1].

Solar PV Thermal (PVT) panel, for example, make use of the heat develop on the solar panel by transferring the heat to a water contained in a tank. A simple system would have a water pump running during the day or at certain hour of the day. In this project, a microcontroller (MCU) will be installed as the main controller for a water pump. The operation and speed of the motor pump will be varied depending on the temperature difference between the solar panel and the water tank.

### 1.1 Objective

The objective of this project is:

1. To design and implement a temperature controller on a hybrid device – Photovoltaic Thermal (PVT) Solar Panel.
2. To extract the heat develop on the solar panel and channeled the heat into the water in a water tank effectively by varying the speed of the motor pump.
3. To keep the water temperature on the tank higher than the temperature on the solar panel.

## 2. Methodology

This is a quantitative study. The controller will read the temperature on the PVT panel and the temperature on a water tank. Based on the difference in the temperature, the controller will drive a water pump to circulate the water at different speed to get the best heat exchange efficiency.

### 2.1 System Design and Modelling

This section describes the design of the system. The hybrid device controller consists of a PIC16F876A microcontroller (MCU), two Texas Instrument LM35 Precision Centigrade temperature sensor, a TOSHIBA Photocoupler TLP781, and a BESTRAM TECH 24V water pump. A JHD162A 16x2 Liquid Crystal Display (LCD) is used to display the temperature on the PVT panel and on the tank.

The PIC16F876A microcontroller acts as the main interface between the sensing circuit and the driving circuit. It read the input voltage from the temperature sensors and convert the analog reading into a 10-bit digital number. The MCU will then read the first 8-bit of the digital number and do a calculation to get the value of the temperature. By comparing the temperature difference, it will send a digital signal to the photocoupler. The high output ($T_H$) and low output ($T_L$) is delayed based on the temperature difference in a way to make the pump to run faster, slower or stop. This digital output from MCU will turn on or turn off the photocoupler, which acts as a switch to the pump.

The Texas Instrument LM35 is a precision integrated-circuit temperature sensors that has an output voltage linearly proportional to the Centigrade temperature [2]. It is rated for full -55°C to +150°C and with a 0.5°C ensured accuracy. The output is a linear +10 mV/°C. It has 3-pins whereby 1-pin is grounded, 1-pin is the output, and the last pin is 5V input voltage.

The TOSHIBA TLP781 photocoupler consists of a photo transistors optically coupled to a gallium arsenide infrared emitting diode with having high isolation voltage [3]. It will receives a signal from the MCU which will turn on or turn off the diode and eventually turn on or off the transistor. As the transistor is turn on, the pump will turn on as well. Due to the natural characteristic of the photocoupler, the switching is almost instantaneously and without bouncing.

The BESTRAM TECH 24V water pump can operate with an input DC voltage of 6V to 24V at rated current 1050 mA. It can withstand fluid temperature ranging from 0°C to 95°C. The pump motor is a brushless DC motor with no spark work. The pump will turn on when the photocoupler is in ON state and will be off when the photocoupler is in OFF state. This water pump will circulate the water between the solar panel and the water tank. Its speed is determined by the temperature difference on the PVT panel and the water tank.

Fig. 1 below shows the block and flow diagram of the controller system.

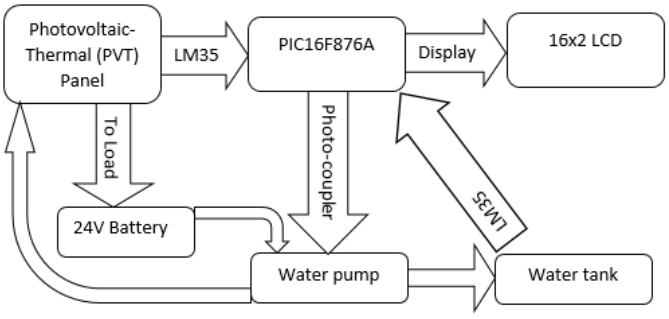


Fig. 1: Block and flow diagram of the controller system.

The program is written in C language using MPLAB IDE v8.63 and is compile using HI-TECH C Compiler v9.81. The code algorithm is shown in Fig. 2 below.

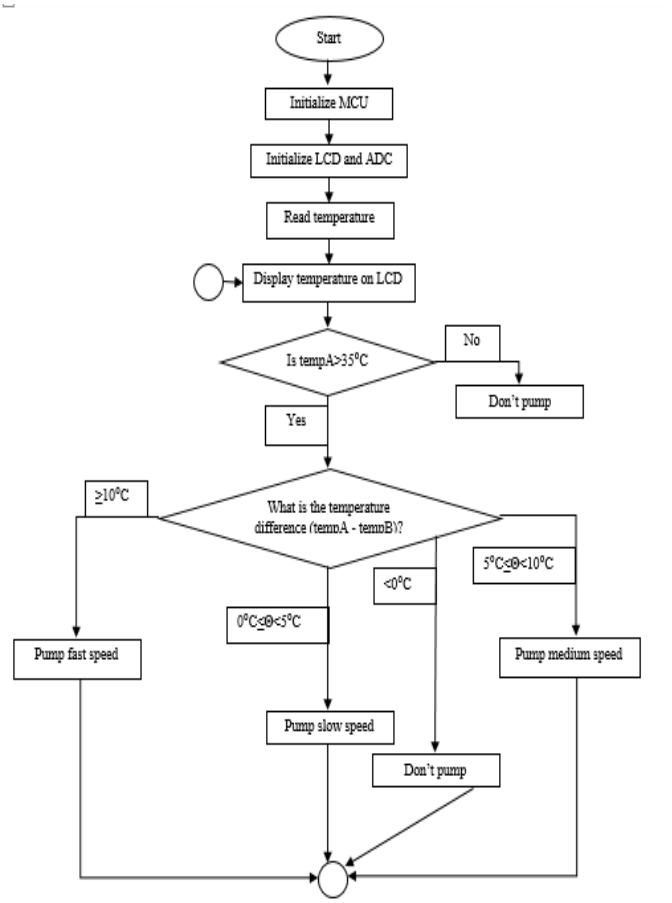


Fig. 2 The program algorithm

## 2.2 Simulation

The circuit is drawn on PROTEUS 8 for circuit simulation purposes. Fig. 3 below shows the circuit drawn in PROTEUS 8. After the circuit is drawn, the hex file created by the HI-TECH C Compiler is loaded into the MCU, and the simulation is run. The simulation is to see whether the motor will run when temperature on the PVT panel (tempA) is higher than 35°C.

The circuit is divided into sensing circuit, display circuit, and drive circuit. Based on Fig. 3, the sensing circuit is on the left-hand side (LHS) of the figure, which consists of two LM35 model. On the other hand, the display circuit consists of the 16x2 LCD, while the drive circuit is the circuit on the top right-hand side (RHS) of the figure.

## 2.3 Data Collection and Testing

The PVT module will be placed outdoors under direct sunlight at varying weather conditions. The tests will be divided into several parts. Firstly, temperature are measured without the controller running to see the temperature develop on the PVT in one day. Next, the temperature is measured while the pump is running at full speed, medium speed, and slow speed for 5 minutes respectively, to see the change in the temperature. Between each 5-minutes test, a gap of 5 minutes is given for the PVT panel to heat up to its normal temperature.

With the data obtained, the voltage drop versus speed of the pump can be determined. As such, the algorithm can be further improved in a way that the speed of the motor pump is varied depending on the temperature difference of the PVT panel and water tank.

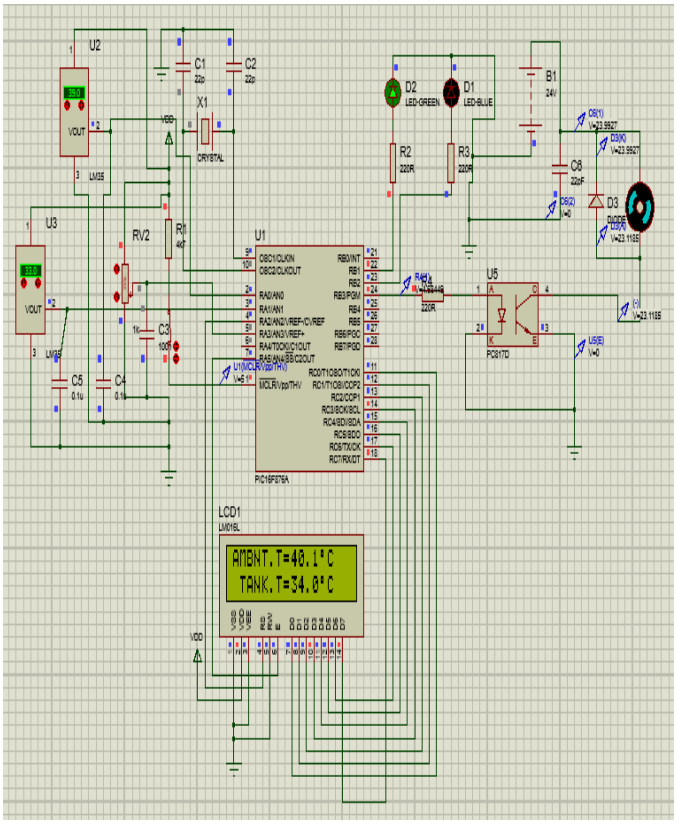


Fig. 3 Circuit develop on PROTEUS

## 3. Conclusions

The controller controls the speed of the motor on the water pump, in a way to enable efficient heat exchange from the solar panel, to the water in the water tank. Theoretically, the design will work but a hardware experiment need to be done to prove the theory.

In the near future, the hardware need to be assembled and tested. The results obtained will be used to improve the algorithm, so that the objectives could be achieved. Also, the results obtained later could help in determining other changes, if needed.

## References

[1] *Aneta Hazi et al, "Energy efficiency of the PVT system used in industry," Univ. of Bacau, Bacau, Romania, 2011.*

[3] *TOSHIBA, "TLP781, TLP781F", August 2008.*

[2] *Texas Instrument, "LM35 Precision Centigrade Temperature Sensors", Oct. 2013.*

# Raised Access Floor Panel and Pedestal Design Optimization

Afiq Asyraf Bin Mazli[1], Thein Chung Ket[1*]

[1]*School of Engineering, Taylor's University, Malaysia,*

**Corresponding email: ChungKet.Thein@taylors.edu.my*

*Abstract*— **Raised access floor system is the array of elevated removable panels installed on top of the building concrete slab held by adjustable supports (pedestals) to provide an underfloor space. The floor panel and pedestal are modelled using computer aided design software and bounded by design variables and constraints before analysed using Finite Element Analysis software. The final model is expected to have higher ratio of (loading capabilities to its mass) and greater cost effectiveness.**

*Keywords*— Raised Access Floor, Pedestal, Finite Element Analysis

## 1. Introduction

### 1.1 Background

In the recent years, raised access floors (RAF) systems are receiving more attention and are featured in latest commercial buildings. Generally, RAF system is the arrangement of elevated of removable floor panels (typically cement-filled, size of 600mm × 600mm × 30mm) installed on top of the building concrete slab held by adjustable supports (pedestals) to provide an underfloor space [1].

RAF systems are supported by the underlying structural floor on pedestals. The pedestals are made up of a base plate, post and an adjustable head. The load from the base plate is transferred to the structural subfloor which is normally made from either aluminum or steel. The pedestal usually must touch the base (subfloor surface) fully and held by adhesive [2].

The space (height) between the RAF panels hold by pedestals and the concrete slab is 150mm, but may range from 70mm to 1200mm according to additional requirements.

The main objectives of this research which correlate with each other include; to increase the loading capabilities of floor panel, reduce the cost of floor panel, improve the (stiffness / mass) plus (performance / price) ratio for access floor panel and pedestal .

## 2. Methodology

### 2.1 Floor Panel

#### 2.1.1 Design Variables

The design variables are the parameters that can be modified in the design process [3]. In this research, the design variable includes the design of flooring panels, pedestal, and materials chosen. The researcher is free to design the floor panel, according to suitability from the literature reviews or any raw ideas obtained.

As for the materials chosen for this study, the current material chosen is ASTM A36 Steel, which is a type of mild steel. This material is chosen due to the strength, cost-effective and easy to handle (manufacture). The related material properties of ASTM A36 steel is tabulated in Table 1.

Table 1. Related Material Properties of ASTM A36 Considered in the Study

| Properties | Value | Units |
|---|---|---|
| Elastic Modulus | 2e+011 | N $m^{-2}$ |
| Poisson's Ratio | 0.26 | N/A |
| Density | 7850 | kg $m^{-3}$ |
| Yield Strength | 2.5e+008 | N $m^{-2}$ |

#### 2.1.2 Design Constraints

The dimension of floor panel is 600mm x 600mm, while the depth of the panel will be studied in the FEA. The length and width of panel is standardised to follow the majority size of the flooring panels used by RAF suppliers.

Based on European (EU) Standard EN12825, a safety factor of 2 is chosen. It is the common safety factor used in the application of raised access floor system in the EU countries. The reason why EU standard is chosen, even though the location of study is in Malaysia is because there are no standardization yet for ASEAN countries.

There are four class of floor panels available based on EU Standard EN12825, as shown in Table 2. Class 2 is chosen to be the ultimate load for the RAF panels. It is the medium class available for normal use, since the study is focussing more on the use of RAF system in office or residential buildings [4].

Table 2. Classes of Ultimate Loads Based on European Standard EN12825 [4]

| Class | Grade | Ultimate Load (kN) |
|---|---|---|
| 1 | Light | ⩾4 |
| 2 | Medium | ⩾6 |
| 3 | Heavy | ⩾8 |
| 4 | Extra Heavy | ⩾9 |

Furthermore, the deflection of the floor panel must not exceed the stated value in accordance to Table 3 when working load is applied [4]. Class A is chosen among the three classes so that the results obtained can be used in most application of RAF.

Table 3. Classes of Deflection Based on European Standard EN12825 [4]

| Class | Maximum Deflection (mm) |
|---|---|
| A | 2.5 |
| B | 3.0 |
| C | 4.0 |

#### 2.1.3 Model Generation

During the computer aided design (CAD) process, data obtained from the research study will be used to design different alternatives for the flooring panel and pedestal.

The alternatives designs then will be tested under different loading simulations before picking the optimum design. These processes are called finite element analysis (FEA). To get a more realistic analysis, finite (boundary) element method will need computational support and closely model the ground as a range to help identify the ground-slab interaction behaviour [5].

For the best current model, the meshing used for the floor panel is solid mesh, and the mesher used is curvature based mesh. The total nodes and elements obtained from the meshing is 26446 and 15755 respectively. Figure 1 shows the example of meshing produced.

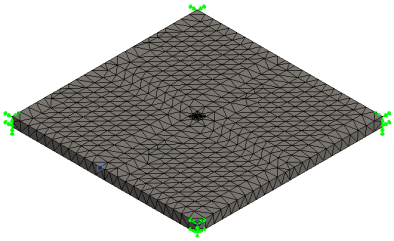

Figure 1. Example of Meshing Produced during Model Generation

There are 5 different loading case that will be modelled and analysed using FEA software. The different loading case are shown in Figure 2 and Figure 3. The concentrated middle loading is shown together (combined) with the impact loading because the point of force is the same, but the impact loading is applied with certain amount of height.

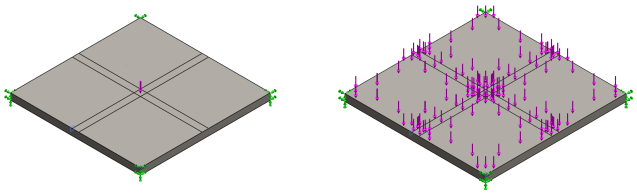

Figure 2. Different Loading Cases on the Floor Panel. (Left – Concentrated Middle Loading, Right – Uniform Loading)

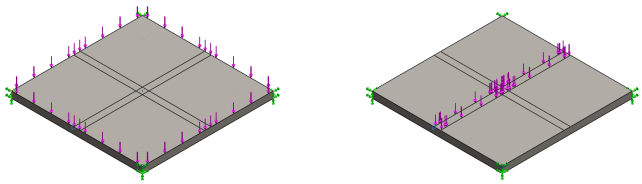

Figure 3. Different Loading Cases on the Floor Panel. (Left – Side Loading, Right – Rolling Load)

### 2.1.4 Analysis

Final comparisons will be made to find the best combinations that provide the best (stiffness / mass ratio) and (performance / price ratio). Different models that fulfil all the design requirements will undergo further analysis and comparisons to find the optimum solution to achieve the objectives.

## 2.2 Pedestal

### 2.2.1 Design Variables

The design of pedestal too can be improved from the existing design, or the researcher is able to completely design a new concept of pedestal that can withstand better load.

### 2.2.2 Design Constraints

Another boundary condition that needs to be considered when using FEA is that the RAF panels will be supported with 4 support panels that will act as pedestals.

The standard also specify that the pedestal vertical load bearing capabilities which states that the understructure must be able to support four times the working load of the system tested, which is 24kN without being distorted or damaged [4].

### 2.2.3 Model Generation

Model of the final pedestal are yet to be finalized. Final model of pedestal will undergo the similar loading cases as the floor panels.

### 2.2.4 Analysis

Same analysis will be done as explained in Sub-chapter 2.1.4.

# 3. Results & Discussion

## 3.1 Floor Panel

The results of the simulations are tabulated in Table 4 and 5. The results shows that both the designs are able to withstand the ultimate load chosen (6 kN) based on EU Standard EN12825, but the mass of final floor panel is improved compared to the initial design. For visualization purpose, a screenshot of the simulation is showed in Figure 4.

Table 4. Maximum Stress and Deflection for Initial Design

| **Initial Design** | Concentrated | Uniform | Side | Rolling |
|---|---|---|---|---|
| Maximum Stress (MPa) | 2.003 | 77.334 | 55.196 | 99.664 |
| Maximum deflection (mm) | 4.776e-003 | 2.01 | 0.984 | 2.17 |
| Mass (kg) | 25.674 | | | |

Table 5. Maximum Stress and Deflection for Final Design

| **Optimized Design** | Concentrated | Uniform | Side | Rolling |
|---|---|---|---|---|
| Maximum Stress (MPa) | 2.281 | 88.115 | 61.167 | 102.093 |
| Maximum deflection (mm) | 5.669e-003 | 2.18 | 1.113 | 2.43 |
| Mass (kg) | 16.304 | | | |

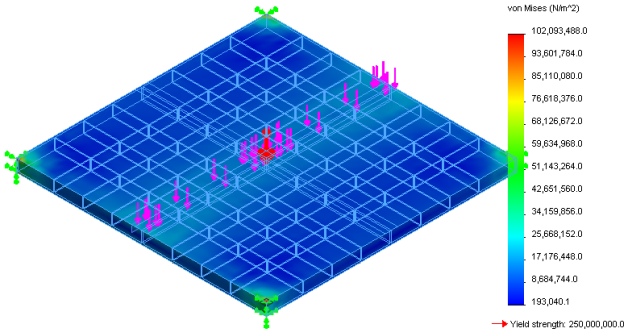


Figure 4. Example of Simulation to obtain the Max Stress on a Floor Panel

# 4. Conclusions

It is concluded that this study is able to achieve its objective. The mass of floor panel managed to be reduced significantly, without affecting capabilities of the floor panel, which improve the (stiffness / mass) ratio. Since the mass of panel is proportional to its price, thus (performance / price) ratio is increased too. As for the pedestal, it is expected that the results will be similarly successful as the floor panel, where all the objectives are met.

**References**

[1] A. Larsson, "High Performance Raised Access Flooring Containing Industrial By-Products," in *1st Civil and Environmental Engineering Student Conference*, London, 2012, pp. 1-6.
[2] Department of the Army and the Air Force, *Technical Manual: Raised Floor Systems*, 1st ed. Washington, United States of America: Joint of Departments of the Army and Air Force USA, 1990.
[3] Zafer Gürdal, Raphael T. Haftka, and Prabhat Hajela, *Design and Optimization of Laminated Composite Materials*, 1st ed. Ontario, Canada: John Wiley & Sons, 1999.
[4] C.E.N, "European Standards - Raised Access Floor," European Committee for Standardization, Brussels, EN 12825:2001 E, 2001.
[5] Frank R. Neal, *Concrete Industrial Ground Floors*, 2nd ed. London: Thomas Telford Publishing, 2002.

# Experimental Investigation of Design Parameters of A Thermo-acoustic Refrigerator

Khawaja Asad Akhtar, Abdulkareem Shafiq Al-Mahdi*

*Department of Mechanical Engineering, School of Engineering, Taylor's University,*

**Corresponding email: abdulkareem.mahdi@taylos.edu.my*

*Abstract*— **Refrigeration is used to preserve food and also to prevent contamination. Traditional refrigerators however pose a few problems. One of the problems being the refrigeration medium which if exposed to can be harmful to health. These media are also not environmental friendly. TAR is considered to be one of the viable options to replace the current refrigerator. The technology of thermo-acoustic refrigeration has been in focus for some time now. Thermo-acoustic means the effect that is a result of the sound waves creating a heat gradient and vice versa. In this paper, a thermo-acoustic refrigerator was built and modified. The model consists of speaker, resonator tube, amplifier and a stack. Different parameters related to the performance of TAR were varied and their effects on the temperature change were recorded. It was found that using Acrylic tubes resulted in a 27% better temperature change than PVC tubes. Also using a shorter tube resulted in a greater temperature change.**

*Keywords*— Thermo-acoustic, refrigerator, temperature change, tube, stack

## 1. Introduction

In the present world, refrigeration and air conditioning are an integral part of our lives. Whether it's about creating a comfortable environment at home or for different industrial use, refrigeration and air conditioning are everywhere. However, the current cooling techniques generate greenhouse gases and at the same time these techniques are costly [1]. Also the media in these refrigerators are highly flammable and their direct exposure is not healthy. A new innovative technique known as thermo-acoustic refrigeration can be used to help solve these issues. A thermo-acoustic refrigerator reduces the effect of global warming, also helps to cut down the cost and at the same time it is sustainable. The effect that arises from sound waves creating a heat gradient and vice versa is what is meant by the term thermo acoustic [2]. A study was conducted on the optimum frequency and temperature difference by Abakr, *et al.* [3]. Another study was conducted on the effect of wave patterns and frequency on the cooling of TAR by Abakr, *et al.* [4].The main objective of this project is to study the effect of different design parameters of the TAR and how these parameters affect the performance of TAR.

## 2. Experimental Design and Procedure

Figure. 1:Experimental setup of thermo-acoustuc refrigerator.

In this paper 4 different experiments have been conducted. Figure 2 describes the main steps. In the first experiment the previous work by [5] was verified. In the second experiment a study was conducted where Acrylic tubes were used with the stack positioned at different lengths in the tube. The frequency was set at 270 Hz using an amplifier and applied for 4 minutes. The temperature change was measured using the thermocouple at hot and cold ends. The third experiment was the same as the second one except that the Acrylic tube was replaced with PVC tube. The last experiment involved studying effect of different tube lengths on temperature change. In this experiment PVC tubes were used and the frequency was set at 270 Hz and applied for 4 minutes. The stack position was changed in terms of ratio and the respective temperature difference was measured using a thermocouple at hot and cold ends.

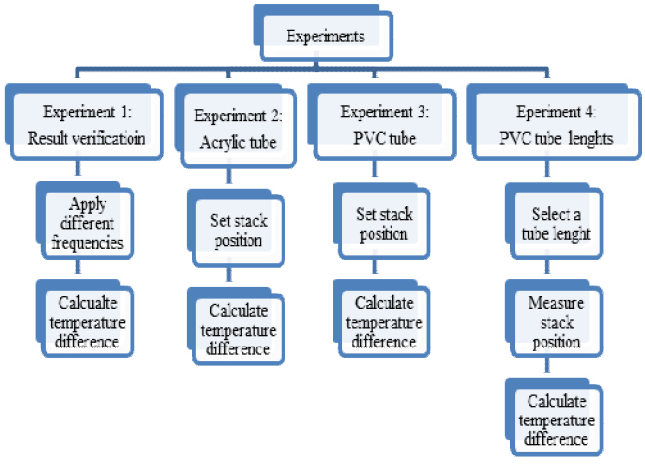


Figure 2: Flow chart of experiments.

## 3. Results and Discussion

The prototype built in the previous work by [5] was used in the current study to verify the previous results and study the effects pf different design parameters of TAR and compare the results and select the optimum design. At different frequencies ranging from 230 Hz to 300Hz, the temperatures at hot and cold ends were

recorded using a thermocouple. Figure 3 shows the results obtained by the previous and current studies. It can be seen from the graph that the maximum temperature was obtained at 270Hz for both the current and final year studies .In the previous work a maximum temperature difference of 25˚C was recorded while in the current study a maximum temperature difference of 24˚C was recorded.

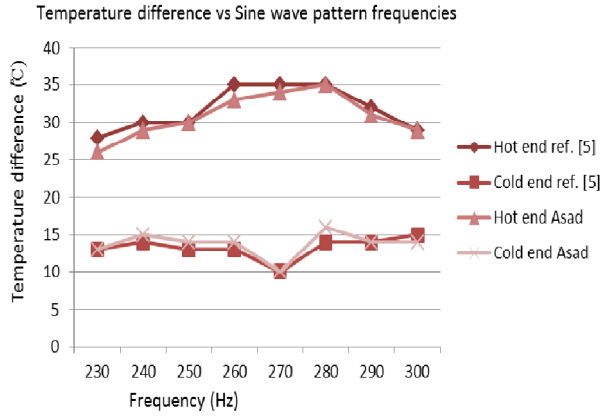


Figure. 3: Comparison of current results with the results of Ref. [5].

An experiment was conducted to investigate the effect of the type of material used for the resonator tube will have on the temperature change at different stack positions. The stack position was measured from the top of the tube to the hot end. Tubes made out of Acrylic and PVC were used. Both tubes used were 26.5 cm long and their internal diameter was 40 mm. The frequency was set as 270 Hz and was kept constant for all the experiments. Figure 4 shows the results of the experiments conducted.

Figure. 4: Comparisn between acrylic and PVC resonator tubes.

It can be observed from the graph obtained that Acrylic resonator tube recorded a maximum temperature difference of 15˚C at a distance of 60 mm, whereas PVC resonator tube recorded a maximum temperature difference of 11˚C at a distance of 35 mm. Also what can be observed is that using the Acrylic resonator tube resulted in higher temperature difference for all the distances compared to the PVC resonator tube.
Looking at the difference in temperature change between Acrylic and PVC it can be suggested that more heat loss occurs through PVC compared to Acrylic.

A following experiment was conducted to study the effect of resonator tube length on the temperature difference. In this experiment, 3 different lengths of PVC tubes were used. The lengths measured 30 cm, 40 cm and 50 cm respectively. The internal diameters of the tubes were 40 mm each and the applied frequency was set at 260 Hz. At different ratios ranging from 0.6 to 0.9 the temperature difference for every length of PVC tube was recorded. The ratios were calculated by dividing the distance of from the hot end of the stack from the bottom of the tube with the total length of the tube. Figure 5 shows the results obtained.

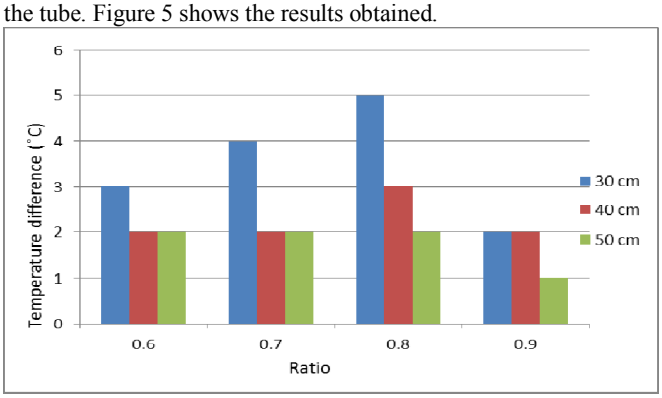


Figure. 5: Comparison between different lengths of PVC tubes.

From the results obtained above it can be seen that as the ratio increases from 0.6 to 0.8 a higher temperature difference is obtained within the 30 cm tube but at 0.9 the temperature difference decreases. For the 40 cm tube the temperature difference is constant between 0.6 to 0.7 and increases at 0.8 but declines at 0.9. For the 50 cm tube the temperature difference remains constant from 0.6 to 0.8 but decreases at 0.9.
However, at all different ratios the 30 cm tube records a higher temperature difference throughout all the ratios, whereas the 50 cm tube records the least temperature difference throughout all the ratios The reason for longer tubes not producing a higher temperature could also be due to the fact that air is very poor conductor of heat and hence the transfer of heat isn't very effective.

## 4. Conclusion and recommendation

The results of the previous study were verified. Different parameters such as the effect of stack position on the temperature change, the effect of using different materials and the effect of using different lengths of tube were studied.
Based on the study conducted, Acrylic tubes have a better temperature difference by 27% compared to PVC tubes. On the other hand 1 meter Acrylic costs RM 95 and 1 meter PVC tube costs RM 6. Also PVC tubes can withstand greater pressure than acrylic tubes. Hence for the experiments and this study in general PVC tubes were the preferred choice.
It was also known from the study that shorter tubes resulted in a better temperature difference than longer tubes.
The current and previous studies obtained a maximum temperature at a frequency of 270 Hz hence this frequency was selected as the operating frequency for the experiments conducted in this study.

## Acknowledgment

I am very grateful to Dr. Yousif from the University of Nottingham Malaysia for his valuable advices for this project.

## References

[1] Newman, J.; Cariste, B.;Queiruga,A.; Davis. I,. Plotnick, B.; Gordon, M. and Martin, S. (2006). *Thermoacoustic Refrigerator*, GSET Research Journal, p.8.

[2] Bamann, T.C.; Howard, C.Q.; and Cazzalato, B.S.(2005). *Review of flow through design in thermoacoustic refrigeration.* School of Mechanical Engineering, The University of Adelaide, Australia.

[3] Abakr, Yousif A., Al Atabi, Mushtak, and Baiman, Chen (2013). Investigation of an atmospheric pressure thermo acoustic cooling system varying its operating frequency. *Journal*

*of Engineering Science and Technology* (*JESTEC*), 8(3), 364-371.

[4] Abakr, Yousif A., Al Atabi , Mushtak, and Baiman, Chen (2011). The influence of wave patterns and frequency on thermo-acoustic cooling effect. *Journal of Engineering Science and Technology* (*JESTEC*), 6(3), 392-396.

[5] Mekdad, M. G. M., and Al-Obaidi, ASM (2013). , Design and analysis of a thermo-acoustic refrigerator. Final year project, School of engineering, Taylor's University, Malaysia

# Numerical Simulation of Stirling Engines for Solar Air Conditioning Unit

Dominic Ang Ding Xiong[1], Lim Chin Hong[2*]

Department of Mechanical Engineering, School of Engineering, Taylor's University, Malaysia

**Corresponding email: ChinHong.Lim@taylors.edu.my*

*Abstract*— **This research attempts to use numerical simulation to maximize the power and torque output for a Gamma Stirling engine. The Stirling engine was modelled in a simplified 2D model, to see how the change in displacer design can improve the engine output. Experiment of an actual small scale Stirling engine will be used to calibrate the numerical model. The objective of this research is to show how the current gamma Stirling engines can be improved and use solar thermal to power air conditioning units.**

*Keywords*— numerical simulation, Gamma Stirling engine, air conditioning

## 1. Introduction

In recent years, Stirling engine technology has progress to advanced level where it is used in space and submarines [1]. Stirling engines are external combustion engine that operates with various heat sources including recycled and solar heat. Over the last 20 years, dish stirling engine powered by solar has been used to produce electricity ranging from 2kW to 50 kW has been built in Japan, Russia, Germany and United States [2]. With the rise of energy cost, any alternative sources to fossil fuel are much welcomed. For the year 2011, about 99% electricity produced in Malaysia was from fossil fuels [3]. With cooling being one of the highest consumption of electricity, it is essential to find ways to reduce the cooling cost. One alternative that has been around is using absorption chiller. Since solar is the main source in this research, solar absorption chiller is in the interest of study. However, electrical driven compressor has a higher coefficient of perfromance (COP) compared to solar absorbtion chiller [4]. COP of electrical powered compressor are normally more than 1 while the COP of solar absorption chiller ranges from 0.35-0.6 [5]. Therefore the aim is to use the Stirling engine and connect it directly to the compressor of a commercial air-conditioning unit, thus lowering the cost needed for cooling. As the stirling engine is used to power the compressor directly, there will be no power loss through the wires as compared to the solar dish stirling system which produces electricity.

The aim of this research is to use ANSYS to create a 2D numerical model of the gamma Stirling engine that is calibrated with experimental results. The model can then be configured for different displacer design to maximize power and torque output of the engine with the sun's thermal heat to operate a commercial air-conditioning unit. The aim of changing the displacer design is to increase the temperature mixing in the cylinder. This area of research is new, as no other researcher has been investigating the change of piston or displacer design in a Stirling engine.

## 2. Research Methodology

The research started out with extensive literature review on the basic of Stirling engines and it's developments for the last few years. The review mainly focused on how various researchers used numerical simulation to simulate the Stirling engines output. The numerical simulation used in this research is ANSYS, using Fluent to simulate the gas flow, temperature and pressure in the engine. Next was to model the actual Gamma Stirling engine. However, the engine model was simplified to 2D to ease the computing power needed. No mechanical losses were considered in the model. Before any simulation can be done, the model had to be mesh. Mesh interface feature was used to allow the displacer to move without affecting the adjacent mesh on the sides of the displacer. Dynamic meshing was used to control the speed and stroke of piston and displacer in the cylinder. User-defined function (UDF) is used to configure the dynamic meshing. This allows the researcher to control the movement of the piston with an equation that is derived from the horizontal movement of the piston with respect to the flywheel arrangement of the actual Stirling engine. The model will then be simulated with results from the experiment.

Equation for displacer

$$x = R - Rcos(\theta + 90°) + L - \sqrt{L^2 - (Rsin(\theta + 90°))^2} \quad (1)$$

Equation for power piston

$$x = R - Rcos\theta + L - \sqrt{L^2 - (Rsin\theta)^2} \quad (2)$$

Fig 2 shows the parameters of equation (1) and (2) derived from the Stirling engine motion.

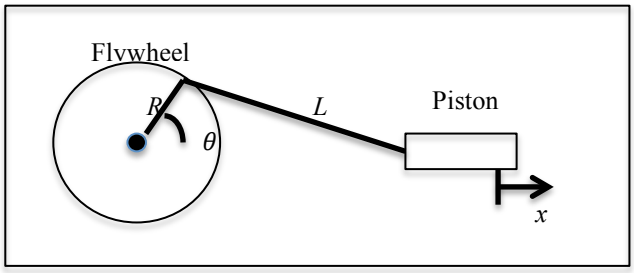


Fig 2. Gamma Stirling configuration for UDF equation

Experiment was done with the actual Stirling engine to see the operating speed of the flywheel at a certain temperature. Once the model is calibrated with the experimental results, the Stirling engine model piston displacer and hot cylinder configuration can then be change to simulate the power and torque output of the engine. Fig.3 shows the different displacer configuration that was tested. The displacer and hot cylinder was changed to a concave shape design. The idea is to create better temperature mixing in the engine. All the results will then be compiled to show the best configuration.

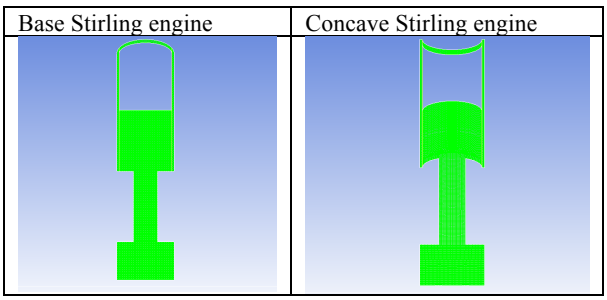


Fig.3 Meshing of Base and Concave Stirling engine.

## 3. Results and discussion

From the simulation, it was found out that the concave design gave a better force output from the same heat source. The heat source was set at 900$w/m^2$. Fig 4. shows the force output from both engines. The power piston produces power twice per cycle, during expansion and

compression. It can be seen that the concave design produces much higher force during expansion compared to the base design. Compression force output difference was closer.

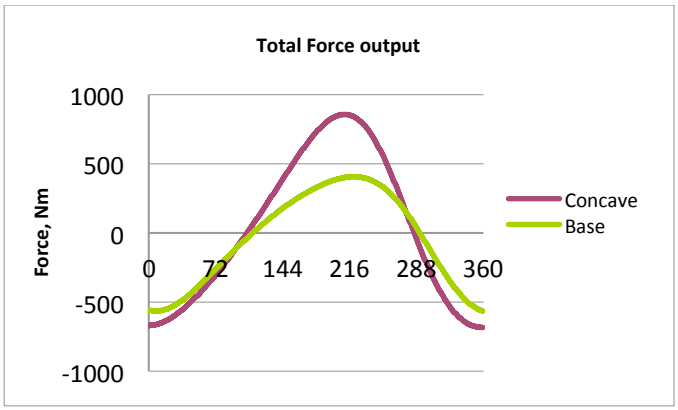


Fig.4 Force out put from both engines

The temperature contour of both engine at crank angle 288° is shown at Fig.5. It can be seen generally, that there is a lower temperature difference between the hot and cold cylinder in the base Stirling engine compared to concave Stirling engine. Chin-Hsiang Cheng *et al.* in their research shows that with higher temperature difference between the displacer and piston areas, higher engine output can be produced[6]. The concave displacer design creates swirl within the hot cylinder, thus allowing the working fluid to heat up faster and expand. This design also increases the displacer area, which Youssef Timoumi *et al* showed in their research increases the engine output[7]. With the increase in area, the swirling also creates turbulence within the regenerator, thus allowing the hot working fluid to mix faster with the cooled working fluid, hence the bigger temperature difference in Concave design. Chin-Hsiang Cheng *et al.* in their research use numerical simulation to show that by the temperature of the heat source, the work output and thermal efficiency increased [8]. Both engine were subjected to the heat source but due to better thermal efficiency, engine output is improved.

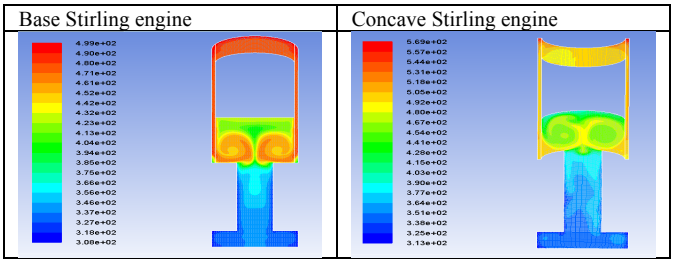


Fig.5 Temperature contour at 288° crank angle.

Fig.6 shows force output of piston and force needed to power the displacer. It can be seen that the base displace requires more force compared to the Concave design. The reason is that part of the force needed to power Concave displacer is supplement by the negative pressure around the displacer. Due to the concave of the displacer, more swirls are being made in the area above and below the displacer. These swirls create lower pressure in the middle, similar like a tornado. Hence before the displacer undergoes expansion, negative pressure occurs below the displacer, as shown in Fig. 7 at crank angle 0°. The same goes when just before the displacer undergoes compression at crank angle 144°, negative pressure occurs above the displacer. The negative pressure creates a suction effect, hence less force required for it during expansion and compression. The displacer of the base Stirling engine also produces swirls shown in Fig.7, crank angle 0°. However, it does not occurs directly blew the displacer, hence the suction effect is much less compared to concave Stirling engine

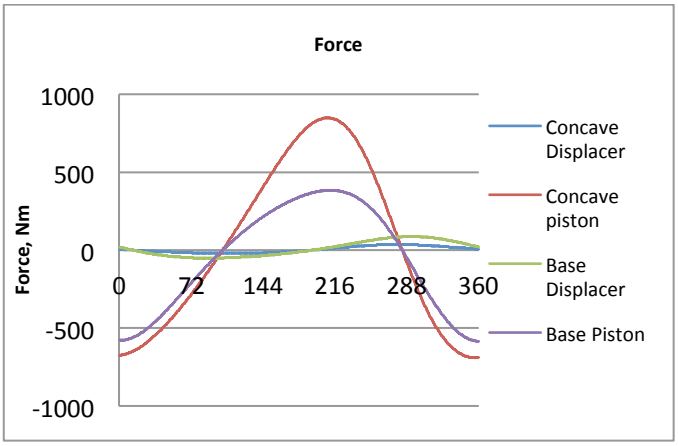


Fig.6 Force for Displacer and piston

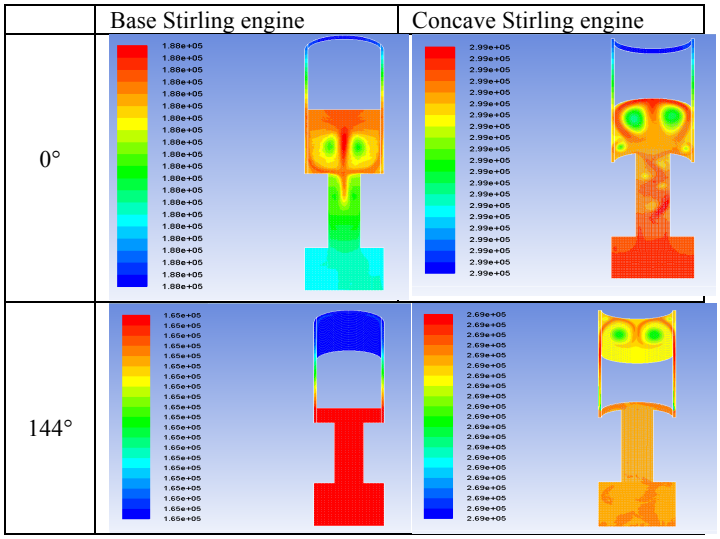


Fig.7 Pressure Contours for both engines

## 4. Conclusion

With the rising cost of cooling increasing as the population increased, it is essential to find ways to reduce the cost of cooling. The research aims to reduce the cooling cost by using solar thermal Stirling engine to power the commercial air-conditioning unit. By changing the displacer design within the Gamma Stirling engine, the research aims to optimize the output and efficiency of current Gamma Stirling engines.

## References

[1] Vineeth CS (2011). *Stirling Engines: A Beginners Guide*. India: Vineeth CS. pp11.

[2] Mancini, T., & Heller, P. (2003). Dish-Stirling Systems: An Overview of Development and Status [J], J. *Solar Energy Eng*., 125 (2), pp135-151.

[3] Haslenda Hashim, Wai Shin Ho. (2011). Renewable energy policies and initiatives for a sustainable energy future in Malaysia Reviews. *Renewable and Sustainable Energy Reviews*. 15 pp4780– 4787.

[4] M. Shekarchiana M. Moghavvemi, F. Motasemi and T.M.I. Mahlia. (2012). Cost Benefit Analysis and Energy Savings of Using Compression and Absorption Chillers for Air Conditioners in Hot and Humid Climates. *AIP Conf. Proc*. 1440, pp521-523.

[5] Rifat. A. Rouf. (2013). Solar Adsorption Cooling: A Case Study on the Climatic Condition of Dhaka. *Journal of Computers*. 8 (5), pp1101-1108.

[6]Chin-Hsiang Cheng, Hang-Suin Yang. (2012). Optimization of geometrical parameters for Stirling engines based on theoretical analysis. *Applied Energy*. 92, pp395-405.

[7]Chin-Hsiang Cheng, Hang-Suin Yang. (2012). Optimization of geometrical parameters for Stirling engines based on theoretical analysis. *Applied Energy*. 92, pp395-405.

[8] Chin-Hsiang Cheng, Ying-Ju Yu (2010). Numerical model for predicting thermodynamic cycle and thermal efficiency of a beta-type Stirling engine with rhombic-drive mechanism. *Renewable Energy*. 35, pp2590-2601.

# Evaluation of The Measurement Accuracy of the Lift of NACA 0012 as a Function of Angle of Attack at Subsonic Speed

Lim Wei Kit[1], Abdulkareem Sh. Mahdi Al-Obaidi[2*]

*Department of Mechanical Engineering, School of Engineering, Taylor's University Malaysia*

**Corresponding email: abdulkareem.mahdi@taylors.edu.my*

*Abstract*— **This paper presents the evaluation of the measurement accuracy of the lift of NACA 0012 in a subsonic wind tunnel. Validation of the data acquisition system of Taylor's subsonic wind tunnel was done by comparing the lift coefficient of NACA 0012 with theoretical results as well as computational fluid dynamics model to the lift coefficient obtained from the wind tunnel. Lift coefficient obtained from the CFD supports the theoretical results whereas the lift coefficient obtained from wind tunnel experiments has a larger percentage error.**

*Keywords*— Wind-tunnel, airfoil, lift coefficient, computational fluid dynamics.

## 1. Introduction

Airfoil performance at subsonic speeds leads to a great impact to flying bodies ranging from manned aerial vehicles to unmanned aerial vehicles. In the wind tunnel laboratory of Taylor's University in Malaysia, particularly in the area of fluid mechanics and aerodynamics, a wind tunnel measurement system to obtain aerodynamic data needs to be verified. Based on the methodology by Barlow et al., this paper presents the evaluation of the measurement of lift on an airfoil as a function of angle of attack at subsonic speeds using Taylor's University subsonic wind tunnel [1]. Verification was performed with a NACA 0012 airfoil and data obtained was compared with published as well as numerical data for verification [2]. The wind tunnel data acquisition equipment is verified to determine if it is suitable for measuring aerodynamic performance of airfoils for education purposes.

## 2. Experimental Approach using Wind Tunnel

NACA 0012 airfoil performance measurements described below were conducted in the subsonic Taylor's wind tunnel, which is an open-type wind tunnel with a contraction ratio on 3.4:1. The rectangular rest sections measures 0.3 m by 0.3 m in cross section and 0.885 m in length. Test section speeds can be varied between 3.33 m/s up to 32.3 m/s by a 0.63 m in diameter fan, which is powered by a 3HP. 415V/50Hz motor.

For the case of Taylor's wind tunnel experiments only three types of dimensionless parameters are considered for matching of dynamic similarity, which are Reynolds number, Mach number and Froude number. [3] Matching of Mach and Froude number is not an important parameter in this experiment as it is a subsonic experiment and model motion is not involved therefore dynamic similarity can be achieved by equating the Reynolds number of both model and prototype [4].

$$Re_m = \frac{\rho_M V_M L_m}{\mu_M} = Re_p = \frac{\rho_p V_p L_p}{\mu_p}$$

where $\rho$ is the density of the air, $V$ is the velocity of model or prototype, $L$ is the characteristic length of model or prototype and $\mu$ is the dynamic viscosity of air. Through this equation, the required velocity for the wind tunnel can then be obtained. All obtained data is collected manually and then processed using a software where the general equations used to calculate the coefficient of lift is as follows;

$$C_L = \frac{F_L}{0.5\rho_p V_p^2 A_p}$$

### 2.1 Experimental Set-up

In this experiment, the NACA0012 airfoil was tested at a Reynolds number of 200,000, which corresponds to a wind tunnel velocity of 26.278 m/s where $\frac{S_m}{S_{reference}} = 1.15$.

Figure 1 shows the mounting used for the airfoil in the test section of the wind tunnel and experiments were conducted starting from an angle of attack of -20° up to 20° with an interval of 5°

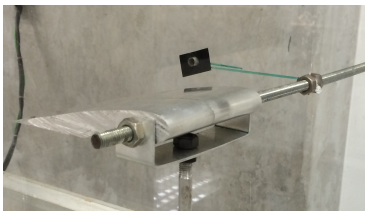

Fig 1 Mounting of the NACA0012 airfoil in the wind tunnel.

## *3.* Numerical Approach using Computational Fluid Dynamics (CFD)

ANSYS FLUENT 14.0 software was used to simulate the aerodynamics of the NACA 0012 airfoil to obtain the lift coefficient and result obtained is used to cross check the theoretical results. The turbulence model chosen for this numerical approach is the Spallart-Allmaras turbulence model and this is due to the simplicity of the equation thus leading to a shorter simulation time. The Spallart-Allmaras turbulence model consists of a single equation, which is modified specifically for the use airfoil simulation. [5]

Figure 2 shows the full scale drawing of the cross section of the NACA 0012 airfoil and the meshing conditions surrounding the airfoil. Based on FLUENT, the mesh consists of 160,740 nodes and edge sizing with a bias factor of 6000 and 170 divisions was selected at the far end of the far-field domain to increase numerical accuracy of the results as mesh nodes becomes finer as it shifts nearer to the wall of the airfoil. For most aeronautical applications where the magnitudes of viscous and turbulent effects are similar it is preferable to keep the range of $y^+$, smallest as possible between 5 and 30. [6] This is to ensure that the simulation runs as close as possible to the airfoil. For this simulation, the $y^+$ value denoted by FLUENT is 12.

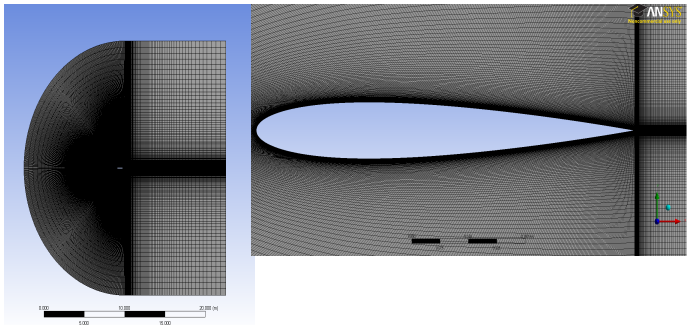

Fig. 2 Domain and meshing of the NACA 0012 airfoil.

Simulation was conducted with the NACA 0012 airfoil over different angles of attack ranging from 0° up to 15° with an increment of 5°.

## 4. Results and Discussion

First a CFD simulation was conducted to determine the total lift coefficient of the NACA 0012 airfoil at different angle of attack. This was compared to theoretical results by Abott to justify the accuracy of the simulation. Next an experiment was conducted in the wind tunnel to obtain the lift force of NACA 0012. Results obtained are compared to the theoretical and numerical results.

Figure 3 shows the relationship obtained from the CFD simulation, and wind tunnel experiment in comparison with the theoretical results. It is possible to see that the lift coefficient as a function of angle of attack for the numerical NACA0012 airfoil in very good agreement with the theoretical. Comparing with the numerical values of $C_L$, all the values are almost similar to the theoretical values except for the highest possible angle of attack, which is 15° as the highest theoretical value plotted is just 14°.

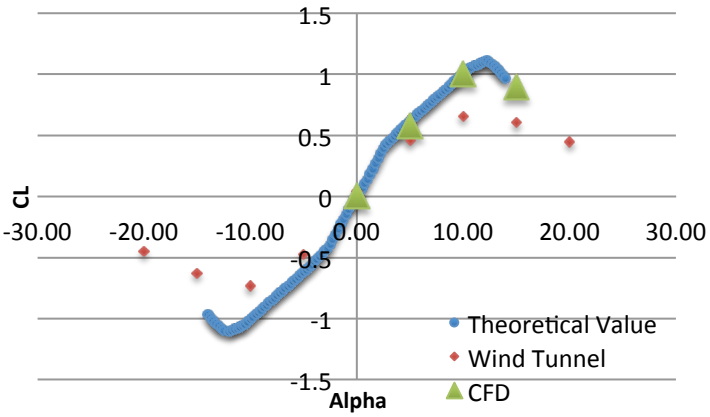


Fig. 3. Variations of lift coefficient against angle of attack.

Table 1. Percentage error obtain from CFD simulation.

| Alpha | CFD, $C_L$ | Theoretical, $C_L$ | Percentage error, % |
|---|---|---|---|
| 0 | -0.000012 | 0 | 0 |
| 5 | 0.6158 | 0.6195 | 0.60 |
| 10 | 1.0030 | 1.0066 | 0.36 |
| 15 | 0.9531 | 0.9628 | 1.01 |

Based on table 1, the highest error during simulation occurred during an angle of attack of 15° at a percentage of 1.01%. With the largest error being at 1.01%, it can be said that the results obtained in the CFD simulation corresponds and complements with the theoretical results.

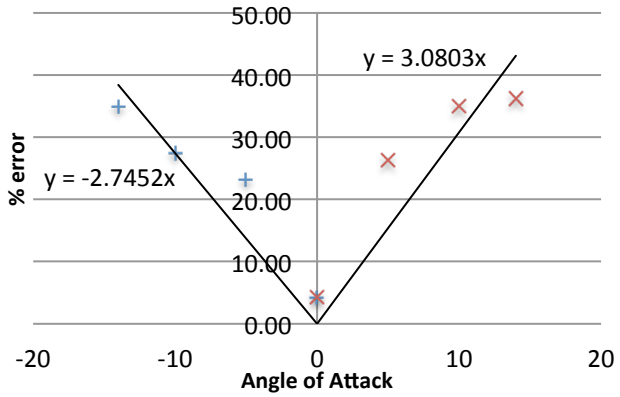


Fig. 4. Percentage error of coefficient of lift from wind tunnel.

Concerning on the percentage of errors shown in Fig. 4, it is shown that the percentage error increases from positive angle of attack of 0° to 5° and it slowly reduces slightly to 20° therefore it is safe to assume that the percentage error increases linearly with angle of attack. The same occurs for the negative angle of attack accept there are some discrepancies in the percentage error at 5° angle of attack. A possible cause for this maybe due to random errors during experiment.

Figure 4 shows the percentage error obtained in the coefficient of lift of NACA 0012 during a wind tunnel experiment. It is seen that the percentage error increases with increasing angle of attack with the lowest error estimated at 4% at 0° and up to 37% at 14 degrees. The large percentage error in lift coefficient as angle of attack increases increase is expected due to model mounting limitation in the wind tunnel such that a strut to change angle of attack passes through the airfoil model as seen in Fig. 1 and prevents total lift force experience by the airfoil to be transferred down to the wind tunnel's force transducer. This further explains that at angle of attack 0° the percentage error recorded is minimum at 4% as due to theoretical results the airfoil experiences no lift at 0°. A small percentage of discrepancies in lift coefficient are also assumed to be primarily caused by the imperfections in milling of the NACA0012 airfoil shape and also some inaccuracies during the experiment.

Based on Fig. 4, almost similar errors are recorded for the positive and negative angles of attack and it can be estimated that there will be an error of $y = 3x$ for $x$ angle of attacks in lift coefficients when running airfoil experiments in Taylor's subsonic wind tunnel.

## 5. Conclusions

In conclusion, the CFD simulation of the NACA 0012 proves to be inline with theoretical published results whereas a reasonable large error of 37% in lift coefficient is recorded from wind tunnel experiment. Some improvements could be done to minimize the error percentage such as the strut to change angle of attack can be removed.

## Acknowledgment

A great appreciation to Sunny Lee and Mike Ooi who have been very responsive in providing me necessary information to get the project to completion.

## References

[1] Jewel B. Barlow, William H. Rae, Alan Pope. (1999). *Low Speed Wind Tunnel Testing 3rd Edition,* John Wiley & Sons

[2] Abbott, I H & Von Doenhoff, A E. (1959). *Theory of Wing Sections: Including a Summary of Airfoil Data*. Dover Publications.

[3] N. A. Ahmed (2013). *Wind Tunnel Designs and Their Diverse Engineering Applications*. United States of America: InTech. 560.

[4] Heller, V. (2011) Scale effects in physical hydraulic engineering models. *Journal of Hydraulic Research, 293-306*

[5] Deck, S. (2002) Development and application of Spallart-Allmaras one equation turbulence to three-dimensional supersonic complex configurations. *Aerospace Science and Technology,* 6(1) 171-183

[6] Nor Elyana Ahmad, Essam Abo-Serie & Adrian Gaylard. (2010). *Mesh Optimization for Ground Vehicle Aerodynamics*. *CFD Letters*. 2 (1), 2-5.

# Advance Personalized Learning: Software based approach

Low Kean Peng[1*], Douglas Tong [2]

[1,2]*Mechanical Engineering, Taylor's University, Malaysia*

**Corresponding email: keanpeng.low@taylors.edu.my*

*Abstract*— **Every student has a different learning style to learn something. Advance Personalized Learning style is the learning style tailored to suit the learner only using technology. The education system in Malaysia has been following a one-size-fits-all method from primary to secondary school. The students are tested at the end of the year and major exam such as Ujian Penilaian Sekolah Rendah (UPSR), Penilaian Menengah Rendah (PMR) and Sijil Pelajaran Malaysia (SPM). Multiple Intelligence (MI) by Howard Gardner, is used as the approach for this personalized learning software based approach. A group of students from the faculty of Engineering will be chosen as subjects to be studied. The subjects will be tested whether do they have their own learning style and the proposed advance personalized learning skill will assist them in their studies. A quantitative analysis will be done on surveys and results of the data collected. The results of the survey and data acquitted from the software will illustrate the chosen model is successful in assisting students in their studies and deepen their interest in engineering.**

*Keywords*— Personalized learning style, Industry, PHP, HTML, Multiple Intelligence

## 1. Introduction

Bloom's taxonomy has been one of the main guidance to understand humans' intelligent and a guidance to understand the learning process [1]. There are debates as researchers which found learning capability is linked to multiple intelligent (MI). It is a theory proposed by Howard Gardner [2]. There are certain subjects that are important to the industry but difficult for the student to learn such as Fluid Mechanics, Thermodynamics and Solid Mechanics. The objectives of this research project including; identifying the learning profile of the chosen group of mechanical engineering students in Taylor's University, finding out the subjects / topics which are required by the industries but the subject is a challenge for the students, develop an advance personalized learning style; a software approach solely based on Multiple Intelligence theory, conducting the experiment the effectiveness of the advance personalized learning style and finally comparing and analyze of the effectiveness of the approach.

## 2. Research Methodology

The research of this final year project is an on-going process. It will be divided into four stages. The first stage is to perform research on case studies and journals to understand more about personalized learning, the work done regarding engineering education. This is important as case studies and journal will show the insights of the final year project and can be used as reference. The second stage is research on proper survey method. Survey is mainly divided into two types which are quantitative and qualitative survey. The chosen type of survey is vital as it will assist the analysis of the data. The third stage of research is to understand more about Multiple Intelligence (MI) and the method of profiling. The last stage will be conducting research on web based application or normal application as this is a software based approach advance personalized learning.

The survey is also divided into three parts and the three surveys must be done one after another. The first part of the survey is to identify The first part of survey that will be carried out is to identify the subjects that the industries feel important but difficult for students. The acquired subject will broaden the topics of students having difficulties and thus it will be easier to carry out the last survey. The second survey will be the topics that students feel bored or not interesting and difficult to understand. The topic that students chosen will be selected as the topic that program will assist the students in to help them understand the topic and develop their interest in it. The last survey that will be carried out is for the students to choose which software based approach they will prefer such as mobile apps, computer software or web based software.

Conceive, Design, Implement and Operate (CDIO) method will be the fundamental design of the software. The current most downloaded application and most visited websites will be studied and examined. This can create a proper plan on the user interface and the outlook of the program. During the design stage, drafts of the user interface, the student profile and the program outlook will be drawn and the codings required will be identified. In the implement stage, the creating software program such as C++, HTML 5 and JAVA will be used. For the last operation stage, the program will be tested to ensure the program performs smoothly.

The approach in this research project is profile the students and understanding their learning method and skill. Thus, program must have the selection of suitable survey questions to profile the students. After that, the students are required to use the program to assist them to understand the topic. At the end of the program, exercises will be used to test the students understanding on that specified topic. A survey will be available to survey whether the student has increased their understanding and interest in the topic and whether the program helps. Simultaneously, their test and final exam results will be collected to be analyzed in order to check their performance.

Pareto Analysis will be done on the survey stage of the research methodology. This is to identify the subject and topic that will be programmed to assist the students. Quantitative studies will be done instead of qualitative as quantitative can represent a group and higher number of people. Results of the students whether improved will be collected from the test and their final exam. The exercises available in the software will be collected to check their understanding on the subject manner. ANOVA analysis will be lastly to be done to demonstrate the percentage of improvement from the students.

## 5. Results and Discussion

After several case studies, Multiple Intelligence (MI) was chosen as the approach after comparing with Myers-Briggs Type Indicator (MBTI) and Kolb's Experiental Learning Model [4]. MBTI was not chosen as the model does provide sufficient evidence whether difference in gender is one of the factor affecting the academic studies and interest of the learner [3]. The model only suggested that the learner ability affected by the student's personality. It also does not suggest that there are other factors affecting the learning profile of a student such as the environment or intelligence. Kolb's model only suggested that students of the four classifications only affect their studying ability [3]. MI classifies students according

to the intelligence or talent they have such as musical, linguistic, logical, visual, bodily, interpersonal, intrapersonal, naturalist and existential.

After research regarding the software type; web based application or normal application, web-based is selected as the software. The selection was done as web-based application allows the students to access it easily as long as they are connected to internet. It also allows the data to be easily collected as the student's log and performance can be recorded in a selected server. Apache Xampp will be the selected server as the storage of the database. It is a free server. The usage of xampp allows the building of the database. From there, all data can be retrieved and populate it to the web system.

PHP and HTML will be chosen as the language for the web programming instead of C++ and JAVA. Java is a strongly-typed language. It requires explicit statements of intent to function and that it is backed by a compiler. Java contains lots of strict restriction on the inputs and outputs expression. If these exact expressions are not expressed correctly, the compiler will fail and the program is unable to function until errors are resolved. There are certain drivers and jar files like jdbc has to be used. The database for Java requires certain driver and jar file.

PHP is weakly typed language. It is more flexible as it requires less formal knowledge on programming. It only uses phpmyadmin as the database. The first advantage of PHP is, aside from being free in terms of cost. The open-source language is widely accessible on every Web-hosting platform for public usage. PHP works universally across platforms. The justification for this manner is that the code is processed entirely on the server side and can be delivered as dynamic content to the viewer. PHP can be also used for large scale operations.

## 7. Conclusions

Advance Personalized Learning will definitely able to encourage the engineering students to be interested in subjects and topics that they find difficult to understand or learn. This is important as the needs to produce capable engineers graduate to ensure the working industry able to meet the codes and standard. Multiple Intelligence theory will demonstrate the student's performances. More improvement can be done after the analysis of the student is done. Web based application is the software approach as it provides flexibility on the student and the research.

## Acknowledgment

I wish to thank my supervisor Mr.Douglas for his guidance and support throughout the final year project.

## References

[1] Kementerian Pelajaran Malaysia, *Dasar Pendidikan Malaysia*, Malaysia: Giga Wise Network, 2012

[2] Howard Garder, *Multiple Intelligence*, United States of America: Basic Books, 2006

[3] Felder, R.M, and Silverman, L.K., "Learning and Teaching Styles in Engineering Education", *Engineering Education*, Vol.78, No.7, 1988

[4] [12] Richard M. Felder and Rebecca Brent, "Understanding Student Differences", *Journal of Engineering Education*, 2005

# Sintering Behaviour of Hydroxyapatite-Forsterite Nanocomposite

Michael Loon Chee Yan[1], Jeffrey Chin Kong Leong[2*]

*Department of Mechanical Engineering, School of Engineering, Taylor's University, Malaysia*

**Corresponding email: jeffreykongleong.chin@taylors.edu.my*

*Abstract*— **This paper attempts to investigate the potential achieved when hydroxyapatite and forsterite nanopowders are combined into a single nanocomposite. The research was initiated with an exhaustive literature review of recent materials and journals. The respective nanopowders were then prepared using the mechanochemical method of synthesis, after which the samples are pressed and sintered and its mechanical properties attained and evaluated. It is the sole objective of this paper to show the importance of this research and the future implications it could have on the biomedical and bioceramics industries.**

*Keywords*— Sintering, hydroxyapatite, forsterite, nanocomposite

## 1. Introduction

Through the study of recent research, it has been discovered that although the bones of a human being have the ability to regenerate upon minimal fracture, it is all the same subjected to fracture under load bearing applications in particular [1]. Due to this occurrence of fractures, there is hence a call for bone transplants to take place which has been deemed to be costly and fairly risky because of the potential transfer of viruses in the process [2]. Extensive research has also contributed that bioceramics are an ideal alternative to the risky bone transplants, in that bioceramic materials can be employed as implants. When the subject of bioceramics is discussed, the talk lately has been often on the topic of hydroxyapatite (HA), which has been found to have desirable biocompatibility and similarity to that of the human bones and teeth [3]. On the other hand, some research has also been performed of an alternate or complementing bioceramic known as forsterite. The effort placed into this research has not been exhaustive but it has been discovered that forsterite too possesses desirable biocompatibility with the human tissue structure. The distinction lies in that forsterite possesses more desirable mechanical properties when compared to HA. It is in this light that this research will be carried out, with the hopes of producing a nanocomposite with superior mechanical properties that the ones currently available.

The aims of this research are three-fold. Firstly, it is to effectively synthesize HA-forsterite nanocomposite. Secondly, this research aims to study the optimum sintering conditions of the nanocomposite with superior mechanical properties at lower temperatures so that it is suitable for the majority of medical applications. Last but not least, this research wishes to enquire into the effects and implications on grain size and mechanical properties when HA and forsterite are combined to form a single nanocomposite.

## 2. Research Methodology

The research will be performed adopting the flow depicted in the flow chart present in Figure 1 below.

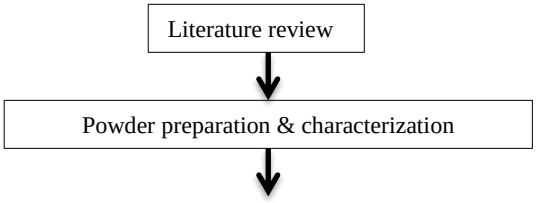


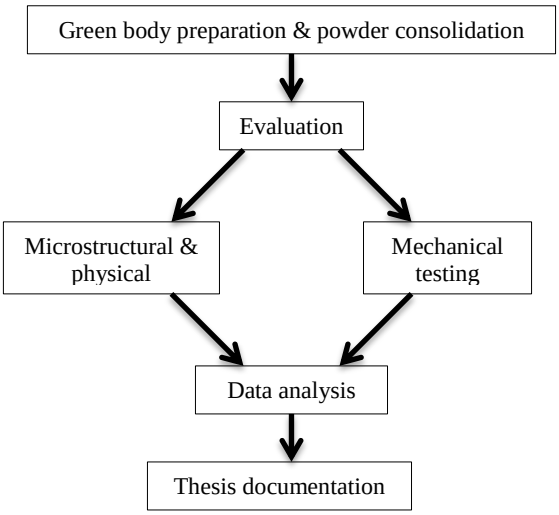


Fig. 1 Flow chart depicting the manner in which this research will be carried out

The research was initiated with an exhaustive literature review in order to stay up to date with the latest developments and progress in the bioceramic field. The review was much focused upon the progress and improvement of HA and the methods employed by various researchers in the process. The literature review has been an ongoing process in this research. Meanwhile, the respective HA and forsterite powders were prepared using the mechanochemical synthesis method. This particular method was chosen over the other methods due to its simplicity. Furthermore, the mechanochemical method is a conventional one, enabling more relevant evaluation and analysis when this research is compared to other work in the later stages. The samples were then pressed via isostatic pressing and sent for sintering using the sintering profile displayed in Figure 2 below.

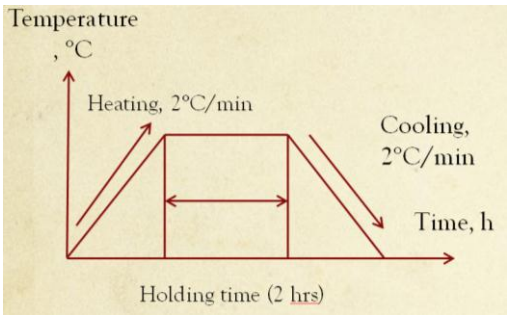


Fig. 2 The sintering profile to be used in this research

The samples will be sintered to different temperatures and percentage weights of forsterite. The samples created are displayed in Table 1 below. Upon sintering, the samples will be polished and grinded before experiments are carried out on them in order to define its properties. Microstructural tests such as bulk density and phase analyses, along with mechanical testing such as hardness and fracture toughness tests will be carried out, upon which all data will be neatly tabulated and evaluated in comparison with current work.

Table 1. The manner in which the samples will be displayed

| Forsterite wt. % | Sintering Temperatures, °C | | | |
|---|---|---|---|---|
| | 1000 | 1100 | 1200 | 1300 |
| 0 | A1 | B1 | C1 | D1 |
| 10 | A2 | B2 | C2 | D2 |
| 20 | A3 | B3 | C3 | D3 |
| 30 | A4 | B4 | C4 | D4 |
| 40 | A5 | B5 | C5 | D5 |
| 50 | A6 | B6 | C6 | D6 |

## 3. Predicted Results & Discussion

### 3.1 Biocompatibility & Properties

Biocompatibility can be defined as *"the potential for a material to perform with another host"* [4]. HA [$Ca_{10}(PO_4)_6(OH)_2$] belongs to the complex apatite family and is a variant of the calcium phosphate compound. Calcium phosphate happens to be a major constituent in the structure of the human bone tissues. Hence, HA possesses very similar chemical composition and crystalline structure to the human bones, confirming its biocompatibility [5]. In addition, HA can be infused as implants into the human body without incurring any negative consequences such as poisoning [6]. Besides these, HA has desirable osteogenic ability, enabling rapid new bone ingrowth [7]. Lastly, the presence of apatite within HA allows a more dependable enforcement of implant to take place to the human bone tissue [8]. In a similar way, forsterite [$Mg_2SiO_4$] has been recently discovered and as time went on, more research has been placed into this area of developing forsterite. The magnesium constituent of forsterite allows it to be a catalyst for metabolism [9], while its silicon constituent enables quick growth of the human skeletal system [10]. These facts seem to suggest that forsterite indeed, in the same manner as HA, has desirable biocompatibility. In a research on the preparation and characterization of forsterite by Ni [11], they prepared forsterite via the sol-gel synthesis method and their results pointed to the fact that forsterite was considered to have desirable biocompatibility. Therefore, it can be said that combining two biocompatible materials would ultimately produce a superior biocompatible material.

### 3.2 Mechanical Properties

Although HA seems to be very desirable to act as a sustainable implant material, its weaknesses suggest otherwise to a certain extent. Also through research, it has been discovered that HA in fact has some undesirable mechanical properties such as brittleness, low flexural strength and low fracture toughness ( < 1 $MPam^{1/2}$) [12]. Due to these inefficiencies, a pure HA implant would be unable to withstand load bearing applications that typical human bones are heavily subjected to. It has also been discovered through other studies, on the other hand, that forsterite has superior mechanical properties as compared to calcium phosphate ceramics such as HA. In the study by Ni [11], through the sol-gel method of powder preparation were successful in attaining a fracture toughness of 2.3 $MPam^{1/2}$ and a maximum flexural strength of 181 MPa when sintered at 1450ºC. In an alternate piece of research, Fathi [13] was able to attain a superior fracture toughness of 4.3 $MPam^{1/2}$ for forsterite when partnering the sol-gel method and two step sintering. Therefore, it can be seen that in terms of mechanical properties, where HA is weak, forsterite seems to be strong, evidence to the argument that the combination of these bioceramics would produce an even stronger one. There have been numerous attempts in order to improve the mechanical properties possessed by HA in particular. Among these, an interesting research by Jiang [14] notes a patented NanoMech NanoSpray coating used before sintering. The critical result produced was that HA was able to withstand up to 10 N of load which was not significantly superior to its original properties. In another study using the chemical precipitation method of synthesis, Aw [15] achieved a mere 0.9 $MPam^{1/2}$ fracture toughness at 1050ºC sintering temperature. Hence, it can be summarized that researchers have attempted altering methods of preparation of HA in order to improve the mechanical properties of HA. However, little or no work has been done to combine HA with another material in these years of attempts. That is precisely what is hoped to be achieved as a result of this research.

## 4. Conclusions

Due to the fact that HA is biocompatible but possesses undesirable mechanical properties, it is appropriate that work be done in order to produce a stronger bioceramic. It has also been found that the biocompatibility of forsterite and its superior mechanical properties puts it in a position to well complement that of HA. Some previous work done on HA alone showed that the fracture toughness achieved was as low as 0.12-0.31 $MPam^{1/2}$ [16] and 0.48-0.67 $MPam^{1/2}$ [17]. A recent research that combined HA, forsterite and bioglass showed improvement with a maximum fracture toughness of 0.972 $MPam^{1/2}$ [18]. Therefore, in terms of improving these properties, this research of combining mere HA and forsterite proves to be one with much potential, pushing the bioceramic and biomedical field to greater limits. Furthermore, the applications to which this work can be implemented will greatly improve the success of the already existing medical field.

## References

[1] U. Kneser, D. J. Schaefer, E. Polykandriotis & R. E. Horch. (2006). Tissue engineering of bone: the reconstructive surgeon's point of view. *J. Cell. Mol. Med., 10* (1) 7-19.

[2] L. L. Hench (2000). The challenge of orthopaedic materials. *Current Orthopaedics, 14,* 7-15.

[3] S. J. Kalita, A. Bhardwaj & H. A. Bhatt (2007). Nanocrystalline calcium phosphate ceramics in biomedical engineering. Mater. Sci. Eng. C., 27, 441-449.

[4] D. F. Williams (2008). On the mechanism of biocompatibility. *Biomaterials*, 29, 2941-2953.

[5] S. Pramanik, A. K. Agarwal, K. N. Rai & A. Garg (2007). Development of high strength hydroxyapatite by solid-state sintering process. *Ceram. Inter.*, 33, 419-426.

[6] M. H. Fathi & A. Hanifi (2007). Evaluation and characterisation of nanostructure hydroxyapatite powder prepared by simple sol-gel method. *Mater. Lett.*, 61, 3978-3983.

[7] P. O'Hare, B. J. Meenan, G. A. Burke, G. Byrne, D. Dowling, J. A. Hunt (2010). Biological responses to hydroxyapatite surfaces deposited via a co-incident microblasting technique. *Biomaterials*. 31 (1), p515-22.

[8] E. Marini, P. Ballanti, G. Silvestrini, F. Valdinucci, E. Bonucci, E (2004). The presence of different growth factors does not influence bone response to hydroxyapatite: preliminary results. *J Orthopaed Traumatol*. 5 (1), p34-43.

[9] E. M. Carlisle, Silicon: a possible factor in bone calcification, Science 167 (1970) 279-280.

[10] J. Althoff, P. Quint, E. R. Krefting, H. J. Hohling, Morphological studies on the epiphyseal growth plate combined with biological and X-ray microprobe analysis, Histochemistry 74 (1982) 541-552.

[11] N. Siyu, C. Lee, C. Jiang, Preparation and characterization of forsterite ($Mg_2SiO_4$) bioceramics, Ceramics International 33 (2007) 83-88.

[12] N. Y. Mostafa, Characterization, thermal stability and sintering of hydroxyapatite powders prepared by different routes. Mater. Chem. Phys. (2005), 94, 333-341.

[13] M. H. Fathi, M. Kharaziha, Improvement of mechanical properties and biocompatibility of forsterite bioceramic addressed to bone tissue engineering materials. *Mater.* 3 (2010), 1455-1458.

[14] J. Wenping, C. Jiping, K. Dinesh, A. Agrawal, P. Malshe, L. Huinan, Improved mechanical properties of nanocrytalline HA coating for dental and orthopedic implants, *Mater, Res. Soc. Symp. Proc.* (2009) 1140.

[15] K. L. Aw, Sintering behaviour of hydroxyapatite bioceramic derived from wet chemical method (2009). 1(1).29.

[16] S. Zhang, Y. S. Wang, Z. T. Zeng, K. A. Khor, W. Weng, D. E. Sun, *Thin Solid Films 516* (2008) 5162-5167.

[17] H. Li, K. A. Khor, P. Cheang, Biomaterials 23 (2002) 85-91.

[18] M. Mazrooei Sebdani, M. H. Fathi. Novel hydroxyapatite-forsterite-bioglass nanocomposite coatings with improved mechanical properties, *Journal of Alloys and Compounds* (2010) 2273-2276.

# Developing an Integrated Approach to Base Pan Finite Element Model Correlation

Mohamad Haris bin Husni @ Rusli[1*], Mohammad Hosseini Fouladi[1], Yap Kim Haw[2]

[1]*School of Engineering, Taylor's University, Malaysia,* [2]*CMD/CAE, Panasonic Appliances Air-Conditioning R&D (M) Sdn. Bhd., Malaysia*

**Corresponding email: m_haris03@yahoo.com*

*Abstract*— **Dynamic behaviours of a base pan for air-conditioning unit are numerically and experimentally investigated. The main outcome of this investigation is to develop an integrated approach of these two methods for model correlation of base pan's finite element model. The processes for numerical solving, pre-test planning, experimenting and correlation analysing are presented. Results from model correlation are essential for model validation which updates dynamics behaviour of FE model to closely represent the actual model.**

*Keywords*— Modal Testing, Finite Element Model Analysis, Experimental Model Analysis, Model Correlation Analysis, Impact Hammer Testing, Base Pan

## 1. Introduction

Base pan is one of air-conditioner outdoor unit's components. Base pan is used to support other components of the units such as condenser, evaporator and compressor. However, the base pan always tends to vibrate during operations. Normally, the heat exchangers, the compressor and the fan are the major components, which can be a primary source of vibration [1]. The components also may provide a vibration transmission path through the mountings of the compressor and the interconnecting copper tubes to the base pan of the outdoor unit [2]. These excessive vibrations of base pan will generate noise during the operations as well as may cause structure failure of the base pan.

In order to evaluate contribution of the base pan to the noise or vibration, it is important to understand the dynamic behaviour of the unit's base pan structure. This makes the study of structural dynamics (vibration) analysis for the base pan is essential for a better part design.

Modal analysis will help to study the dynamic behaviour of the base pan. There are two approaches of doing modal analysis which are numerically (AMA) and experimentally (EMA). FE modal correlation will compares the behaviour from results obtained in AMA to EMA as part of validation process.

## 2. Background and Framework

### 2.1 Numerical Modal Analysis (Normal Mode Solution)

Computation of a structure's dynamic behaviours (natural frequencies and mode shapes) is performed by solving an eigenvalue problem. In this particular problem, eigenvalues (natural frequencies) and eigenvectors (mode shapes) will be solved. Since damping is ignored in the analysis, the eigenvalues are real numbers [3]. The solution of the equation of motion for natural frequencies and normal modes requires a special reduction form of the equation of motion as shown in Eq. (1).

$$[M]\{\ddot{u}\} + [K]\{u\} = 0 \quad (1)$$

where:

$\{\ddot{u}\}$ = acceleration vector, $\{u\}$ = displacement vector, $[K]$ = stiffness matrix, $[M]$ = mass matrix

The solution of Eq. (1) is assumed has a form as shown in Eq. (2) which also can be form into Eq. (3) after substitution. The parameters are extracted from Eq. (3) using Lanczos method. The assumption for the whole process is that the structure is time-invariant and linear [4].

$$[x] = [a]e^{j[\omega]t} \quad (2)$$

$$([K] - \lambda_i[M])[a_i] = 0 \quad (3)$$

where:

$[a]$ = vector of displacement, $[\omega]$ = vector of natural frequencies, $t$ = time

$\lambda_i$ = eigenvalues, $[a_i]$ = eigenvectors

### 2.2 Pre-test Planning

Pre-test helps to design an optimum test condition by determine measurement and excitation locations and creating Test-Analysis Model (TAM). TAM is reduced representation of finite element model (FEM) which allows modal analysis to be more manageable. The location of excitation and test response measurement also can be optimised by the selection of TAM's degree of freedom.

FEM model's stiffness and mass matrices can be reduced by using Guyan Reduction method so that TAM can be obtained from it and the degree of freedom is corresponding to modal test sensor location

The accuracy of a TAM is evaluated based on how well the reduced modal properties approximate those of the original FEM model. In perfect reduction, the diagonal value of the Modal Assurance Criterion (MAC) will have unity value whereas the off-diagonal terms will have zero value [5]. The MAC values can be determined by using Eq. (4). The same application of MAC plot also can be used to determine the excitations and measurements locations from TAM.

$$MAC_{ij} = \frac{(\phi_i^T \phi_j)^2}{(\phi_i^T \phi_i)(\phi_j^T \phi_j)} \quad (4)$$

where $\phi_i$ and $\phi_j$ are the mode shape vectors

### 2.3 Experimental Modal Analysis

Experiment model analysis stage can be divided into several phases which are experiment setup, data acquisition and result evaluation. During experiment setup, decision on test system configuration will be made. It will include decision on type of support structure (boundary conditions), assumptions and excitation type.

Next phase is data acquisitions which involve acquisition of frequency response function (FRF) to serve as input to the modal parameter estimation stage. During data acquisition phase, three major strategies need to be applied so that a good FRF can be acquired. The strategies are transducer consideration, leakage and windowing and lastly sampling [6].

The result obtain from data acquisition phase will be evaluated so that its reliability can be guaranteed. The method of evaluation of the data is divided into three ways which are frequency check, reciprocity check and coherence.

### 2.4 Modal Correlation Analysis

Correlation is a process to determine the degree of agreement between two sets of frequencies and mode shapes. Frequencies can directly compared or by plotting on simple graph. However, to compare mode shapes require more complicated process since mode shapes are vector. The methods to compare the mode shapes are by using Modal Assurance Criterion (MAC).

By using the software, the test frequency response function can be reviewed. The test mode shapes also can be animated together with

overlaying the test geometry and sensor locations to the analysis model [7]. The software also provides a visual comparison by displaying shapes and synchronised side by side animation.

## 3. Application and Results

### 3.1 Numerical Analysis with Siemens NX Nastran Solver

CQUAD4 and CTRIA3 shell elements were selected to model the base pan. 53528 elements, 3mm in size were generated with 52596 nodes. There were 50417 CQUAD4 and 3111 CTRIA3 elements were noted. The threshold values of elements were checked to ensure the quality of mashing. The highest aspect ratio was 4.95; whereas warp was 4.97 and lastly skew value was 59.86.

The model was simulated by using structural analysis setup with linear and steady state time dependency. The results obtained were tabulated in Table 1.

Table 1. Comparison of Natural Frequency between Numerical and Experimental Modal Analysis

| Mode | Natural Frequencies (Hz) | | % Difference |
|---|---|---|---|
| | Numerical | Experimental | |
| 1 | 104.4 | 106.1 | 1.60 |
| 2 | 123.0 | 111.8 | 0.91 |
| 3 | 140.7 | 148.4 | 1.05 |
| 4 | 168.7 | 168.6 | 0.99 |
| 5 | 193.0 | 195.7 | 1.01 |

### 3.2 Pre-test Planning Configuration

30 DOF for excitations and 7 DOF for uni-axial sensors' placement were used to create TAM. These sensors' locations were chosen based on the MAC plot which the off-diagonal highest value was 0.176. For excitation DOF, the highest value for MAC plot off-diagonal was 0.008.

Fig 1 shows the test configuration blue datum represent excitation location whereas red datum represents measurement locations.

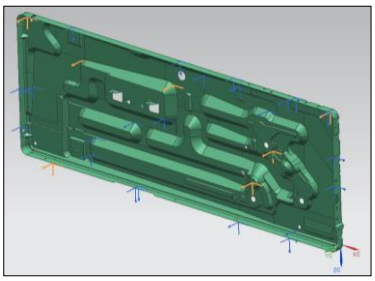

Fig. 1 Pre-test Configuration for Sensors and Excitation Points

### 3.3 Modal Testing Results

The structure was tested in free condition which means it will not attached to ground at any of its coordinates. The structure was assumed to be linear, observable and time-invariant. The structure was excited by using impact hammer roving method.

The structure was suspended using an elastic string with the flat surface was facing down. All the sensors were fixed to respective measurement locations using beeswax. An impact hammer was used to hit the excitation points accordingly. All the hitting sequence was determined during pre-test phase. The accelerometers used for response measurement were B&K 4517 and the hammer was B&K 8204.

The analysis mode chose was baseband, frequency span was set to 400Hz with 200 lines, thus made the signal duration become 500ms. Transient window was chose to filter hammer's signal whereas exponential window for response signal. Coherence measurements corresponding to the FRF showed acceptable correlation at most of the resonances. The measurements of FRF were averaged four times using linear modes. Any overload and double hit impacts were rejected.

The natural frequencies and associated mode shapes of the base pan were estimated based on the FRF's acquired. All these parameters were estimated using curve-fitting method which include real and normalisation function. Natural frequencies obtained from modal test data were compared with numerical result and tabulated in Table 1. In order to capture all the desired modes, the modes were selected between 100 and 200Hz.

### 3.4 Modal Correlation Analysis

Figure 2 show virtual comparison of mode 1.

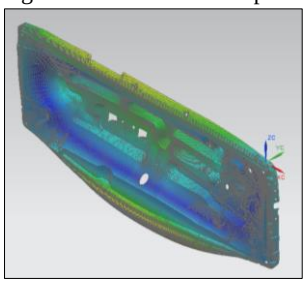

Fig. 2a Mode 1 from Numerical Analysis

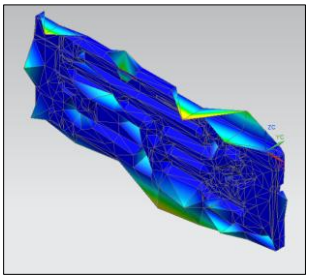

Fig. 2b Mode 1 from Experimental Modal Analysis

## 4. Discussion

From comparison of natural frequencies, it shows that all the modes well correlated since the percentage differences were not bigger than 2%. However by virtual comparison, the modes correlated poorly. Poor correlation was caused by difference between the static displacements and the mode shape which is known as "scaling". The scaling happen due to normal mode shape cannot mimic a true physical dislocation when there is applied load [5].

Insufficient measurement of DOF also may contribute to the error because of limited sensors placement. There also might be some information left out during parameters estimation process which the TAM cannot animate the desired mode shapes.

## 5. Conclusions

Modal data obtained from modal analysis is a very helpful piece of information that can assist in the design of base pan. The visualisation and understanding of mode shapes will be very significant in the design process because it can helps to recognise area of weakness in the design as well as area that need to be improved.

For this particular case, initial results have proven that reasonably well correlation in term of natural frequencies. Highest percentage difference was 1.6%. However, visual comparison shown that some improvement need to be implement for reducing the scaling effect. After correlation analysis is satisfied, modal updating can be done.

## References

[1] Steven E. Marshall, "Reducing Compressor Noise while Considering System Interactions," in *International Compressor Engineering Conference Paper*, Bristol, 2002.

[2] Parag H. Mathuria and Macinissa Mexache, "Mounting Design of a Compressor for Improving Sound Rating of an Out-door Unit," Ohio, 2006.

[3] Siemens Product Lifecycle Management Software Inc. (2001) NX Nastran Basic Dynamic Analysis User's Guide.

[4] Jimin He and Zhi-Fang Fu, *Modal Analysis*, 1st ed. Delhi: Butterworth-Heinemann, 2001.

[5] Mossimo Giorelli, "Methodology for Correlating Experimental and Finite Element Modal Analyses on Valve Trains," Worcester, 2002.

[6] National Instruments, The Fundamentals of FFT-Based Signal Analysis and Measurement in LabVIEW and LabWindows/CVI, 2009.

[7] NX CAE, NX FE Model Correlation: Compare simulation with test data, 2011.

# Drag Optimization Mechanism for Taylor's Race Car

Mohammed Mohaymen Khan[1], Abdulkareem Sh. Mahdi Al-Obaidi [2*]

[1,2]*Mechanical Engineering, Taylor's University, Malaysia*

**Corresponding email: abdulkareem.mahdi@taylors.edu.my*

*Abstract*— **The time is one of the most important factor in achieving the destination in a car race. One factor which contributes in reducing the time is drag force. This paper proposes a method to optimize the drag force of a car during the race. An increase in the drag was observed when cooling channel to direct the airflow into the radiator was installed in the car. Simulink was used for real-time simulation of the linear motion of the car to observe the performance of the car by optimizing the drag coefficient. It was concluded that if the drag coefficient of the car is optimized from 0.6702 to 0.5853 or 0.6217 then it is possible to achieve better speed and to cover more distance in less time as compared to the car with fixed value of drag coefficient.**

*Keywords*— Drag Coefficient, Drag Optimization, Cooling Channel, Performance of the Car, Simulink, Airflow, Velocity, Distance.

## 1. Introduction

Taylor's University Racing Team (TRT) designed and manufactured and open wheel race car. After the test run it was observed that the temperature of the engine increases gradually due to the blockage of the airflow into the radiator which was placed at the back of the driver seat [1]. It is important to avoid the engine from overheating to improve its efficiency and to prevent its failure [1]. In order to cool down the engine a cooling channel (flat plate) was installed to direct the airflow into the radiator as shown in Figure 1 [1]. An extensive study was conducted by Lee and Al-Obaidi to calculate the drag and its affect by changing the angle of attack of the cooling channel [1]. This resulted in additional drag, having this channel at the given angle is not required but it is required only when the temperature of the engine reach its maximum limit.

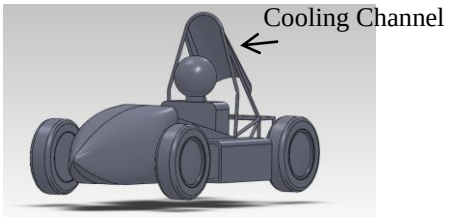


Figure 1. Car model with cooling channel [1]

The main objective of this research is to design a control system which adjusts the angle of the cooling channel depending on the temperature of the engine. This involves the study of the effect of an optimization of the drag coefficients ($C_d$) on the performance of the open wheel race car. For this study the drag coefficient is considered as a variable because the angle of the cooling channel has to be adjusted during the race to provide minimum possible drag when the temperature of the engine is normal and vice versa.

## 2. Research Methodology

It is important to carry out the real time simulation of the car to study the effect of the drag optimization on the performance of the race car such as the velocity and distance covered in time. Tasora (2008) studied the lateral acceleration and reaction of suspension with respect to time at simulated maneuver by developing the computer based simulator tool for optimizing the design of the car [2]. Bruna and Spiridon (2013) studied the effectiveness of numerical modeling of aerodynamic by adopting the aircraft airfoil on sports car to determine the $C_d$ at different angle of attack and concluded that engineering student can design complex aerodynamic model and obtain accurate results [4, 5].Lot and Simos (2013) studied the methodology for lap time optimization of a sports hybrid electrical vehicle with give characteristics on a particular track [3]. To study the effect of the drag optimization on the velocity, distance and acceleration with respect to it is important to simulate the car on the race track. This can be achieved through Matlab, Simulink.

### 2.1 Mathematical Modeling

To simulate the motion of car on the race track a mathematical model was developed. Newton's second law was used to create the mathematical model as shown:

$$\sum F = ma \quad (1)$$

$$\iint m\ddot{x} = \iint F_w + F_t - F_d - F_r \quad (2)$$

where, $\sum F$ represents the forces acting on the car.

$F_t$ is the thrust of the car in Newton .

$F_w$ is the weight of the car in Newton.

$$F_w = mg \quad (3)$$

$F_d$ is the drag force of the car in Newton.

$$F_d = \frac{1}{2}\rho v^2 AC_d \quad (4)$$

$F_r$ is the friction force acting on the car in Newton.

$$F_r = \mu mg \quad (5)$$

where $m$ is mass in $kg$, $g$ is gravity in $m/s^2$, μ is friction coefficient, $C_d$ is drag coefficient, $v$ is velocity in m/s, $A$ is reference area in $m$ and $\rho$ is mass density of fluid in $kg/m^3$.

### 2.2 Simulink

Simulink model is created to simulate the car motion and study the effect of different drag on the performance of the car. This Simulink model is only able to simulate the real-time linear motion of the car. Table 1 shows the main characteristics of the car.

Table 1.Main Characteristics of Race Car

| | | | |
|---|---|---|---|
| **Mass of car (m)** | 250 kg | - | - |
| **Driver and fuel mass (m)** | 80 kg | | |
| **Friction Coefficient(μ)** | 0.6 | - | - |
| **Drag Coefficients ($C_d$)** | 0.6702 | 0.6217 | 0.5853 |
| **Maximum Speed(v)** | 13.8 m/s | - | - |

The values from the table 1 were used in the Simulink model as shown in Figure 2.

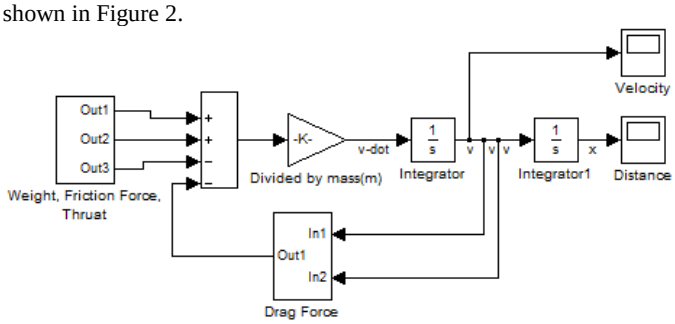


Figure 2. Simulink model for linear motion of the car

As mentioned the drag coefficient is considered as a variable as it has to be adjusted and readjusted during the race to improve the performance of the car such as time required to complete one lap is minimum. When the temperature of the engine is normal the cooling channel will be adjusted at angle to reduce the overall drag of the car without allowing the air entering into the radiator. Similarly when the engine starts to heat up the cooling channel will adjust its angle to

allow the air into the radiator to cool down the engine which would result in additional drag.

## 3. Results and Discussion

The drag coefficient of the car with the cooling channel at different angle of attack was calculated by Lee and Al-Obaidi as shown in Figure 3 to determine the minimum possible drag coefficient at particular angle of the cooling channel [1].

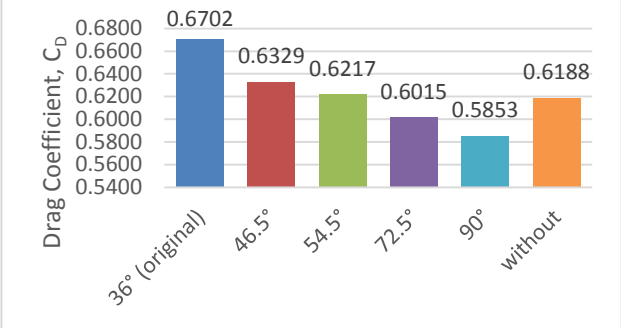


Figure 3. Drag Coefficients at different angels of cooling channel

Figure 3 clearly shows that the drag coefficient is higher when the cooling channel is fixed at its original position at an angle of 36 ° and if the angle of the cooling channel is readjusted a decrease in the drag coefficient was observed which could affect the performance of the car. These drag coefficients were substituted in the Simulink model to determine performance of the car by observing the change in velocity and distance with respect to time. Figure 4 shows the time taken by the car to reach a distance of 5 km when different drag coefficients were used.

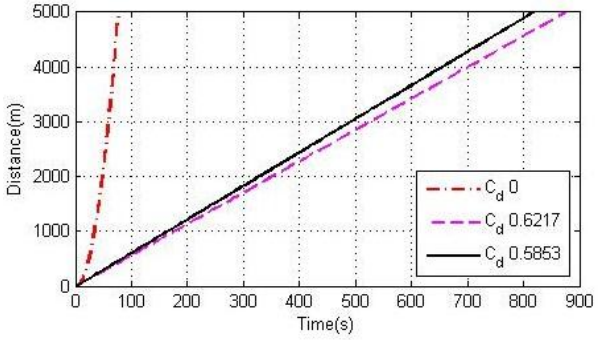


Figure 4. Distance vs. time at different Drag Coefficient

From Figure 4 it can be observed that when the drag coefficient is set as zero it only takes around 100 s for car to reach 5000 m. But when the angle of the cooling channel is adjusted to 36 degree to allow the air into the radiator for the cooling of the engine the drag coefficient is increased to 0.6702 and it takes 880 s to cover a distance of 5000 m. Similarly when the angle of the cooling channel is adjusted to 90 degree the drag coefficient is increased to 0.5853 it takes 820 s to reach 5000 m. This clearly proves that the higher the drag coefficient the more time the car is going to take to complete one full lap.

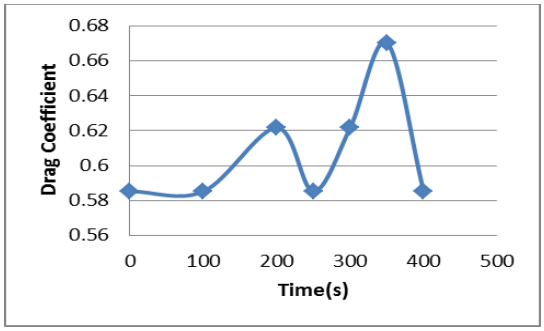


Figure 5. Change in Drag coefficient over Time

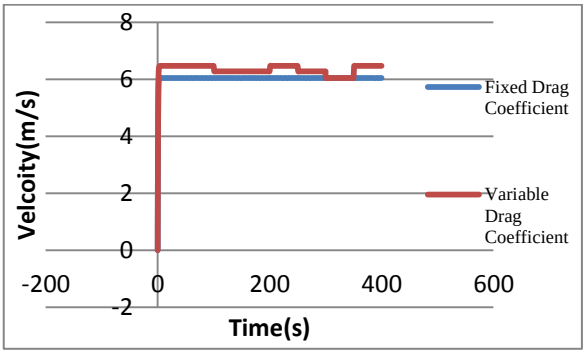


Figure 6. Velocity vs. Time at fixed and variable drag coefficient

Figure 6 shows the velocity with respect to time when the drag coefficient is kept constant and as a variable. It was observed that if the cooling channel is kept at its original fixed angle of 36° at a drag coefficient of 0.6702 the maximum velocity attained by the car would be 6 m/s. And if the drag coefficient is changed during the race the change in the velocity with respect to time can be observed. The car started the race at minimum drag coefficient of 0.5853 and achieved a maximum velocity of around 6.5 m/s. Later during the race after 100 s the engine started to heat up and the angle of the cooling channel was adjusted to 54.5° to allow the air into the radiator to cool down the engine this resulted in an increase of the drag coefficient to 0.6217 and decreased the velocity of the car to 6.25 m/s. After 200 s when the temperature of the engine had returned to normal the angle of the cooling channel was readjusted to 90° with drag coefficient of 0.5853 and the change in velocity from 6.25m/s to 6.5 m/s was observed. At 300 s and increase in the temperature of the engine was observed and the cooling channel was adjusted to its original position of 36° with a drag coefficient of 0.6702 and a decrease in the velocity to 6 m/s was observed. Figure 5 shows the change in the drag coefficient over the time span of 400s during the race. This clearly proves that if the drag coefficient of the race car would be optimized by changing the angle of cooling channel instead of fixing the cooling channel at a particular angle it would decrease the time required for the completion of the one lap due to the continues change in the velocity of the car.

## 4. Conclusions

Based on the numerical simulation it can be concluded that the drag coefficient plays an important role on the performance of the race car and this could increase or decrease the opportunity of winning the race. If the drag coefficient of the car is optimized during the race it is possible to achieve better speed and to cover more distance in less time as compared to the car with fixed value of drag coefficient.

Future studies include the simulation of the car on a complicated race track with curves and turns to study the effect of the optimization of the drag on the performance of the car. As well as optimizing the angle of the cooling channel and drag to provide airflow into the radiator depending on the temperature of the engine.

## References

[1] Lee, C., S., & Al-Obaidi, A., S., M. (2013). "*Calculation and Optimization of the Aerodynamic Drag of Open-Wheel Race Car,*" Submitted thesis for FYP, School of Engineering, Taylor's University.

[2] Tasora, A. (2008). *"Real-Time Simulation of a Racing Car,"* International Workshop on Research and Education in Mechatronics, 1(9), 1-7.

[3] Lot, R., & Evangelou, S., A. (2013). "*Lap Time Optimization of a Sports Series Hybrid Electric Vehicle*," Proceeding of the World Congress on Engineering: Vol. 3, pp.(1-6), London, U.K.

[4] Bruna,M., P., and Spiridon, E. (2013).*"Numerical Modelling of Aerodynamics for Applications in Sports Car Engineering."* Proceedings of the 2013 Maui International Engineering Education Conference. pp. 1-10.

[5] Bruna M., P., (2011). "*Engineering the race car wing: Application of the vortex panel numerical method*." Journal of Sports Engineering. 13(4),195-204.

# Vibration Control in Human Powered Vehicle

Muhammad Fadhli bin Ab Wahab[1], Dr. Hosseini Fouladi[1*], Dr. Satesh Namasivayam[1*]

[1]*School of Engineering, Taylor's University, Malaysia*

**Corresponding email: thereds15@yahoo.com*

*Abstract*— **This project was about the study of the effect of vibration on the Human Powered Vehicle (HPV). The amount of the HPV's vibration must be comply with the standards given by the SIRIM. The type of analysis used in this study was numerical analysis, which was done using ANSYS software to conduct the simulation on the chassis of the HPV. At the end of the project, two factors were decided. One of them was the most suitable type of suspension to be used while the other one was the most suitable position of the suspension on the HPV.**

*Keywords*— numerical analysis, ANSYS, vibration

## 1. Introduction

Human powered vehicle (HPV) is defined as a vehicle that operates using human muscle power (Fehlau, 2003). The purposes of this type of vehicle are environmentalism, lower cost, exercise and leisure. One common example of HPV is bicycle (Little, 2006).

The project about the human powered vehicle is developed during the 3rd year in mechanical engineering degree programme. However, it was found out that the produced HPV still has many aspects that can be improved, such as it vibrates when driven through a rough surface of the road. In order to improve its overall quality, the impact of vibration on the HPV must be studied.

Fig 1 HPV Produced by the Students

The objectives of the project were:

- ✓ To conduct the numerical analysis on the chassis of the HPV using ANSYS software.
- ✓ To apply the knowledge gained from the results of the numerical analysis and comply it with the standards given by SIRIM.

## 2. Methodology

At the start of the project, the first step was to select the suitable parameters and boundary conditions to be applied. The area of study in this project was to focus only on the chassis of the HPV, neglecting other parts such as the tires and the pedals. The purpose of this was to make the analysis become simpler and easy to understand. The 3D model of the chassis was shown in Figure 3. The type of material used for the chassis was structural steel and its total weight was 15 kg. The type of meshing used was 3D meshing and the size of the meshing was set to be medium. This type of meshing was used since it was suitable for a solid model and also considered to be sufficient enough to provide the detailed result. The flow chart of the project was shown in Figure 2.

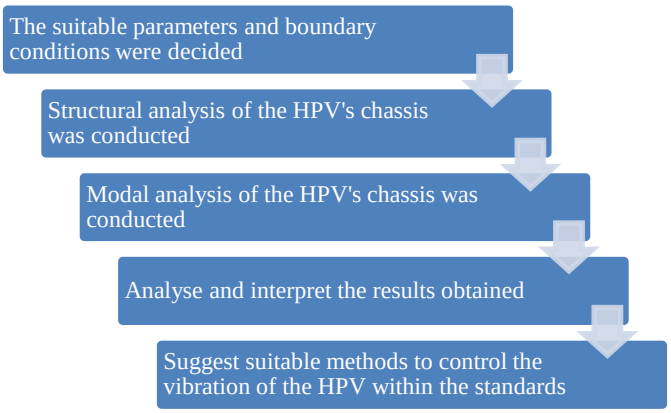


Fig 2 Flow Chart of Research Methodology

Afterwards, the structural analysis of the HPV's chassis was conducted. The objective was to determine the amount of deflection of the chassis when all the forces were applied to it and also the position of the maximum deflection. The amount of deflection was assumed to be directly proportional to the amount of vibration the chassis experiences. First, the analysis was done without involving the damper in order to find the amount of deflection it experiences when an excitation force was applied to it. The weight of the driver was kept constant at 60 kg. The result obtained was then being compared with the standards provided by SIRIM to check whether it is within the desired amount or not. It was realized that the result obtained was not compatible with the standards, so the damper must be applied to the HPV's chassis in order reduce the amount of deflection. The structural analysis was again repeated by applying the damper to the system. The analysis was being repeated several times until the most suitable amount of damper was decided to be used.

Fig 3 3D Model of HPV's Chassis

After that, the modal analysis of the HPV's chassis was conducted. The objective was to check whether the chassis vibrates near its natural frequency when it was driven on a rough road surface. The damper was not involved during the first analysis. The results obtained shown that there were few natural frequencies that the chassis encountered when it was driven. So a damper must be applied to the system in order to prevent the HPV from vibrating heavily. This can be done by shifting its natural frequency outside from its working frequency range. This analysis also were being repeated several times until the most suitable amount of damper was decided to be used.

The data collected from both the structural and modal analysis will be compared and analysed. The information gained from the data collected, such as its behavior was explained in detail. When the numerical analysis was carried out, it was essential for the analysis to be within the scope so that the project will not stray from its objective and should be able to achieve it at the end. The problems encountered during the experiment must also be stated and after that give some suggestions to improve the experiment in the future.

After completing all the studies, the suitable methods to control the vibration of the HPV are to be developed. There are many techniques of how to suppress the vibration. In this research, the most suitable technique chosen was to apply the bike suspension to the chassis. The bike suspension chosen also must satisfy both the structural and modal analysis so that the amount of vibration can be efficiently controlled.

## 3. Results and Discussion

### 3.1 Result of Static Structural Analysis

The result obtained shown that the maximum deflection of the HPV's chassis (5 mm) occurred on the middle of the chassis, which was near to the position of the driver's seat. From this it was known that the driver experienced almost the maximum amount of vibration the HPV experienced. Besides that, the amount of maximum vibration also did not comply with the standards given by SIRIM. So the safety and comfort of the driver was affected from this amount of vibration.

In order to reduce the vibration, damper was applied at the bottom of the driver's seat. The most suitable damper chosen had a stiffness value of 200 GPa. After the damper was applied, the maximum deflection reduced to 2.5 mm, which was half of the original value. This amount of vibration the chassis experienced also complies with the standards so the driver's comfort and safety were maintained in this situation. The minimum and maximum deflection that happened on the HPV was shown on Figure 4 below.

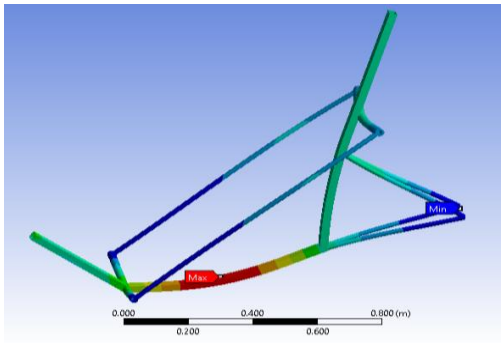


Fig 4 Result of Static Structural Analysis

### 3.2 Result of Modal Analysis

From this analysis, it was shown that the chassis experienced 5 natural frequencies when it was operating in the range of working frequency. The working frequency was assumed to be within 1 to 200 Hz. So it experienced a high amount of vibration since it vibrated near to its natural frequencies.

The natural frequencies was shifted outside the range of working frequency by applying a damper to the system. The type of damper which was decided earlier in the structural analysis was applied first. However, there were still 2 natural frequencies that happened within the range of working frequencies. So the damper's stiffness was changed to 250 GPa. There was no natural frequency that happened when this damper was used, so this damper was the most suitable to be used in the system. This damper also were applied back to the structural analysis in order to check whether it affects the results. The maximum and minimum deflection of the chassis was shown in Figure 5 below.

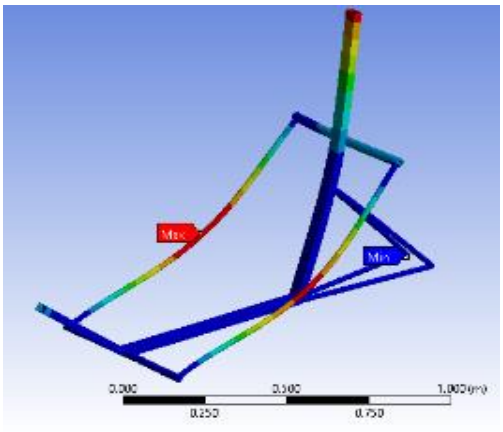


Fig 5 Result of Modal Analysis

## 4. Conclusions and Recommendations

In conclusion, it is essential to control the vibration of the Human Powered Vehicle (HPV) within the standards given by ISO. This is to ensure that the health and comfort of the user is well-maintained at all times. In order to do that, numerical analysis must be carried out first before producing the product. This is to understand more about the vibration experienced by the HPV, such as the source of the vibration, HPV's natural frequency and also the amount of vibration itself.

In the future, it is recommended to conduct both numerical analysis and also experimental analysis. The purpose of this is to validate whether the result obtained from the numerical analysis is the same with a real life. In order to do this, the complete 3D model of the HPV must be used rather than just the chassis of the HPV so that both the results will be familiar and can be compared.

## Acknowledgment

Firstly, I would like to thank Dr. Hosseini Fouladi who has guided me during the process of this project. Besides, I also would like to thank my parents who gave me so much support in terms of both moral and financial support. Last but not least, I also would like to give my thanks to Taylor's University for giving me an opportunity to produce my own project's paper.

## References

Fehlau, G., 2003. The Recumbent Bicycle. 2nd ed. Verlag Kiel, Germany: Moby Dick.

Little, J., 2006. Way Out There: The Best of Explore. 1st ed. Vancouver, Canada: Greystone Books Ltd.

# Development of tissue engineering skin culture system

NG KUN YONG[1], YONG LENG CHUAN[2*]

[1] *Mechanical Engineering, Taylors University, Malaysia,* [2]*School of Engineering, Taylors University, Malaysia*

**Corresponding email: Lengchuan.yong@taylors.edu.my*

*Abstract*— **Tissue-engineering skin is to accelerates regeneration of skin wounds and reduce the period of pain feeling during regeneration. Epithelium consists of fibroblast, keratinocytes, melanocytes, glands and others. The objective of this project is to design other culture methods to reduce the production cost and time needed to culture sufficient numbers of cells before implement to patient where mass production might be needed to fulfil society demand. Fibroblast has been selected to test the functionality of the design.**

*Keywords*— tissue engineering skin, culture system, fibroblast

## 1. Introduction

Biomimetic human skin is artificial to reduce the curing time needed for human skin to regenerate and minimize the time needed for wound healing process. Human epidermis mainly consists of fibroblast, keratinocytes, melanocytes and glands where it has a multilayer structure. The typical practice of culture the multi-layered epithelium skins are to culture fibroblast and keratinocytes with the assistance of human fibrin matrix as a scaffold along with calcium chloride[1].Keratinocytes mainly found in the outer layer of the epithelium skins where is provide the first line protection to human body. Besides that, keratinocytes cells are the cells that has air interface with outside air. Culturing human skin can be improved using a well-established animal-derived trypsin. [2] The time consuming of the culture of epithelial cells has contribute to expensive curing methods. Compare to natural regeneration, tissue engineering skin has a significant of reduce wound healing time needed although it is still expensive to due to long culture time needed and not popular yet in society. The gold standard of clinical application of skin substitution is to use skin grafting. The limitation of skill grafting is that the injured part that applied skin grafting need to have some remains of cells likes fibroblast, keratinocytes and melanocytes. This is because skin grafting method is to help cells to proliferate by providing extra-cellular matrix (ECM). If the injury of skin has reached no cells remain in the skin, skin grafting might not be the first line curing method. There are few companies has been trying to improve the culture method, reduce culture time needed and make the culture methods more easy to implement, but there is still no significant improvement of culture method. With the latest culture methods, around 1 to 2 weeks is needed to cure skin injured. The most significant improvement for culture technology is by Nunc Company that introduces Thermo-culture plate where the cells can be detached from culture plate when the temperature changes. This is considered the significant improvement because the cells that culture in culture plates wells cannot be detached or the cells will be damaged.

The main objective of this project is to design a culture system for culturing epidermis of human skin with lower cost of production, higher production rate and higher efficiency of transferring cultured cells. Fibroblast cells have been selected to test the functionality of the design.

## 2. Research methodology

This project has implement Conceive, Design, Implement and Operate (CDIO) design concept as advice. The 5 main phases of this project are conceiving stage, design stage, implement stage, operate stage and testing stage. Phase 1 is idea conceive, phase 2(a) material selection, 2(b) design, phase 3 building of prototype, phase temperature control and timer and phase 5 testing of prototype.

This project belongs to a quantitative study where it includes mathematic modeling and assesses the functionality of the prototype of this project through experiment. This project is to design and develop tissue engineering skin culture system that enables to produce artificial epithelium with simply method and lower production cost. Fibroblast cells have selected to test the functionality of the prototype. This is because fibroblast is one of major cells in dermis layer where act as a support for keratinocytes cells at epidermal. Hence, the cell chosen to test the functionality of the prototype is fibroblast cells. Well establish of fibroblast also contribute to be selected to verify this prototype.

Flow chart for research methodology

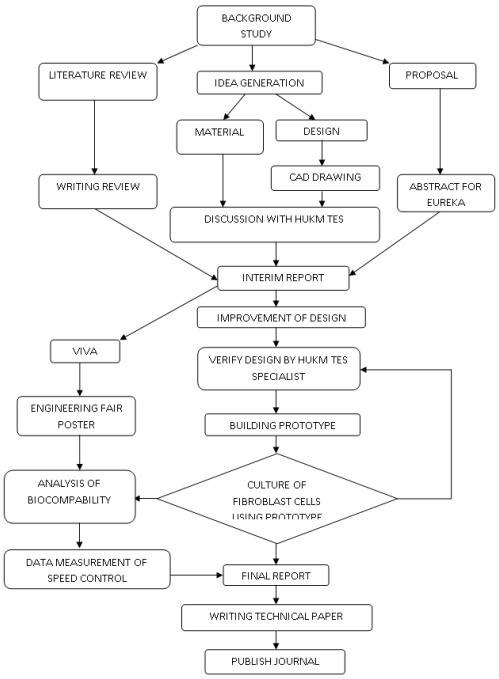


## 3. Structure of skin

The three main layers of skin are epidermis in the outermost layer, dermis medium layer and the hypodermis inner layer. The thickness of the outer most is around 0.1-0.2 mm. At this layer, the main cells types are keratinocytes and melanocytes. The function of this layer is to provide vital barrier function. [4] The dermis medium layer consists of fibroblast which is the main cellular components of this layer. There are enzymes in this layer will produce wound healing affect and revive process of skin. The enzymes are continuing produced by elastin and glycosaminoglycan (GAGs). This is because fibroblast producing extracellular matrix (ECM) and provides all cell types with nutrients by the vascular system. Besides that, sweat glands, sebaceous and hair follicles are found at dermis and epidermis layer. Hypodermis consists of white blood cells macrophages, fibroblasts, plasma cells, adipose cells, glands and

fibers like collagen and elastin [5]The simplified structure of skin has been shown in figure 1 below.

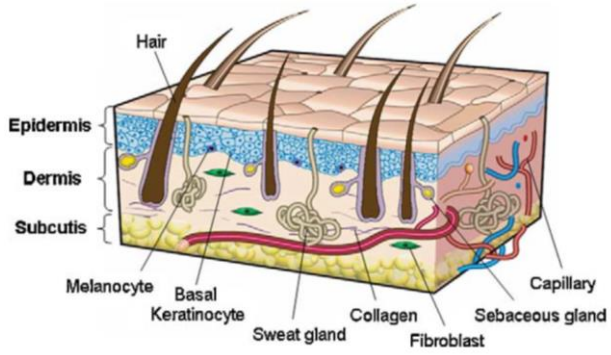


Figure 1 –The simple structure of skin [3]

## 4. Development event of tissue engineering skin

Around 2011, by using the concept of skin micrographs to rejuvenate the epidermis of full-thickness wounds and combined the hydrogel and foam dressing. It has proven can be regenerate 5cm X 5cm full-thickness wounds with a split-thickness skin graft to expansion. [6] The main weakness of full-thickness skin graft (FTSG) or split-thickness skin graft (STSG) is where skin graft has a change of failure which will lead to the grafted skin not healing the wound and it needs to repeat the skin graft from beginning. This will cause even longer time needed for patient to recover and painful feeling of the failure of skin graft.

Around 2013, full thickness skin regeneration without scarring was proven by introducing RNAi functionalized collagen-chitosan[7] Besides that, Nunc Company introduced temperature- responsive cell culture surface. By using Immobilized polymer poly (N-isopropylacrylamide) or also name as PIPAAm which is the skin grafted issue culture polystyrene (TCPS) surface, it able to release the adherent cells that culture in the surface when the temperature reduce to below 32 degree Celsius. [8] This is because that material has change to hydrophilic and binds water when the temperature goes below 32 degree Celsius. The main challenge for this technology is expensive and need experience people to handle the culture system. As a result, this project is trying to simplify the culture method and make it cheaper compare to these technologies. There is area of improvement of multi-culture plate where it just stacks the culture flask together. Furthermore, the available design in market are unable to reduce the workload of culturing cells and it only help to make culture flask more organize when putting in incubator.

## 5. Improvement of culture flask design

The improvement of culture plate has been designed to simplify skin culture system for stage 4 cell culture which is proliferate stage before it apply to patient. The common practice after separate glow of keratinocytes and fibroblast, both types of cells are required to remove from the culture flask and combine both cells in another culture flask or other culture plate. Since position of keratinocytes is always above of fibroblast position, the design has allowed user to presetting the position of cells during proliferate culture stage and enable to mix those cells by removing the slide in between both different culture space of cells. The temperature needs to be reduced to below 32 degree Celsius before removing the slide. This is because the slide is coated by isopropylacrylamide (PIPAAm) and allows cells to detach from culture slide, so that the cells will not damage when removing the slide where the cells used to attach and proliferate. This design has reduced loss of healthy cells when transferring from one culture flask to another flask. One of the main reason for long culture time is needed is where the cells needs to be cultured to the desired numbers of cells and the numbers of cells is always very huge. This is because some of the healthy cells are expected to be damaged or loss when transferring from culture plate to patient injured body part. By reducing loss of cells using this design where it leads to increases of efficiency of transferring of cells. This has contributed to reduce the number of cells needs to be cultured due to higher efficiency of transferring cells. Lower desire number of cells need to be cultured will directly reduce the time needed of culture cells before it transfer to patient. The cost of cell culture has been reduced because of lower time needed to culture. Besides the cost of culture cells is reduced, it also reduce the number of days of patient suffer while waiting for the desired cell to be cultured and transfer. If we able to cure patient with shorter time, it will contribute doctor in hospital able to serve more patient or help more patient. Figure 2 below has shown that the design of the culture plate.

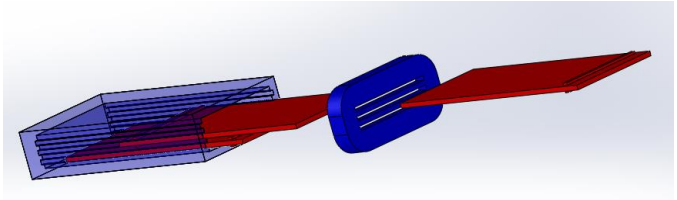

Figure 2—The prototype of culture flask design

## 6. Conclusions

As a conclusion, this project is trying to reduce culture time taken and simply the culture method where it reduces the workload of culture cells and increase the efficiency of transferring cultured cells to the patient. In this project, it only tested with fibroblast cells to prove the concept of the design.

## References

[1] P. de la Puente and D. Ludeña, “Cell culture in autologous fibrin scaffolds for applications in tissue engineering.,” *Exp. Cell Res.*, vol. 322, no. 1, pp. 1–11, Mar. 2014.

[2] A. El Ghalbzouri, S. Commandeur, M. H. Rietveld, A. a Mulder, and R. Willemze, “Replacement of animal-derived collagen matrix by human fibroblast-derived dermal matrix for human skin equivalent products.,” *Biomaterials*, vol. 30, no. 1, pp. 71–8, Jan. 2009.

[3] G. C. Gurtner, S. Werner, Y. Barrandon, and M. T. Longaker, “Wound repair and regeneration,” *Nature*, vol. 453, no. 7193, pp. 314–321, 2008.

[4] C. N. Grover, R. E. Cameron, and S. M. Best, “Investigating the morphological, mechanical and degradation properties of scaffolds comprising collagen, gelatin and elastin for use in soft tissue engineering.,” *J. Mech. Behav. Biomed. Mater.*, vol. 10, pp. 62–74, Jun. 2012.

[5] H. N. Kim, A. Jiao, N. S. Hwang, M. S. Kim, D. H. Kang, D.-H. Kim, and K.-Y. Suh, “Nanotopography-guided tissue engineering and regenerative medicine.,” *Adv. Drug Deliv. Rev.*, vol. 65, no. 4, pp. 536–58, Apr. 2013.

[6] F. Hackl, E. Kiwanuka, J. Philip, P. Gerner, J. P. E. Junker, E. J. Caterson, and E. Eriksson, “Skin micrografts regenerate the epidermis of full-thickness wounds when transplanted with random orientation and covered with a hydrogel and foam dressing,” *J. Am. Coll. Surg.*, vol. 213, no. 3, p. S92, Sep. 2011.

[7] X. Liu, L. Ma, J. Liang, B. Zhang, J. Teng, and C. Gao, “RNAi functionalized collagen-chitosan/silicone membrane bilayer dermal equivalent for full-thickness skin regeneration with inhibited scarring.,” *Biomaterials*, vol. 34, no. 8, pp. 2038–48, Mar. 2013.

[8] C. C. Flasks, S. Pipettes, S. Flasks, C. Slides, and F. Units, “Thermo Scientific Nunc Surfaces & Materials.”

# Investigation of Sintering Time on the Mechanical Properties of Un-doped Y-TZP Ceramics

ChyiShen Wong[1*], S.Sivakumar [2]

[1,2]*Mechanical Engineering, Taylor's University, Malaysia*

**Corresponding email:chyishen18@gmail.com*

*Abstract*— In this research, commercially available 3mol% Y-TZP powder was subjected to different sintering schedule with temperatures ranging from 1250-1500°C by presureless sintering with a holding time of 1 minute to 2 hours using a standard cooling rate of 10°C/min. Mechanical evaluation in terms of Bulk density, Young's modulus, Vickers hardness and fracture toughness were carried out in order to investigate the effects of sintering time and sintering temperature on the 3Y-TZP ceramics. Sintering time was found to be an important factor governing the density of the sintered 3Y-TZP samples. It was found that longer holding times resulted in higher densities. Moreover, it was also found that 3Y-TZP samples with holding times of 2 hours, 1 hour, and 30 minutes and 1 minute exhibit the same trend in mechanical properties magnitude variation.

*Keywords*— Sintering, Y-TZP, Mechanical Properties, Ramp rate, Densification, Monoclinic, Tetragonal, Cubic

## 1. Introduction

Yttria-Tetragonal Zirconia Polycrystals (Y-TZP) that stabilised by 2.5 to 3 mol% yttrium oxide has been the most popular type of ceramic material due to its excellent flexural strength (>1000 MPa) and high fracture toughness (> 5 $MPam^{1/2}$). As such, Y-TZP ceramic is used in many diverse applications including cutting tools, dies, thermal barrier coatings, piston, valves, knives, bioimplants, etc. Pure undoped Y-TZP (ZrO2) exhibits phase transformation with a sequence from monoclinic (m) to tetragonal (t) and finally to cubic (c) configuration[1]. The sintering time affects the transformations between different polymorphs which are essential for the processing and yielding various mechanical properties of Zirconia ceramics [2]. Studies in phase transformation of Zirconia ceramics from various literatures stated that the tetragonal (t) to monoclinic (m) phase transformation is highly related to the high temperature hysteresis of approximately 200°C (for undoped Y-TZP) and a finite volume change of 4-5% [3]. Densification strategies are imperative in the sintering and fabrication of ceramic components in order to accomplish finer sintered grain sizes and full densification. Sintering process of zirconium ceramics is completed through one cycle of heating, holding and cooling [4]

In this research, commercially available 3mol% Y-TZP powder was subjected to different sintering schedule with temperatures ranging from 1250-1500°C by presureless sintering with a holding time of 1 minute to 2 hours using a standard cooling rate of 10°C/min. The main objective of this research was to sinter samples which exhibit high mechanical properties, small grain sizes whilst maintaining the tetragonal phase stability.

## 2. Research Methodology

### 2.1 Sample Preparation

The 3% mol yttria-stabilized zirconia used in this research was manufactured by Kyoritsu Ltd., Japan under the code name KZ-3YF.

| Powder Characteristics | |
|---|---|
| Yttria (mol%) | 3 |
| Average particle diameter (μm) | 0.2 |
| Specific surface area | 16 |
| Bulk Density (g/cm³) | 6.09 |
| Bending Strength (MPa) | 1100 |
| Fracture Toughness (MPam½) | 4-6 |
| Hardness (GPa) | 13 |

Table 1: Starting properties of Y-TZP powder

The undoped powder were uniaxially compacted at about 1 kN into discs and rectangular bars using mold and die assembly and cold isostatically pressed at 200 MPa. The green samples were subjected to presureless sintering using rapid heating furnace at various temperatures ranging from 1250°C to 1500°C. A ramp-rate of 10°C/min and holding time of 1 minute to 2 hours were applied in this research. The sintered samples were firstly ground and polished prior to density measurement, Vickers hardness testing, XRD and SEM evaluation.

### 2.2 Characterization

The mechanical and physical properties of the sintered samples were determined using various equipments and method of calculations.

| Physical evaluation |
|---|
| ***Sintered bodies preparation*** – Grinding using series of silicon carbide paper followed by polishing using diamond paste down to 1 μm surface finish |
| ***Phases present*** – X-Ray Diffraction |
| ***Microstructure evaluation*** – Scanning Electron Microscope |
| **Mechanical testing and evaluation** |
| ***Bulk density*** – Archimedes's principle |
| ***Hardness*** – Vickers Hardness Tester |
| ***Fracture toughness*** – Vicker's indentation method |
| ***Strength measurement*** – Instron Universal Testing Machine (UTM) |
| ***Modulus of Elasticity*** – Grindosonic type MK5 'Industrial' |

Table 2: Methods of physical and mechanical evaluation

## 3. Results and Discussion

In conclusion, the holding time and temperature plays a significant role in affecting the mechanical properties (i.e. bulk density, Young's modulus, Vickers hardness and fracture toughness) of 3Y-TZP ceramics. Although the variation in the mechanical properties observed as the temperature progresses regardless of the holding time employed is relatively large and thus significant, an interesting observation can be made based on the results is that much of the variation that occurred, seems to have taken place when the temperature of 3Y-TZP samples was within the temperature range of 1250°C to 1350°C. Little fluctuation in magnitude of the mechanical properties of 3Y-TZP samples was observed above 1400°C until the maximum temperature of 1500°C was reached. Table 3 shows the variation both in magnitude and in percentage of the mechanical properties at three temperature ranges which are 1250°C to 1400°C, 1400°C to 1500°C and 1250°C to 1500°C for 3Y-TZP samples sintered with a holding time of 1 minute. 3Y-TZP samples with holding times of 2 hours, 1 hour, and 30 minutes were found to exhibit the same trend in magnitude variation. Thus it can be inferred from this result that sintering temperatures of 3Y-TZP within the range of 1400°C to 1500°C did not cause a significant change in the mechanical properties when compared to Y-TZP sintered from 1250°C to 1400°C.

| Mechanical Properties | Temperature Range (°C) | | |
|---|---|---|---|
| | **1250 to 1400** | **1400 to 1500** | **1250 to 1500** |
| **Bulk Density ($Mgm^{-3}$)** | 4.392→5.917 (35%↑) | 5.917→5.895 (0.4%↓) | 4.392→5.895 (34%↑) |
| **Young's Modulus (GPa)** | 110.2→200.2 (82%↑) | 200.2→205.4 (3%↑) | 110.2→205.4 (86%↑) |
| **Vickers Hardness (GPa)** | 4.91→13.1 (167%↑) | 13.1→10.24 (22%↓) | 4.91→10.24 (108%↑) |
| **Fracture Toughness ($MPam^{1/2}$)** | 4.69→5.12 (35%↑) | 5.12→5.14 (0.4%↑) | 4.69→5.14 (9.6%↑) |

Table 3: Variation in magnitude of the mechanical properties of Y-TZP ceramic sintered with 1 minute holding time at three temperature ranges.

Based on the observation, it can be inferred that the 3Y-TZP sintered within the range of 1250°C to 1400°C underwent micro-structural changes that would inevitably change the mechanical properties of these samples. However, at 1400°C (minimum temperature at which mechanical properties do not vary significantly) with a holding time of 1 minute yielded ceramics with acceptable mechanical properties rendering these samples fit for structural application.

| | **Typical recommended properties for Y-TZP*** | **Properties for samples sintered at 1400°C / 1min. holding time** |
|---|---|---|
| **Bulk Density ($Mgm^{-3}$)** | > 95 | 97 |
| **Young's Modulus (GPa)** | > 180 | 200.2 |
| **Vickers Hardness (GPa)** | > 10 | 13.1 |
| **Fracture Toughness ($MPam^{1/2}$)** | 4 - 7 | 5.12 |

***Introduction to Zirconia, Magnesium Elektron Ltd., UK (No. 113,1986)***

Table 4: Mechanical properties comparison of 3Y-TZP sintered at 1400°C with 1 minute holding time

Based on the above, 3Y-TZP sample sintered at 1400°C with a holding time of 1 minute fits well within the postulated criterion for 3Y-TZP that are deemed fit for industrial application.

## 4. Conclusion and recommendation

The current study was carried out to evaluate the possibility of fabricating 3Y-TZP ceramics with mechanical properties that are desirable to ensure that these fabricated ceramics do not fail under hostile humid environment. The main parameter that was manipulated in order to achieve these objectives was the sintering holding time and sintering temperature. Sintering time was found to be an important factor governing the density of the sintered 3Y-TZP samples. It was found that longer holding times resulted in higher densities. Moreover, it was also found that 3Y-TZP samples with holding times of 2 hours, 1 hour, and 30 minutes and 1 minute exhibit the same trend in mechanical properties magnitude variation.

More detailed study on the ramp rate employed in the sintering profile could lead to a better densification. Employing a lower ramp rate to reduce the onset temperature of sintering might be useful in attaining 3Y-TZP with higher density.

## Acknowledgment

Foremost, I would to thank my supervisor Dr. Sivakumar for the effort, guidance and the motivation that he has given me throughout this research. It has been a great pleasure working with him as valuable knowledge in the area of material engineering was shared to me.

## References

[1] Basu, B., J. Vleugels, O. Van Der Biest, Transformation behavior of yttria stabilized tetragonal zirconia polycrystal composites, Journal of Materials Research (2001), pp. 2158-2169

[2] Basu, B., Toughening of Yttria-Stabilised Tetragonal Zirconia Ceramics, International Material Reviews (2005), pp. 239-256(18)

[3] J.A. Brito-Chaparro, A. Reyes-Rojas, M.H Bocanegra-Bernal, A. Aguilar-Elguezabel, Elucidating of microstructure of $ZrO_2$ ceramics with additions of 1200 ºC heat treated ultrafine MgO powders: Aging at 1420 ºC, Materials Chemistry and Physics (2007), pp. 45-53

[4] S. Ramesh, S. Sivakumar, Effects of two stage sintering on the properties of Y-TZP ceramics, University Malaysia Pahang (2011)